INFLUENCE OF PROPERTIES OF FLY ASH FROM DIFFERENT SOURCES ON THE MIX DESIGN AND PERFORMANCE OF GEOPOLYMER CONCRETE

A thesis submitted in fulfilment of the requirements for the degree

of

Doctor of Philosophy

by

Chamila Madusanka Gunasekara

B.Sc.Eng (Hons), M.Eng

Civil and Infrastructure Engineering

School of Engineering

College of Science, Engineering and Health

RMIT University

Melbourne, Australia.

July 2016

DECLARATION

I certify that except where due acknowledgement has been made, the work is that of the author alone; the work has not been submitted previously, in whole or in part, to qualify for any other academic award; the content of the thesis is the result of work which has been carried out since the official commencement date of the approved research program; any editorial work, paid or unpaid, carried out by a third party is acknowledged; and, ethics procedures and guidelines have been followed.

Madurapperumage Chamila Madusanka Gunasekara

6th July 2016

ACKNOWLEDGEMENT

I wish to express my heartfelt gratitude and appreciation to my principal supervisors, Prof. Sujeeva Setunge and Dr. David W. Law, for their warm-hearted encouragement, advice, mentoring, and research support throughout the course of this research.

I would like to acknowledge the Civil and Infrastructure Engineering, School of Engineering, RMIT University for providing me the post graduate research scholarship to conduct studies.

I wish to thank the Civil and Infrastructure Engineering laboratory staff, Pavel Ryjkov, Kevin Dung Le and Xiang Gao, and in particular Saravanan Mani who greatly assisted in preparing the test specimens. I would also like to express my appreciation to all technical staff in Chemical Engineering laboratory and Rheology & Materials Processing Centre (RMCP), and Dr. Ashish Kumar from MEP Instruments Pty Ltd. in facilitating the laboratory experiments.

I also express my appreciation to Phillip Francis in RMMF (RMIT Microscopy & Microanalysis Facility) and his technical staff, in particular, Peter Rummel and Dr. Matthew Field for their scientific and technical assistance. I further wish to thank School of science, RMIT University for providing their laboratories, chemistry and Nuclear Magnetic Resonance (NMR) Spectroscopy, to complete the research works.

I wish to appreciate the assistance of the administrative staff at School of Engineering of RMIT University. I further wish to express my thanks to Cement Australia Pty Ltd. and Flyash Australia Pty Ltd for the supply of fly ash throughout these three years.

I am indebted to my beloved parents, for their continuous encouragement and support throughout my years of education. I sincerely dedicate this thesis to them. My deepest gratitude is for my wife, Shasheeka, for her unconditional love, support, patience, encouragement and understanding. Our sons, Adeesha and Pamitha, have been a great source of inspiration, light and love in brightening my days of research over this period and beyond. I would also like to express my gratitude to all my teachers, from primary school up to post graduate level, for their contribution and support.

Last, but not the least, I would like to thank all my colleagues and friends for their continuous support and understanding.

ABSTRACT

Geopolymer concrete produced using 100% fly ash as the main binder replacing Portland cement (PC) has been the focus of the research study. A major challenge in the specification of geopolymer mix designs is the variability in the fly ash used and the impact of that variability on the performance of the geopolymer produced. The research to date has concentrated on the properties of these materials, with distinct variations in performance noted. Little research has been undertaken on understanding the chemistry behind these variations and in characterizing the components of the fly ash and the activators and how their interaction and relative concentrations determine the performance and properties of the geopolymer concrete produced in long term.

This research study aimed at developing a fundamental understanding of the physical, mineralogical and chemical properties of fly ash on the performance of 100% fly ash based geopolymer concrete. The broader literature review was conducted initially to identify properties of fly ash affecting compressive strength of geopolymer. Then a comprehensive experimental programme was designed and executed with a wide range of state of the art techniques to understand the specific influence of individual properties of fly ash and combined effect which affects the compressive strength of geopolymer. The key factors affecting the performance of geopolymers made from a total of five chemically and physically distinct fly ash is reported. The key factor identified as influencing the strength was the workability, with a flow in the range between 110 ± 5% and 140 ± 5% required for optimal performance. In this flow range, the strength of geopolymer is governed by the specific surface area of precursor fly ash coupled with the quantity of amorphous phase up to 20μm in particle size. In addition a negative zeta potential of the fly ash was identified as assisting gel formation with the smaller the negative zeta potential of the geopolymer product the larger the quantity of gel formation and higher the compressive strength observed. The uniformity of the distribution of SiO_2 and Al_2O_3 in the fly ash is observed to directly influence the dissolution of the amorphous surface layer in the initial geopolymerization process and control the aluminosilicate gel precipitation and gel–phase creation. This study shows that the higher the uniformity of distribution, and more stable the conversion of aluminium from octahedral to tetrahedral coordination the higher the aluminium amalgamation with silicates leading to production of a three dimensional polysialate–siloxo

polymeric gel network with high rigidity and stability, which in turn results in higher compressive strength. A high CaO content in fly ash further leads to high compressive strength.

The second phase of this study was dealing with the performance of geopolymer concrete up to one year using a range of fly ash with same mixing process, providing a systematic long term study of the mechanical and durability properties of a range of geopolymer concrete. Hence, the research data presented here will be extremely useful to understand the long term behaviour of geopolymer concrete made with the wide range of fly ash that are available across the world. The results show a considerable increase in performance observed between 90 and 365 days for all concrete depending on the fly ash properties. This is attributed to an on-going geopolymerization which results in continuing gel formation leading to a more densely packed microstructure, with an associated reduction in meso-pores and macro-pores. The nature of the gel matrix formed, in terms of uniformity and compactness, was observed to determine the mechanical properties. The presence of a high quantity of CaO leads to a densely packed microstructure at an early age, giving high early compressive strength. The nature of the interfacial transition zone formed between coarse aggregate and mortar and its density was observed to govern the tensile strength. An increase in porosity and micro cracks was seen to negatively affect the compactness of the gel matrix, which in turn affects the elastic modulus. The packing density coupled, with the pore size distribution, were observed to determine the permeation and diffusion characteristics of the concrete. A high quantity of meso-pores in the gel paste was observed to increase the water absorption while a high quantity of macro-pores leads to an increase in the water and air permeability of geopolymer concrete. Notably the initial chloride diffusion coefficients are analogous to those observed in Portland and blended cement concretes and also observed to decrease with the age in a similar manner.

At last the applicability of current relationships of Portland cement concrete as specified in Australian Standards (AS) and American Concrete Institute (ACI) for geopolymer concrete have been critically examined. The results indicated that the flexural strength of geopolymer concrete is higher than those predicted using current design equations for Portland cement concrete of similar compressive strengths. However, splitting tensile strength of geopolymer concrete is comparable to those predicted using current design equation for Portland cement concrete for similar compressive strength. It was also observed that ACI stated equation

significantly overestimates the splitting tensile strength of geopolymer concrete. Similarly, Australian Standards overvalues the elastic modulus of geopolymer concrete.

LIST OF PUBLICATIONS

The research outcomes from this Ph.D study have been published in five peer reviewed conference papers. Two journal articles have been published, another one accepted to publish and others are currently in peer review process. The complete list of the publications is provided as follows:

Journal articles

1. **Chamila Gunasekara**, David W. Law, Sujeeva Setunge, Jay Sanjayan (2015). Zeta potential, gel formation and compressive strength of low calcium fly ash geopolymers. *Construction and Building Materials Journal*, 95, pp. 592-599. doi:10.1016/j.conbuildmat.2015.07.175

2. **Chamila Gunasekara**, David W. Law, Sujeeva Setunge (2016). Long term permeation properties of different fly ash geopolymer concrete. *Construction and Building Materials Journal*, 124, pp. 352-362. doi:10.1016/j.conbuildmat.2016.07.121

3. **Chamila Gunasekara**, Sujeeva Setunge, David W. Law (2016). Long term mechanical properties of different fly ash geopolymer concrete. *ACI Structural Journal* (Accepted with minor amendments).

4. **Chamila Gunasekara**, David W. Law, Sujeeva Setunge, Iko Burgar, Robert Brkljaca (2016). Impact of elemental distribution in low calcium fly ash based geopolymers. *Journal of Advanced Concrete Technology* (In peer-review process).

5. **Chamila Gunasekara**, Sujeeva Setunge, David W. Law (2016). Correlation between mechanical properties of fly ash geopolymer concrete. *Journal of Materials in Civil Engineering (ASCE)* (In peer-review process).

6. **Chamila Gunasekara**, Sujeeva Setunge, David W. Law, Nick Willis, Trevor Burt (2016). Engineering properties of geopolymer aggregate concrete. *International Journal of Concrete Structures and Materials* (In peer-review process).

Conference papers

1. **M.P.C.M.Gunasekara**, D.W.Law, S.Setunge (2014). Effect of composition of fly ash on compressive strength of fly ash based geopolymer mortar, *Proceedings of 23rd Australasian Conference on the Mechanics of Structures and Materials (ACMSM23)*, Byron Bay, Australia, 9-12 December.

2. **M.P.C.M.Gunasekara**, D.W.Law, S.Setunge (2014). Compressive strength and microstructural development of fly ash based alkali activated binders, *Proceedings of 2nd International Congress on Durability of Concrete (ICDC2014)*, New Delhi, India, 4-6 December.

3. **M.P.C.M.Gunasekara**, David W. Law, Sujeeva Setunge (2015). A comparative study of durability characteristics and microstructure of five different fly ash based geopolymer concrete, *Proceedings of 14th International Congress on the Chemistry of Cement (ICCC14)*, Beijing, China, 13-16 October.

4. **M.P.C.M.Gunasekara**, David W. Law, Sujeeva Setunge (2015). The effect of type of fly ash on mechanical properties of geopolymer concrete, *Proceedings of Concrete 2015*, Melbourne, Australia, 30th August-2nd September.

5. **Chamila Gunasekara**, David W. Law, Sujeeva Setunge (2016). Comparison of long term strength and permeability properties of different fly ash based geopolymer concrete, *Proceedings of 4th International conference in Sustainable Construction Materials and Technologies (SCMT4)*, Las Vegas, USA, 7-11 August.

TABLE OF CONTENTS

LIST OF FIGURES

LIST OF TABLES

1 INTRODUCTION

1.1 Background

The demand for Portland cement (PC) has been ever increasing in contrast to natural resources for cement production which have decreased. In addition, increased PC production results in significant amount of CO_2 emissions. Schneider et al. (2011) predicted that worldwide cement production would increase from approximately 2.54 billion tonnes in 2006 to 4.38 billion tonnes in 2050 based on 5% growth per year. However, the projected level for 2015 was reached by 2011 (Staniford, 2012). The increase of PC production has a detrimental effect on the global environment, with PC production alone contributing between 4 to 8% of CO_2 emissions worldwide (Gartner, 2004, Meyer, 2009, Chen et al., 2010). A small reduction of PC production could result in significant environmental benefits in terms of CO_2 emission. This has encouraged research into environmentally friendly cementitious materials that produce high strength and good durability while maintaining an acceptable level of energy consumption for production.

Over recent years the concrete industry has consistently moved towards sustainability by incorporating significant amounts of industrial waste and by-product materials such as fly ash in concrete. However, further need to reduce the PC production and consumption has led to research investigating the use of waste materials such as fly ash and blast furnace slag to satisfy the requirement of being the sole binder in concrete. Geopolymer concrete, also known as alkali activated concrete, 100% fly ash concrete, inorganic polymer concrete, or cement free concrete are outcomes of this approach.

Geopolymer concrete differs substantially from PC concrete, as it follows a distinctly different reaction pathway to PC concrete to attain structural integrity. PC concrete is reliant on the presence of calcium-silicate-hydrate (C–S–H) gel for matrix formation and strength development, while geopolymer concrete undergoes polycondensation of alumina and silica oxides in the fly ash, with a highly alkaline activator. The mechanism for geopolymerization involves three principal steps. These are dissolution of alumina and silica oxides of the fly ash in the alkaline activator, transportation of dissolved alumina and silica species and the polycondensation process with the formation of aluminosilicate gel as a main reaction product (Fernandez-Jimenez and Palomo, 2005). In the activation process, the hydroxyl anions acts as a reaction catalyst while the alkali metal cations act as structure forming

elements. The structure of aluminosilicate gel contains Si^{4+} and Al^{3+} randomly distributed along the polymeric chains that are cross linked so as to provide cavities of sufficient size to accommodate the charge balancing hydrated alkali cations.

Fly ash based geopolymer concrete can achieve comparable strengths to PC and blended cement concrete (Guo et al., 2010, Bakharev, 2005a). Hardjito et al. (2004) reported that the Young's modulus, Poisson's ratio and tensile strength of fly ash based geopolymer concrete are comparable to those of PC concrete. Wallah et al. (2006) found that geopolymer concrete undergoes low creep and very little drying shrinkage. Moreover, fly ash based geopolymer concrete have a satisfactory performance in durability characteristics such as better resistance against chloride (Miranda et al., 2005), carbonation (Law et al., 2014), elevated temperature (Kong and Sanjayan, 2010, Junaid et al., 2014, Junaid et al., 2015) and sulphate & acid (Bakharev, 2005b). On the other hand, in terms of CO_2 emission, fly ash based geopolymer concrete production reduces CO_2 emission by 26-45% by the replacement of PC with no adverse economic effects (McLellan et al., 2011, Habert et al., 2011, Stengel et al., 2009). Overall, fly ash based geopolymer concrete has significant potential to reduce use of PC in concrete.

1.2 Research Significance

Variations in the combustion process and inconsistent chemical composition of coal sources result in variability in the chemical, physical and mineralogical properties of precursor fly ash. Thus, the major challenge in design of geopolymer concrete structures is the variability of compressive strength and other material properties of concrete resulting from different sources of fly ash. Table 1.1 illustrates range of compressive strengths reported in literature while using fly ash produced in different power plants. Thus, understanding the distinct properties of the fly ash as the geopolymer precursor and correlating these properties with the compressive strength development of the geopolymer is essential at the real application stage. This initiates two research questions of this study:

1. What parameters influence the compressive strength of geopolymer concrete produced with different fly ash sources?

2. What are the underlying reasons for the different compressive strengths of geopolymer concrete observed with different sources of fly ash?

Table 1.1 Compressive strength of different fly ash based geopolymer mortar

Research Study *(Reference)*	Fly ash Source	Mix design parameters		Optimum compressive strength (MPa)
		[a]Na_2O dosage (%)	[b]Activator Modulus (AM)	
Fernandez-Jimenez and Palomo (2005)	Spanish	5.55 - 14.9	0.037 - 1.23	91.6
Yang et al. (2008)	Malaysian	8.9 - 16.4	0.9	9.5
Adam (2009)	Australian (Gladstone)	7.5 - 15	1.0 – 1.5	79.3
Wardhono et al. (2012)	Australian (Tarong)	15	1.0 - 1.5	30.2
	Australian (Mt.Piper)			54.9

[a]Na_2O dosage = Na_2O in alkaline activator /fly ash; [b]AM = SiO_2/Na_2O in alkaline activator

Published research to date on geopolymer concrete has studied the material properties in short term (up to 90 days) using a single type fly ash, and in each study using a mixing process unique to that study. Hence, the systematic long term research will be extremely useful to understand the long term performance of geopolymer concrete made with a wide range of fly ash that are available across the world. Moreover, evaluating the correlation between long term mechanical properties of geopolymer concrete manufactured using a wide range of fly ash in conjunction with the applicability of current relationships between compressive strength and the mechanical properties based on standards derived for PC concrete is very important. Thus following research questions have been raised concerning the long term performance of geopolymers prior to their adoption as a sustainable alternative to the PC concrete.

3. What is the correlation between long term material properties of geopolymer concrete and mix design and constituent materials?

4. Why permeability and diffusion characteristics of geopolymer concrete change with fly ash type?

5. Can we predict mechanical properties of geopolymer concrete as a function of compressive strength?

To address the arising research questions and to achieve the desired objectives of the research, a comprehensive research program has been formulated. The following sections

will briefly discuss the research objectives that have been derived to address these research questions, along with a description of the overall scope and limitations of this study.

1.3 Aim and specific Objectives

Aim of this research study is to develop a fundamental understanding of the physical, mineralogical and chemical properties of precursor fly ash on the performance of fly ash based geopolymer concrete.

The specific objectives will include;

1. Identify properties of fly ash affecting strength of geopolymer mortar.
2. Understand the specific influence of individual properties of fly ash and combined effect which affect the strength of geopolymer mortar.
3. Validate any hypothesis developed using further experiments.
4. Evaluate long term performance of geopolymer concrete produced using different fly ash types.
5. Examine applicability of current relationships between mechanical properties and compressive strength of PC concrete stated in standards for geopolymer concrete.

1.4 Research Scope

Low calcium, class F precursor fly ash from five different coal power stations in Australia has been investigated. The compressive strength of fly ash geopolymer mixes was examined over a range of activator modulus at a fixed Na_2O dosage in order to optimize the best mix design of both geopolymer mortar and concrete for each specific fly ash. A series of tests have been conducted on geopolymer mortar as the first phase of the research. These results have been analysed to explain the effects of the chemical, physical and mineralogical properties of precursor fly ash on the strength evolution of geopolymers. The long term performance of mechanical and durability properties of four different fly ash geopolymers was being investigated in the second phase of research. The influence of properties of precursor fly ash on the geopolymer material properties are studied through comprehensive microstructural and pore-size distribution analysis.

1.5 Organization of thesis

This thesis is organized into eight chapters as described below:

Chapter 1 is the introductory chapter which presents the background of the research, discusses the significance of the research and the research questions, discusses the objectives of the study, states the scope of the research with limitations of the study, and finally provides a brief outline of the overall thesis.

Chapter 2 initially discusses current PC production and its related issues to the environment. Next, the use of fly ash in concrete as cement replacement materials and the alkali activation of fly ash as well as the reaction mechanism are discussed briefly. Finally the identified factors affecting the properties of fly ash based geopolymer concrete from the existing literature, and performance of the geopolymer concrete over time, in terms of mechanical and durability are presented.

Chapter 3 presents the details of the materials and the experimental methods used. A series of tests had been conducted using state of the art techniques to characterise precursor fly ash and geopolymer matrices. The experimental methods used to investigate long term material properties of geopolymer concrete are listed here in detail.

The research conducted to understand the factors affecting the suitability of fly ash as a source material for geopolymers has been split into two chapters, Chapter 4 and Chapter 5. In **Chapter 4**, variation of chemical, physical and mineralogical properties of precursor fly ash and their impact on the compressive strength development of geopolymer mortar produced by a wide range of low calcium Australian fly ash are covered comprehensively.

Chapter 5 presents further research conducted for understanding the factors affecting suitability of fly ash as a source material for geopolymers. This chapter presents the microstructural studies undertaken to identify the elemental oxide distribution within the fly ash particles and how this affects the geopolymerization mechanism and the compressive strength achieved. The pore-structural changes with the degree of geopolymerization is also examined deeply and then correlated with the compressive strength of final geopolymer systems.

Chapter 6 compares the test results of the long term mechanical properties in different fly ash based geopolymer concrete with the comprehensive microstructural analysis. The applicability of current relationships between compressive strength and the mechanical properties based on standards derived for PC concrete is examined for the fly ash geopolymer concrete. The new regression models derived for geopolymer concrete are also presented.

Chapter 7 describes the long term permeation and diffusion characteristics of geopolymer concrete produced with wide range of fly ash. The pore-structure and microstructural changes of different fly ash geopolymers have been deeply examined and correlated with the observed variations in order to discuss the long term durability of geopolymer concrete.

The final chapter, **Chapter 8**, discusses the overall conclusions of this research and provides recommendations for future research, which can be carried out as an extension of the presented work.

2 LITERATURE REVIEW

2.1 Introduction

2.1.1 Portland cement production

Concrete is the most abundant construction material and PC, a major component of concrete, is the largest volume of construction material produced in the world. The manufacturing process of PC (Figure 2.1) consists essentially of grinding the raw materials, mixing them intimately in certain proportions and burning in a large rotary kiln at a temperature of up to about 1450℃ when the material sinters and partially fuses into balls known as clinker. The clinker is then cooled and ground to a fine powder, with some gypsum added, and the resulting product is the commercial PC so widely used throughout the world.

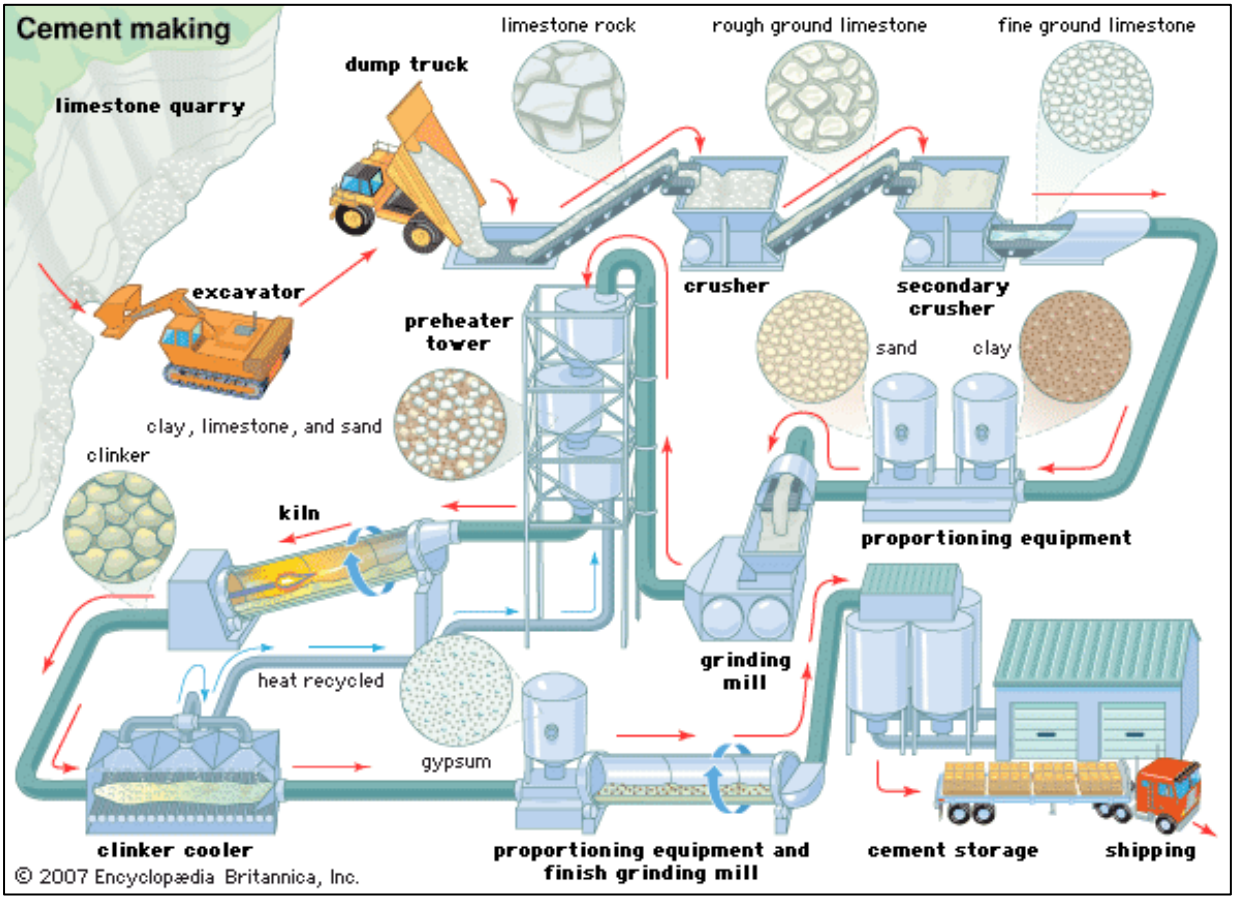

Figure 2.1 Portland cement manufacturing process

Schneider et al. (2011) reported that global PC production will increase from 2.54 billion tonnes in 2006 to 4.38 billion tonnes in 2050 based on 5% growth per year. Major growth is foreseen in countries such as China and India as well as in regions like the Middle East and

Northern Africa (Figure 2.2). However, Staniford (2012) reported that the projected level of PC production for 2015 had already been reached in 2011. This is an environmentally alarming trend with respect to the diminishing of natural resources and global warming.

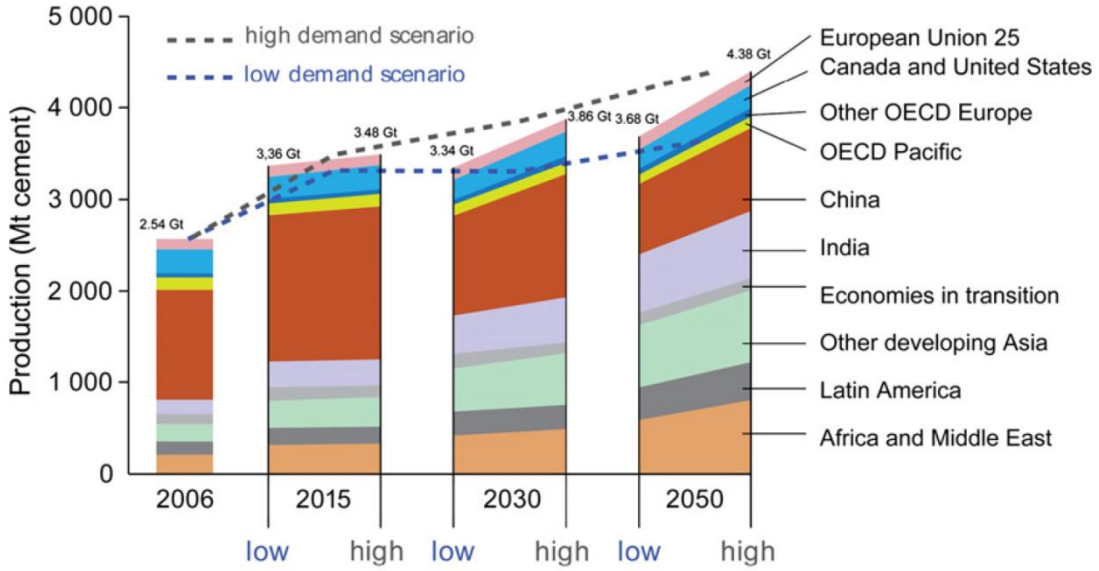

Figure 2.2 Global Portland cement production (Schneider et al., 2011)

2.1.2 CO_2 emission and other environmental issues

The PC manufacturing process is an energy intensive process (Berry et al., 2009) and one of the highest CO_2 emitting industries in the world. It contributes between 4% to 8% of the current anthropogenic CO_2 emissions worldwide (Gartner, 2004, Meyer, 2009, Chen et al., 2010), with the production of 1 tonne of cement producing from 0.6 up to1 tonne of CO_2, depending on the power plant (Peng et al., 2013, Li et al., 2011, Huntzinger and Eatmon, 2009). Berry et al. (2009) reported that the contribution of PC production to global greenhouse gas emissions is 1.6 billion tons. In Australia alone, the total greenhouse gas emissions from PC production increased by 5.2% between 1990 and 2005 (Wood, 2009). The projected trend of global CO_2 emission by PC industry from 1990 to 2050 is shown in Figure 2.3.

It is estimated that up to 0.54 tonne of CO_2 per tonne of clinker is released during calcination, in which limestone is transformed into lime, and 0.46 tonne of the CO_2 emitted is the result of burning fuel to provide the thermal energy necessary for calcination to occur (Lawrence, 2003). Thus the primary difference between the cement industry and most other industries is

that fuel consumption is not the dominant driver of CO_2 emission. Hence, a small reduction of PC production could result in significant environmental benefits in terms of CO_2 emission.

In contrast, production of one tonne of PC requires about 2.8 tonnes of raw materials (mainly limestone), including fuel and other materials. In addition to the CO_2 emission, PC production generates 5 to 10 % of dust, i.e. altogether about 6000 to 14000m^3 dust-containing air-streams are generated per one tonne of cement production. Overall, PC manufacturing industry is facing challenges such as increase in cost of energy, requirements to reduce CO_2 emissions, mitigation of additional environmental issues and the supply of raw materials in sufficient qualities and quantities.

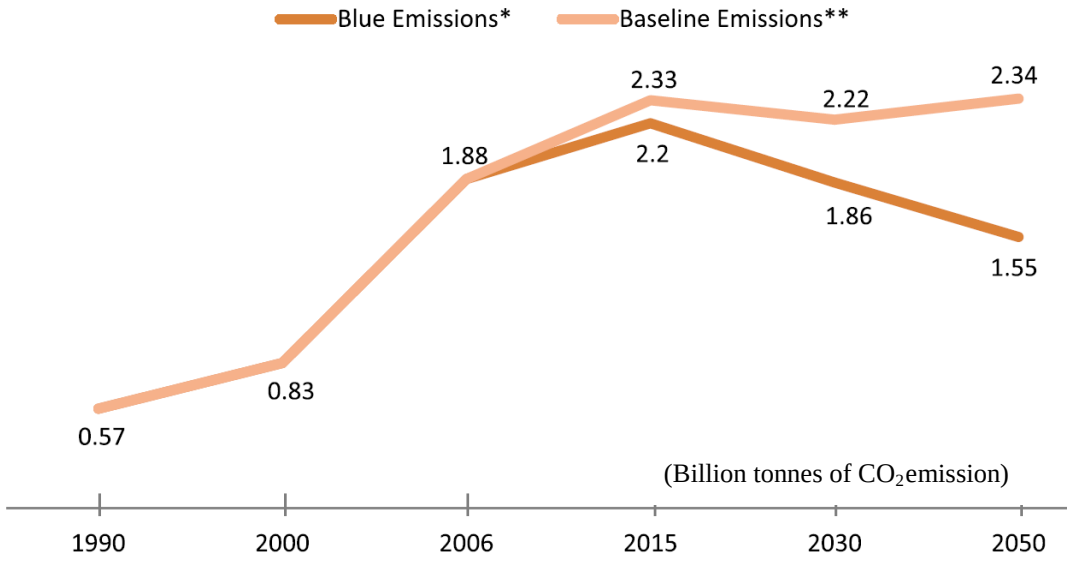

*Blue emission: Future emissions by considering application of mitigation technologies and policies.
**Baseline emission: Expected emissions without applying any mitigation actions.

Figure 2.3 Global CO_2 emission by cement plant (Boden et al., 2009, Benhelal et al., 2013)

2.1.3 Durability issues in aggressive environments

PC concrete is a durable construction material in a mild environment with proper design. However it has been long documented that reinforced concrete structures located in aggressive environments can suffer from deterioration due to ingress of aggressive agents such as chloride, carbon dioxide and acid. Most of the chemical attacks on PC concrete are in the form of a reaction between aggressive agents and the cement matrix, i.e. reaction with the $Ca(OH)_2$ and C–S–H, the major hydration products that provide the strength and binding properties, that are vulnerable to chemical degradation.

The durability of concrete has a direct relationship to its service behaviour, design life, and especially the safety. Catastrophic damage resulting from steel reinforcement corrosion, alleged to be driven by chlorides from de-icing salts and pH reduction from carbonation, has been noted among bridge decks (Bentur et al., 1997, Broomfield, 2006). Cracking in the concrete mass facilitates the ingress of chlorides and other harmful agents, hence accelerating the deterioration of the reinforcing steel.

Sulphate attack is another important durability and serviceability concern for PC concrete used in construction. The external sulphate attack on PC concrete structures show that reactions involve $Ca(OH)_2$, C–S–H and the aluminate component of hardened cement paste (Scrivener and Young, 1997). As a result of these reactions, expansion and cracking are caused by ettringite and gypsum formation, while softening and disintegration are caused by destruction of C–S–H (Scrivener and Young, 1997, Taylor and Gollop, 1997), resulting a deterioration of concrete structures.

2.2 Use of fly ash as alternative cementitious material

2.2.1 Fly ash production

Fly ash, known also as pulverized-fuel ash is the ash precipitated electrostatically or mechanically from the exhaust gasses or coal-fired power stations (Figure 2.4). It is the most common waste pozzolanic material in the world. Typically coal is pulverized and blown with air into the boiler's combustion chamber where it immediately ignites, generating heat and producing a molten mineral residue. Boiler tubes extract heat from the boiler, cooling the flue gas and causing the molten mineral residue to harden and form ash. The bottom ash which contains coarse particles fall to the bottom of the combustion chamber, while the lighter fine ash particles remain suspended in the flue gas. Prior to exhausting the flue gas, fly ash is removed by particulate emission control devices such as electrostatic precipitators.

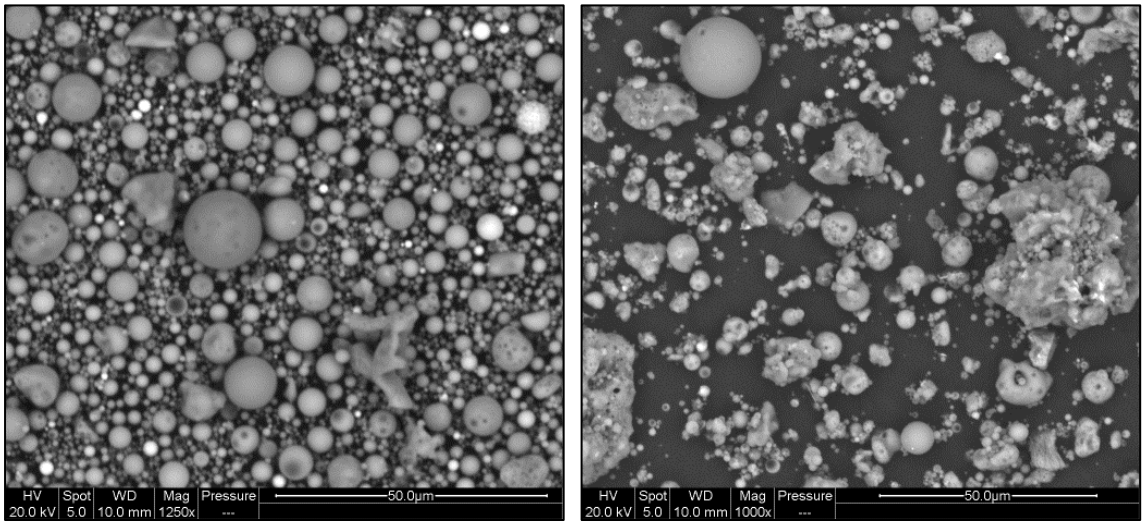

Figure 2.4 Fly ash precursor (a) Gladstone & (b) Port Augusta Power Station in Australia

Fly ash production had increased to 900 million tonnes per year by 2008 and it is anticipated to increase up to about 2000 million tonnes in 2020 (Malhotra, 2008). While about 45% of this is being utilized for various purposes including cement and concrete production the balance is disposed in landfills and storage lagoons at significant cost, posing a potential risk to local aquifers due to the possible leaching of heavy metals. Because of the increasing load of toxic metals in the landfill, the threat to ground water contamination is potentially increased.

Fly ash mainly consists of silica, alumina and iron oxides. Other minor constituents of fly ash are oxides of calcium, magnesium, sulphur, alkali, phosphorus, manganese and titanium. According to ASTM C618 standard (ASTM, 2012), fly ash can be divided into three groups as class F, class C and class N, based on the major chemical substances.

2.2.2 Fly ash usage in concrete

Fly ash is a pozzolanic material which reacts with $Ca(OH)_2$ from cement hydration to form C-S-H gel. This is the primary reaction when fly ash is used as a supplementary cementitious material. When used with PC, fly ash will only start to react when some cement hydration has taken place. This delay causes blended PC concrete to develop strength slowly at early ages compared to PC alone (Wang et al., 1994). However, properly cured concrete with fly ash as part cement replacement produces a denser product because the sizes of the pores are reduced by the reaction products of fly ash. This results in a continuous increase in compressive strength and will ultimately achieve an acceptable strength. The use of fly ash as a partial

replacement material in PC concrete has led to many advantages in fresh and hardened concrete, especially in terms of durability characteristics. The PC concrete with fly ash can be beneficial in reducing the permeability to wear and aggressive agents such as chloride and sulphate (Neville, 1996).

In contrast, the special shape of the fly ash particles helps to reduce the amount of mixing water in PC concrete. That means, concrete placement characteristics can be improved significantly by using fly ash in the concrete mixtures (Baweja and Nelson, 1998). In precast concrete, the benefit of fly ash can be translated into better workability, resulting in sharp and distinctive corners and edges with a better surface appearance. Added to this, the fine particles in fly ash can help to reduce bleeding and segregation which lead to improved pumpability and finishing properties. Overall, use of fly ash in PC concrete can lead to many improvements in concrete performance. However, a limit of up to 40% fly ash replacement is recommended with to maintain acceptable strength and durability (Neville, 1996).

2.2.3 Fly ash activation in alkaline media

Research has shown that it is possible to use fly ash as a sole binder by activating it with alkalis such as caustic alkalis, silicate salts, non-silicate weak acid salts, aluminates, aluminosilicates, and non-silicate strong acid salts (Sarker, 2011, Adam, 2009, Rangan, 2008, Duxson et al., 2007a, Fernández-Jiménez et al., 2006b, Hardjito et al., 2004). The product of this reaction is C-S-H gel, i.e. the product formed during the hydration of cement. However, a second type of reaction mechanism is possible and involves the activation of fly ash to form aluminosilicate polymers through a condensation and polymerisation process (Palomo et al., 1999, Davidovits, 1991). This is fundamentally different from a straight activation process and is a characteristic of a geopolymeric reaction. The term geopolymer was applied by Davidovits (1991) and is used to differentiate the geopolymer reaction from other types of alkali-activated material such as alkali-activated slag since the hydration product is more polymer than C-S-H gel.

2.3 Fly ash based Geopolymer

2.3.1 Fly ash use as a source material

The naturally occurring aluminosilicate materials could be a source materials for geopolymers (Xu and Van Deventer, 2000). Many researchers have used metakaolin as a

source material of aluminosilicate for geopolymer production due to its pure aluminosilicate content (De Silva et al., 2007, Duxson et al., 2005, Xu and Van Deventer, 2000, Davidovits, 1991, Cwirzen et al., 2014). However, the major disadvantage of use of metakaolin is the high-cost of production in bulk stage. Fly ash is a possible source material for geopolymer concrete production by activating it with a high alkaline solution (Talha Junaid et al., 2015, Fernández-Jiménez et al., 2006a, Duxson et al., 2007a, Molyneaux et al., 2007, Rangan, 2008). The presence of calcium in high quantities may interfere with the polymerisation process and alter the microstructure (Gourley, 2003), thus low calcium, Class F fly ash is preferred as a source material for geopolymer production compared to high calcium, Class C fly ash (Palomo et al., 1999, Swanepoel and Strydom, 2002a).

Fly ash production had increased to 900 million tonnes per year by 2008 and it is anticipated to increase up to about 2000 million tonnes in 2020 (Malhotra, 2008). While about 45% of this is being utilized for various purposes including cement and concrete production the balance is disposed in landfills and storage lagoons at significant cost, posing a potential risk to local aquifers due to the possible leaching of heavy metals. Hence, production of fly ash based geopolymer concrete not only reduces the CO_2 emission by 26-45% with the replacement of cement (McLellan et al., 2011, Habert et al., 2011, Stengel et al., 2009), but also convert a waste product into a useful by-product, conserving landfills and storage lagoons (Khale and Chaudhary, 2007). The added advantage over use of metakaolin is the low-cost of production in bulk amounts.

2.3.2 Reaction mechanism and hydration products

In discussing the molecular structure of geopolymer, the term polysialate was coined as a descriptor of the aluminosilicate network structure. The tetrahedral structures, i.e. SiO_4 and AlO_4, are linked in an alternating fashion sharing oxygen atoms to compose the sialate network (Figure 2.5) which has often been described to be similar to a sodalite network (Davidovits, 2000).

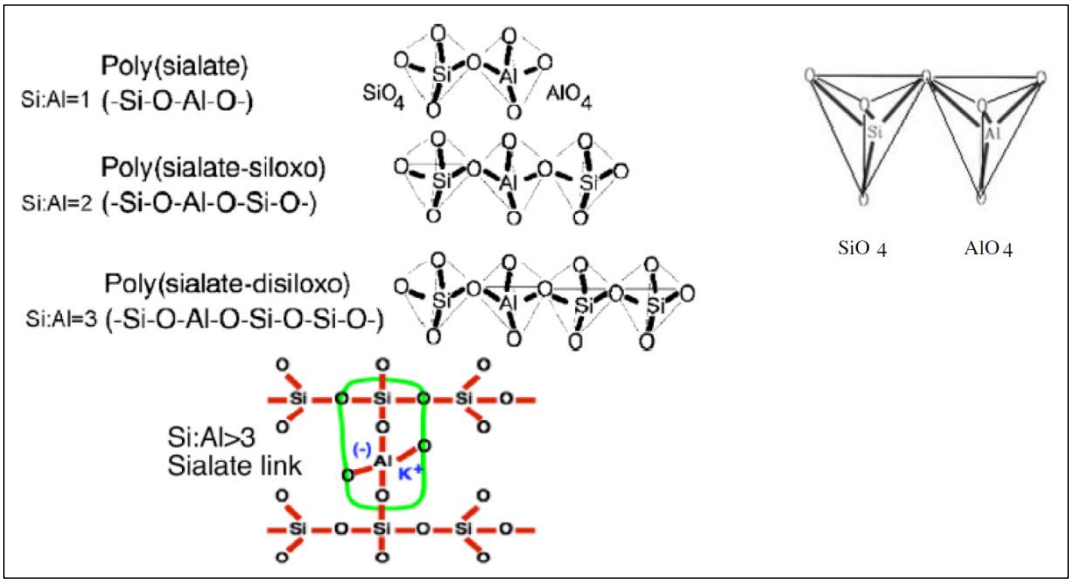

Figure 2.5 Aluminosilicate structure and nomenclature (Davidovits, 2005)

Due to the negative charge of the Al^{3+} in IV-fold coordination, positive ions must be present to balance out this charge. The alkali silicates or hydroxides used as the activating agents achieve this requirement by providing either potassium (K^+) or sodium (Na^+) ions into the matrix. The aluminosilicate have been grouped in three families depending on the atomic ratio of Si/Al that may be 1, 2, or 3 (Davidovits, 1994).

The geopolymerization process itself is an exothermic polycondensation reaction involving alkali activation by a cation in solution. Duxson et al. (2007a) presents a highly simplified reaction mechanism for geopolymerization by outlining the key processes occurring in the transformation of a solid aluminosilicate source into a synthetic alkali aluminosilicate gel (Figure 2.6).

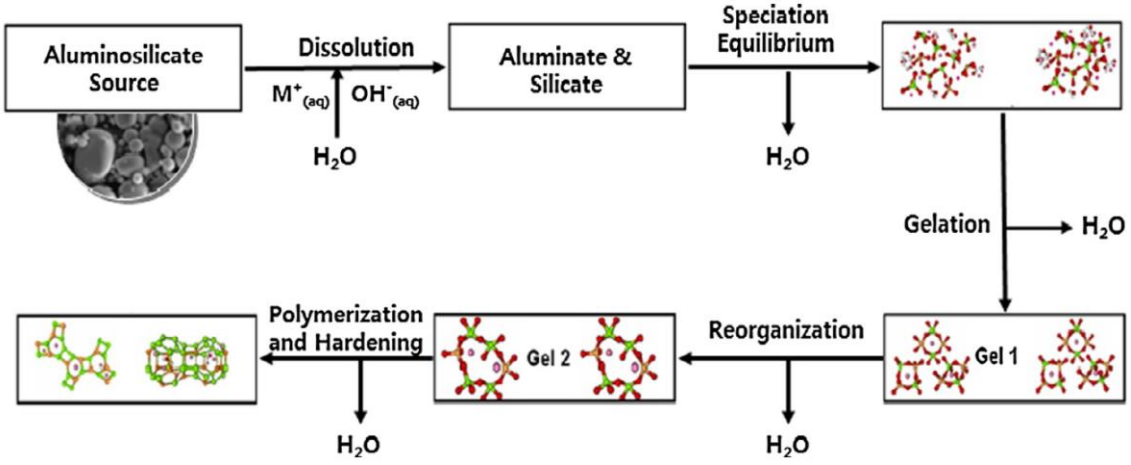

Figure 2.6 Conceptual model for geopolymerization (Ryu et al., 2013, Duxson et al., 2007a)

During the geopolymerization process, the slow growth of crystalline structures becomes evident as the nuclei of the polymerized gel reaches in critical size. The matrix crystallinity is relative to the rate by which precipitation occurs: fast reactions between alkali and fly ash do not allow time for growth of a well-structured crystalline environment. Therefore, most hardened geopolymer concrete are referred to as zeolitic precursors rather than actual zeolites. The final product of geopolymerization is an amorphous, semi-crystalline cementitious material (Duxson et al., 2007a, De Silva et al., 2007).

The chemical composition of the geopolymer material is similar to natural zeolitic materials, but the microstructure is amorphous. The polymerization process involves a substantially fast chemical reaction under alkaline conditions on Si-Al minerals, resulting in a three-dimensional (3-D) polymeric chain and ring structure consisting of Si-O-Al-O bonds (Davidovits, 1994). The formed gel product contains alkaline cations which compensate for the deficit charges associated with the aluminium at silicon substitution. An intermediate, aluminium-rich phase is first formed which then gives way to a more stable, silicon rich 3-D aluminosilicate gel product (Xie and Xi, 2001).

Moreover, Fernández-Jiménez et al. (2005) also illustrated the alakli activation of fly ash by a descriptive model (Figure 2.7). The dissolution process starts with an attack to the fly ash particles by high alkaline solution. As a result of the reaction, products are generated both inside and outside the shell of sphere until the ash particle is completely or almost completely consumed (Figure 2.7 a-c). At the same time, precipitations of reaction products occur as the alkaline solution penetrates the larger sphere and fill up the interior space with the reaction product, forming a dense matrix (Figure 2.7b). Due to the substantial precipitation of reaction products, some portions of smaller particles are covered with the products providing a crust which prevents contact with alkaline solution (Figure 2.7e) resulting in an unreacted fly ash particle. As a consequence, several morphologies may co-exist in a single paste: unreacted particles, particles attacked by the alkaline solution but which maintain their spherical shape, reaction product and so on (Figure 2.7d).

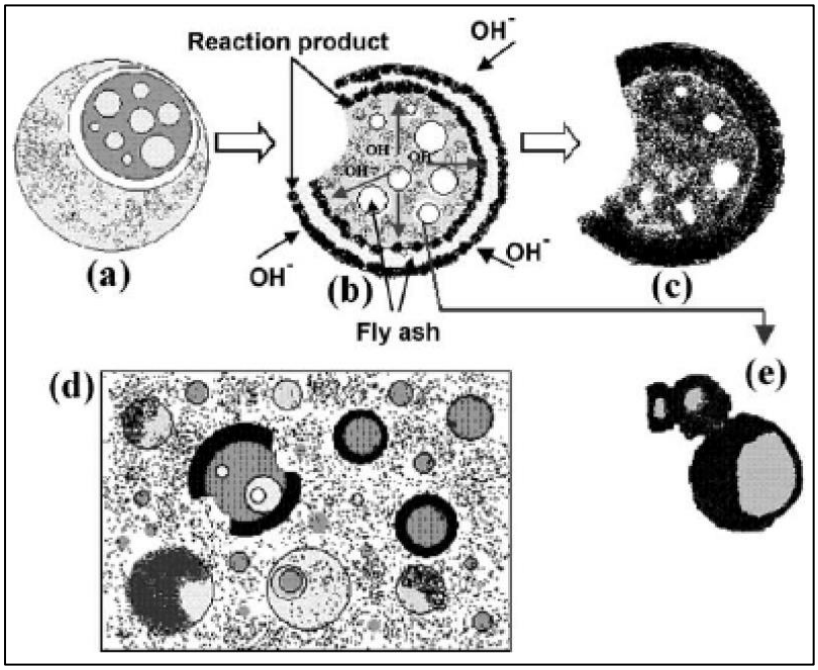

Figure 2.7 Descriptive model of fly ash-alkali activation (Fernández-Jiménez et al., 2005)

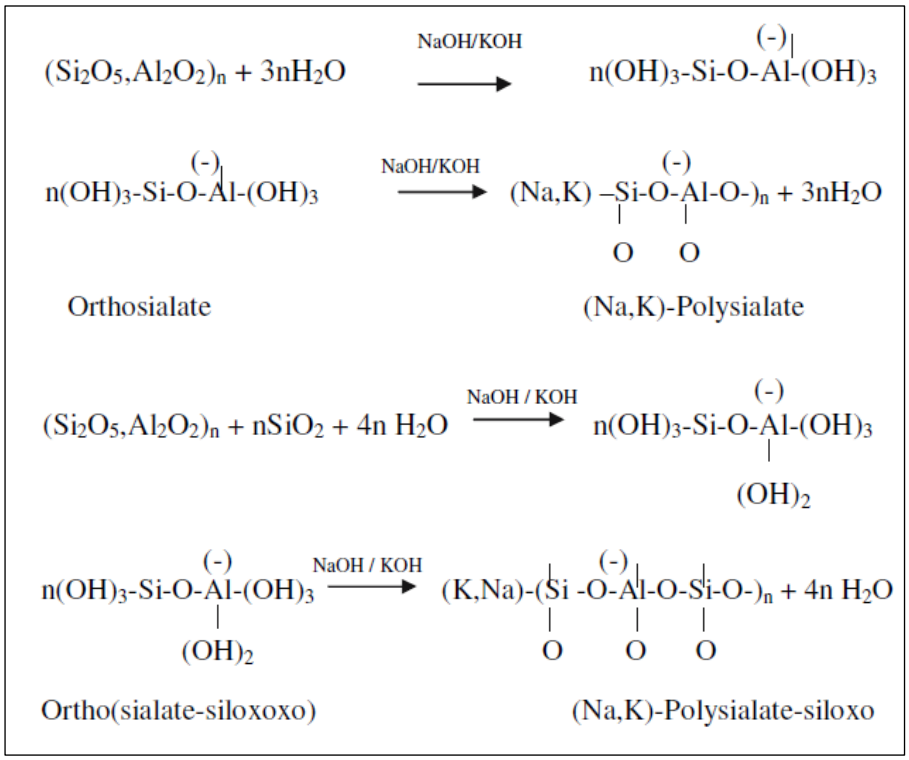

Figure 2.8 Geopolymeric reactions (Khale and Chaudhary, 2007)

The geopolymeric reactions involved in initial pozzolanic activation to final microstructural development is shown in Figure 2.8 (Khale and Chaudhary, 2007). The significant observation noted is the water in geopolymer mix doesn't participate in the geopolymeric

reaction. That means the water content in geopolymer mix only contributes to its workability during the handling process. Moreover, water is expelled from the geopolymer matrix during the curing and further drying periods. This is in contrary to the chemical reaction of water in the PC concrete mix during the hydration process.

2.3.3 Microstructure and its development

The geopolymerisation process mainly proceeds by mechanisms through the highly alkaline media when parts of fly ash are firstly dissolved in strong alkali solution and then a new geopolymer structure is developed in this solution as shown in Figure 2.9. The Na^{+} and Ca^{2+} ions play an important role while entering the Si–O–Al–O skeleton and in which they compensate the loading on Al atoms. Incorporation of those cations into Si–O–Al–O chains improves the strength of the final aluminosilicate gel structure (Khale and Chaudhary, 2007).

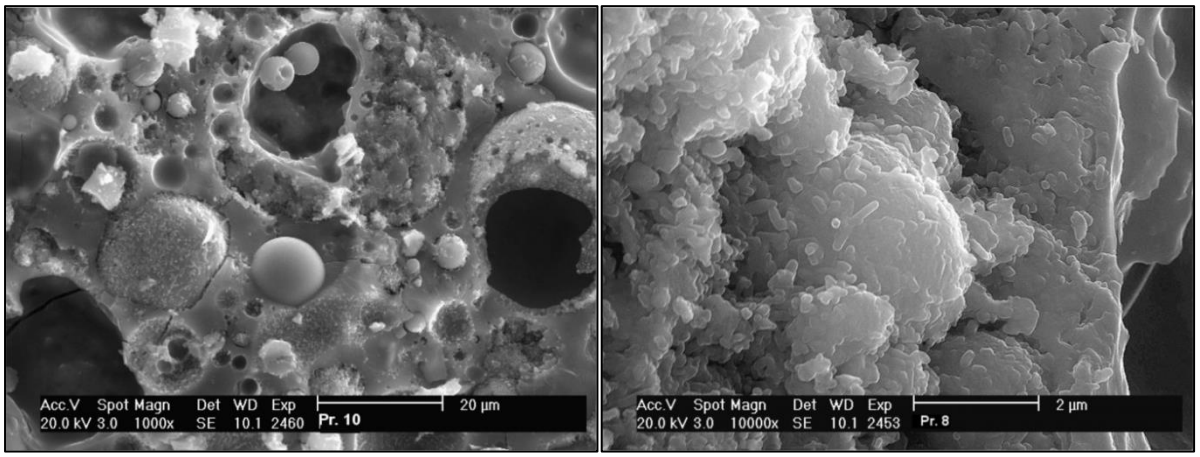

Figure 2.9 Typical appearance of fly ash based geopolymer (Škvára et al., 2006)

Fernández-Jiménez et al. (2005) reported the microstructural development of fly ash based geopolymer with respect to its degree of geopolymerization. They observed the changes detected in the fly ash geopolymer microstructure as a consequence of the sodium hydroxide dissolution attack in four different heat curing periods of 5 hours, 20 hours, 7 days and 60 days at 85^{o}C. Figure 2.10(a) shows the characteristic morphology of the raw fly ash. This ash consists of a series of spherical vitreous particles of different micron sizes. Whilst usually hollow, some of these spheres may contain other particles of a smaller size in their interiors. Figure 2.10(b) shows the first changes detected in the geopolymer microstructure under heat curing for 5 hours at 85^{o}C. A low to moderate degree of reaction (about 45.35%) was observed at this stage. Here, the spheres seem to be almost intact or appear within other

spheres, depending on the degree of local reactivity. Actually, in the early stages of the process, the alkaline dissolution dissolves part of the shells of the spheres, exposing the smaller particles (trapped inside the larger ones) to the alkaline attack as well.

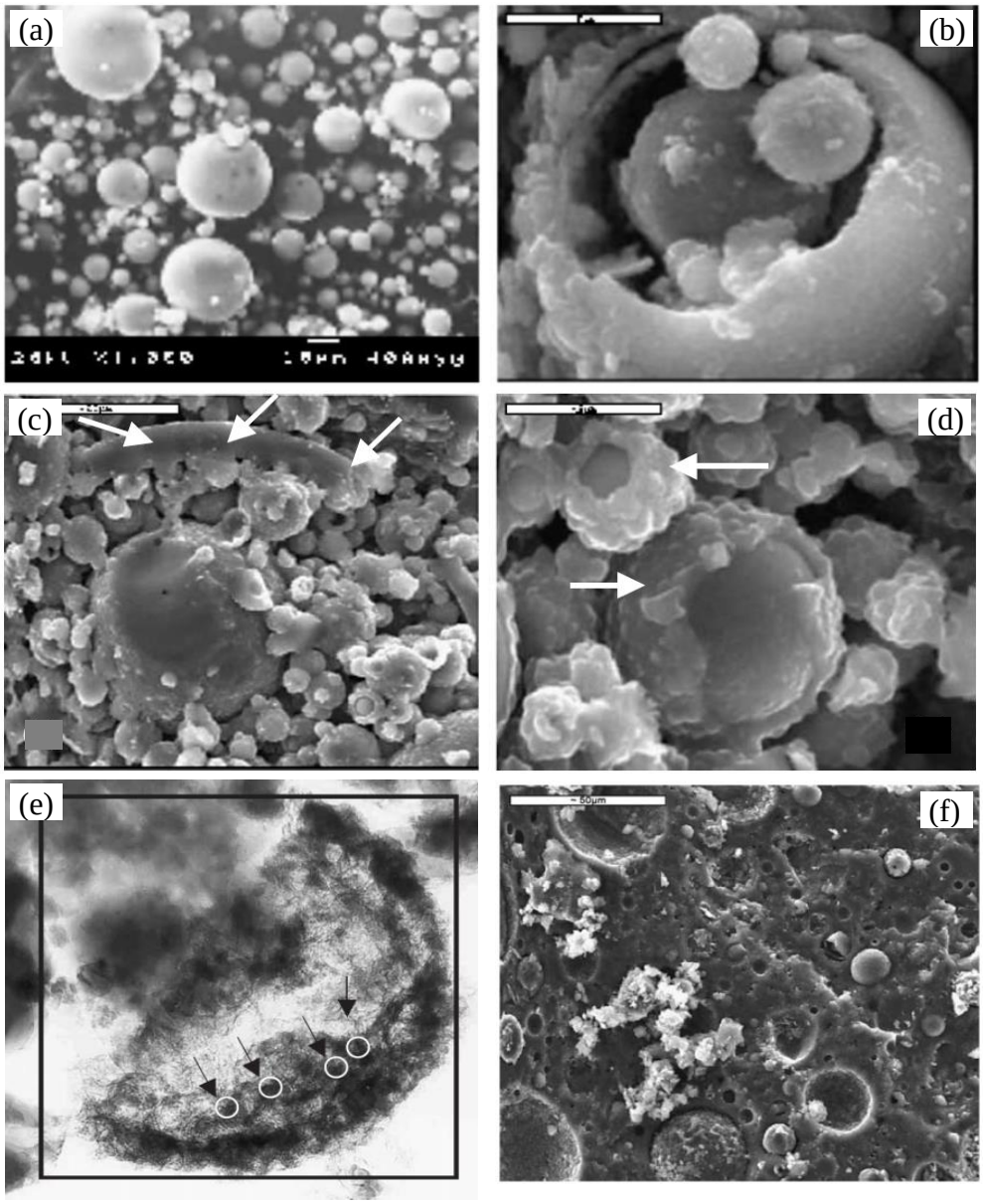

Figure 2.10 Microstructural development of geopolymer (Fernández-Jiménez et al., 2005)

Figure 2.10(c) and Figure 2.10(d) shows fly ash particles in a more advanced stage of the geopolymeric reaction, i.e. about 50% of reaction achieved after being heat cured for 20 hours at 85^{o}C. Figure 2.10(c) shows that the reactive process of a large fly ash sphere has been frozen. The main reaction product from the alkaline activation, i.e. aluminosilicate gel, precipitated around this large fly ash particle and gets compacted with the additional gel

produced from the other fly ash particles. Additionally, some alkali-reacted small fly ash particles in Figure 2.10(d) coexisted with the unreacted/partially reacted fly ash spheres. Hence those fly ash particles obviously would react with alkali very slowly.

Figure 2.10(e) shows the fly ash activated with sodium hydroxide for 7 days at 85^{o}C (Fernández-Jiménez et al., 2005). The spherical morphology of some fly ash particles becomes evident through transmission electron microscope (TEM) image. The large spherical fly ash particle underwent a long reaction process. Some small particles (25–35 Å diameters) have been identified inside this large particle. They were embedded into the aluminosilicate gel produced during the reaction process. Finally, Figure 2.10(f) shows the fly ash activated with sodium hydroxide for 60 days at 85^{o}C (Fernández-Jiménez et al., 2005). Highly compacted geopolymer matrix has developed after the long heat curing period which led to 66.83% degree of reaction. The non-reacted fly ash particles were embedded into the matrix.

2.3.4 Porosity and its distribution

A higher degree of geopolymerization leads the formation of a larger quantity of aluminosilicate gel. This gel fills the cavities between unreacted fly ash particles and pore spaces, thus refining the size of these pores. The total specific pore volume of the geopolymers depends on the fly ash particle size. The finer fly ash particle size results in the denser paste and hence the reduced pore volume in the specimens (Nazari et al., 2012).

In PC concrete, the porosity is divided into gel pores and capillary pores (Jennings et al., 2008). The gel pores are formed within the gel, and their diameter is in the range of a few nanometres. Capillary pores correspond to the spaces originally filled with water, and not filled by reaction products. The size of capillary pores range from a few nanometres to several dozen of micrometres. The air voids range from several dozen of micrometres to millimetres size (Gallucci et al., 2007). In practice, there is an overlap in gel and capillary pore systems in the range of about 5–20 nm. The formation of capillary pores is characteristic of cement systems, while their formation in geopolymers is less distinct, because the gel takes up most of the space (Ma et al., 2013).

In geopolymers, according to the IUPAC classification, porosity is generally classified as macro-porosity (pore size > 50nm), meso-porosity (2 nm < pore size < 50nm) and micro-porosity (pore size < 2nm) (Sing, 1985). The macro-pores represent the gaps between

unreacted fly ash particles. Meso-pores are typical pores between geopolymer phases, while micro-pores exist within the gel network (Zheng et al., 2010).

Duxson et al. (2005) found that the Si/Al ratio affects the microstructure of geopolymers, and hence the pore structure. Specimens with a Si/Al < 1.4 exhibit a microstructure comprising clustered dense particulates with large interconnected pores. Specimens with a Si/Al > 1.65 appear homogeneous exhibiting a porosity evenly distributed with small pores. According to the Figure 2.11**,** the pore volume distribution of geopolymers can be observed to shift into smaller pores as the Si/Al ratio increases. The pore size distribution of the geopolymer sometimes can be observed as a bimodal distribution due to large quantities of interconnected pores in combination with some level of crystallinity in alkali-activated systems. Overall, an increase in nominal Si/Al ratio results in large changes in the microstructure and porosity distribution of geopolymers.

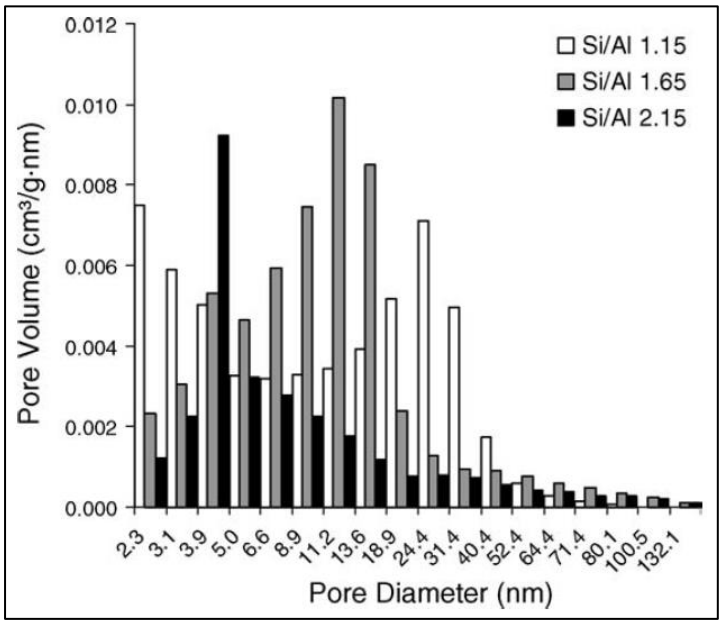

Figure 2.11 Pore volume distribution of geopolymers (Duxson et al., 2005)

2.4 Factors affecting the properties of fly ash based Geopolymer

2.4.1 Activator Modulus and Na_2O dosage

Activator modulus (AM) and Na_2O dosage are important parameters in geopolymer mix design. The AM is defined as the mass ratio of SiO_2/Na_2O in alkaline activator while the Na_2O dosage is the ratio of Na_2O/fly ash (Equation 2.1 and 2.2, respectively).

$$\text{AM} = \frac{\text{SiO}_2 \text{ in alkaline activator solution}}{\text{Na}_2\text{O in alkaline activator solution}} \quad (2.1)$$

$$\text{Na}_2\text{O dosage} = \frac{\text{Na}_2\text{O in alkaline activator solution}}{\text{fly ash}} \quad (2.2)$$

When alkaline activator consists of both sodium based silicate and hydroxide, it is hard to reflect the effect of the Na^+ concentration in the geopolymer mixture. Hence, literature (Adam, 2009) suggested that use of Na_2O dosage as mix design parameter is a good indicator of the Na^+ concentration in the initial geopolymer mix. Bakharev (2005a) also suggested an alternative method as Na_2O dosage in terms of the mass ratio of Na to fly ash. However, the Na_2O in the activator solution to fly ash for the sodium silicate based activator is more suitable since the grade of sodium silicate solution is usually specified by the ratio of SiO_2 to Na_2O which makes the mix design calculations easier.

Rangan (2008) reported that the variations in the AM significantly modifies the degree of geopolymerization of the dissolved species in the alkaline activator solution, thus determining the mechanics and overall properties of the geopolymer concrete. Lin et al. (2014) showed that a high SiO_2/Na_2O ratio (i.e. between 1.6 and 2.0) was required to synthesize geopolymers with the higher compressive strength. Zuda et al (2006) reported that higher percentages of soluble silica in geopolymer systems retards dissolution of the fly ash material due to increased saturation of the ionic silica species.

Table 2.1 Activator modulus and Na_2O dosage used in fly ash based geopolymers

Research Study *(Reference)*	Geopolymer product	Mix design parameters	
		Na_2O Dosage (%)	Activator Modulus (AM)
Fernandez-Jimenez and Palomo (2005)	Mortar specimen	5.55 - 14.9	0.037 - 1.23
Yang et al. (2008)		8.9 - 16.4	0.9
Adam (2009)		7.5 - 15	1.0 – 1.5
Wardhono et al. (2012)		15	1.0 - 1.5
Hardjito & Rangan (2005)	Concrete specimen	5.30 – 5.70	1.31 – 1.36
Wallah & Rangan (2006)		5.70	1.31
Sumajouw & Rangan (2006)		6.80	1.09
Adam (2009)		7.50	0.75 – 1.25
Wardhono et al. (2012)		15	1.0 - 1.5

The typical AM and Na_2O dosages that have been used in fly ash based geopolymers are given in Table 2.1. The data shows that a higher Na_2O dosage is required for fly ash activation (5.3-16.4%). Adam (2009) found that Na_2O dosage of 15% provided the optimum compressive and tensile strength properties for fly ash geopolymer concrete. This is attributed to the polymerisation process which requires highly alkaline solutions to dissolve the silica and alumina ions in the fly ash precursor. The extent of dissolution of silica and alumina oxides and the Si/Al ratio in fly ash are significant factors in the geopolymerisation reaction (Davidovits, 1991).

2.4.2 SiO_2/Al_2O_3 ratio

Davitovits (1991) has suggested that certain synthesis limits exist for the formation of a strong geopolymeric gel product. The satisfactory SiO_2/Al_2O_3 composition for the initial geopolymer mix will lie in the range from 3.3 to 4.5. In addition, the M_2O/SiO_2 from 0.2 to 0.48, the H_2O/M_2O from 10 to 25, and M_2O/Al_2O_3 from 0.8 to 1.6 in initial geopolymer mix is required for the stronger gel formation. Here, "M" is represented by alkali cations such as Na^+ or K^+. De Silva et al. (2007) further reported that the setting time of the geopolymer system is primarily controlled by the alumina content and increases with increasing SiO_2/Al_2O_3 ratio in the initial mix. If the Al_2O_3 content increases, in other words when the SiO_2/Al_2O_3 ratio is lower, the resulting products acquire low compressive strength.

2.4.3 Alkali-hydroxide concentration

Alkali hydroxide concentration is another significant factor influencing geopolymerization. Hardjito et al. (2004) reported that the solubility of fly ash increased with the increase of hydroxide ion concentration in the activator solution, resulting in high compressive strength of resultant geopolymer concrete. Rattanasak and Chindaprasirt (2009) examined the changes of fly ash surface after reacting with three sodium hydroxide solutions with different concentrations. Figure 2.12 shows the significant differences of fly ash surface under different concentration levels. For an example, fly ash which reacted with 5M sodium hydroxide solution showed less sign of reactivity while forming small spherical units of aluminosilicate gel with diameter of 0.5–2.0 μm on the surface. However, when the alkali concentration increased, the dissolution of the fly ash surface also increased, Figure 2.12(c-d), and formed the large amount of gel while merging of the small spherical gel.

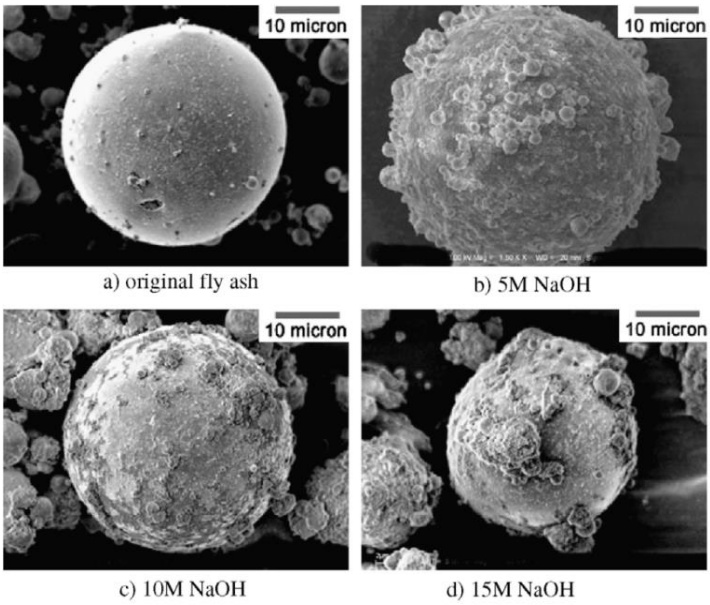

Figure 2.12 Fly ash surfaces leached with NaOH (Rattanasak and Chindaprasirt, 2009)

Wang et al. (2004) reported that higher sodium hydroxide addition accelerated the chemical dissolution but depressed ettringite and $Ca(OH)_2$ formation during the binder hydration. This reduction in the $Ca(OH)_2$ content resulted in the superior strength and durability performance for the geopolymer concrete (Poon et al., 2003). However, Palomo et al. (1999) mentioned that there is a limit for the alkali concentration increase, after that an excess of OH^- ion concentration in the activator solution decreased the compressive strength.

Wang et al. (2004) performed studies using cement kiln dust-fly ash system with 2% and 5% sodium hydroxide. They reported that, addition of 5% sodium hydroxide tends to increase the strength of the binder at early ages (below 7 days) but the strength decreased at later ages. It is hypothesised that the excessive sodium hydroxide resulted in undesirable morphology and non-uniformity of the hydration products in the pastes, thereby reducing the binder strength. Kaps and Buchwald (2002) reported that measurable strength could not be achieved below sodium hydroxide content of 15% whereas above 25% there was no improvement in the strength.

When using potassium hydroxide as an activator solution, the 10M potassium hydroxide showed the highest compressive strength of 60 MPa, but the strength decreased on increasing the potassium hydroxide concentration from 10M to 15M, probably due to excess K^+ ions in the framework (Cheng and Chiu, 2003). The potassium hydroxide leached substantially more silica and alumina as compared to the sodium hydroxide. Addition of K_2O was found to

benefit the compressive strength and also to reduce the occurrence of cracking (Van Jaarsveld et al., 2003, Xu and Van Deventer, 2002).

2.4.4 Alkali silicate to alkali hydroxide liquid ratio

The ratio of sodium silicate to sodium hydroxide plays an important role in the compressive strength development. The addition of sodium silicates to the mix design increases mechanical properties beyond the ability of a hydroxide activator alone. However, care must be taken to regulate the ratio between each substance. Hardjito et al. (2004) reported that the ratio of sodium silicate to sodium hydroxide plays a vital role in the development of mechanical properties of geopolymer concrete. The higher the mass ratio of sodium silicate to sodium hydroxide liquid, the higher is the compressive strength of geopolymer concrete. On the other hand, the matrix activated with potassium silicate and potassium hydroxide obtained the greatest compressive strength while sodium silicate and sodium hydroxide activated matrices were generally weaker followed by potassium silicate and sodium hydroxide. Since K^+ ion is more basic it allows a higher rate of solubilized polymeric ionization and dissolution, leading to a dense polycondensation reaction that provides greater overall network formation and an increase in the compressive strength of the matrix (Phair and Van Deventer, 2001).

The composition of alkali silicate solution can be expressed by modulus of solution, i.e. the SiO_2/Na_2O ratio. Increasing the SiO_2/Na_2O ratio affects, in the positive sense the degree to which, polymerisation occurs. Commercial liquid sodium silicates have a modulus of 1.6-3.85. Sodium silicate liquids outside of this range have limited stability and are not practical. The pH value is the most important characteristic determining stability of high-modulus silicate solution, that is, their inclination to the formation of gel or coagulation (Bondar et al., 2011, Xu and Van Deventer, 2000).

2.4.5 pH level

The strength of the geopolymer concrete can be affected by the value of pH. The setting time of the `geopolymeric mix decreased as the pH of the activating solution increased. At lower pH values the geopolymeric mix remained viscous and behaved like cement while at higher pH, the mix attained a more fluid gel composition, which was less viscous and more workable (Phair and Van Deventer, 2001). Higher solubility of monomers would be expected

for potassium hydroxide compared to sodium hydroxide because of the higher alkalinity. With increasing pH there will be a predominance of smaller chain oligomers and monomeric silicate available to react with soluble aluminium. Further, with an increase in pH, soluble aluminium increases and reacts with calcium available for reaction. In contrast, a lower pH-value of the solution leads to lower monomer concentration (Duxson et al., 2005, Phair and Van Deventer, 2001). Hence, it is clear that a pH range 13–14 is most suitable for the formation of the geopolymers with higher mechanical strength.

2.4.6 Curing temperature and curing time

The curing temperature is an important factor in the setting of the geopolymer concrete. At ambient temperature, fly ash reaction is extremely slow and the pozzolanic reaction is accelerated by increasing temperature. An increase of curing temperature in the range of 30^{o}C to 90^{o}C, was observed to increase the compressive strength (Wang et al., 2004, Hardjito et al., 2004). This is the opposite of PC concrete, i.e. PC concrete cured at elevated temperature exhibit expansion behaviour which leads to cracking, resulting in loss of strength, decreased service life and potentially other durability problems (Ramlochan et al., 2003).

Khale and Chaudhary (2007) state that, processing at ambient temperature was unfeasible due to a delayed on set of setting, and this could be avoided by the thermal treatment. They also reported that curing at 75^{o}C for 4 hours completed a major part of the geopolymerization process and resulted in satisfactory properties of the geopolymer concrete. Similarly, Swanepoel and Strydom (2002b) investigated utilization of fly ash and kaolinite clay in the geopolymeric material. The compressive strength after 7 and 28 days was highest (6 MPa and 7 MPa respectively) for the sample heated at 60^{o}C for 48 h. Palomo et al. (1999) observed the compressive strength of 60 MPa, after curing fly ash at 85^{o}C for 5 hours, and stated that temperature is especially important for 2 hours to 5 hours of curing. Wang et al. (2004) reported that cement kiln dust-fly ash geopolymer cured at 24^{o}C obtained lower compressive strength as 6.9 MPa and 13.8 MPa at 28 and 56 days, respectively. However, curing temperature increase up to 50^{o}C resulted in an increase of compressive strength by two-fold.

In addition to the curing temperature, curing time is also an important parameter, i.e. prolonged curing time improves the polymerization process resulting in higher compressive strength. Palomo and Lopez (2003) noted that geopolymers developed compressive strength

of 45 MPa in just 24 hours of curing. However, literature (Hardjito et al., 2004, Swanepoel and Strydom, 2002b, Palomo et al., 1999) reported that an increase in strength for curing periods beyond 48 hour is not very significant. On the other hand, Puertas et al. (2000) noted that prolonged curing at elevated temperature breaks the granular structure of the geopolymer. This results in dehydration and excessive shrinkage due to contraction of gel, without transforming to a more semi-crystalline form. This results in an adverse effect on the compressive strength of the hardened geopolymer. Therefore, successful geopolymer concrete production can be achieved via proper balancing of curing temperature and curing time.

2.4.7 Relative humidity

Van Jaarsveld et al. (2002) showed that geopolymer cured at higher humidity in sealed bags did not improve the compressive strength. This behaviour is in contrast with what is expected from the curing of PC concrete, which gains strength when cured under higher humidity. This behaviour is corroborated by the FTIR analysis as the absorption peaks around 1033 cm^{-1} corresponding to the asymmetric stretching of Si–O and Al–O bonds which were affected by curing of samples in sealed bags and their wave numbers were slightly lower than for the samples cured without bags. A lower wave number is indicative of weaker inter-tetrahedral bonding and could contribute to the lower compressive strength for the geopolymer samples cured in the sealed bags. The saturated atmosphere in the bags, resulted in conditions more suitable to the formation of the slightly weaker bonds.

2.4.8 Liquid/solid ratio

The liquid/solid ratio is another important parameter at geopolymer mix design stage. Similar to a strength vs. water/cement ratio trend in PC concrete, compressive strength of geopolymer concrete decreases with the increase of liquid/solid ratio. Hence, water content in the geopolymer mix played an important role on the properties of geopolymer binders (Hardjito and Rangan, 2005, Barbosa et al., 2000, Xie and Kayali, 2014).The minimum water/cement ratio is approximately 0.4 by weight for PC (Neville, 1996), whereas the fresh geopolymeric material is readily workable even at low liquid/solid ratio (Palomo et al., 2004). The quantity of water contained in the geopolymer mix is generally defined as sum of water contained in the alkali silicate, alkali hydroxide and added water, while the quantity of solid is the sum of

the mass of fly ash and the solid contained in the alkaline activator solution (Hardjito et al., 2004).

2.4.9 Fly ash properties

The properties of fly ash have a significant effect on the resultant geopolymer properties. Calcium oxide content in fly ash has a significant influence on the properties of the fresh mixture as well as the properties of the final hardened product (Van Jaarsveld et al., 2003). The setting time increases exponentially as the calcium oxide content decreases below 20%, however the decrease in calcium oxide is accompanied by a decline in the compressive strength of the resulting geopolymer. Hence, the calcium oxide content range of 5–15% might be considered desirable for most applications (Diaz et al., 2010). Fly ash with a high glass phase content will also lead to a higher degree of geopolymerization, therefore higher compressive strength (Alvarez-Ayuso et al., 2008).

Particle size distribution has a significant impact in the reactivity of fly ash. A higher amount of fine particles will result in higher surface area, and therefore higher reactivity, resulting in higher compressive strength (Van Jaarsveld et al., 2003, Fernandez-Jimenez and Palomo, 2003). Thus, grinding of fly ash might be under taken to enhance its suitability for geopolymerization. The utilization of higher combustion temperatures also supports a finer grain size distribution.

The presence of unburned carbon in fly ash, even in relatively small amounts, will require higher activator solution to fly ash ratio, which results in an adverse effect on the compressive strength of the hardened geopolymer paste as well as an economic disadvantage in the manufacturing of the geopolymer concrete (i.e. activator solution represents a major cost item in the production of geopolymer concrete). Therefore, similar to particle size distribution, unburnt carbon content (loss on ignition) is also an important characteristic of raw fly ash (Diaz et al., 2010, Van Jaarsveld et al., 2003, Fernandez-Jimenez and Palomo, 2003).

2.5 Mechanical properties of fly ash based Geopolymer concrete

Geopolymer concrete is a complex and non-uniform material of which the stress-related mechanical characteristics are influenced not only by the behaviour of each constituent material but also by the interactions among these materials. The mechanical properties of fly

ash based geopolymer concrete, both short term and long term, addressed in literature mainly consists of compressive strength, flexural strength, splitting tensile strength, modulus of elasticity and poison's ratio together with the behaviour of stress-strain variation (Sarker et al., 2013, Ryu et al., 2013, Li et al., 2013, Neupane et al., 2012, Diaz-Loya et al., 2011, Rangan, 2008, Duxson et al., 2007a). Sofi et al. (2007a) has shown that mechanical properties of fly ash based heat cured geopolymer concrete are comparable to the PC concrete, and the methods of calculations used in the case of reinforced PC concrete beams can also be used to predict the shear strength of reinforced geopolymer concrete beams. Also the structural performance of reinforced concrete depends on the bond between concrete and the reinforcing steel. Geopolymer concrete exhibited superior bond strength to PC concrete, and the existing design equations for bond strength of PC concrete with steel reinforcing bars can be conservatively used for the calculation of bond strength of geopolymer concrete (Sofi et al., 2007a, Sarker et al., 2007). Moreover, Sumajouw and Rangan (2006) examined the behaviour and failure modes of reinforced geopolymer concrete columns and beams, and found that those were similar to the observed reinforced PC concrete columns and beams.

Hardjito and Rangan (2005) worked with fly ash based geopolymer concrete and found that the geopolymer concrete has a comparable compressive strength and lower modulus of elasticity to that of PC concrete for up to 90 days of their investigation. However, the splitting tensile strength of geopolymer concrete was found to be higher than the values recommended by Australian Standard (2009) for PC concrete.

Fernandez-Jimenez et al. (2006a) also reported similar findings while working with fly ash based geopolymer concrete, and mentioned that geopolymer concrete has a high compressive and flexural strength, but lower modulus of elasticity compared to PC concrete within the first 90 days. According to the authors, it might be possible that fly ash geopolymer concrete exhibits a similar behaviour to high performance PC concrete. The values of compression modulus of elasticity based on formulae proposed by different codes proved to be unreliable. This was attributed to the existence of variables which had not been taken into consideration in the formula, but nevertheless influenced the properties.

Diaz-Loya et al. (2011) worked with a series of fly ash and found that geopolymer concrete seems to possess similar mechanical behaviour to that of PC concrete. The relationship between the flexural and compressive strengths of geopolymer concrete can be expressed using a statistically derived equation that resembles that given by the American Concrete

Institute (2008) for PC concrete. The relationship between the modulus of elasticity and the compressive strength of geopolymer concrete is similar to that of PC concrete, however, their relationship is linear, whereas for PC concrete it follows a power curve. They further state that the modulus of elasticity of geopolymer concrete can be represented as a function of both density and compressive strength, and that the density of geopolymer concrete can be accurately predicted by the fineness of fly ash.

Neupane et al. (2014) investigated the mechanical properties of different grades of fly ash based geopolymer concrete and the applicability of the Australian Standards compared against the same grade of PC concrete. It showed that uniaxial tensile and flexural tensile strengths attained by geopolymer concrete are higher than the prescribed value by Australian standards (2009) for the same grade of concrete. However, modulus of elasticity is found to be almost equal with the calculated value from Australian standards (2009) and similar to the grade of PC concrete.

Sofi et al. (2007b) examined the mechanical characteristics of inorganic polymer concrete and found that density of this concrete was equal to that of PC concrete. Moreover, the splitting tensile and flexural strength of the inorganic polymer concrete compares favourably with the models presented by several standards for PC concrete. Although the difference between splitting tensile and flexural strength of inorganic polymer concrete mixes has been found to be approximately 2 MPa, similarities in strength gain between the concrete mixes were apparent. On the other hand, inorganic polymer concrete showed higher values of Poisson's ratio which are similar to high strength concrete.

Ryu et al. (2013) investigated the compressive strength and splitting tensile strength of fly ash based geopolymer concrete produced by activating with a higher molarity of sodium hydroxide as an alkaline activator, which provided higher compressive strength together with a considerable impact on the early strength. The use of a mix of sodium based hydroxide and silicate with a mix ratio of 1:1 was shown to activate the geopolymerization of fly ash and achieve remarkable compressive strength development. That strength figures reached the criterion of high strength concrete, and verified the potential of fly ash as a 100% replacement for cement. In contrast, they examined the splitting tensile strength of fly ash based geopolymer concrete is about 7.8 to 8.2% of the measured compressive strength, which is similar to that of PC concrete. However, they concluded that gathering a larger amount of

data is necessary to obtain a more reliable relationship between the compressive and the splitting tensile strength of geopolymer concrete.

Wardhono (2015) worked with fly ash based geopolymer concrete and found that the relationship between the mechanical properties, i.e. compressive strength, tensile strength and modulus of elasticity, and ultrasonic pulse velocity (UPV) follows a positive linear relationship with concrete age, which is comparable to that of PC concrete. Thus, an increase of mechanical properties is followed by an increase of UPV. The increase in mechanical properties of fly ash geopolymer concrete is also associated with a decrease of porosity and water absorption. These findings confirm that the quality of fly ash based geopolymer concrete is improving with time.

2.6 Durability properties of fly ash based Geopolymer concrete

It is essential that every concrete structure should continue to perform its intended function by maintaining the required strength and serviceability during the specified service life. It follows that concrete must be able to withstand the processes of deterioration to which it can be expected to be exposed. Such concrete is said to be durable. Inadequate durability manifests itself by deterioration which can be due either to external factors or to internal causes within the concrete itself. The various actions can be physical, chemical or mechanical.

Physical causes of deterioration include the effects of high temperature or the differences in thermal expansion of aggregate and the hardened cement paste. An important cause of damage is alternating freezing and thawing of concrete and the associated action of de-icing salts. Mechanical damage is caused by impact, abrasion, erosion or cavitation.

The chemical causes of deterioration include the alkali-silica and alkali-carbonate reactions. External chemical attack occurs mainly through the action of aggressive ions, such as chlorides, sulphates, or of carbon dioxide, as well as many natural or industrial liquids and gases. The damaging action can be of various kinds and can be direct or indirect. Young et al. (1998) showed that chemical attack by acids can be particularly severe where the pH is less than 4 and even worse where the acid solution has a velocity that is able to cause mechanical abrasion. Chemical resistance of cement paste is directly related to its permeability, with less permeable pastes being more resistance to chemical attack. Hence, in the long term

performance, the permeation properties are highly important in controlling the durability of concrete in order to resist the ingression of deleterious substances into the concrete (Basheer et al., 2001). Moreover, they reported that the main transport processes which describe the movement of aggressive substances, such as chloride, sulphate, water and carbon dioxide, through concrete are distinguished as diffusion, absorption and permeability.

Diffusion:

The process whereby a liquid, gas or ion migrates through concrete is driven by a concentration gradient. The rate of diffusion is significantly affected by the characteristics of the penetrating substance and the chemistry of the concrete, as well as the concentration gradient and the size of capillary pores. The diffusion progress of a gas is very slow in saturated concrete, thus this property is a significant factor that need to be taken into account for a concrete in above-ground structures such as buildings or bridges, where concrete is in a partially dry condition.

Absorption:

Absorption is the process whereby, the transport of liquids in the pores of hardened cement paste is transported by surface tension capillary action under ambient conditions. The concrete takes in liquid by capillary suction to fill the pore space available. Capillary suction can occur in dry or partially dry concrete. This transport mechanism is particularly relevant to coastal structures where chloride salts are deposited on the concrete surface and then absorbed into the concrete.

Permeability:

The process whereby, a fluid flows through a concrete under the action of a pressure differential. The flow rate follows Darcy's law for laminar flow through a porous medium and depends on the pressure gradient and the size of interconnected pores. The concrete has to be in the saturated state with relevant pores being continuous and greater than 120 nm to allow the flow process. Permeability is a relevant property to assess the durability and serviceability of structures which have constant contact with water, such as dams, foundation and underground structures.

2.6.1 Water absorption and Permeability

Olivia and Nikraz (2011) investigated the influence of water/binder ratio, aggregate/binder ratio and alkaline/fly ash ratio on the water absorption and permeability of fly ash based

geopolymer concrete. They found that the water absorption was less than 5%, and it decreases with a decrease in the water/binder ratio, an increase in the aggregate/binder ratio, and an increase in the alkaline/fly ash ratio. They further reported that the measured water permeability of geopolymer concrete ($2.46–4.67x10^{-11}$ m/s) is lower than that of PC concrete due to its denser paste and smaller pore inter-connectivity.

Wongpa et al. (2010) worked with inorganic polymer concrete produced from fly ash combined with rice husk–bark ash and found that the alkaline solution/fly ash ratio is the major parameter controlling the water permeability. The Paste/Aggregate ratio also affects water permeability in a similar way to the alkaline solution/fly ash ratio, however, with less impact. Higher alkaline solution/fly ash ratio and Paste/Aggregate ratio result in lower compressive strength and higher water permeability. They further showed that the water permeability of concrete was significantly related to its compressive strength.

Ma et al. (2013) studied the pore structure and water permeability of fly ash geopolymer with varying silica and alkali content, curing age and curing temperature. The examined pore structure of geopolymer paste differed significantly from that of PC paste. The aluminosilicate gel formed during geopolymerization was uniformly distributed in the matrix, thus large capillary pores were not observed, but some large cavities were detected. They found that development of the pore structure of fly ash geopolymer with time is considerably slower than that of PC paste. The effect is even more pronounced with increased curing. Thus, extending the curing time under heating is beneficial for the pore structure development of geopolymer. An increase of both silica and alkali content also result in a lower total porosity and a finer pore system.

In contrast, Ma et al. (2013) observed that the water permeability of fly ash geopolymer paste is higher than that of PC paste, especially at later ages. Thus, prolonged curing time under heating could significantly increase the water permeability of geopolymer. Additionally, higher silica content leads to significantly reduced water permeability at later ages, however higher alkali content has a negative effect on water permeability at later ages.

Law et al. (2014) worked with geopolymer concrete made from fly ash activated with sodium silicate and sodium hydroxide, and observed a non-linearity in the sorptivity data in the initial stages of geopolymer compared to the PC concrete. This non linearity is hypothesized as being due to an increased bleeding in geopolymer concrete giving a cement rich surface layer

allowing higher initial absorption. The sorptivity values of the geopolymer concrete are comparable to those of PC concrete of similar strength.

2.6.2 Chloride attack

Chloride attack is one of the most important aspects of the durability of PC concrete, because it is the primary cause of corrosion of reinforcement. Due to high alkalinity of PC concrete a protective oxide film is present on the surface of steel reinforcement. The protective passive layer can be lost due to the presence of chloride in the presence of water and oxygen. Chloride ions are transported through the concrete matrix via diffusion, capillary absorption, and hydrostatic pressure/convection (Elakneswaran et al., 2009, Stanish et al., 2005).

Absorption takes place during wetting and drying cycles. During these cycles, chlorides are absorbed by the suction of water containing the chlorides into the concrete pores. Chloride ions are also introduced by hydrostatic pressure, which causes the permeation of chloride ions through the matrix. Diffusion is the mechanism that is capable of bringing chlorides to the level of the reinforcing steel, thereby accelerating the corrosion of the rebar. The most important characteristic related to the ingress of chloride ions is the pore structure of the cement past matrix which affects the porosity of concrete (Stanish et al., 2005). Lower porosity of a concrete leads to a reduction of the ingress of chloride ions into the concrete.

Law et al. (2014) showed that chloride diffusion coefficients of the fly ash geopolymer concrete are comparable with those for PC and blended cement concrete. This would indicate a high level of resistance to chloride ingress for fly ash geopolymer concrete. However, in terms of long term performance, PC and to a greater extent blended cement concrete show a reduction in the chloride diffusion coefficient with time. This improved performance is attributed to on-going hydration of the concrete with time. For geopolymer concrete, which is produced by heat curing, little if any further reaction will take place, demonstrated by a minimal increase in compressive strength with time when compared to PC and blended cement concrete cured at ambient temperatures. Hence, it may be expected that little improvement in the diffusion coefficient will occur in geopolymer concrete over time when compared with PC and blended cement concrete. Moreover, they observed the chloride diffusion coefficient after 20 years would be similar in both geopolymer and PC concrete.

Lloyd et al. (2010) worked with 100% fly ash and fly ash/sag based geopolymers and showed that geopolymer cement is prone to alkali leaching leading to a reduction in the pH which is

essential to prevent steel corrosion. They also report that the presence of calcium is crucial for having durable steel-reinforced concrete which is a potential concern in low calcium, aluminasilicate geopolymers.

Miranda et al. (2005) worked with alkali-activated fly ash binders and observed that geopolymer binders have superior pH conditions than PC binders. Activated fly ash mortars passivate reinforcing steel as rapidly and effectively as PC mortars. They reported that pH decreased with hydration reaction development, however an alkaline condition remained even after 5 years, as carbonation did not occur.

Kupwade-Patil and Allouche (2013) investigated the durability of steel reinforced-concrete specimens made from three alkali-activated fly ash stockpiles and PC in cyclic wet-dry chloride environment over a period of one year. Geopolymer concrete was found to exhibit lower average diffusion coefficients, chloride contents, and porosity compared with their PC concrete counterparts. Furthermore, only micro-level indications of corrosion products were observed at the matrix-rebar interface for some geopolymer concrete, whereas multiple gross corrosion products were observed among the PC concrete specimens. Thus, geopolymer concrete made from low calcium, class F fly ash exhibited a significantly higher resistance to chloride-induced corrosion compared with PC concrete, as well as geopolymer concrete made from high calcium, class C fly ash.

2.7 Current implementation of Geopolymer concrete

A geopolymer concrete building was recently constructed at the University of Queensland in Brisbane (Wallis, 2013). The building contains 33 precast floor panels as shown in Figure 2.13 made from modern structural geopolymer concrete by mixing with two industrial by products as fly ash and blast furnace slag.

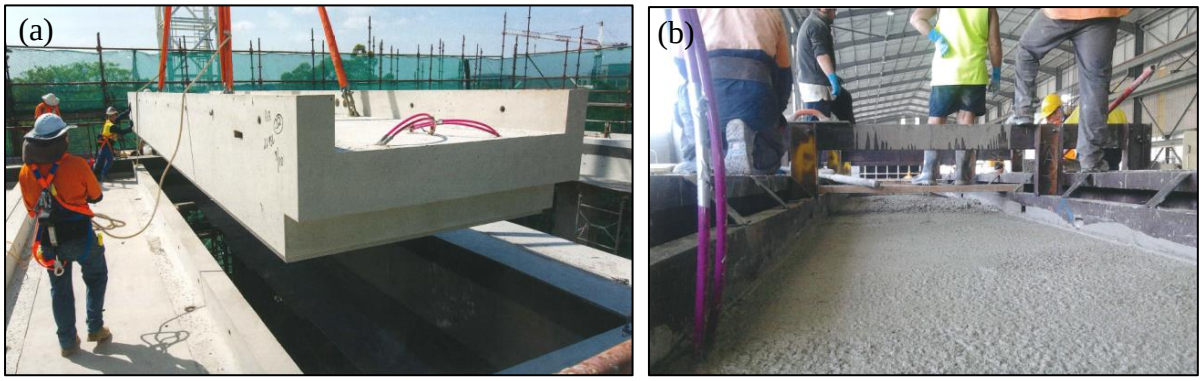

Figure 2.13 (a) Placing of precast geopolymer concrete panel, and (b) Concrete finishing in the precast factory (Wallis, 2013)

Moreover, a new regional airport has been constructed using geopolymer concrete in Toowoomba, Queensland, Australia (Corbett, 2014). That was the largest geopolymer concrete pavement project in the world. Above geopolymer concrete was produced by recycled slag and recycled fly ash in combination with chemical activators. The project initially estimated that 6600 tonne of CO_2 emission reduction will result from using environmentally friendly geopolymer concrete in the airport apron and taxiway pavements instead of conventional PC concrete. A high capacity wet-mix mobile batch plant was set up at the airport project site during the construction of the 2.87km runway. Around 30,000m^3 of geopolymer concrete has been used in the airport. Large quantities of the geopolymer concrete are also used in the construction of the buildings in the project, as well as in the adjacent business park precinct. The airport's concrete pavements have a flexural tensile strength of 4.8MPa and typical depths of 400-440mm. The airport will be able to cater for larger air planes such as Boeing 747s, 737s and Airbus A330s.

Gourley and Johnson (2005) have reported the details of geopolymer precast concrete products on a commercial scale. The products included sewer pipes, railway sleepers, and wall panels. Reinforced geopolymer concrete sewer pipes with diameters in the range from 375mm to 1800mm have been manufactured using the facilities currently available to make similar pipes using PC concrete. Tests performed in a simulated aggressive sewer environment have shown that geopolymer concrete sewer pipes outperformed comparable PC concrete pipes by many folds. They also reported the good performance of reinforced geopolymer concrete railway sleepers in mainline tracks and excellent resistance of geopolymer mortar wall panels to fire.

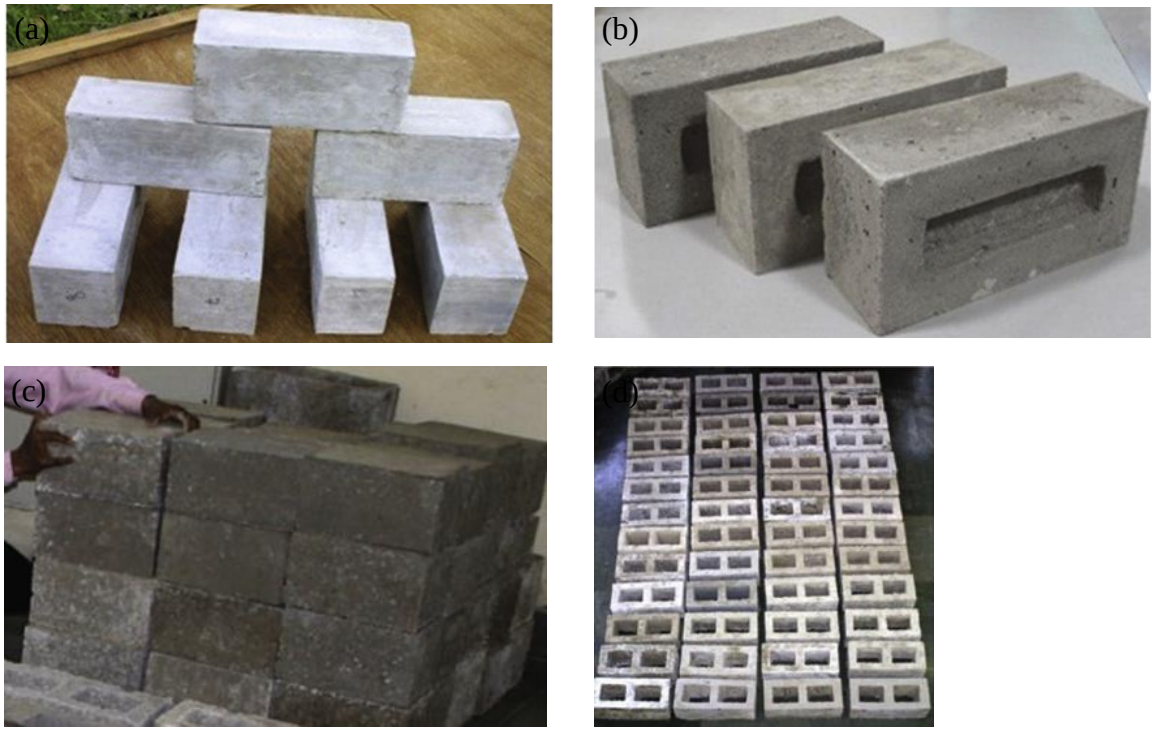

Figure 2.14 (a) Solid bricks, (b) Foamed bricks, (c) Solid blocks, and (d) Hollow blocks (Singh et al., 2015)

Singh et al. (2015) investigated the suitability of geopolymer concrete in making various geopolymer bricks and blocks shown in Figure 2.14. Geopolymer bricks were produced using fly ash based geopolymer mortar by providing 80^{o}C heat curing for 2 hours. The bricks are obtained with density of 1900-2100 kg/m^{3}, water absorption of 10–15% and dry compressive strength of 12–25 MPa. Furthermore, solid geopolymer blocks and hollow geopolymer blocks were produced on a machine using fly ash geopolymers. The solid geopolymer blocks obtained 10 MPa compressive strength with density of 2100 kg/m^{3} and water absorption less than 10%. On the other hand, the hollow geopolymer blocks achieved 5 MPa strength with a density of 1200 kg/m^{3}.

2.8 Characterization of fly ash and its geopolymer

The morphology and composition of the fly ash can vary significantly between different sources. Thus, a variety of techniques is used to characterise fly ash by measuring their own physical, mineralogical and chemical properties. Moreover, the properties of resultant geopolymers, such as solubility, cation exchange capacity, porosity distribution and rheological behaviour can be examined through novel test methods.

- X-ray Fluorescence (XRF) analysis:

The XRF is a non-destructive analytical technique which can be used to determine the elemental composition of raw fly ash precursors. XRF analysers determine the chemistry of a fly ash sample by measuring the fluorescent x-ray emitted from a sample when it is excited by a primary x-ray source. Each of the elements present in a fly ash sample produces a set of characteristic fluorescent x-rays that is unique for that specific element. Thus, XRF spectroscopy is an excellent technology for qualitative and quantitative analysis of different fly ash based on their chemical composition.

- Energy Dispersive X-ray (EDX) analysis:

The EDX, referred to as EDS or EDAX, is a non-destructive x-ray technique and can be used to identify the elemental composition and elemental distribution of fly ash. EDX systems are attachments to Scanning Electron Microscopy (SEM) or Transmission Electron Microscopy (TEM) instruments where the imaging capability of the microscope identifies the specimen of interest. The data generated by EDX analysis consist of spectra showing peaks corresponding to the elements making up the true composition of the sample being analysed. Elemental mapping of a fly ash sample and image analysis are an additional capabilities of the SEM/EDX system.

- SEM analysis:

The SEM/EDX is widely used for the surface analysis of fly ash. High resolution images of surface topography, with excellent depth of field, are produced using a highly focused, scanning primary electron beam. The primary electrons enter a surface with an energy of 0.5 – 30 kV and generate many low energy secondary electrons. The intensity of these secondary electrons is largely governed by the surface topography of the raw fly ash or resultant geopolymer sample. An image of the sample surface can thus be constructed by measuring secondary electron intensity as a function of the position of the scanning primary electron beam. High spatial resolution is possible because the primary electron beam can be focused to a very small spot (< 10 nm). High sensitivity to topographic features on the outermost surface (< 5 nm) can be achieved when using a primary electron beam with an energy of lower than 1 kV.

In addition to low energy secondary electrons, backscattered electrons and X-rays are generated by primary electron bombardment. The intensity of backscattered electrons can be correlated to the atomic number of the element within the sampling volume. Hence, some qualitative elemental information can be obtained. The analysis of characteristic X-rays emitted from the sample gives more quantitative elemental information.

- X-ray Diffraction (XRD) analysis:

The XRD uses X-rays to investigate and quantify the crystalline nature of fly ash and its geopolymer by measuring the diffraction of X-rays from the planes of atoms within the material. It is sensitive to both the type of and relative position of atoms in the material as well as the length scale over which the crystalline order persists. Thus, it can be used to measure the crystalline content of materials, identify the crystalline phases present, determine the spacing between lattice planes and the length scales over which they persist, and to study preferential ordering and epitaxial growth of crystallites.

- Fourier Transform Infrared (FTIR) spectroscopy analysis:

The FTIR spectroscopy can be used to identify chemical bonds present in a fly ash and its geopolymer molecule by producing an infrared absorption spectrum. The spectra produce a profile of the sample, a distinctive molecular fingerprint that can be used to screen and scan samples for many different components. FTIR is an effective analytical instrument for detecting functional groups and characterizing covalent bonding information during geopolymerization. FTIR can also be combined with some other novel techniques, such as Infrared-spectroscopy coupled to Thermo gravimetric Analysis (FTIR/TGA), Nuclear Magnetic Resonance spectroscopy (NMR), and Near Infrared (NIR) and Raman scattering, which provides complementary data regarding a geopolymers molecular structure.

- Solid state Magic Angle Spinning-Nuclear Magnetic Resonance (MAS-NMR) analysis:

The solid state ^{29}Si, ^{27}Al and ^{23}Na MAS-NMR have been used previously to evaluate and compare the different types of (reactive) aluminium–silicates in fly ash precursors and their corresponding geopolymers (Valcke et al., 2014, Oh et al., 2014, Temuujin et al., 2010, Fernández-Jiménez et al., 2006b, Favier et al., 2015). While this was mostly done qualitatively, a few reported that NMR spectra were deconvolved for semi-quantitatively evaluating the type of aluminium–silicate phases in geopolymers. The ^{29}Si MAS-NMR is

capable of distinguishing SiO_4 tetrahedra of cross-linked density ranging from 0 to 4, the relative concentration of which may be determined from peak intensities. Therefore ^{29}Si MAS-NMR can provide valuable information on the type of the various cross-linked SiO_4 tetrahedra. In addition, each replacement of Si by Al in the second coordination sphere of a Si atom, characteristic shift effects are observed in ^{29}Si MAS-NMR which make it possible to determine the number of tetrahedral Al connected via oxygen bridges to a given SiO_4 tetrahedron. The ^{27}Al MAS-NMR can provide additional information of the geopolymer formation process since there is a well-defined ^{27}Al shift differences among AlO_6 (octahedral coordinates) at 0–16 ppm, and AlO_4 (tetrahedral coordinates) at 55–80 ppm and AlO_5 (five-fold coordinated species) at 25–35 ppm. The ^{23}Na MAS-NMR spectrum can indicate amount of well resolved Na^+ sites formed at the geopolymerization, corresponding to the presence of crystalline hydrated Na compounds.

- Atomic Absorption Spectrometry (AAS) analysis:

The AAS is an analytical technique that measures the concentrations of elements. Atomic absorption is so sensitive that it can measure down to parts per billion (ppb) of a gram in a sample. The technique makes use of the wavelengths of light specifically absorbed by an element. They correspond to the energies needed to promote electrons from one energy level to another, higher, energy level. Several studies exist studying the leachability of fly ash in water and alkaline media to check the available major ion concentration at the geopolymerization.

- Mercury Intrusion Porosimetry (MIP) and Brunauer-Emmett-Teller (BET) surface area Analysis:

The MIP uses the non-wetting properties of mercury to gain information on pore characteristics of geopolymer concrete, such as porosity, pore volume, pore size distribution and density. During a typical porosity analysis in MIP analyser, a higher pressure is needed to force intrusion of mercury in smaller pores, whereas mercury intrusion in larger pores already occurs at low pressure. In this way a wide dynamic range of pore sizes can be measured and a pore size distribution can be obtained. Porosity is especially important in understanding the formation, structure, and potential use of many substances. The porosity of a material affects its physical properties and, subsequently, its behaviour in its surrounding environment. The

adsorption, permeability, strength, density, and other factors influenced by a substance's porosity determine the manner and fashion in which it can be appropriately used.

In addition to MIP, the BET surface area analysis is a useful technique which provides precise specific surface area evaluation of fly ash by nitrogen multilayer adsorption measured as a function of relative pressure using a fully automated analyser. The technique encompasses external area and pore area evaluations to determine the total specific surface area in m^2/kg yielding important information in studying the effects of surface porosity and particle size in many applications.

- Zeta potential analysis:

Zeta potential is a measure of the magnitude of the electrostatic or charge repulsion/attraction between particles, and is one of the fundamental parameters known to affect stability. Its measurement brings detailed insight into the causes of dispersion, aggregation or flocculation, and can be applied to improve the formulation of dispersions, emulsions and suspensions.

- Rheological characteristics analysis:

To realise its potential as a construction material, geopolymeric systems must be capable of being moulded, compacted, extruded or otherwise formed. Thus, developing mix formulations through a study of the effect of binder formulations on rheology is very important. Furthermore, rheology is a dynamic property of microstructure. Viscometry has been established as a sensitive and fundamentally sound technique that can be used to determine the fundamental rheological properties of the geopolymer binders, such as yield stress and plastic viscosity. This has been shown to give good predictions of the rheology of fresh concrete of related composition. Industry standard tests such as slump and flow table will also provide the information regarding flowability of concrete.

2.9 Summary of Chapter 2

The PC production consumes vast amounts of fuel and raw materials using processes that are energy intensive and emit large amounts of greenhouse gases, contributing 4–8% of anthropogenic CO_2 emissions worldwide. This on-going issue has inspired research into environmentally friendly green concrete utilizing alkali-activated cements, widely known as

geopolymers, using materials containing alumina and silicates such as fly ash. The latest estimated figures show the reduction of CO_2 emission due to the replacement of PC with geopolymer is between 26–45% with no economic sacrifices.

Geopolymer concrete differs substantially from PC concrete, as it follows a distinctly different reaction pathway to attain structural integrity. PC concrete is reliant on the presence of C-S-H gel for matrix formation and strength development, while geopolymer concrete undergoes polycondensation of alumina and silica oxides in the fly ash, with high alkaline activator. The mechanism for geopolymerization involves three principal steps, these are dissolution of alumina and silica oxides of the fly ash in the alkaline activator, transportation of dissolved alumina and silica species and the polycondensation process with the formation of aluminosilicate gel as a main reaction product.

A major challenge faced by the construction industry in adopting geopolymer material is the variability of fly ash from different sources and the effect this can have on the compressive strength of geopolymers produced. To date a number of parameters have been reported in literature as affecting the compressive strength of geopolymers, such as activator modulus and Na_2O dosage, SiO_2/Al_2O_3 ratio, alkali hydroxide concentration, alkali silicate to hydroxide ratio, pH level, curing temperature and time, relative humidity, liquid to solid ratio and properties of source material.

Previous studies found that the fly ash geopolymer concrete has a comparable compressive strength, flexural strength and splitting tensile strength, but lower elasticity modulus to that of PC concrete. Moreover, the literature suggested that fly ash based geopolymer concrete is suitable for structural applications and the current available design codes for PC concrete can be used for the design of geopolymer concrete structures. The durability resistance of fly ash geopolymer concrete against water permeation and chloride attack has been widely reported in literature. The most of them have shown that fly ash geopolymer concrete have a satisfactory performance, however many of them were conducted over a short term periods by using a single type of fly ash as the source material.

The comprehensive literature reviews indicted that the properties of fly ash has a significant impact on the properties of resultant geopolymer concrete. A major gap in knowledge is the lack of a systematic study where the properties of geopolymer concrete produced using

different sources of fly ash are studied in long term. Comprehensive research program presented in this thesis addresses the gap in knowledge.

3 MATERIALS AND RESEARCH METHODOLOGY

3.1 Overview

This chapter presents the detail of the materials and the experimental methods used. Low calcium, class F precursor fly ash from five different coal power stations in Australia has been investigated. The compressive strength of fly ash geopolymer mixes was examined over a range of activator modulus at a fixed Na_2O dosage in order to optimize the best mix design of both geopolymer mortar and concrete for each specific fly ash. A series of tests have been conducted on geopolymer mortar as the first phase of the research. These results have been analysed to explain the effects of the chemical and physical properties of precursor fly ash on the strength evolution of fly ash geopolymers. The long term performance of mechanical and durability properties of different fly ash geopolymer concrete has been investigated in the second phase of research. The influence of the properties of precursor fly ash on the long term geopolymer performance is studied through comprehensive microstructural and pore-structural analysis and other state of the art techniques.

3.2 Planning of the Research Program

A comprehensive research program developed to achieve the research objectives stated in Chapter 1 is shown in Figure 3.1. The laboratory experiments were intended to conduct in two stages, as Phase 1 and Phase 2:

Phase 1: The series of experiments were conducted to investigate factors affecting the compressive strength of different fly ash based geopolymer mortar, as shown in Figure 3.2.

Phase 2: The long term performance of mechanical and durability properties of different fly ash based geopolymer concrete has been investigated, as shown in Figure 3.3.

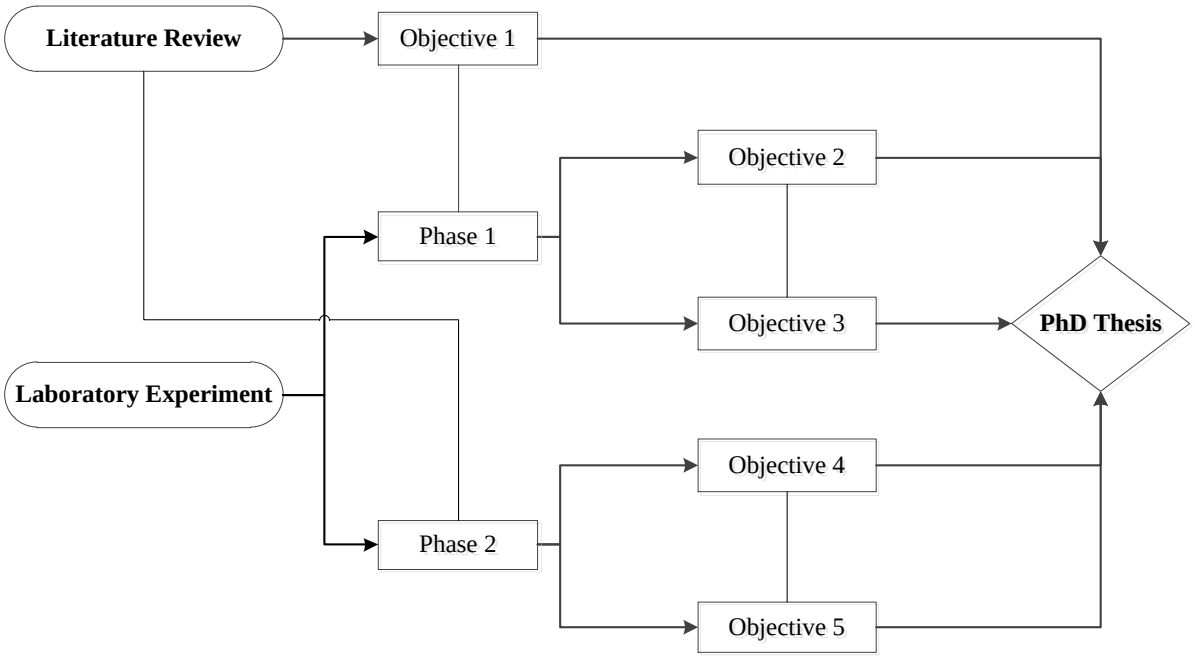

Figure 3.1 Research Program - Overview

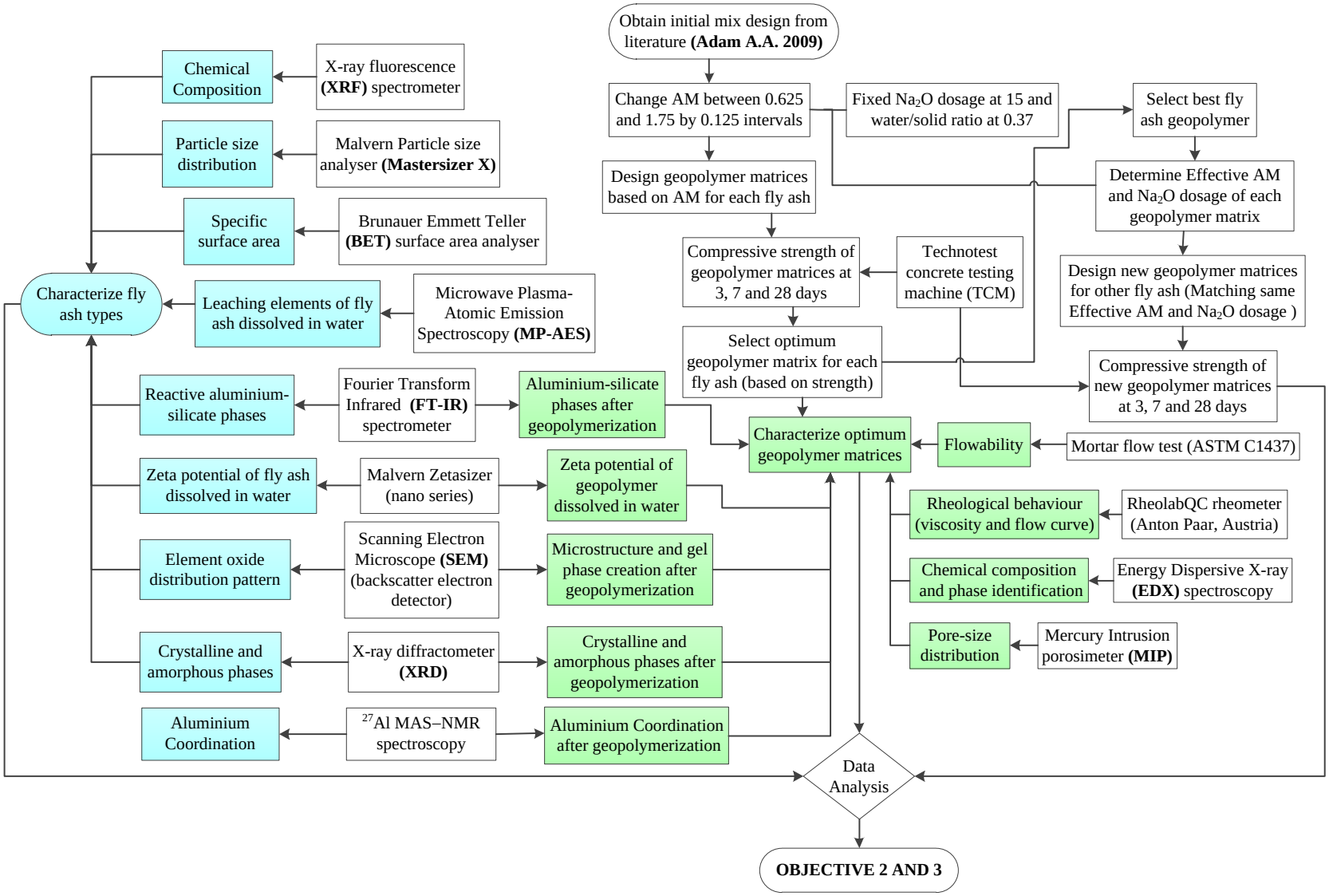

Figure 3.2 Phase 1: Compressive strength of geopolymer mortar - Overview

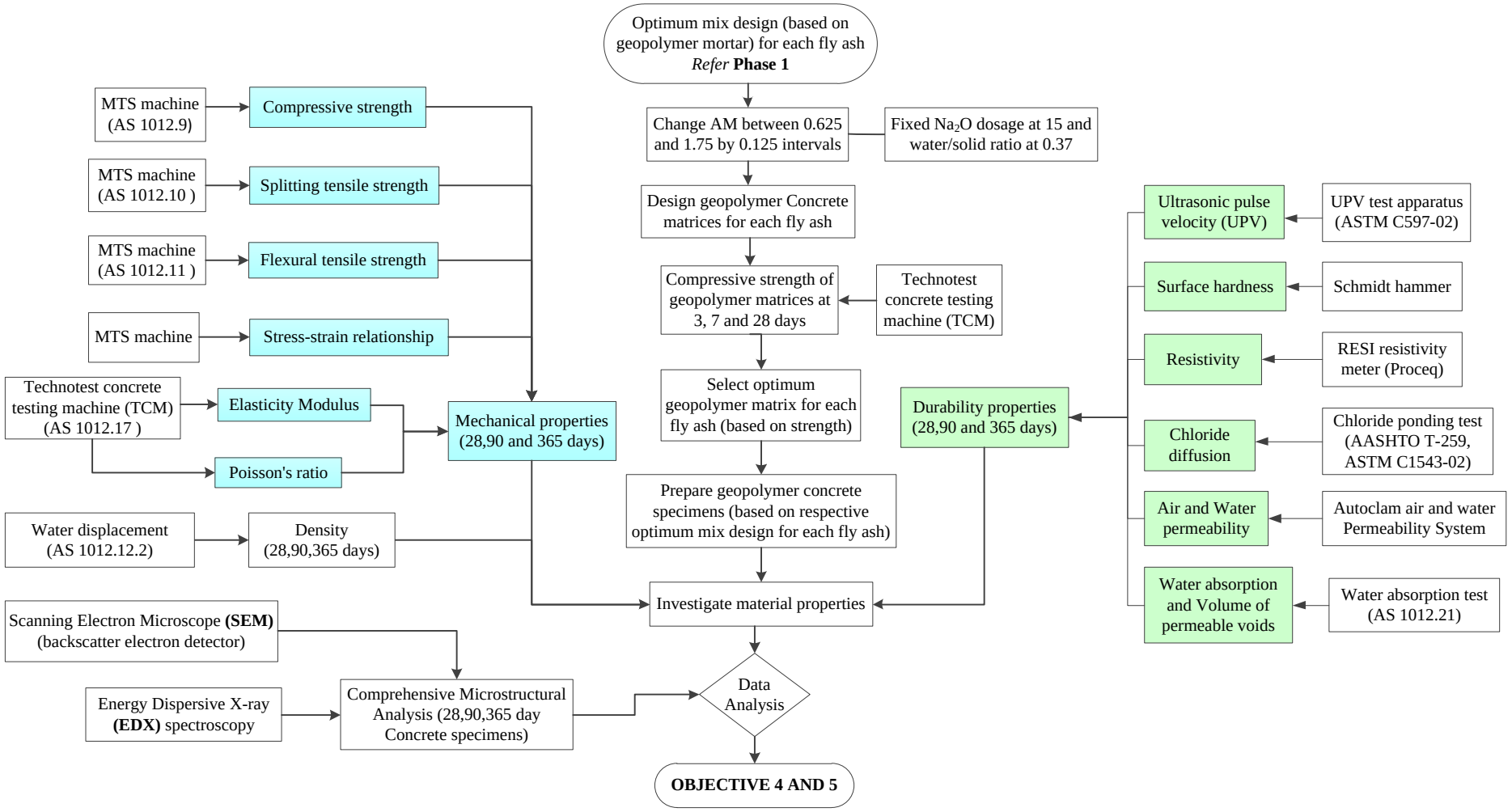

Figure 3.3 Phase 2: Long term material properties of geopolymer concrete - Overview

3.3 Preparation of geopolymer mortar

3.3.1. Materials used – Geopolymer mortar

3.3.1.1. Fly ash

Fly ash used in the investigation was dry, low calcium class F fly ash conforming to AS 3582.1 standard (1998b), obtained from five different power plants as Gladstone, Tarong, Port (Pt.) Augusta, Collie and Mount (Mt.) Piper in Australia. The location map of power plant and the scanning electron microscopy image of fly ash are shown in Figure 3.4. The chemical composition and the particle size distribution of the fly ash, as determined by X-ray fluorescence (XRF) analysis and Malvern Particle size analyser (Mastersizer X) respectively, are summarized in Table 3.1, Figure 3.5 and Table 3.2.

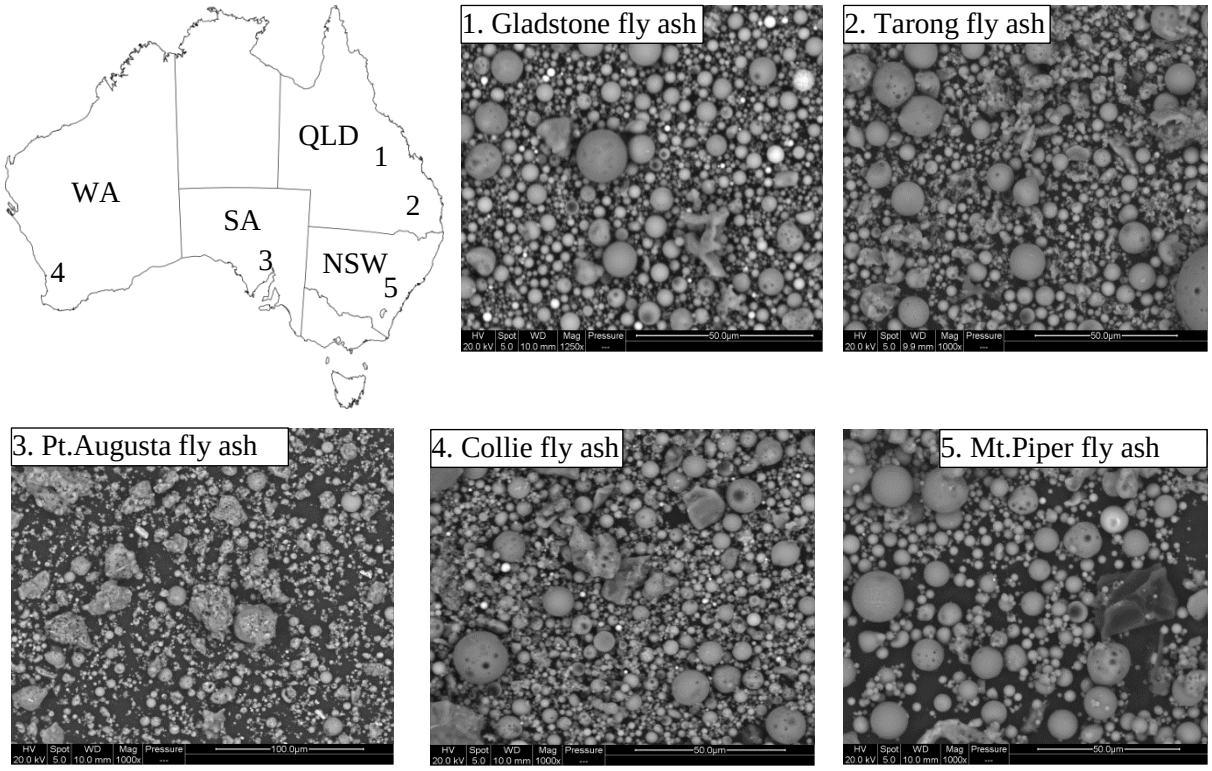

Figure 3.4 Fly ashes obtained from five different power stations

Table 3.1 Chemical composition of low calcium fly ash

Chemical oxide	Component (wt. %) of each fly ash				
	Gladstone	Pt.Augusta	Collie	Mt.Piper	Tarong
SiO_2	50.82	49.97	52.67	65.18	73.12
Al_2O_3	29.89	31.45	29.60	25.30	21.50
$SiO_2 + Al_2O_3$	80.71	81.42	82.27	90.48	94.62
SiO_2 / Al_2O_3	1.7	1.6	1.8	2.6	3.4
Fe_2O_3	10.26	3.22	11.27	1.90	1.36
CaO	3.24	5.03	0.94	0.63	0.29
K_2O	0.58	1.87	0.65	3.65	0.63
TiO_2	2.05	2.54	1.83	1.53	1.84
P_2O_5	1.61	1.77	1.13	1.21	1.06
MgO	0.80	1.54	0.72	0.00	0.00
Na_2O	0.00	1.85	0.00	0.00	0.00
SO_3	0.28	0.33	0.48	0.23	0.00
LOI[a]	0.43	0.51	0.63	1.30	1.16

[a] Loss on Ignition (unburnt carbon content)

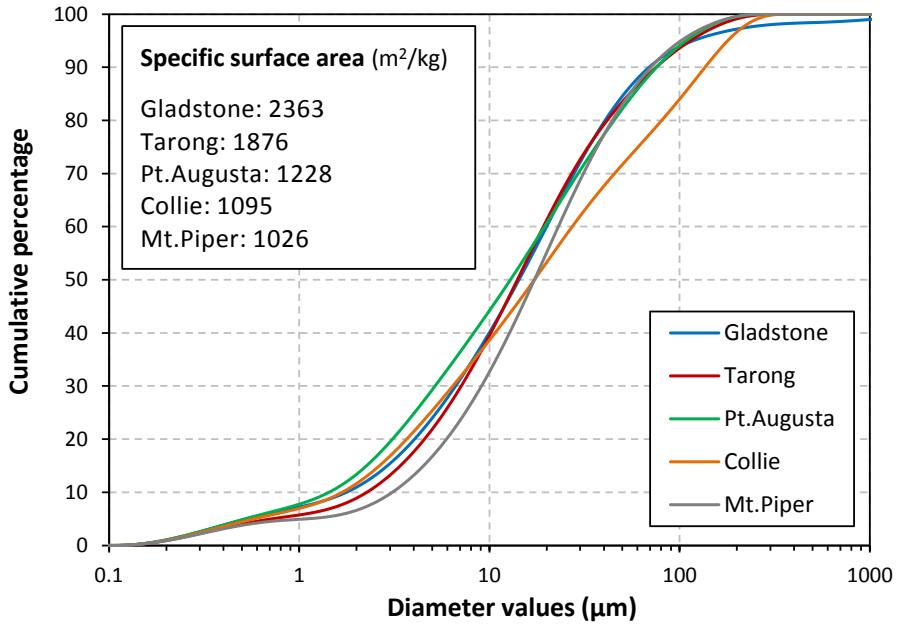

Figure 3.5 Cumulative percentage passing vs. particle size

Table 3.2 Particle size distribution of low calcium fly ash

X	Passing (%) at X of each fly ash				
	Gladstone	Pt.Augusta	Collie	Mt.Piper	Tarong
5 micron	24.8	30.1	26.1	17.4	22.7
10 micron	43.1	46.7	40.9	36.0	43.0
20 micron	61.9	62.1	54.6	57.1	63.0
30 micron	73.2	71.4	62.7	69.9	73.6
40 micron	79.8	77.4	67.7	77.4	79.3
45 micron	82.7	80.2	70.0	80.7	81.8
50 micron	85.3	82.9	72.3	83.8	84.2
60 micron	89.6	87.9	76.7	89.0	88.3
70 micron	91.2	90.1	79.0	91.2	90.2
80 micron	92.6	92.1	81.3	93.0	91.9
90 micron	93.8	93.8	83.6	94.6	93.4
SSA[a]	2362.7	1228.3	1095.3	1025.5	1875.5

[a]Specific surface area (m^2/kg)

Brunauer Emmett Teller (BET) method by N_2 absorption was used to determine the specific surface area of fly ash materials. Moreover, the amorphous percentage and available crystalline phases of specific fly ash were obtained by X-ray diffraction (XRD) analysis, which are shown in Figure 3.6 and Table 3.3.

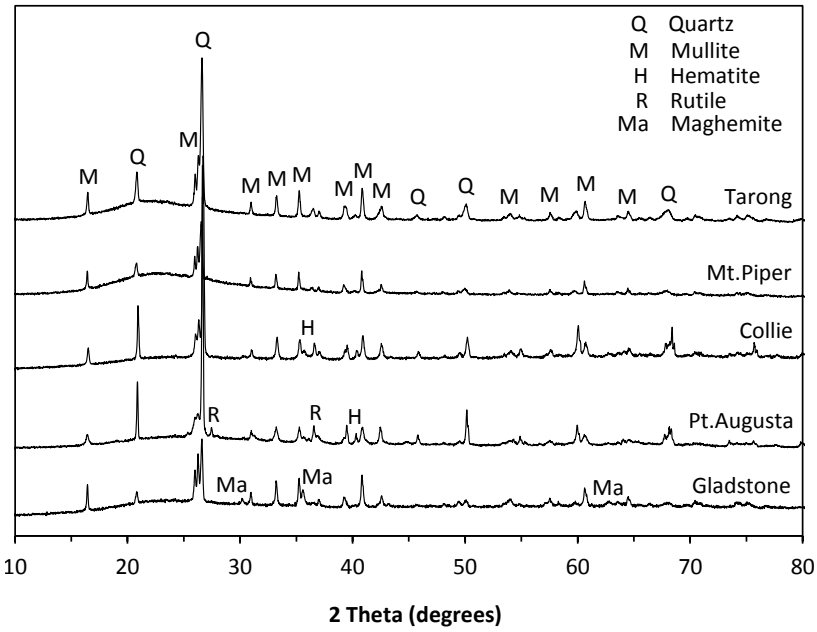

Figure 3.6 Crystalline phases of low calcium fly ash

Table 3.3 Quantitative analysis of amorphous & crystalline percentage of fly ash

Mineralogical composition (%)		Gladstone	Pt.Augusta	Tarong	Collie	Mt.Piper
Amorphous		71.8	59.5	66.3	72.5	79.2
	Quartz	6.8	29.2	14.8	18.2	7.2
Crystalline	Mullite	17.9	7.5	18.9	8.7	13.6
	Others	3.5	3.8	0	0.6	0

3.3.1.2. Alkaline activator

The alkaline liquid used in geopolymers consisted of a mixture of commercially available sodium silicate solution with a specific gravity of 1.53 and an alkaline modulus ratio (Ms) equal to 2 (where Ms = SiO_2/Na_2O, Na_2O = 14.7% and SiO_2 = 29.4% by mass), and sodium hydroxide solution (15 M). Previous studies had shown that a use of 15 M sodium hydroxide produced the highest strength for geopolymer mortar (Adam, 2009). The sodium hydroxide solution was prepared by dissolving commercial grade sodium hydroxide pellets with 99% purity in deionised water at least one day prior to usage. Sodium silicate solution was supplied by PQ Australia (Pty) Ltd., and the relevant properties of the solution are based on the Material Safety Data Sheet (MSDS), which is tabulated in Table 3.4.

Table 3.4 Properties of Sodium Silicate solution (Source: MSDS-PQ Australia)

Product Name	D™
Wt. Ratio SiO_2/Na_2O	2.00
$\%Na_2O$	14.7
$\%SiO_2$	29.4
Density @ 68°F(20°C) °Be'	50.5
Density @ 68°F(20°C) lb/gal	12.8
Density @ 68°F(20°C) g/cm^3	1.53
pH	12.8
Viscosity Centipoises	400
Characteristics	Clear to opalescent liquid

3.3.1.3. Fine sand

Locally available river sand in uncrushed form with a specific gravity of 2.5 and a fineness modulus of 3.0 served as fine aggregate. Properties were determined in accordance with AS 1141.5 standard (2000a). Typical grading of the fine aggregate is shown in Table 3.5.

Table 3.5 Grading of the fine aggregate

Sieve size	% retained	% Passing	Specification (% Passing)
4.75 mm	0	100	87-100
2.36 mm	1.8	98	86-96
1.18 mm	6.4	94	75-90
600 um	27.7	72	58-72
300 um	69.4	31	31-39
150 um	96.4	4	5-15
75 um	99.6	0	0-4

3.3.2. Mix designs and proportions – Geopolymer mortar

3.3.2.1. Mix design on Activator Modulus (AM)

The initial mix design of fly ash geopolymer mortar was adopted from previous research conducted at RMIT University, Melbourne, Australia (Adam, 2009). The absolute volume method (Neville, 1996) was used in determining the proportion of cementitious materials, fine aggregate (i.e. sand), chemical activator, and water.

Nine mix designs based on AM (Equation 2.1 and Appendix A1) were used in this investigation. The mix proportion used in each mix design is summarized in Table 3.6. The AM is varied by blending liquid sodium silicate and sodium hydroxide in different proportions. The Na_2O dosage is kept to 15% by mass of alkali for all mix designs. Adam (2009) had shown that a Na_2O dosage of 15% produced the highest compressive strength for fly ash geopolymer mortar.

Table 3.6 Mix design details of fly ash geopolymers based on AM

Geopolymer Mix design	Relevant AM	Mass ratio of materials for 1 liter (kg)					
		Fly ash	Sand	Added free water	Activator Solution		Na_2SiO_3 / NaOH
					Na_2SiO_3	NaOH	
AM - 0.625	0.625	1	2.75	0.083	0.257	0.374	0.7
AM - 0.75	0.75	1	2.75	0.067	0.383	0.312	1.2
AM - 1.0	1.0	1	2.75	0.067	0.510	0.234	2.2
AM - 1.125	1.125	1	2.75	0.044	0.574	0.219	2.6
AM - 1.25	1.25	1	2.75	0.042	0.638	0.175	3.6
AM - 1.375	1.375	1	2.75	0.024	0.699	0.157	4.4
AM - 1.5	1.5	1	2.75	0.015	0.765	0.117	6.5
AM - 1.625	1.625	1	2.75	0.001	0.796	0.098	8.1
AM - 1.75	1.75	1	2.75	0.000	0.867	0.072	12.0

For all the mortar mixes, the sand to fly ash ratio is fixed to 2.75 according to ASTM C109/C109M standard (2013a) while the ratio of volume of sand to the total volume of mortar mixer was kept at 60%. The water to solid ratio is fixed to 0.37. The quantity of water contained in the mix is defined as sum of water contained in the sodium silicate, sodium hydroxide and added water, while the quantity of solid is the sum of the mass of fly ash and the solid contained in the alkaline activator solution. Instead of using water to binder ratio, the water to solid ratio was used due to the high quantity of solid contained in the alkaline activator. This solid comprised of Na_2O and SiO_2 as well and reduced the workability of fly ash geopolymer, especially at higher dosages of Na_2O. Hence, the use of water to solid ratio for mix designs of fly ash geopolymer mortar enabled a more consistent workability to be achieved during the mixing process. The mortar specimens investigated, with reference to the fly ash type and mix design based on AM, are shown in Table 3.7.

Table 3.7 Tested fly ash geopolymer specimens relating to mix designs based on AM

Geopolymer	Geopolymer (GP) mix design								
	AM 0.625	AM 0.75	AM 1.0	AM 1.125	AM 1.25	AM 1.375	AM 1.5	AM 1.625	AM 1.75
Gladstone	-	-	*G1.0	G1.125	**G1.25**	G1.375	G1.5	-	-
Pt.Augusta	-	-	PA1.0	PA1.125	**PA1.25**	PA1.375	PA1.5	-	-
Collie	-	-	C1.0	C1.125	C1.25	**C1.375**	C1.5	-	-
Mt.Piper	MP0.625	**MP0.75**	MP1.0	-	MP1.25	-	MP1.5	-	-
Tarong	-	-	T1.0	-	T1.25	-	T1.5	**T1.625**	T1.75

G-Gladstone; PA-Port Augusta; C-Collie; MP-Mount Piper; T-Tarong fly ash

*Note: G1.0 is defined as Gladstone fly ash geopolymer mortar with mix design of AM-1.0.

3.3.2.2. Mix design on Effective Activator Modulus (AM_{eff})

In order to account for the variations in the chemical composition of the different fly ash materials the SiO_2 and Na_2O content of the different fly ash materials was accounted for by including these in the AM to give an effective activator modulus (AM_{eff}), as shown in Equation 3.1 (Appendix A2).

$$\text{Effective AM } (AM_{eff}) = \frac{SiO_2 \text{ in alkaline activator solution and fly ash}}{Na_2O \text{ in alkaline activator solution and fly ash}} \quad (3.1)$$

$$\text{Effective } Na_2O \text{ dosage} = \frac{Na_2O \text{ in alkaline activator solution and fly ash}}{\text{fly ash}} \quad (3.2)$$

Mix designs based on the AM_{eff} of the Gladstone geopolymer were used in this investigation, as the Gladstone was the material with the highest compressive strength. The calculated AM_{eff} of Gladstone geopolymer mixes, G1.0, G1.25 and G1.5, were 4.5, 4.8 and 5.0, respectively. The AM_{eff} of G1.125 and G1.375 geopolymer mixes overlapped with the G1.0 and G1.25 mixes, respectively.

The revised mix proportion used in each mix design based on calculated AM_{eff} is summarized in Table 3.8. In the modified design the Na_2SiO_3 and NaOH quantities were varied to modify the AM-0.75, AM-1.0, AM-1.25 and AM-1.5 mix designs to give an AM_{eff} of 4.1, 4.5, 4.8 and 5.0, respectively for the Pt.Augusta, Collie, Mt.Piper and Tarong materials. The effective Na_2O dosage which was calculated by considering Na_2O content in fly ash (Equation 3.2) is fixed at 15% for all geopolymer mixes. The tested mortar specimens are shown in Table 3.9.

Table 3.8 Mix design details of fly ash geopolymers based on AM_{eff}

GP	Original GP mix	Modified Mix design	Relevant AM_{eff}	Mass ratio of materials for 1 liter (kg)					
				Fly ash	Sand	Water	Activator Solution		Na_2SiO_3 / NaOH
							Na_2SiO_3	NaOH	
Pt.Augusta	PA0.75	AM_{eff}-4.1	4.1	1	2.75	0.111	0.329	0.261	1.3
	PA0.875	AM_{eff}-4.3	4.3	1	2.75	0.097	0.377	0.246	1.5
	PA1.0	AM_{eff}-4.5	4.5	1	2.75	0.078	0.510	0.176	2.9
	PA1.25	AM_{eff}-4.8	4.8	1	2.75	0.055	0.638	0.117	5.5
	PA1.50	AM_{eff}-5.0	5.0	1	2.75	0.031	0.769	0.057	13.4
Collie	C1.0	AM_{eff}-4.5	4.5	1	2.75	0.067	0.437	0.268	1.6
	C1.25	AM_{eff}-4.8	4.8	1	2.75	0.042	0.569	0.207	2.7
	C1.50	AM_{eff}-5.0	5.0	1	2.75	0.016	0.696	0.149	4.7
Mt.Piper	MP1.0	AM_{eff}-4.5	4.5	1	2.75	0.062	0.332	0.381	0.9
	MP1.25	AM_{eff}-4.8	4.8	1	2.75	0.057	0.351	0.350	1.0
	MP1.50	AM_{eff}-5.0	5.0	1	2.75	0.049	0.421	0.307	1.4
Tarong	T0.75	AM_{eff}-4.1	4.1	1	2.75	0.037	0.218	0.525	0.4
	T0.875	AM_{eff}-4.3	4.3	1	2.75	0.030	0.253	0.506	0.5
	T1.0	AM_{eff}-4.5	4.5	1	2.75	0.021	0.331	0.441	0.8
	T1.25	AM_{eff}-4.8	4.8	1	2.75	0.021	0.427	0.387	1.1
	T1.50	AM_{eff}-5.0	5.0	1	2.75	0.014	0.505	0.339	1.5

Table 3.9 Tested fly ash geopolymer specimens relating to mix designs based on AM

GP	Geopolymer (GP) mix design				
	AM_{eff} - 4.1	AM_{eff} - 4.3	AM_{eff} - 4.5	AM_{eff} - 4.8	AM_{eff} - 5.0
Pt.Augusta	*PA4.1	**PA4.3**	PA4.5	PA4.8	PA5.0
Collie	-	-	C4.5	**C4.8**	C5.0
Mt.Piper	-	-	MP4.5	**MP4.8**	MP5.0
Tarong	T4.1	**T4.3**	T4.5	T4.8	T5.0

*Note: PA4.1 is defined as Port Augusta fly ash geopolymer mortar with mix design of AM_{eff} - 4.1.

3.3.3. Mixing, Casting and Curing – Geopolymer mortar

Mixing, casting and curing process of geopolymer mortar is shown in Figure 3.7. The fly ash and sand were initially mixed using a 5 litre Hobart mixer for 4 minutes with a speed of 150 rev/min. Activator solution, i.e. sodium silicate and sodium hydroxide, and water was added to the dry mix and mixed firstly by hand using a mixing tool for 1 minute. The whole mix was then blended in a Hobart mixer for 4 minutes with a speed of 150 rev/min and further 2 minutes with 300 rev/min. Immediately after mixing the geopolymer mortar was placed in 50x50x50 mm^3 Teflon moulds and vibrated using a vibration table for 20 seconds. After vibration the moulds were kept at room temperature for 1 day and then cured in a dry oven for 24 hours at $80^{o}C$ temperature. Moulds were removed from the oven and left to cool to room temperature before demoulding, and then kept at room temperature until being tested.

Figure 3.7 Mixing, casting and curing of geopolymer mortar

3.3.4. Testing – Geopolymer mortar

Compressive Strength – Mortar

The compressive strength test was performed on the 50 mm^3 specimens in accordance with AS 1012.9 standard (1999a) and a loading rate of 0.34 $(N/mm^2)/S$ using a Tecnotest concrete testing machine as shown in Figure 3.8. Average compressive strength of three mortar specimens was reported.

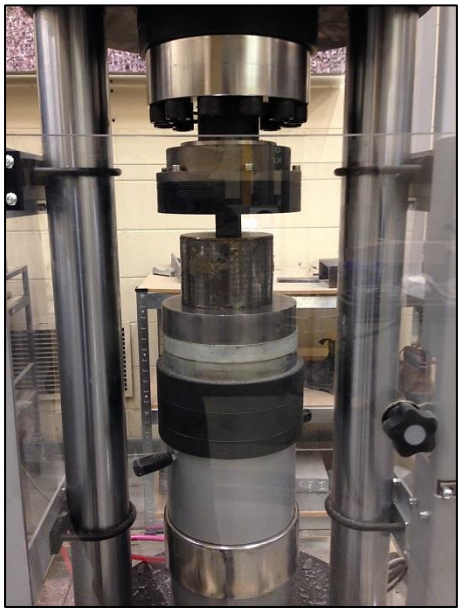

Figure 3.8 Compressive strength test of geopolymer mortar

Leaching of Elements –

Leaching test was performed in order to examine the solubility of five fly ash in water. Initially, the 5% weight of fly ash is dissolved in deionized water for 24 hours using an overhead rotating mixer. After that, the fly ash was filtered from 0.45µm size filter papers and a sample from the solution was taken and acidified with 2% volume of concentrated HNO_3 to prevent precipitation. Finally the concentration of the desired elements was analysed with Microwave Plasma-Atomic Emission Spectroscopy (MP-AES).

Zeta potential –

Malvern Zetasizer (nano series) was used to measure the zeta potential of fly ash particles and optimum geopolymer matrices well-dispersed in deionized water (5% weight suspension). Before each set of measurements, the instrument was calibrated using potassium tungstosilicate solution, and all calculations were performed using the Zetasizer software (v. 7.11).

Mineralogical composition –

Amorphous and crystalline phases of fly ash and resultant geopolymers were determined by X-ray diffraction (XRD) test. XRD data was obtained using a Bruker AXS D4 Endeavor wide angle X-ray diffractometer with copper anode at 40 kV and 35mA. After 28 days

samples were cut into thin slices, then ground into fine particles and filtered using 75 micron sieve to obtain the required powder samples for testing.

Microstructural Analysis –

The backscatter electron imaging and X-ray imaging (mapping) were performed using Quanta Scanning Electron Microscopy (SEM) apparatus with 15kV of energy. The elemental analysis was done using an Oxford Aztec EDS attached to the SEM. The specimens were cut using a diamond saw to a size of 2–4 mm in height and 5–10 mm in diameter and then carbon coated and mounted on the SEM sample stage with conductive, double sided carbon tape before being analysed.

Fourier transforms infrared (FT-IR) Analysis –

FT-IR absorption spectra were recorded in the range 4000–450 cm^{-1} using a Perkin–Elmer-Spectrum 100 FT-IR spectrometer, equipped with the universal attenuated total reflectance (ATR) top plate and diamond crystal. Spectra were recorded at a spectral resolution of 4 cm^{-1} and a scan speed of 0.2 cm/s and data were normalised according to the Spectrum software (Perkin–Elmer). The samples were manually ground and filtered using 75 micron sieve to achieve required powder for testing.

Nuclear Magnetic Resonance (NMR) Analysis –

Solid state MAS-NMR (magic-angle spinning nuclear magnetic resonance) spectroscopic experiments were performed using an Agilent 500 MHz DD2 Console equipped with a triple resonance solid state MAS probe. The ^{27}Al spectra were acquired at 25 °C using the 'onepul' pulse sequence with 1024 accumulations. The samples were loaded into 4mm rotors and rotation frequencies of 10 kHz were used. The ^{27}Al MAS-NMR spectra were obtained with a repetition delay time of 2 s and a 40 ms acquisition time for quantitative analysis. The samples used for analysis were manually ground and filtered using 75 micron sieve to achieve required powder before testing.

Mercury Intrusion Porosimetry (MIP) Analysis –

Pore size and pore volume distribution analysis was conducted using Auto pore IV 9500 (V1.09) Micrometrics mercury intrusion porosimeter. Prior to MIP analysis, the geopolymer monoliths (1x1x2 cm^3) were dried in an oven at 105^{o}C for 48 hours.

Rheological behavior –

The rheological behavior of optimum geopolymer samples were measured using a Haake VT550 rheometer with a 4-bladed vane of 22mm diameter and 40mm height of , in a large cup of 55mm diameter. The shear rate range used for the suspension was 0.1-100 s^{-1}. Before each measurement, the geopolymer was mixed by hand to avoid settling of particles and to provide a homogenous mix, left to rest for 30 seconds to dissipate residual stresses induced by mixing, before testing.

Flowability –

Standard mortar flow test was conducted using flow table in accordance with ASTM C1437 (2013b), as shown in Figure 3.9. This test was conducted to examine the mortar flowability in optimum geopolymer matrices.

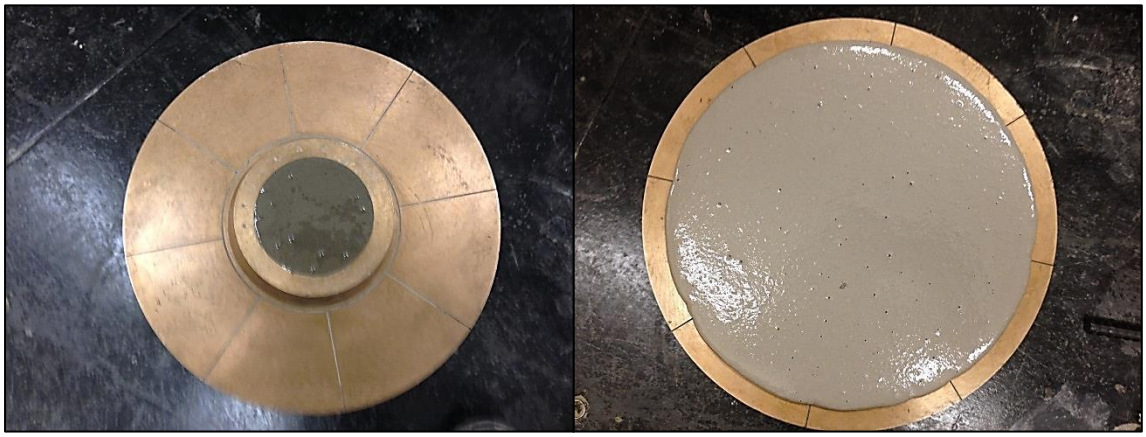

Figure 3.9 Standard mortar flow test for geopolymer mortar

3.4 Preparation of geopolymer concrete

3.4.1. Materials used – Geopolymer concrete

3.4.1.1. Fly ash

Fly ash used in the investigation was dry, low calcium class F fly ash conforming to AS 3582.1 standard (1998b), obtained from five different power plants as Gladstone, Tarong, Pt.Augusta, Collie and Mt.Piper in Australia. The chemical composition of the fly ash used for preparation of geopolymer concrete slightly differed from the previous batch used for preparation of geopolymer mortar, though obtained from the same power station. The new chemical composition of fly ash is determined by XRF analysis and tabulated in Table 3.10.

However, the other properties of fly ash, i.e. particle size distribution, specific surface area and mineralogical composition, are similar and described in Section 3.3.1.1.

Table 3.10 Chemical composition of low calcium fly ash

Chemical oxide	Component (wt. %) of each fly ash				
	Gladstone (GFA)	Port Augusta (PAFA)	Collie (CFA)	Mount Piper (MPFA)	Tarong (TFA)
SiO_2	47.87	49.37	53.82	66.63	75.66
Al_2O_3	28.0	31.25	29.95	24.40	19.0
$SiO_2 + Al_2O_3$	75.87	80.62	83.77	91.03	94.66
SiO_2 / Al_2O_3	1.71	1.58	1.80	2.73	3.98
Fe_2O_3	14.09	4.47	9.24	0.84	1.38
CaO	3.81	4.80	1.03	0.78	0.30
K_2O	0.62	2.21	0.79	3.90	0.63
TiO_2	1.99	2.94	2.19	1.66	1.83
P_2O_5	1.81	1.65	1.28	1.21	1.00
MgO	0.93	1.28	0.58	0.0	0.0
Na_2O	0.41	1.30	0.75	0.36	0.15
SO_3	0.27	0.24	0.34	0.21	0.03
LOI[a]	0.43	0.51	0.63	1.30	1.16

[a] Loss on Ignition (unburnt carbon content)

3.4.1.2. Alkaline activator

The alkaline liquid used in geopolymers consisted of a mixture of commercially available sodium silicate solution and sodium hydroxide solution. The properties of the sodium silicate and sodium hydroxide used are described in Section 3.3.1.2.

3.4.1.3. Fine sand

Locally available river sand in uncrushed form with a specific gravity of 2.5 and a fineness modulus of 3.0 was used to prepare geopolymer concrete specimens. The properties of fine sand used are described in Section 3.3.1.3.

3.4.1.4. Coarse aggregates

Coarse aggregates were prepared in accordance with AS 1141.5 (2000a). The moisture condition of the aggregate was kept at a saturated surface dry condition prior to mixing. The coarse aggregate used in this study was crushed basalt aggregate of two-grain sizes: 7 mm (2.58 specific gravity and 1.60% water absorption) and 10 mm (2.62 specific gravity and

0.74% water absorption). The water absorption values for both aggregate size were below the acceptable value of 2% (AS, 2014a). Combined aggregates were finally used to prepare geopolymer concrete specimens. The final combined aggregate volume was a combination of 38% of 10mm, 19% of 7mm and 43% of sand. The typical grading of the combined aggregate is shown in Table 3.11.

Table 3.11 Grading of the combined aggregates

Sieve size	Aggregate			Combined aggregate
	7mm	10mm	Sand	
13.2 mm	100.0	100.0	100.0	100.0
9.5 mm	100.0	100.0	100.0	100.0
6.7 mm	96.0	100.0	100.0	99.2
4.75 mm	36.0	21.0	100.0	57.8
2.36 mm	3.0	2.0	98.0	42.8
1.18 mm	0.0	1.0	94.0	38.6
600 µm	1.0	0.0	72.0	31.9
300 µm	0.0	0.0	31.0	14.2
150 µm	0.0	0.0	4.0	1.5

3.4.2. Mix designs and proportions – Geopolymer concrete

The mix design in each fly ash geopolymer concrete was initially selected, based on previous tests on mortar specimens given in Section 3.3.2.1. The blended sodium silicate and sodium hydroxide solutions are characterized by the activator modulus as shown in Equation 2.5. The activator modulus was then varied by 0.125 intervals, starting from the optimum mix design of the geopolymer mortar as shown in

Table 3.12, to determine the optimum 28-day compressive strength for the geopolymer concrete. The Na_2O dosage is kept to 15% by mass of alkali while the total aggregate in the concrete was kept to 64% of the entire mixture by volume for all mixes. The ratio of ingredients (fly ash, chemical activator, aggregate, and water) was calculated based on the absolute volume method (Neville, 1996), as a result, the total weight of binder and water was varied to keep the volume of material and water/solid ratio (0.37) constant. The water in the mix was taken as the sum of water contained in the sodium silicate, sodium hydroxide and added water. The solid is taken as the sum of fly ash and the solid in alkali activator solution (i.e. solid in the sodium silicate solution and sodium hydroxide solution). Table 3.13 summarizes the mix details for all fly ash based geopolymer concrete.

Table 3.12 Tested concrete specimens in each fly ash based geopolymer (GP) concrete

GP	Mix design								
	AM - 0.625	AM - 0.75	AM - 1.0	AM - 1.125	AM - 1.25	AM - 1.375	AM - 1.5	AM - 1.625	AM - 1.75
Gladstone	-	-	-	G1.125	*G1.25	G1.375	G1.5	-	-
Pt.Augusta	-	-	-	PA1.125	*PA1.25	PA1.375	PA1.5	-	-
Collie	-	-	C1.0	C1.125	C1.25	*C1.375	C1.5	-	-
Mt.Piper	MP0.625	*MP0.75	MP1.0	-	-	-	-	-	-
Tarong	-	-	-	-	-	-	T1.5	*T1.625	T1.75

*Optimum mix design for geopolymer mortar, Section 3.3.2.1

G-Gladstone; PA-Pt.Augusta; C-Collie; MP-Mt.Piper; T-Tarong fly ash

Note: G1.125 is defined as Gladstone fly ash geopolymer concrete with mix design of AM-1.125.

Table 3.13 Mix design details of geopolymer concrete (kg/m^3)

Mix	Fly ash	Aggregate (kg)			Activator (kg)		Added
	(kg)	Sand	7 mm	10 mm	Na_2SiO_3	NaOH (15 M)	water (kg)
AM -0.625	427	718	317	634	136	147	33
AM -0.75	425	714	315	631	163	132	30
AM -1.0	421	708	313	626	217	104	20
AM -1.125	420	706	312	624	241	92	15
AM -1.25	418	702	310	621	266	78	12
AM -1.375	416	699	309	618	292	65	8
AM -1.5	414	697	308	616	317	52	3
AM -1.625	412	693	306	612	342	39	0
AM -1.75	409	687	304	607	365	26	0

3.4.3. Mixing, Casting and Curing – Geopolymer concrete

Mixing, casting and curing process of geopolymer concrete is shown in Figure 3.10. The mixing of geopolymer concrete was carried out using a 120 litre concrete mixer. The dry materials (fly ash, fine sand and coarse aggregates) were mixed first for 4 minutes. Then activator and water were added to the dry mix and mixed continuously for approximately 8 minutes until the mixture was glossy and well combined. The mixture was then poured into different moulds based on experiment method, i.e. 100mm^3 cubic Teflon moulds for compressive strength test, 100ϕx200mm^3 cylindrical PVC moulds for compressive strength, elasticity modulus, Poisson's ratio, stress-strain relationship and density tests, 150ϕx300mm^3 cylindrical PVC moulds for splitting tensile strength test, 100x100x350mm^3 rectangular timber moulds for flexural strength test, 100x200x200mm^3 rectangular timber moulds for

ultrasonic pulse velocity, surface hardness and resistivity tests, 100x300x300mm^3 rectangular timber moulds for air & water permeability tests, and 100ϕx50mm^3 cylindrical PVC moulds for water absorption test. All specimens were vibrated using a vibration table for 1 minute to remove air bubbles. After vibration the moulds were kept at room temperature for 1 day and then heat cured in an oven for 24 hours at 80°C temperature. The inside surfaces of the moulds were coated with a high performance silicon spray to prevent the samples from sticking to the mould surface during the heat curing process. Moulds were removed from the oven and left to cool to room temperature before demoulding, and then kept at room temperature (23±2 °C) until being tested. Three concrete specimens were tested for each case (experiment) and then average test results were reported in the thesis.

Figure 3.10 Mixing, casting and curing of geopolymer concrete

3.4.4. Testing – Geopolymer concrete

Compressive Strength – Concrete

The compressive strength test was performed on both 100mm^3 cubical and 100ϕx200mm^3 cylindrical geopolymer concrete specimens in accordance with AS 1012.9 (1999a) standard and a loading rate of 20 MPa/min using a MTS machine with a loading capacity of 1000 kN, as shown in Figure 3.11. The MTS machine was computer controlled with the testing specifications and data acquisition configured by the MTS Test-star controller and software. Three concrete cubes were tested for each data point at 3, 7 and 28 days after casting for each mix design during the optimisation process. Three concrete cylinders were tested for each data point at 28, 90 and 365 days for the optimum mix design for each fly ash geopolymer. Average compressive strength of three concrete specimens for each case was reported.

Figure 3.11 Compressive strength test of geopolymer concrete

Flexural tensile strength – Concrete

The flexural tensile strength test which is also known as modulus of rupture test, was carried out on the MTS machine with a loading rate of 1 MPa/min in accordance with AS 1012.11 (2000c) standard, as shown in Figure 3.12. The setup of the flexural tensile strength test followed a four point bending test, and specimens of optimum mix in each fly ash geopolymer was measured by loading 100mmX100mm concrete beam with a span length of 300mm. Three prism specimens were tested for each data point at 28, 90 and 365 days after casting and average flexural strength for each case is reported.

Figure 3.12 Flexural strength test of geopolymer concrete

Splitting tensile strength – Concrete

The splitting tensile strength which is further expressed as indirect tensile strength, of the geopolymer concrete specimens was experimentally measured in according to AS1012.10 (2000b) standard, as shown in Figure 3.13. Test was performed on the MTS machine which was equipped with the splitting tensile strength test equipment with a loading rate of 1.5 MPa/min. To obtain the splitting tensile strength for specimens of optimum mix in each fly ash geopolymer, a cylinder of dimension 150x300mm (diameter x height) was subjected to compressive loading along its length and were tested at the age of 28, 90 and 365 days after casting. Three specimens were tested for each data point and average splitting tensile strength for each case is reported.

Figure 3.13 Splitting tensile strength test of geopolymer concrete

Modulus of elasticity and Poisson's ratio – Concrete

The static modulus of elasticity and Poisson's ratio tests were performed on the Technotest concrete testing machine coupled with the compressometer/extensometer with a loading rate of 0.25 MPa/sec according to AS 1012.17 (1997) standard, as shown in Figure 3.14. Both tests were undertaken by subjecting cylinder specimens of dimension 100x200mm (diameter x height) to uni-axial compression by loading up to 40% of the average compressive strength of three similar concrete specimens. Three cylinders of optimum mix in each fly ash geopolymer were tested for each data point at 28, 90 and 365 days after casting, and average elasticity modulus and Poisson's ratio is reported. In the Poisson's ratio test, the first and second readings were discarded which was used for the setting of the gauges, and thus next three readings were used for the average value.

Figure 3.14 Elasticity modulus and Poison's ratio tests of geopolymer concrete

Stress-Strain relationship – Concrete

Stress-Strain relationship for optimum fly ash geopolymer concrete mixes was established using MTS machine connected with the data acquisition test rig, with a loading rate of 1 MPa/min. Two strain gauges attached to the specimen of 100x200mm (diameter x height) cylinder within middle third height were used to measure the strain. Three cylinders were tested for each data point at 28 days after casting, and average stress and strain values for each case was used to establish the stress-strain relationship.

Air and Water permeability – Concrete

The air and water permeability tests were performed using the Autoclam Permeability System (Basheer et al., 2007, Claisse et al., 2003) as shown in Figure 3.15. The both permeability tests were conducted at 28, 90 and 360 days after casting for each optimum mix design. Three cube specimens of 100x300x300 mm^3 were tested and average values for each case was considered for the analysis. Air and water permeability tests were carried out at one location on each specimen.

In air permeability test, the pressure inside the apparatus is increased to slightly above 0.5bar and the decay in pressure is monitored every minute from 0.5bar for 15 minutes or until the pressure has diminished to zero. A plot of natural logarithm of pressure against time is linear, hence the slope of the linear regression curve between the 5^{th} and 15^{th} minute for tests lasting

for 15 minutes is used as an air permeability index, with units of Ln(Pressure)/min. When the pressure becomes zero before the test duration of 15 minutes, the data from the beginning of the test is used to determine the slope.

The water permeability test is conducted at the same specimen, but one day after the former test. Water is admitted into the test area through a priming pump and the pressure inside is increased to 0.5bar at the end of the priming. The quantity of water flowing into the concrete is recorded every minute for duration of 15 minutes. The quantity of water flowing into concrete plotted against the square root of time is linear, hence the slope of the square root time plot between 5 and 15 minutes is used to report a water permeability index with units $m^3/\sqrt{min}$.

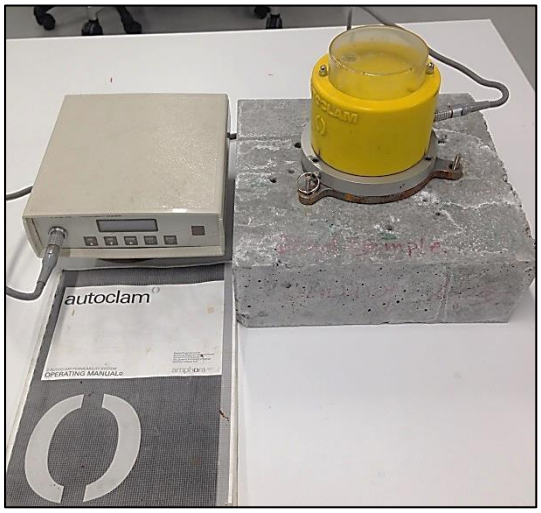

Figure 3.15 Air and Water Permeability test

Water absorption and Permeable voids – Concrete

The water absorption test was carried out in accordance with AS 1012.21 (1999b) standard to determine the immersed absorption. Immersed absorption (*A*i) is the ratio (%) of the mass of water contained in a concrete specimen, and was used to determine the water absorption of fly ash geopolymer concrete specimens. The specimens of 100 mm diameter x 200 mm long cylinders were cut into four equal slices for this test and the result reported is the average of the results for the four slices. Three cylinders were cut into slices and tested for a geopolymer at 28, 90 and 365 days after casting, and average values for each case was considered. Moreover, the Apparent Volume of Permeable Voids (AVPV) in geopolymer concrete was measured using same specimens in accordance to the aforementioned standard at 28, 90 and 365 days.

Chloride diffusion – Concrete

The chloride diffusion coefficient (D_a) and surface concentration (C_s) were determined based on salt ponding test in accordance with AASHTO T-259 (1997b) and ASTM C1543 (2010) standards. The 28-day and 365-day aged 100mm^3 geopolymer concrete cubes were used for the testing. All faces, except top face, were painted with epoxy in order to make the chloride ingress uni-directional. This method facilitated the preparation of chloride specimens without the need for coring. Then, all specimens were immersed in 3% sodium chloride solution for duration of 90 days. In order to prevent the evaporation of chloride solution, the container was closed and solution was renewed in every two weeks. After 90 days, the specimens were removed from the chloride solution and cut into five different thicknesses with the depth increments correspond to 0-10 mm, 10-20 mm, 20-30 mm, 30-40 mm and 40-50 mm. Each slice was then ground and pulverized using a ring mill machine to 150 µm and sent to an accredited laboratory to determine the chloride content according to AASHTO T-260 (1997a) standard. The chloride diffusion coefficient (D_a) and the surface concentration (C_s) were calculated by plotting the chloride profiles and determining the best fit curve using Fick's 2nd Law (Crank, 1975). The reported test results are an average of three samples for each geopolymer.

Ultrasonic Pulse Velocity (UPV) – Concrete

The UPV test is considered as a non-destructive testing (NDT) method and is used to determine the strength and quality of a material based on the speed of a stress wave passing through the medium which is related to the elasticity-density. The UPV was measured in accordance with ASTM C597 (2009) standard using a portable ultrasonic non-destructive digital indicating tester with a 54 kHz transducer, as shown in Figure 3.16. Three cuboid concrete specimens of 200x200x100 mm^3 were tested for each geopolymer at 28, 90 and 365 days after casting, and measured the transit time and the pulse velocity. The reported test results are an average of three samples for each geopolymer.

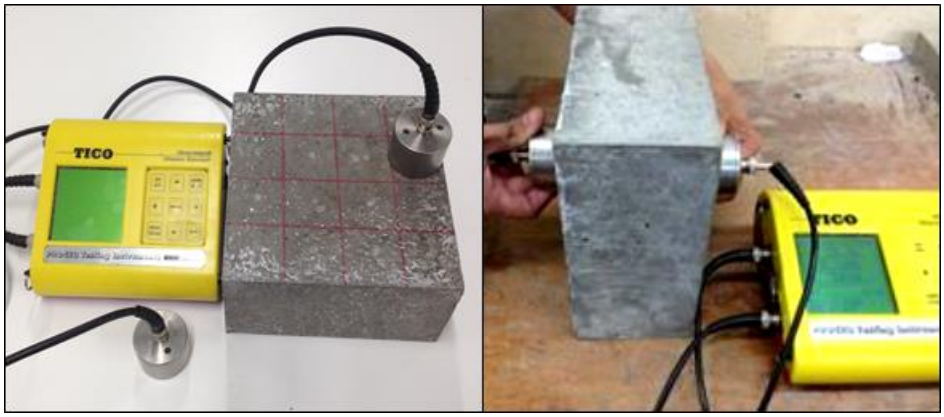

Figure 3.16 Ultrasonic pulse velocity test

Resistivity – Concrete

The resistivity of geopolymer concrete was measured using Wenner probe by the four-point method at 50 mm spacing, as shown in Figure 3.17. This test is designed to measure the electrical resistivity of the concrete specimen in an effective and non-destructive manner and is common practice within the field. The electrical resistivity of concrete is an important parameter in assessing the likelihood of corrosion having initiated. High electrical resistivity of a concrete will tend to slow the corrosion process compared to that of a concrete with a low resistivity (Song and Saraswathy, 2007). The resistivity reading was in a scale of 0 – 100 kΩ.cm. Three cuboid specimens of 200x200x100 mm^3 were tested for each geopolymer at 28, 90 and 365 days after casting, and average values for each data point was considered.

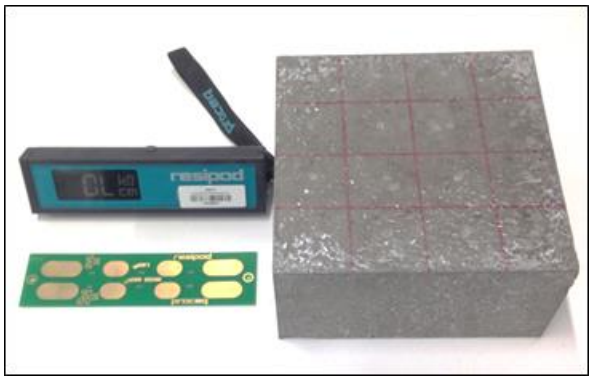

Figure 3.17 Resistivity test

Surface Hardness – Concrete

The surface hardness test, which is also known as Schmidt rebound hammer test was carried out using Schmidt Type N hammer (Figure 3.18) in according to ASTM C805/C805M (2013c) standard. Striking points were uniformly distributed to reduce the influence of coarse aggregates and distribution and averages of the rebound value was calculated. Three cuboid

specimens of 200x200x100 mm^3 were tested for each geopolymer at 28, 90 and 365 days after casting, and average values for each data point was considered.

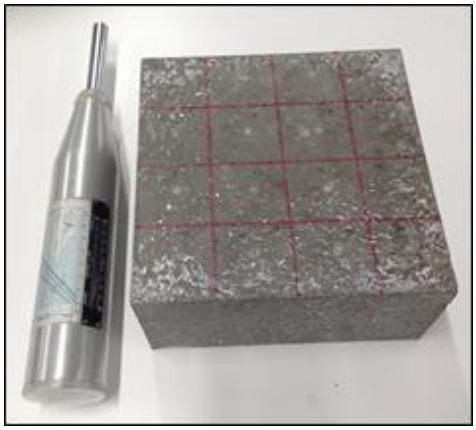

Figure 3.18 Schmidt rebound hammer test

Density – Concrete

The density of geopolymer concrete specimens were estimated using water displacement method in accordance with AS 1012.12.2 (1998a) standard, as shown in Figure 3.19. Three sets of 100x200mm^3 concrete cylinders were tested at 28, 90 and 365 days after casting, and average values for each data point was considered for the analysis.

Figure 3.19 Density test

Workability – Concrete

In order to measure the workability of geopolymer concrete mix, the standard slump test was undertaken in accordance with AS 1012.3.1 (2014b) standard. In this study, all fly ash geopolymers displayed a very high, collapsed slump, thus workability was represented by the average diameter of the slump flow.

3.5 Summary in Chapter 3

Chapter 3 on materials and experimental methods is summarised as follows:

- Fly ash used in the investigation was dry, low calcium class F fly ash, obtained from five different power plants, Gladstone, Tarong, Port Augusta, Collie and Mount Piper, in Australia. Commercially available sodium based hydroxide and silicate solution was used as alkaline activator.

- Mix design of both geopolymer mortar and concrete was based on the activator modulus (AM) with a fixed Na_2O dosage of 15% and fixed water/solid ratio of 0.37 for all fly ash. The AM was changed between 0.625 and 1.75 by 0.125 intervals for both geopolymer mortar and concrete until obtain the optimum mix design for each fly ash.

- The reasons for the variation of compressive strength of different fly ash geopolymer mortar specimens were investigated by using series of state of the art techniques, such as X-ray fluorescence spectroscopy, Particle size analyser, Brunauer Emmett teller surface area analyser, Microwave plasma-atomic emission spectroscopy, Fourier transform infrared spectrometer, Zetasizer, Scanning electron microscopy, X-ray diffractometer, Rheometer, Energy dispersive X-ray spectroscopy, Mercury intrusion porosimeter, and Nuclear magnetic resonance spectroscopy.

- Long term mechanical properties of different fly ash geopolymer concrete, such as compressive strength, flexural strength, splitting tensile strength, modulus of elasticity and Poisson's ratio were investigated up to one year.

- Long term durability properties of different fly ash geopolymer concrete, such as air and water permeability, water absorption and apparent volume of permeable voids, chloride diffusion, resistivity, ultrasonic pulse velocity and surface harness were investigated up to one year.

4 COMPRESSIVE STRENGTH OF GEOPOLYMER MORTAR

4.1 Overview

This chapter presents the test results and discussion related to the **Phase 1** of the experimental study as shown in Figure 3.2 on geopolymer mortars for five Class F fly ash. Compressive strength of the different fly ash geopolymer mortar mixes was examined over a range of activator modulus at a fixed Na_2O dosage in order to optimize the best mix design for specific fly ash. A series of tests have then been conducted using state of the art techniques to investigate the properties of the optimized geopolymer mortar specimens. Experimental results have been analysed to develop an understanding of the effects of the chemical, physical and mineralogical properties of precursor fly ash on the compressive strength evolution of fly ash based geopolymer mortar.

4.2 Optimized mix design of geopolymer mortar

Wang et al. (1994) has reported that there is an inter dependence between the AM and Na_2O content, as the formation of silica gel makes a significant contribution to the compressive strength. When the Na_2O content is kept constant, the alkaline activation effect can be considered constant, the higher the modulus the more the contribution from silica gel and the higher the strength within a certain range. This results in a variable optimum modulus, which depends on the type of source material.

In the present study, the AM is selected to optimize the mix design in order to reduce the unreacted and partially-reacted fly ash spheres in each mix as an increase of these has an adverse effect on the strength of the matrix, in particular at the interface between them and the geopolymer matrix (Steveson and Sagoe-Crentsil, 2005). In addition changing AM significantly modifies the degree of polymerization of the dissolved species in the alkaline-silicate solution (Rangan, 2008). This may result in the formation of different synthesized gel products that determine the compressive strength.

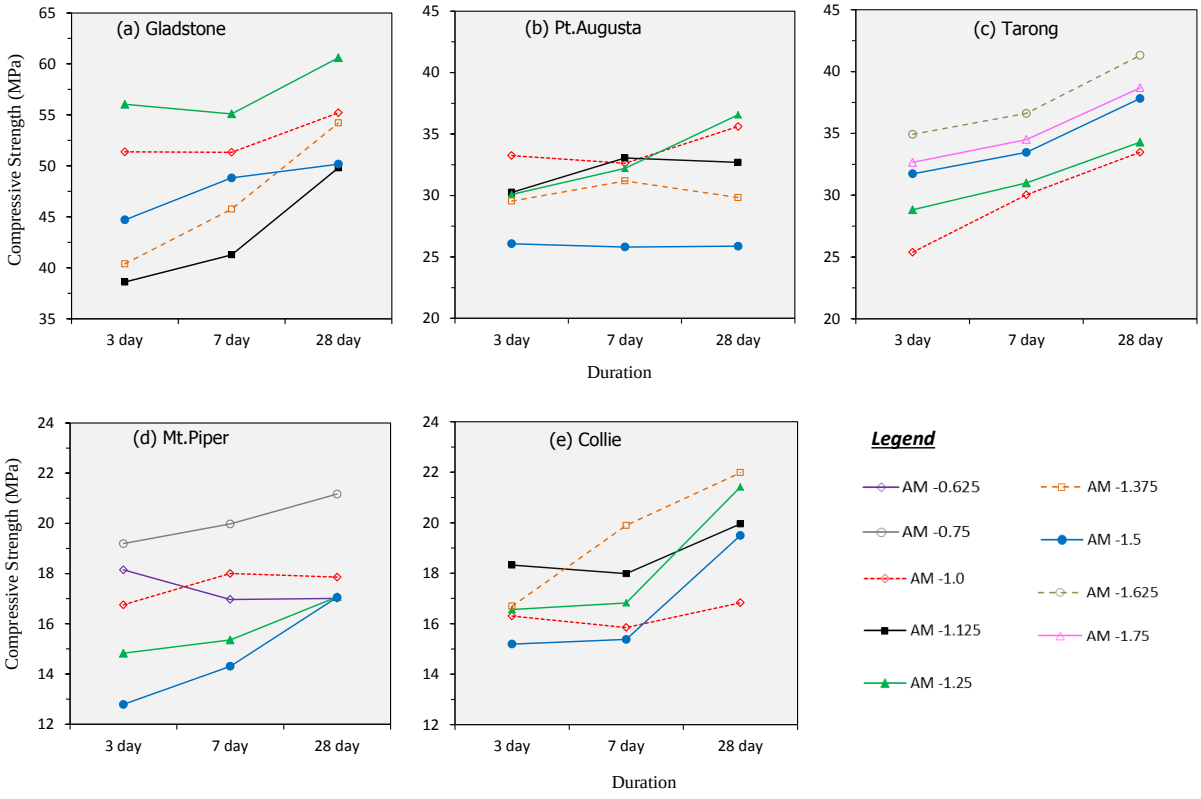

Figure 4.1 Compressive strength vs. age for different Activator Modulus (AM)

Table 4.1 Changing compressive strength with Activator Modulus (AM)

Geopolymer	Mix	Compressive Strength (MPa)		
		3 days	7 days	28 days
Gladstone	G1.0	51.4	51.3	55.2
	G1.125	38.6	41.3	49.8
	G1.25	56.0	55.1	60.6
	G1.375	40.4	45.8	54.2
	G1.5	44.7	48.8	50.2
Pt.Augusta	PA1.0	33.2	32.6	35.6
	PA1.125	30.3	33.0	32.7
	PA1.25	30.1	32.2	36.6
	PA1.375	29.5	31.2	29.8
	PA1.5	26.1	25.8	25.9
Collie	C1.0	16.3	15.9	16.8
	C1.125	18.3	18.0	20.0
	C1.25	16.6	16.8	21.4
	C1.375	16.7	19.9	22.0
	C1.5	15.2	15.4	19.5
Mt.Piper	MP0.625	18.1	17.0	17.0
	MP0.75	19.2	20.0	21.2
	MP1.0	16.8	18.0	17.9
	MP1.25	14.8	15.4	17.1
	MP1.5	12.8	14.3	17.1
Tarong	T1.0	25.4	30.0	33.5
	T1.25	28.8	31.0	34.3
	T1.5	31.7	33.5	37.8
	T1.625	34.9	36.6	41.3
	T1.75	32.7	34.5	38.7

The variation in compressive strength with AM for each fly ash geopolymer is presented in Figure 4.1 and Table 4.1. All reported strengths were mean value of three tested mortar cubes at specific period (Appendix B). Initially, all fly ash materials were tested at AM 1.0, 1.25 and 1.5. Additional testing was then undertaken in 0.125 increments to determine the optimum compressive strength. The Gladstone geopolymer gave the highest compressive strength at all ages and at each AM. The highest value for the Gladstone geopolymer is 60.6 MPa at 28-day, for G1.25 mix. However, all the other fly ash types show variations dependant on age and AM employed. The Mt.Piper and Collie geopolymers show the lowest compressive strength for all compositions and at all ages. While the Mt.Piper has a slightly higher compressive strength than the Collie at AM-1.0 for all three ages, it is always lowest at other AM. The Tarong geopolymer displays a lower compressive strength than Pt.Augusta

for AM-1.0 and AM-1.25 at 3 days, 7 days and 28 days. For the AM-1.5 specimens Tarong geopolymer was significantly higher than Pt.Augusta, with the difference in strength increasing with time.

The optimum 28-day compressive strength of Gladstone, Tarong, Pt.Augusta, Collie and Mt.Piper geopolymer mortar is shown in Figure 4.2. Gladstone geopolymer obtained the highest compressive strength while Mt.Piper and Collie geopolymers achieved the lowest strengths around 22 MPa. Both Tarong and Pt.Augusta geopolymers obtained moderate compressive strengths as ~41 MPa and ~36 MPa, respectively.

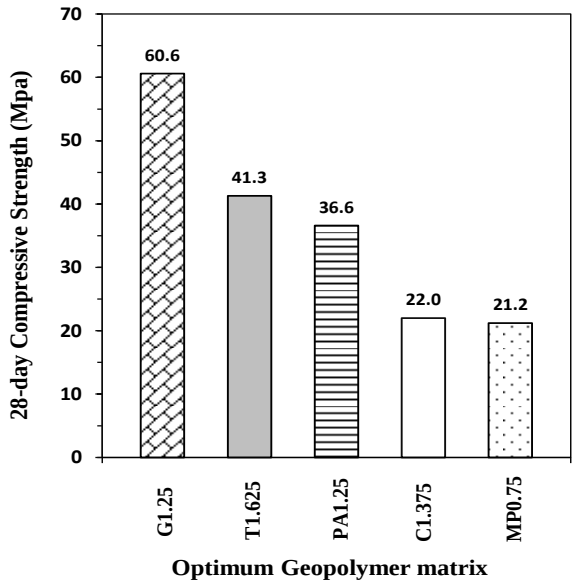

Figure 4.2 Optimum compressive strength of geopolymer mortar

4.3 Compressive strength development

Table 4.2 shows the percentage increase of compressive strength in different fly ash geopolymers at 28 days when compared to the respective 3rd day compressive strengths.

Table 4.2 Compressive strength development

Geopolymer	Mix	Compressive strength (MPa)		Strength gain (MPa)	*Strength development (%)
		3 days	28 days		
Gladstone	G1.25	56.0	60.6	4.6	8.2
Pt.Augusta	PA1.25	30.1	36.6	6.5	21.6
Collie	C1.375	16.7	22.0	5.3	31.7
Mt.Piper	MP0.75	19.2	21.2	2.0	10.4
Tarong	T1.625	34.9	41.3	6.4	18.3

*Percentage increase of strength at 28 days when compared to respective 3rd day strength

Gladstone geopolymer mortar obtained the lowest strength gain though it achieved highest compressive strength at 28 days. On the other hand, Collie geopolymer achieved the highest strength development between 3 and 28 days though it showed the lowest strength at 28 days. Both Pt.Augusta and Tarong geopolymers obtained about 20% of strength gain during this period. Previous studies have reported that the compressive strength of fly ash geopolymer concrete increased with age in the order of 10 to 20% when compared to the 7^{th} day compressive strength for ambient cured specimens (Wallah and Rangan, 2006). This is in contrast to PC concrete which gain significantly more strength over time. In the presence of water the main constituents of PC undergo a continuing hydration process, forming calcium silicate hydrate and calcium hydroxide, which result in strength gain over time (Neville, 1996). The geopolymerization process under the highly alkaline conditions involves a fast chemical reaction that result in a three dimensional polymeric chain and ring structure of Si-O-Al-O bonds (Davidovits, 1994). While Wallah and Rangan (2006) found that the compressive strength of ambient-cured fly ash geopolymer concrete significantly increased with the age. Palomo et al. (1999) have indicated that heat curing enhanced the initial geopolymerization process. The results from this work confirms the findings of Palomo et al. (1999) that heat curing results in little subsequent gain in strength from 3 to 28 days.

4.4 Factors affecting the compressive strength variation

4.4.1. Effect of Activator Modulus (AM)

The optimum 28-day compressive strength of Gladstone, Tarong, Pt.Augusta, Collie and Mt.Piper geopolymers are 60.6, 41.3, 36.6, 22.0 and 21.2 MPa, respectively (Figure 4.2). It was observed that the optimum 28-day compressive strengths occur at a range of different AM. The optimum strength of both Gladstone and Pt.Augusta were obtained at an AM of 1.25, while the optimum strength for Collie was obtained at AM of 1.375, Figure 4.3(a). In Tarong geopolymer, Figure 4.3(b), the AM was varied from 1.0 to 1.75, and optimum 28-day strength was obtained at an AM of 1.625. In Mt.Piper geopolymer, the AM was varied between 0.625 and 1.5 until the highest compressive strength was obtained at an AM of 0.75.

The results show no direct correlation between the AM and the compressive strength, though the lowest AM did lead to the lowest compressive strength. This indicates that chemical composition of the binder material may play an important role in the optimum AM and the ultimate compressive strength of geopolymer. Significant variation in the chemical

composition of the different fly ash was observed, Table 3.1. In particular in the SiO_2, Al_2O_3, CaO, Fe_2O_3 and alkali oxide content.

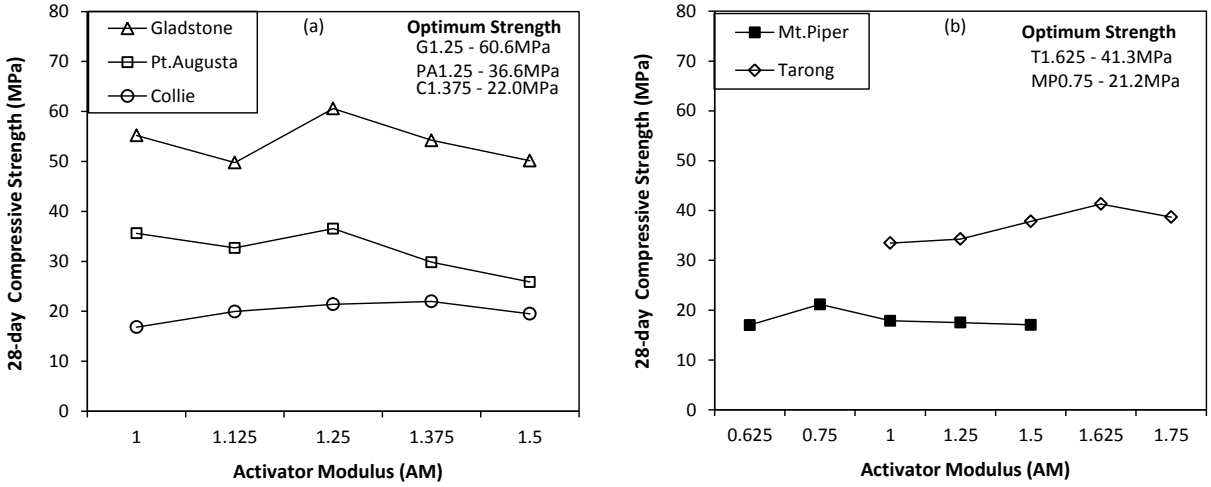

Figure 4.3 Optimum 28-day compressive strength vs. AM

4.4.2. Effect of chemical composition of fly ash

4.4.2.1. Effect of SiO_2 and Na_2O content

To assess the impacts of SiO_2 and Na_2O variations in the fly ash, the effective AM (AM_{eff}), Equation 3.1, was determined for the optimum performing fly ash, the Gladstone. The mix designs were varied for each of the other fly ash geopolymer mortar specimens to replicate the AM_{eff} for the Gladstone geopolymer, Table 3.8. The AM_{eff} was varied from 4.1 to 5.0, as shown in Table 3.9, for Pt.Augusta, Collie, Mt.Piper and Tarong based geopolymers until their optimum 28-day compressive strengths were achieved.

The variation in compressive strength with AM_{eff} of five different fly ash based geopolymer mortar is presented in Table 4.3. The optimized 28-day compressive strength based on AM_{eff} is also shown in Figure 4.4. While a general increase in strength was obtained for the geopolymer mixes with revised mix designs, none of the specimens reached the strength of the Gladstone geopolymer at any AM_{eff}. The highest compressive strength obtained by Pt.Augusta geopolymer, 45.6 MPa, was at the AM_{eff} of 4.3. However, compressive strength of Pt.Augusta decreased significantly with an increase of AM_{eff} from 4.8 to 5.0. The PA5.0 displayed the lowest strength, 12.1 MPa. This may be due to insufficient sodium hydroxide in activator solution which reduces dissolution of fly ash spheres (Thokchom et al., 2009). The Tarong, Collie and Mt.Piper mixes all showed a slight increase for the revised mix designs

based on AM_{eff}, but as for the original mix designs the Collie and Mt.Piper geopolymers showed the lowest compressive strengths for all mix designs, except AM_{eff}-5.0. The MP4.5 had a higher strength than the C4.5, but difference in strength of Mt.Piper and Collie geopolymers reduced with an increase of AM_{eff}.

Table 4.3 Changing compressive strength with AM_{eff}

Geopolymer	Mix	Compressive strength (MPa)	
		3 days	28 days
Pt.Augusta	PA4.1	26.0	34.7
	PA4.3	37.6	45.6
	PA4.5	37.6	39.6
	PA4.8	28.7	31.5
	PA5.0	8.9	12.1
Collie	C4.5	14.8	15.4
	C4.8	20.9	21.6
	C5.0	19.6	21.4
Mt.Piper	MP4.5	21.8	21.1
	MP4.8	22.6	23.3
	MP5.0	21.3	22.6
Tarong	T4.1	26.1	38.2
	T4.3	32.2	41.6
	T4.5	33.9	37.4
	T4.8	31.6	35.4
	T5.0	33.2	37.7

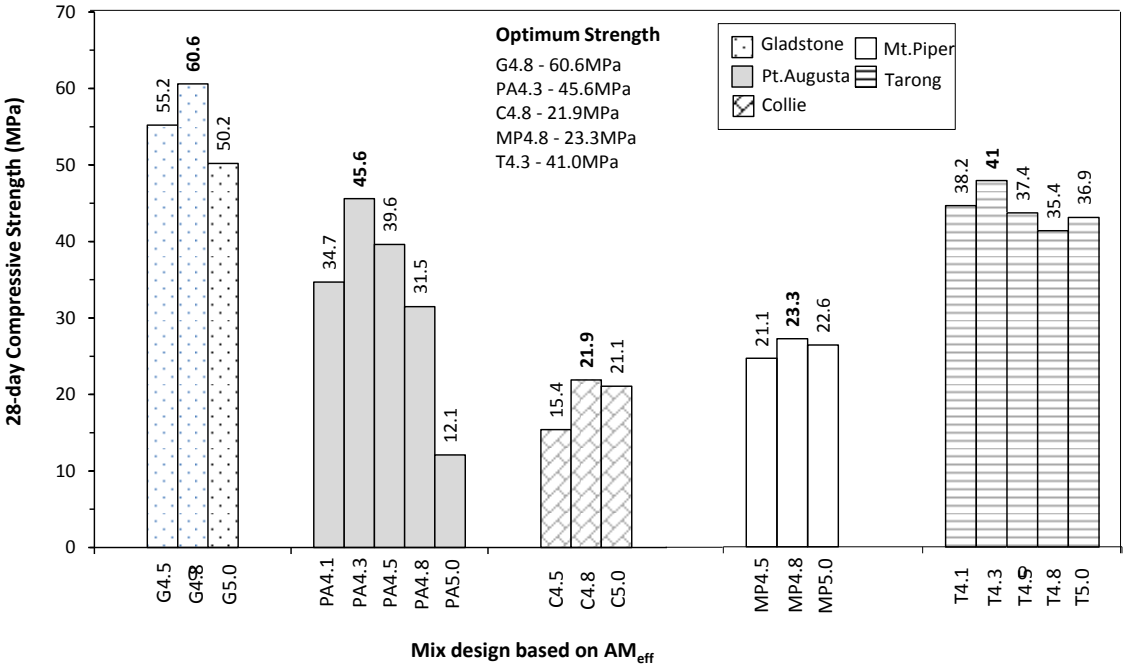

Figure 4.4 The 28-day compressive strength based on AM_{eff}

A comparison of optimum compressive strength obtained by each fly ash geopolymer, based on AM and AM_{eff} is shown in Figure 4.5. The Pt.Augusta geopolymer obtained considerable strength gain (9 MPa) with modified mix designs while Tarong and Collie geopolymers displayed a slight incremental gain in strength. The Mt.Piper geopolymer obtained a 2.1 MPa of strength increase. Therefore the results reported here indicate that even after SiO_2 and Na_2O content in fly ash is taken into account in mix design, a direct correlation between AM_{eff} and compressive strength is not evident. However, the data shows that Collie and Mt.Piper give the optimum compressive strength at same mix design of AM_{eff}-4.8, but both the Pt.Augusta and Tarong geopolymers give the optimum compressive strength at AM_{eff} - 4.3. This would indicate that even taking into account the SiO_2 and Na_2O content of the specific fly ash does not give a universal mix design for the optimum compressive strength. Overall, these results indicate that while the SiO_2 and Na_2O content of fly ash and activator have a significant impact it is not the only factor that determines the optimum mix design.

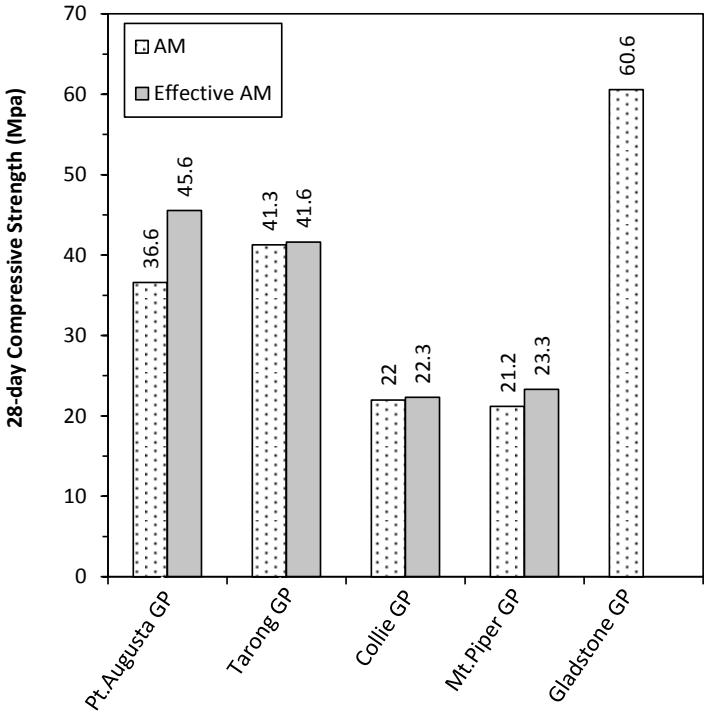

Figure 4.5 Optimum 28-day strength of geopolymers (GP) based on AM and AM_{eff}

4.4.2.2. Effect of SiO_2/Al_2O_3 ratio

Davidovits (1991) has suggested that certain synthesis limits exist for the formation of strong geopolymeric products; the satisfactory composition lies in the range 3.3 to 4.5 for the SiO_2/Al_2O_3 ratio. In this investigation, the SiO_2/Al_2O_3 ratio of Gladstone, Pt.Augusta and

Collie geopolymer mixes at all AM are in this range as shown in Figure 4.6(a)–A. But, the Mt.Piper and Tarong geopolymers gave optimal results in the range between 5.0 and 7.8, Figure 4.6(a)–B. This is in part due to the high SiO_2/Al_2O_3 composition in initial raw materials in Mt.Piper and Tarong. As the AM is defined by considering the activator solution only (Equation 2.1); the SiO_2/Al_2O_3 ratio of Tarong fly ash is twice that of Gladstone fly ash as shown in Table 3.1, thus Tarong geopolymer mixes have a much higher range compared to Gladstone geopolymer mixes. These results suggest that the optimum range will be affected by the chemical composition of the raw fly ash.

The SiO_2/Al_2O_3 ratio of geopolymer mix corresponding to the optimum AM in Gladstone, Pt.Augusta, Collie, Tarong and Mt.Piper are 4.0, 3.7, 4.2, 7.6 and 5.1, respectively. Figure 4.6(b) shows a linear relationship between SiO_2/Al_2O_3 ratio and optimum AM. The optimum AM increases with an increase in the SiO_2/Al_2O_3 ratio. The data shows that four of the five materials follow this linear relationship but the Mt.Piper does not. The Mt.Piper based geopolymer gives the best 28-day strength at AM of 0.75. However, using the relationship derived for the four other mixes the predicted range for the optimum AM is between 1.4 and 1.5.

Mt.Piper has larger unburnt carbon percentage that absorbs the activator solution. This may result in a lowering of the NaOH in activator solution, particularly at higher AM. As reported in the literature (Wang et al., 1994), when alkaline activation is insufficient and thus becomes the main factor slowing down the hydration of the slag, a lower modulus is preferred, otherwise a higher modulus is preferred. Thus, similar to the slag, higher alkali contents in the mixture yield better reactivity with the fly ash (Thokchom et al., 2009). Hence, it appears that the optimum AM of Mt.Piper has shifted to a lower value (0.75) despite the predicted range, between 1.4 and 1.5, as shown in Figure 4.6(b).

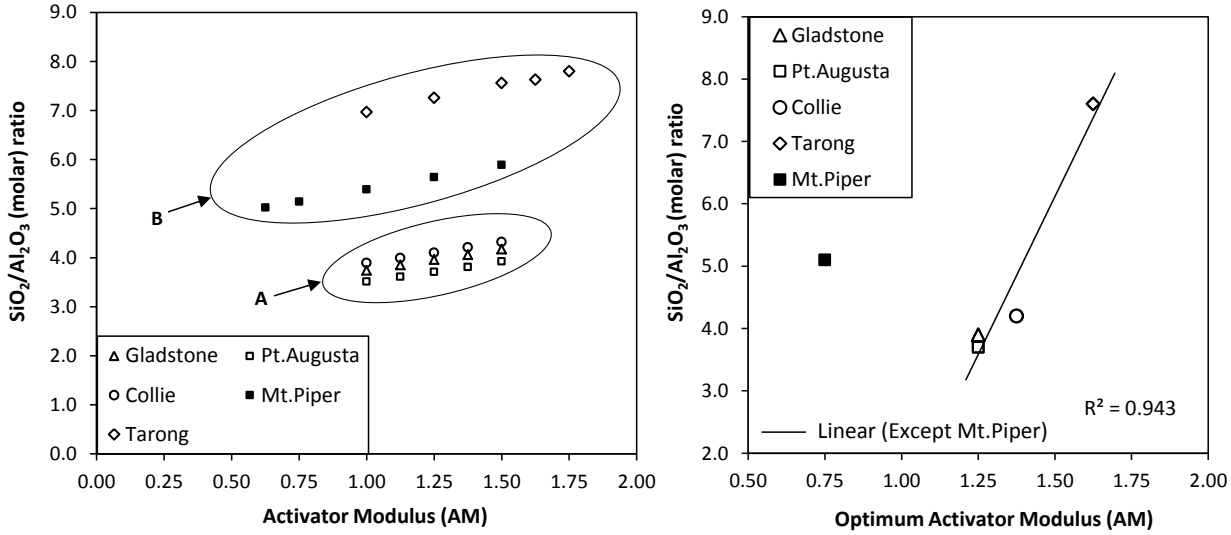

Figure 4.6 SiO_2/Al_2O_3 ratio vs. (a) AM and (b) Optimum AM

Figure 4.7 shows the optimum 28-day strength variation with SiO_2/Al_2O_3 ratio in the different geopolymer matrices. There is a small strength increment with increasing SiO_2/Al_2O_3 ratio up to 4.0. Previous studies also showed a similar trend of increasing strength with an increase of SiO_2/Al_2O_3 ratio and suggested SiO_2/Al_2O_3 ratios around 3.5–4.0 are regarded as the most suitable for optimal strength characteristics in geopolymers (De Silva et al., 2007). However, a significant decrease in compressive strength is observed for the Collie at a ratio of 4.2, and the Mt.Piper at a ratio of 5.1. Tarong, with a ratio almost twice that of G1.25 at a ratio of 7.6, achieved the second highest compressive strength. These results indicate that SiO_2/Al_2O_3 ratio has no clear influence on compressive strength, and that other factors (which are discussed below) are more dominant in determining compressive strength.

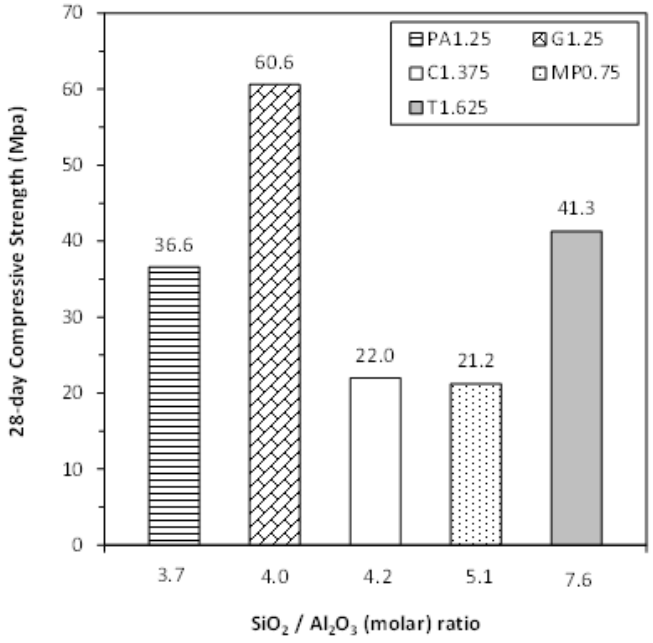

Figure 4.7 Compressive strength vs. SiO_2/Al_2O_3 ratio

4.4.2.3. Effect of CaO and Fe_2O_3 content

The calcium oxide (CaO) content has been reported as an important factor affecting final compressive strength in geopolymers; increasing CaO content in fly ash appears to have a positive influence on the compressive strength of geopolymers (Diaz et al., 2010, Van Jaarsveld and Van Deventer, 1999). Conversely a high percentage of iron oxides (Fe_2O_3) produce relatively low compressive strength in geopolymers (Fernandez-Jimenez and Palomo, 2005). Thus, both CaO and Fe_2O_3 have been hypothesized as affecting the final compressive strength. The optimum 28-day strength vs. CaO content and Fe_2O_3 content are shown in Figure 4.8(a) and Figure 4.8(b), respectively. The PA1.25 has highest CaO with lower Fe_2O_3 content. The G1.25 has second highest CaO with significantly high Fe_2O_3 content, but displayed the best compressive strength out of the five geopolymer mortars and the PA1.25 had the third highest strength. The T1.25 has lowest CaO and Fe_2O_3 content, but achieved the second highest compressive strength. The C1.375 and MP0.75 obtained the same strength having a similar CaO content but their Fe_2O_3 content is significantly different. Overall the data indicates that there is no direct relationship between the CaO and Fe_2O_3 content and compressive strength. As such, while both CaO and Fe_2O_3 content in fly ash have an influence to the final strength of geopolymer mortar, their percentage alone should not be used as a basis for predicting the ultimate compressive strength. More comprehensive discussion related to CaO content in fly ash is discussed in Section 4.5.

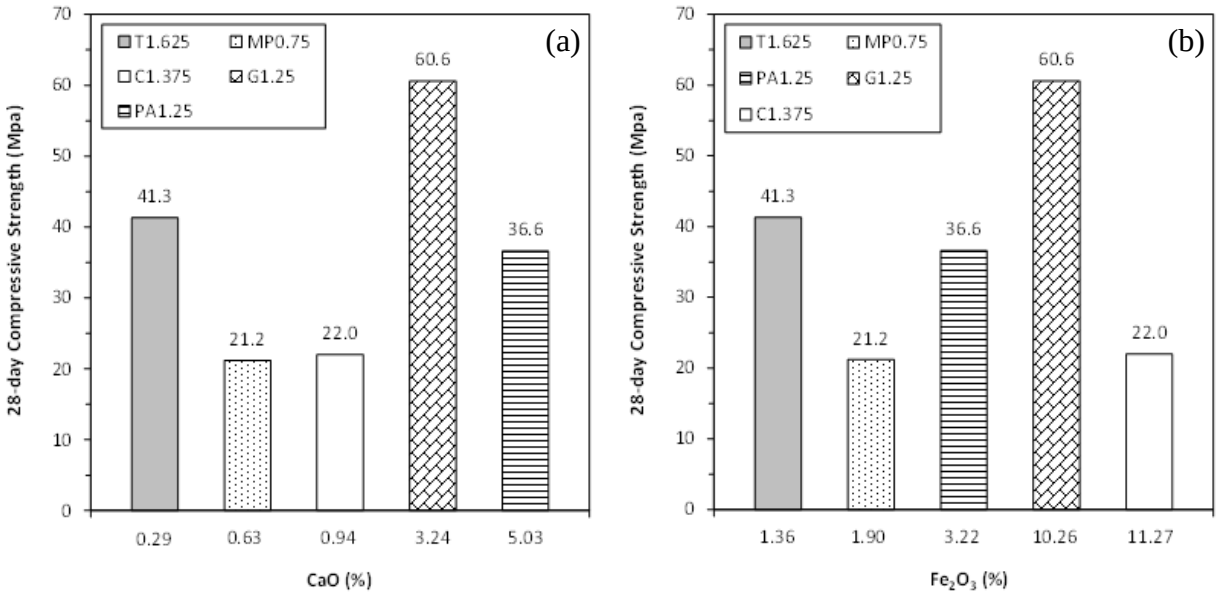

Figure 4.8 Compressive strength vs. (a) CaO content and (b) Fe_2O_3 content

4.4.3. Effect of physical properties of fly ash

4.4.3.1. Particle size distribution and Specific Surface Area (SSA)

The particle size distribution of the raw fly ash has been identified as influencing the compressive strength achieved for the geopolymer mortar produced, with an increase of finesses leading to an increase compressive strength (Van Jaarsveld et al., 2003, Pimraksa et al., 2011, Sathonsaowaphak et al., 2009, Fernandez-Jimenez and Palomo, 2003). Fineness is generally defined as the percentage of particles passing at a specified sieve size. The effect of fineness acts two ways; during the mixing of geopolymer, the activator solution demand rises as the fineness of the fly ash decreases due to the need to fill larger voids among coarser fly ash particles to achieve a workable material. On the other hand, the finer the fly ash particles, the greater the surface area, resulting in a more reactive fly ash, as a significant part of the reaction occurs at the particle-liquid interface. Previous research has reported that when the particle fraction size higher than 45μm is removed, the strength increased (Fernandez-Jimenez and Palomo, 2003). They further examined that when the particle fraction size higher than 45 microns is removed, the compressive strength increased achieving 70MPa in one day.

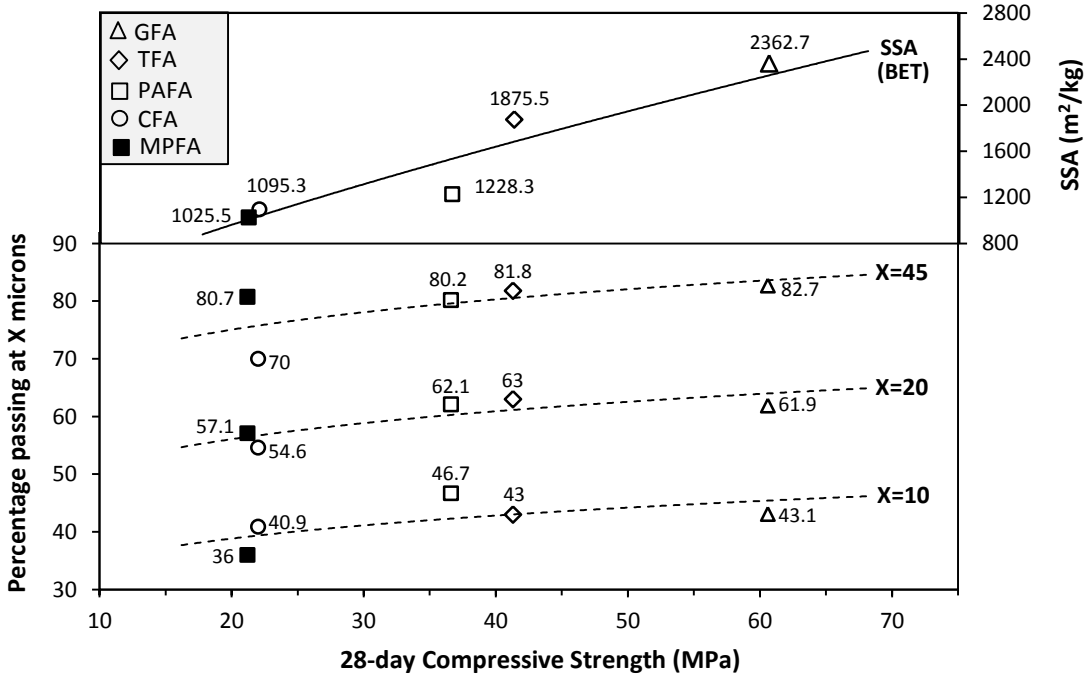

Figure 4.9 Compressive strength vs. Particle size distribution and SSA

Analysis of different particle sizes (10μm, 20μm, 45μm) and the surface area versus the compressive strength is displayed in Figure 4.9. The data shows that the best correlation is achieved between the particles passing the 10μm and 20μm sieve, while the strength vs. specific surface area shows an increase of strength with an increase of surface area. In all cases the Collie and Mt.Piper, which give the lowest compressive strength have the lowest percentage passing the sieve sizes 10 and 20μm. At 45μm, Mt.Piper has a slightly higher percentage passing compared to the Pt.Augusta, while Collie is significantly lower, despite both having very similar compressive strengths. This is contrary to the observation of Fernandez-Jimenez and Palomo (2003), i.e. the percentage of particles with size lower than 45μm between 80 and 90% leads to an optimum compressive strength but is in agreement with the data of Tennakoon et al. (2014b), who observed that the highest compressive strength is obtained with fly ash with the lowest mean particle size in geopolymer mortar samples. A significant difference between the Collie and Mt.Piper with the Gladstone, Pt.Augusta and Tarong is the specific surface area, i.e. Collie and Mt.Piper have lowest surface area. Thus, the lowest compressive strength is achieved by the fly ash with lowest quantity of particles passing at the 10 and 20μm sieve size coupled with smallest surface area.

Mortar samples using Gladstone fly ash has compressive strengths of over 60MPa compared to 36.6MPa for the Pt.Augusta and 41.3MPa for the Tarong. All three fly ash has a very similar percentage passing at both the 10μm and 20μm sieve size. However, considering their specific surface area values, the Gladstone has the greatest followed by Tarong and Pt.Augusta, respectively (Figure 4.9), illustrating that the strength variation of these three materials is well correlated with surface area. This would suggest that while a higher level of particle percentage passing at both the 10μm and 20μm sieve size in the precursor fly ash does improve the performance, specific surface area of fly ash has the higher weighting factor in determining the compressive strength. Overall, the specific surface area of precursor fly ash coupled with the quantity of particles passing at the 10 and 20μm sieve size is strongly contributing to the compressive strength development.

4.4.3.2. Unburnt carbon content

The percentage of unburnt carbon in fly ash has also been identified as a critical factor when assessing the geopolymerization as it acts as an inert particulate and absorbs the activator solution. Therefore, obtaining a workable mixture requires a volume of activator solution beyond that needed to merely activate the source material to account for the activator absorbed by the unburned carbon present in the fly ash. The unburnt carbon can cause more unreacted and partially reacted fly ash spheres in the geopolymer matrix formed, resulting in a lower compressive strength (Diaz et al., 2010, Fernandez-Jimenez and Palomo, 2003).

Optimum 28-day strength vs. unburnt carbon content of fly ash is shown in Figure 4.10. The G1.25 has lowest unburnt carbon content and gives the highest compressive strength. Conversely, the MP0.75 has the highest unburnt carbon content and showed the lowest compressive strength. The C1.375 had a similar strength to MP0.75 but only half of the MPFA's unburnt carbon content. The Collie has lowest fineness ratio at 45 and 20 micron sieve size which would be expected to result in larger voids among coarser fly ash particles giving a smaller particle-liquid interface. This is hypothesized as the reason that C1.375 did not achieve the same strength gain despite having the lower unburnt carbon content.

Tarong has second highest unburnt carbon percentage, more than twice of Pt.Augusta. But, T1.625 gave the second highest compressive strength, followed by P1.25. Tarong had a higher surface area with a larger quantity of fine particles than Pt.Augusta. Moreover, the Tarong had a significantly higher SiO_2 percentage than Pt.Augusta (73% and 49%

respectively). Formation of aluminosilicate gel which develops the strength is dependent on the quantity of Si^{4+} leaching from the fly ash. Other authors have shown that higher amounts of reactive SiO_2 result in a higher degree of geopolymerization and consequently higher mechanical strength (Van Jaarsveld et al., 2003, Fernandez-Jimenez and Palomo, 2003). Thus, overall the effect of higher surface area, higher fine particles and larger quantity of Si^{4+} ion leaching is expected to increase the degree of geopolymerization and concurrent gel formation in Tarong. Hence, this is believed as the cause of the higher strength of T1.625 than PA1.25, though having the second highest unburnt carbon percentage. These results would indicate that unburnt carbon percentage is a negative influence on compressive strength, but combinations of other factors are more dominant in determining compressive strength.

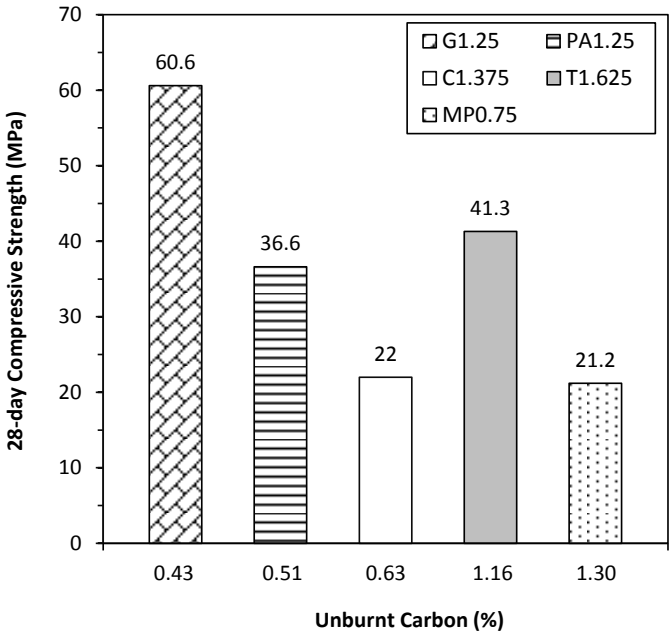

Figure 4.10 Compressive strength vs. unburnt carbon content

4.4.4. Effect of rheological behaviour of geopolymer

4.4.4.1. Effect of workability

The data has shown that the particle size distribution is related to the compressive strength. A parameter that is governed by the material fineness is the workability of the mortar. A very fine material can lead to an increased demand for activator, which can reduce the workability, though it can also result in a higher degree of reactivity and hence an improvement in the

ultimate strength achieved. The workability (flow) verses compressive strength is presented in Figure 4.11.

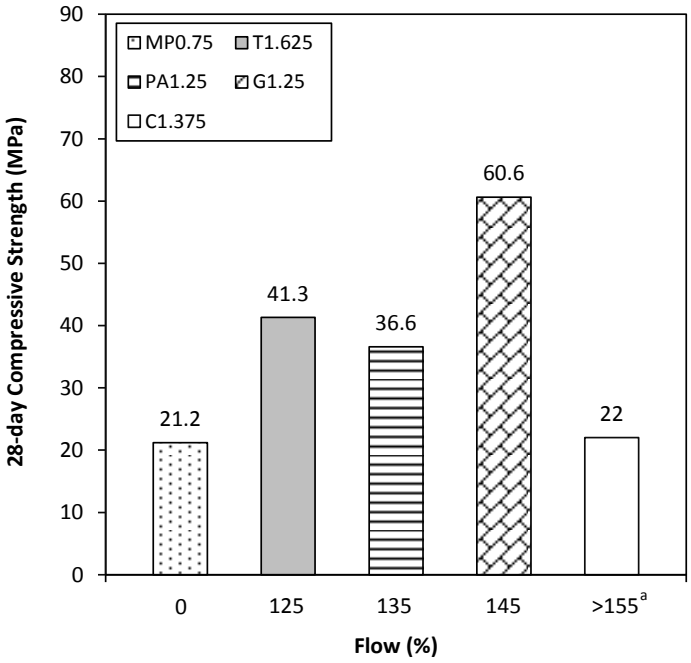

[a]Maximum measureable limit from the flow table

Figure 4.11 Compressive strength vs. workability of geopolymers

A previous study states that the optimal workable flow for high calcium geopolymer mortar is in the range of 110 ± 5% to 135 ± 5% to allow easy placement into the mould (Chindaprasirt et al., 2007). This leads to better compaction, which in turn results in higher compressive strength. In this investigation the Tarong and Pt.Augusta mixes gave a flow value within this range, 125% and 135% respectively, with compressive strengths of 41.3 and 36.6MPa. The Gladstone has the highest fineness ratio which gave the highest compressive strength of 60.6MPa and had a slightly higher workability of 145%.

The Collie mix, however, exceeded the flow table limit, demonstrating very high fluidity during placement into the moulds. The Collie has the lowest percentage passing at 20 and 45μm, the second lowest percentage passing 10μm and the second lowest surface area. This is hypothesised as the reason for the high fluidity. With an increase in fluid content, particle to particle interaction of the fly ash is less due to a larger inter-particle distance and lower particle interference, hence a lower compressive strength is obtained.

The Mt.Piper resulted in a very stiff mix with no flow value and experienced difficulties in obtaining uniform mixing and compaction. This is attributed to the high unburnt carbon

content in the Mt.Piper as shown in Table 3.1. The unburnt carbon in fly ash acts as an inert particulate and absorbs the activator solution. Therefore, obtaining a workable mixture requires a volume of activator solution beyond that needed to merely activate the source material to account for the activator absorbed by the unburned carbon present in the fly ash. Tarong has a higher fineness ratio and greater surface area than Pt.Augusta. However, the Tarong has an unburnt carbon only slightly less than Mt.Piper, and more than twice that of the Pt.Augusta. This is hypothesized as the cause of the slightly lower workability of the Tarong compared to the Pt.Augusta.

The results suggest that the workability does have an influence on the compressive strength, and that the acceptable range of low calcium fly ash geopolymers can be extended to 145% ± 5% from the 135 ± 5% previously identified (Chindaprasirt et al., 2007). A very high or very low flow can both have a negative impact on the compressive strength. The workability itself is influenced by a combination of particle size distribution and the unburnt carbon content, both of which should be considered when assessing the fly ash.

4.4.4.2. Geopolymer matrix vs. Workability

The nature of the geopolymer matrix formed in five different fly ash geopolymer mortar is displayed in Figure 4.12. Gladstone geopolymer has a well compacted, uniform, denser pore structure with the least amount of unreacted/partially reacted fly ash grains. It further contains the fewest number of micro-cracks. This is consistent with the high compressive strength observed in Gladstone. Both the Pt.Augusta and Tarong displayed similar microstructures, being heterogeneous in nature, with an increased number of unreacted/partially reacted fly ash spheres observed. An increased number of micro-cracks were also observed in both Pt.Augusta and Tarong geopolymer matrices compared to the Gladstone. These observations would explain the strength difference between Pt.Augusta and Tarong compared to Gladstone. All three geopolymers are in the acceptable workability range, and show a lower amount of unreacted/partially reacted compounds and micro-cracks than the Collie and Mt.Piper.

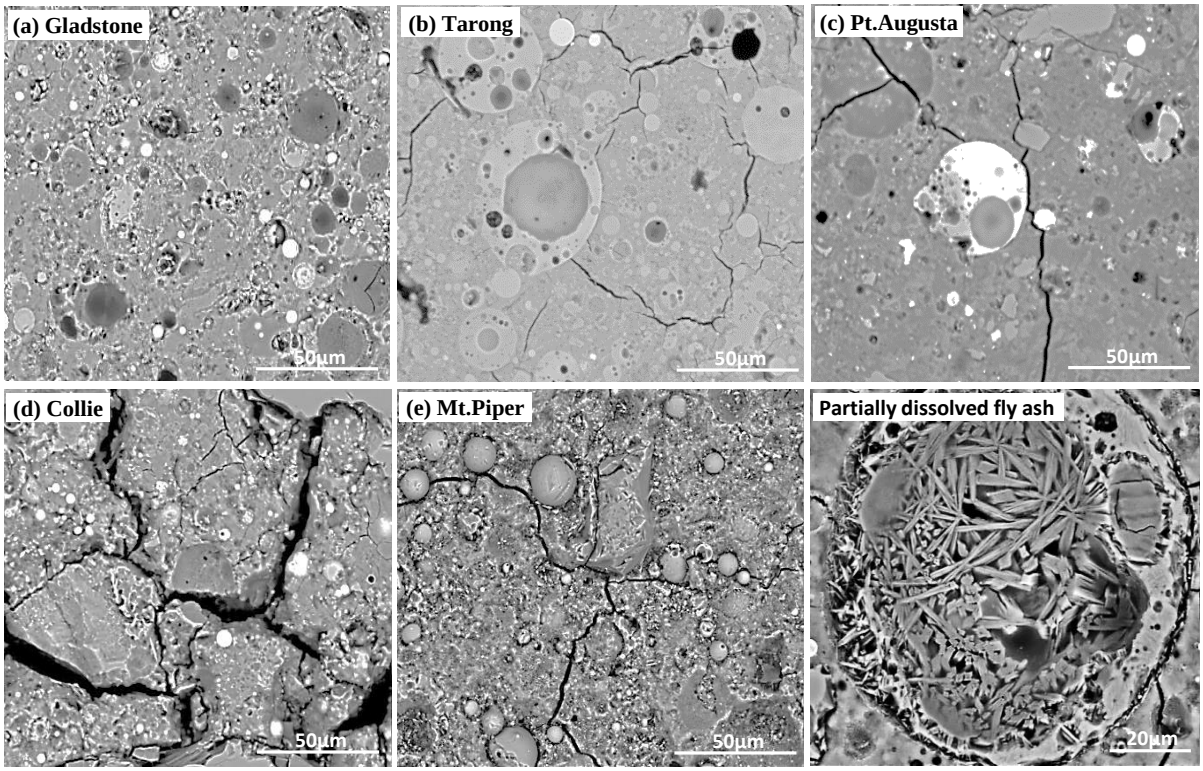

Figure 4.12 SEM image on microstructure of five fly ash geopolymers

The Collie has a microstructure with widely propagated micro-cracks. The width of the cracks was visibly larger than those in the other geopolymer matrices. These cracks separated the material into several small pieces making discontinuities in the matrix. Due to the very high fluidity of the initial mix, Figure 4.11, it is hypothesised that this results in a more rapid dissipation in the geopolymerization process. This would produce the discontinuity identified in the microstructure. The Mt.Piper has a higher amount of unreacted fly ash grains, making up a significant proportion of the total volume of the binder, and a large number of propagated micro-cracks. The Mt.Piper geopolymer mix was very stiff, non-workable and achieving a uniform mix was difficult, which is hypothesised as the reason for the unreacted grains. These materials are composites, hence the strength of the unreacted particles, the interface between them and geopolymer matrix is expected to have a significant bearing on the overall strength of the material (Steveson and Sagoe-Crentsil, 2005). The above observation correlate well with the observed lowest compressive strengths achieved for Mt.Piper and Collie geopolymer types. The results also suggest that the degree of unreacted/partially reacted particles and micro-cracks propagation is dependent upon the workability of the material.

4.4.4.3. Effect of viscosity

The rheological behaviour of concentrated geopolymer mortar was non-Newtonian, and showed a pseudoplastic type of flow behaviour. For geopolymer dispersions the particle size distribution and particle-particle interaction become important controlling factors for the pseudoplastic behaviour. The apparent viscosity of Mt.Piper is difficult to measure due to the lack of workability and high stiffness of the mortar a few minutes after mixing and so the data here are presented only for the other four materials.

The maximum apparent viscosity, η_{max}, of four geopolymers varied significantly though they have the identical water/solid ratio. When η_{max} increases the workability increases in all geopolymers. This runs contrary to the expectation that the higher the viscosity the lesser would be the flowability. The relative viscosity (η/η_{max}) against normalized shear rate $(\dot{\gamma}/\dot{\gamma}_{max})$ is shown in Figure 4.13.

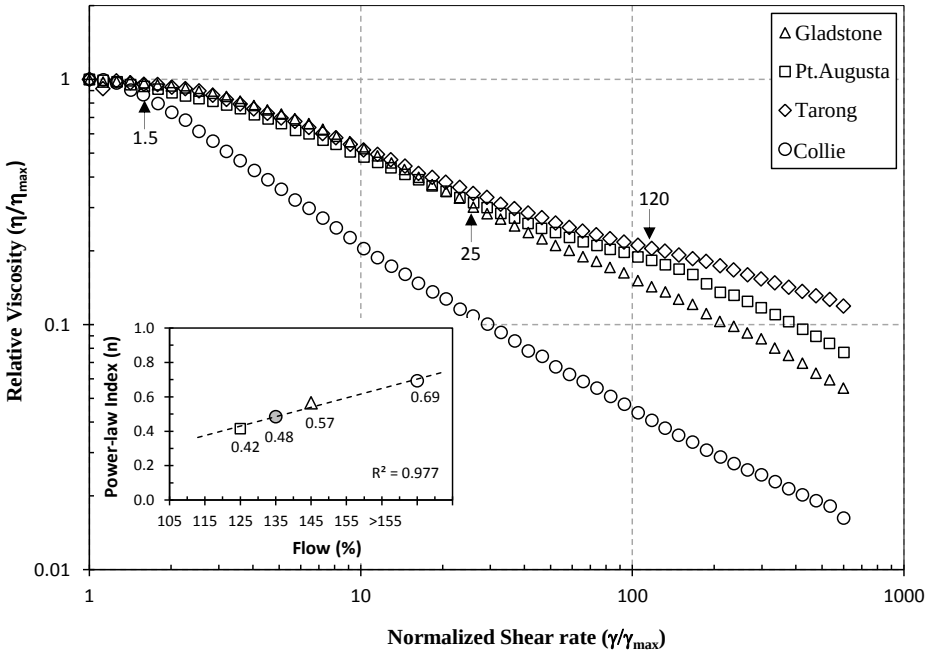

Figure 4.13 Relative viscosity vs. Normalized shear rate

The η_{max} corresponds to the maximum value of viscosity observed in experiments and $\dot{\gamma}_{max}$ is the shear rate at which the decrease in the viscosity with shear rate is first observed. On the normalised scale of Figure 4.13 the response of the Gladstone, Tarong and Pt.Augusta are identical for $\dot{\gamma}/\dot{\gamma}_{max} \lesssim 25$ and $(\eta/\eta_{max}) \sim (\dot{\gamma}/\dot{\gamma}_{max})^{-0.33}$. However for Collie $(\eta/\eta_{max}) \sim (\dot{\gamma}/\dot{\gamma}_{max})^{-0.66}$, indicating a much stronger dependence of the relative viscosity

on the imposed shear rate. For $\dot{\gamma}/\dot{\gamma}_{max} > 25$, the differences between Gladstone and the other two materials become more evident, but only after $\dot{\gamma}/\dot{\gamma}_{max} > 120$, is the difference between the flow behaviours of Pt.Augusta and Tarong significant. The measured workability therefore appears to correlate well with the shear thinning nature of the fluids in the regime where differences in the slopes of the flow curves are most obvious ($\dot{\gamma}/\dot{\gamma}_{max} > 120$). The workability also correlates well with the shear thinning exponent (m) in $(\eta/\eta_{max}) \sim (\dot{\gamma}/\dot{\gamma}_{max})^{-m}$, which decreases as Collie > Gladstone > Pt.Augusta > Tarong. It can be observed from Figure 4.11 that the workability increases in exactly the same order of relative viscosity for the materials tested.

It is interesting to note that when $\dot{\gamma} \rightarrow 0$, the value of η_{max} increases as Collie > Gladstone > Pt.Augusta > Tarong. Also it can be observed from Figure 4.9 that the particle size of Collie is considerably coarser (larger effective diameter). It has recently been shown that the shear thinning exponent, m, depends both on the particle size and the aspect ratio of the particles as well as on the ratio of the volume fraction to the maximum packing fraction (Mueller et al., 2009). Fly ash particles are typically spherical and so the effective particle diameter plays a dominant role in determining the maximum packing fraction. Indeed if the particle diameter is large, the shear thinning exponent, m, would be larger. The evidence provided in Figure 4.9 and Figure 4.13 indicates that the particle size and its distribution significantly influence the workability, i.e. the geopolymer mortar becomes more workable as the quantity of coarser particles increased, although it is difficult to quantify the exact extent.

4.4.5. Effect of mineralogical composition of fly ash

The XRD patterns of fly ash precursors and their resultant geopolymers is shown in Figure 4.14. While the XRD patterns displayed peaks due to crystalline phases; quartz, mullite, rutile and iron oxide (either magnetite or hematite), all fly ash are primarily amorphous in nature. As the geopolymerisation reaction progressed the percentage of amorphous content detected was significantly lower in the geopolymer product than in its fly ash precursor. The intensity of crystalline peaks of fly ash precursors also progressively decreased after the geopolymerization process. However, while both the crystalline and amorphous phases reduced, the amorphous reduction was greater. This would be anticipated as amorphous compounds are easier to dissolve than crystalline compounds during the initial step of the geopolymerization process, yielding higher amounts of reactive SiO_2 and Al_2O_3 to combine

during the transportation/coagulation phase of the geopolymeric reaction. This increases the rate of geopolymerization, thus giving high compressive strength (Wang et al., 2005, Fernandez-Jimenez and Palomo, 2005, Van Jaarsveld et al., 2003).

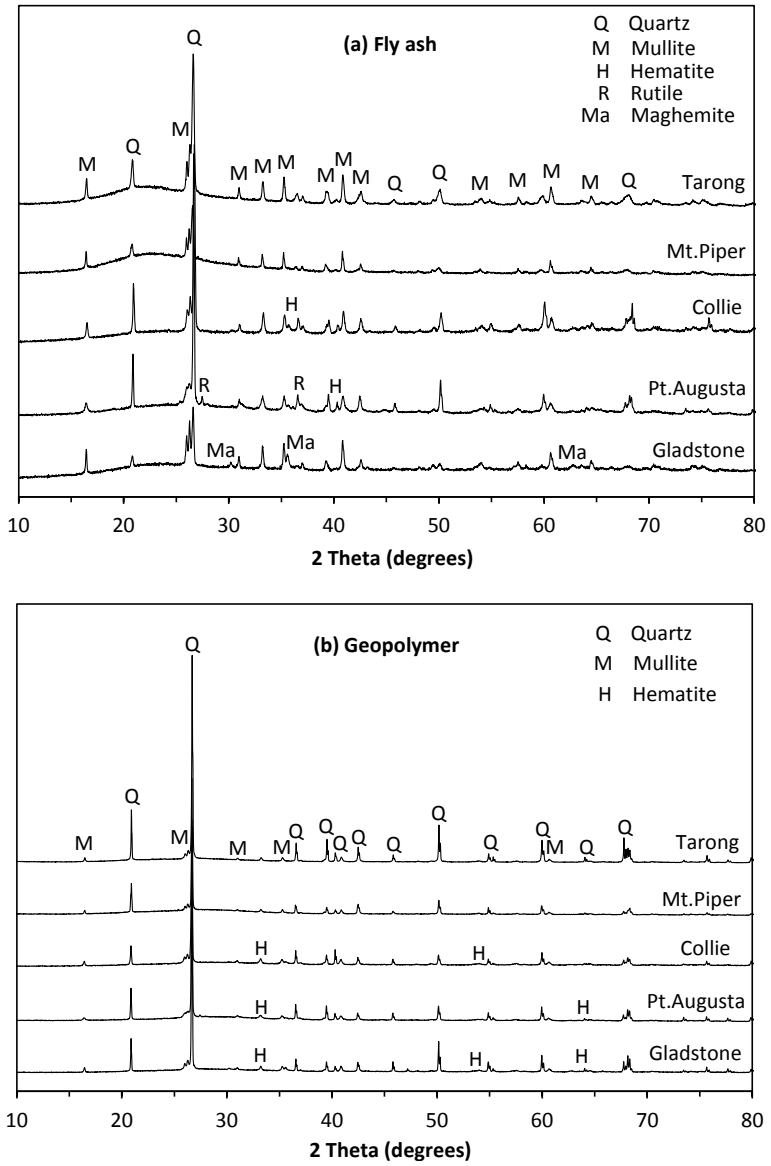

Figure 4.14 Crystalline phases in (a) precursor fly ash and (b) resultant geopolymer mortar

The quantitative analysis of mineralogical composition of fly ash precursors and their resultant geopolymers is shown in Figure 4.15. Moreover, the effect of amorphous percentage in fly ash on the compressive strength of geopolymer mortar is shown in Figure 4.16.

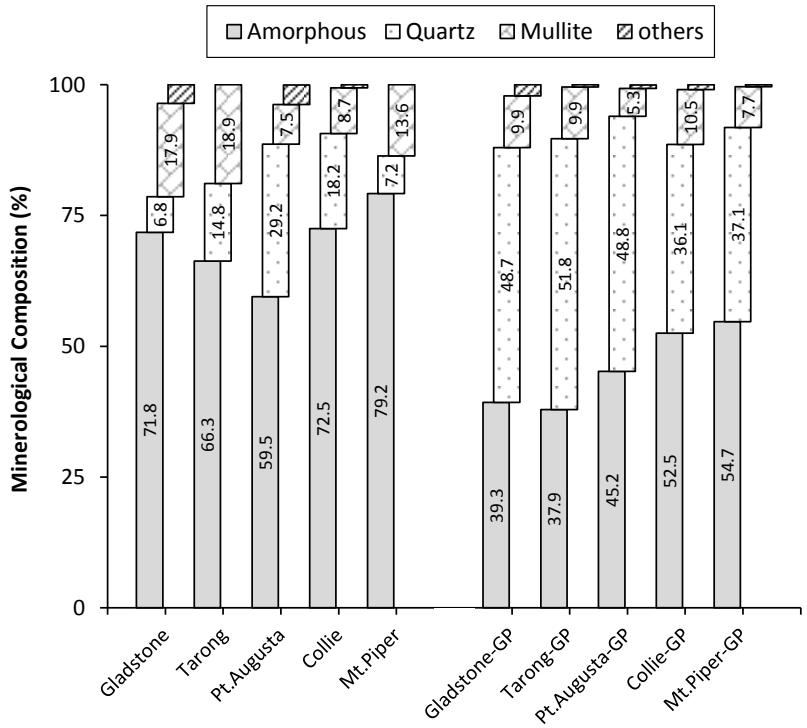

Figure 4.15 Mineralogical composition of fly ash and resultant geopolymers

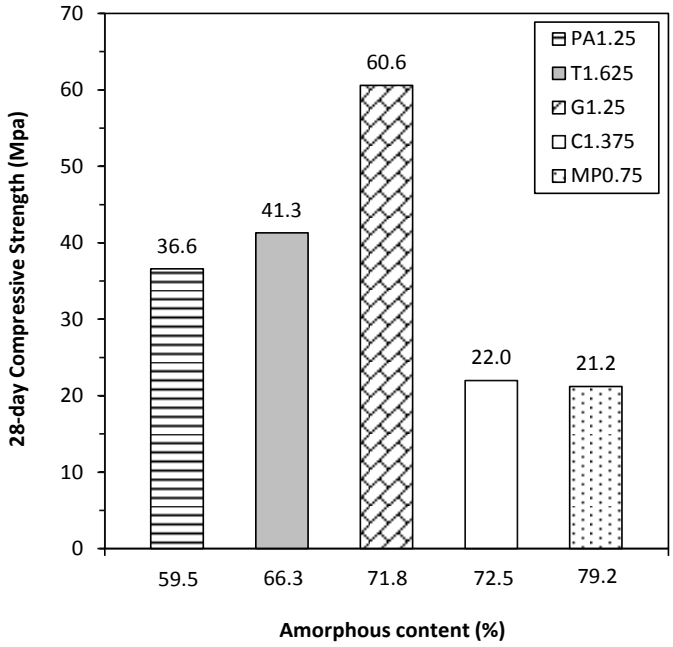

Figure 4.16 Compressive strength vs. amorphous content

According to the quantitative analysis, shown in Figure 4.15, the percentage of amorphous content in the Gladstone, Tarong and Pt.Augusta were 71.8%, 66.3% and 59.5%, respectively. Such differences in the amorphous content could explain the different compressive strength values displayed by fly ash after being subjected to the activation

process. The higher the content of the amorphous percentage in the fly ash, the higher the degree of reactions (Alvarez-Ayuso et al., 2008). Considering the Gladstone, Tarong and Pt.Augusta based geopolymers, their 28-day compressive strength is correlated with the amorphous content in their original fly ash precursors, Figure 4.16; Gladstone having higher amorphous percentage than Tarong and Pt.Augusta, thus G1.25 has higher geopolymerization, resulting in the highest compressive strength. When high contents of quartz and mullite phases present in the fly ash, the reactivity of the Si-Al bearing fraction decreases drastically (Van Jaarsveld et al., 2002). Summation of quartz and mullite in Tarong is lower than Pt.Augusta. The Tarong has a significantly higher SiO_2 percentage than Pt.Augusta (73% and 49% respectively), and the effect of this difference on strength variation is explained in 4.4.2.2.

The Mt.Piper and Collie have the highest amorphous contents, 79.2% and 72.5% respectively. However, in the geopolymer produced, less of this amorphous phase was converted than for both the Gladstone and Tarong materials, both of which gave higher compressive strength. It was noted that the amount of amorphous phase converted in Mt.Piper and Collie was higher than the Pt.Augusta, though the relative percentages were similar. The results would suggest that the reaction of the amorphous phase is a primary factor in the compressive strength produced, but that other factors, such as the particle size, surface area and workability, can impact significantly on the strength of the geopolymer produced.

4.5 Zeta potential and gel formation

The surface layer of fly ash particles contain a significant amount of readily leachable elements (Iyer, 2002), while the elements enriched in the cores of fly ash particles are not directly exposed to leaching and therefore their release are diffusion controlled and also dependent on the dissolution rates of the surface layers (Kukier et al., 2003). Surface associated elements are therefore more susceptible to leaching in an aqueous environment. Table 4.4 tabulates the quantity of cations leached from five different fly ash in water. Moreover, elements leached from fly ash in water and the pH changes in fly ash-water system are shown in Figure 4.17.

Table 4.4 Quantity of cations leached from different fly ash in water

Fly ash	Element Leaching - Concentration (ppm)							pH
	Si	Al	K	Mg	Na	Ca	Total	
Gladstone	5.0	6.2	3.4	1.0	0.5	60.2	76.2	10.8
Port Augusta	4.1	1.6	1.6	3.9	1.5	40.5	53.3	8.7
Tarong	2.1	1.3	0.2	0.5	0.1	4.5	8.6	4.8
Collie	3.3	7.8	1.1	2.4	0.4	6.5	21.5	4.3
Mount Piper	2.4	3.2	1.7	0.6	0.1	9.8	17.9	4.6

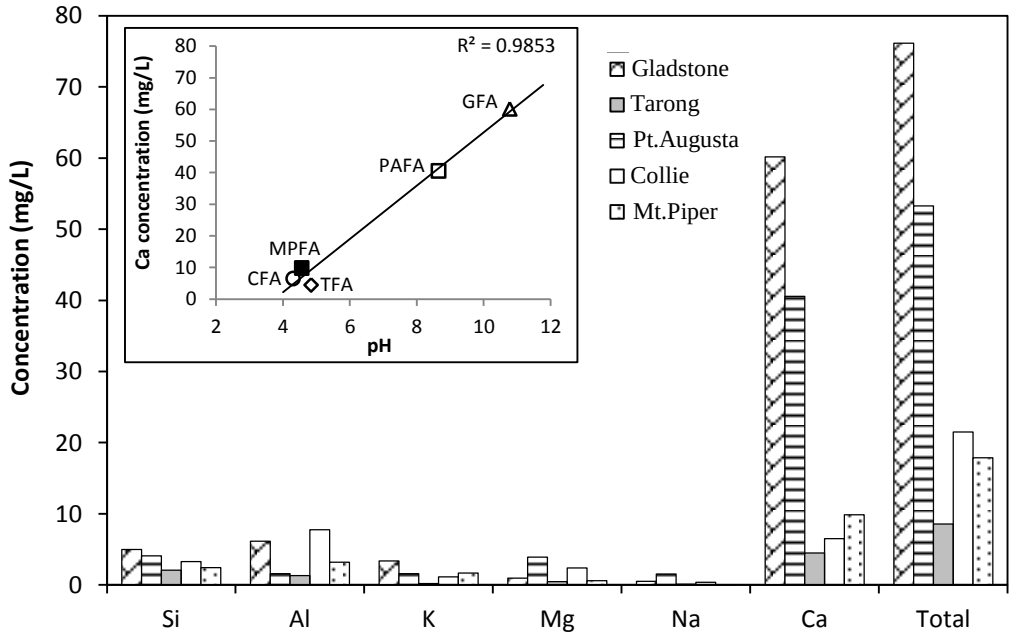

Figure 4.17 Elements leached from fly ash in water and pH changes

The principal element leached from fly ash is Ca, and the extent of this Ca^{2+} ion dictates the pH of the fly ash–water system. Both the Gladstone and Pt.Augusta have high CaO content, Table 3.1, which is reflected in the increased pH in water.

A high concentration of alumina and silica functional groups is present at the surface of the fly ash particles. The most common anionic groups at the surface being silicates ($-O-SiO_2^-$) and aluminates ($-O-AlO^-$) (De Silva et al., 2007), which is shown in Table 3.1. The changing zeta potential with pH in the fly ash-water system is presented in Figure 4.18. It would be expected that the aluminate and silicate surface groups of Gladstone and Pt.Augusta would become more extensively deprotonated due to their higher pH in fly ash-water system and

yield a negatively charged surface. This is confirmed by the significantly higher negative zeta potential in Figure 4.18.

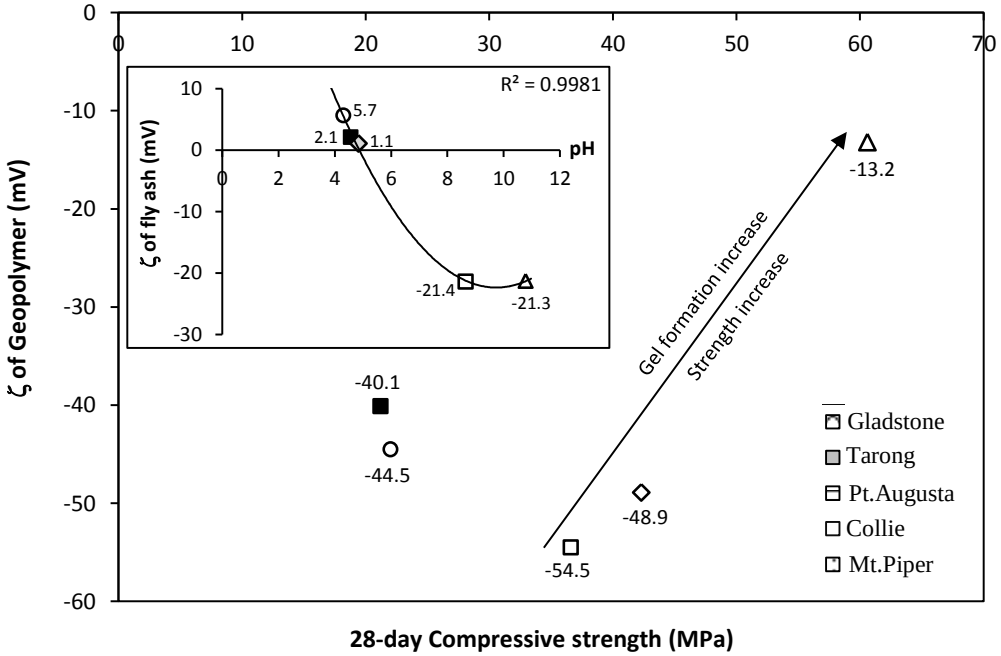

Figure 4.18 Zeta potential (ζ) of fly ash and geopolymer suspensions in water

In contrast, Tarong, Collie and Mt.Piper show a positive zeta potential. The Na^{+}, K^{+}, and Ca^{2+} ions determine the zeta potential of fly ash (Nägele and Schneider, 1989). Aluminate and silicate groups have different charges as a function of pH and can undergo interactions with various ions (Lieberman et al., 2015). These three fly ash have less than 1% of CaO, have less aluminates and silicates at the surface and, as such are acidic, with the pH varying between 4.3 and 4.8, rather than alkaline as for Gladstone and Pt.Augusta. This leads to an accumulation of cations in the double layer, giving these fly ash a slightly positive zeta potential. The fly ash with negative zeta potentials will react more readily, due to the excess of reactive silicate and aluminate groups on the surface. Hence, a negative zeta potential for the fly ash is indicative of a more reactive material.

However, once geopolymerization did occur the zeta potentials of the geopolymers all gave negative values, Figure 4.18. The Gladstone geopolymer has the smallest value, -13.2mV, the other four gave values between -40 to -55 mV, regarded as being in the fairly stable range for agglomeration, while the Gladstone geopolymer is in on the threshold value for agglomeration (Riddick, 1968). The small zeta potential would indicate that the Gladstone geopolymer will more readily form the gel layer and hence could account for the higher

compressive strength observed. When fly ash react with sodium hydroxide aqueous solution, the aluminate species form $[Al(OH)_4]^-$ and the silicate species form either $[SiO(OH)_3]^-$ or $[SiO_2(OH)_2]^{2-}$ (Sagoe-Crentsil and Weng, 2007), hence a negatively charged surface is formed while establishing a double layer. The Na^+ ions of the alkaline activator, will then react with these negatively charged surface groups and form a sodium-aluminosilicate gel layer on their surfaces. Thus, according to the Sagoe-Crentsil and Weng (2007), the accumulation of more Na^+ ions in the double layer while forming gel resulted in a decrease of zeta potential.

It has previously been reported that the time for the supersaturated alumina silicate species solution to form a continuous gel varies considerably with raw material, processing condition and solution composition (Duxson et al., 2007b). The largest specific surface area (2362.7 m^2/kg) coupled with highest quantity of particles passing at the 10 and 20µm sieve size is attributed to the rapid formation of gel in Gladstone geopolymer. Both Gladstone and Pt.Augusta have high CaO content, which produce a more negatively charged surface at on initial dissolution. This is consistent with the observation that the amount of CaO in raw fly ash is an important factor affecting final strength in geopolymers; increasing CaO content in fly ash has been reported as having a positive influence on the compressive strength of geopolymers (Van Jaarsveld and Van Deventer, 1999, Diaz et al., 2010).

4.6 Conclusions in Chapter 4

Five types of geopolymers were synthesized in this study from different Australian fly ash. Overall the data indicates that a number of inter related factors influence the compressive strength of the geopolymer.

- Optimum activator modulus for 28 day compressive strength of geopolymer mortar depends on the chemical composition of the fly ash material. This ranges from 0.75 for Mt.Piper fly ash to 1.625 for Tarong fly ash.

- Effective activator modulus (AM_{eff}) which accounts for the SiO_2 and Na_2O in the fly ash in calculating the activator modulus (AM) does appear to show a positive impact with 28 day compressive strength of geopolymer mortar.

- SiO_2/Al_2O_3 ratio does not show a direct correlation with compressive strength of geopolymer mortar.

- Amount of unburnt carbon in fly ash demonstrates an inverse correlation with the compressive strength. This is explained as due to the absorption of activator solution by unburnt carbon, which reduces the activator available for geopolymerization and workability.

- Workability is a key factor contributing to compressive strength of low calcium fly ash geopolymer and a flow in the range 110 ± 5% to 140 ± 5% is required for optimum performance.

- The workability correlates well with the shear thinning exponent *m* in $(\eta/\eta_{max}) \sim (\dot{\gamma}/\dot{\gamma}_{max})^{-m}$ which depends on the particle size distribution. The flow is governed by the fineness, with the quantity of particles passing at the 10 and 20μm sieve size being the best indicator of the suitability of the fly ash.

- The specific surface area of precursor fly ash coupled with the quantity of particles passing at the 10 and 20μm sieve size is the key factor in the dissolution, coagulation and

gel formation of geopolymers. The higher the surface area and the higher the particles smaller than 20μm, the better the gel formation.

- For those materials whose flow is within the specified range, the amorphous content in the 10 to 20μm range was identified as being critical to the strength development, rather than the total amorphous content.

- A good correlation exists between the zeta potential of the raw fly ash and the CaO percentage, with a high CaO content leading to negative zeta potential.

- The larger the negative zeta potential of the fly ash the higher the compressive strength of the resultant geopolymer. A smaller negative zeta potential of the geopolymer is an indication of more gel formation and hence a high compressive strength.

5 MICROSTRUCTURE AND PORE-STRUCTURE VARIANCE OF GEOPOLYMER MORTAR

5.1 Overview

In Chapter 4 the chemical, physical and mineralogical properties of raw fly ash were discussed and a number of inter related factors influencing the compressive strength identified. The principal factors identified were workability, specific surface area and the quantity of particles in amorphous phase smaller than 20µm size. This chapter discusses the microstructural studies undertaken to identify the elemental oxide distribution within the fly ash particles and how this affects the geopolymerization mechanism and the compressive strength achieved.

Chapter 5 presents the test results of **Phase 1** of the comprehensive experimental study shown in Figure 3.2, as an extension of Chapter 4. The Al_2O_3 and SiO_2 content and their dissolution are identified as key factors in the formation of the aluminosilicate gel and the geopolymer matrix produced. Thus, it is important to determine the distribution of these elements and any potential impact on the properties of the geopolymer produced. The microstructural and pore-structural changes with the degree of geopolymerization is assessed deeply and then correlated with the compressive strength of final geopolymer systems.

5.2 Microstructure of geopolymer mortar

A significant variation in compressive strength was noted between the five fly ash geopolymer mortars, Figure 4.3. The highest compressive strength was observed for the Gladstone fly ash geopolymer (~61 MPa) while the Collie and Mt.Piper fly ash geopolymers displayed the lowest compressive strengths (~21 MPa). Tarong and Pt.Augusta fly ash geopolymers fell in the range between (~41 and ~37MPa, respectively). The microstructure variance of five geopolymer mortar and its influence on aforementioned strength variation are discussed in this chapter.

5.2.1 Element distribution pattern

Figure 5.1 shows the element distribution map of the five different fly ash precursors. The four key elements in geopolymerization, Si, Al, Ca and Fe, are displayed as green, red, blue and purple, respectively. For each element, the higher the intensity (brightness) of the image, the greater the quantity of the corresponding element. For instance, the brightest image for Al belongs to Pt.Augusta fly ash while the less intense image for Si represents the lower quantity of SiO_2 within the Pt.Augusta fly ash, Table 3.1.

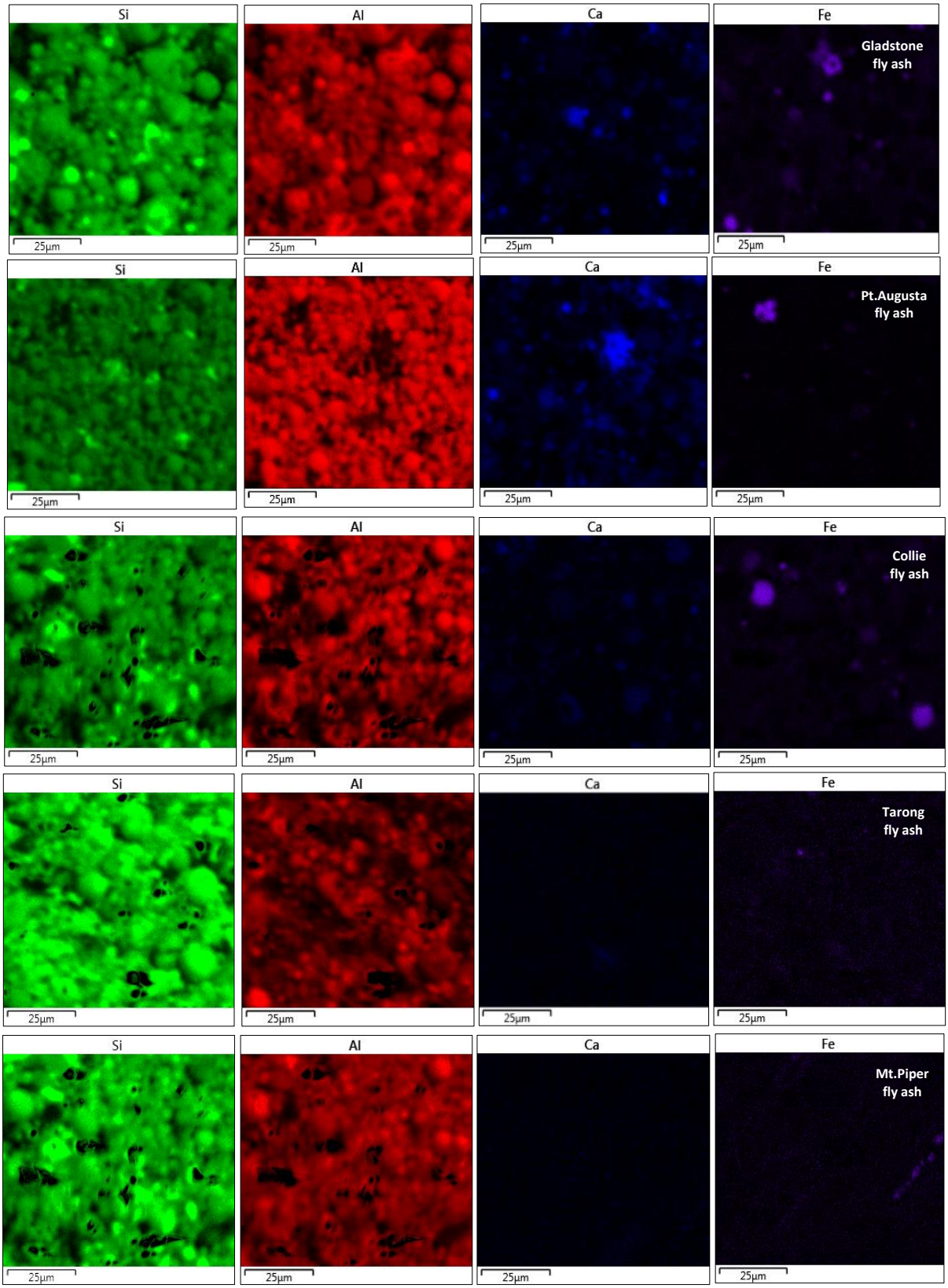

Figure 5.1 X-ray mapping of Si, Al, Ca and Fe distribution in individual fly ash

The overlay image of key elements distribution is displayed in Figure 5.2. Each fly ash precursor has its own element distribution pattern.

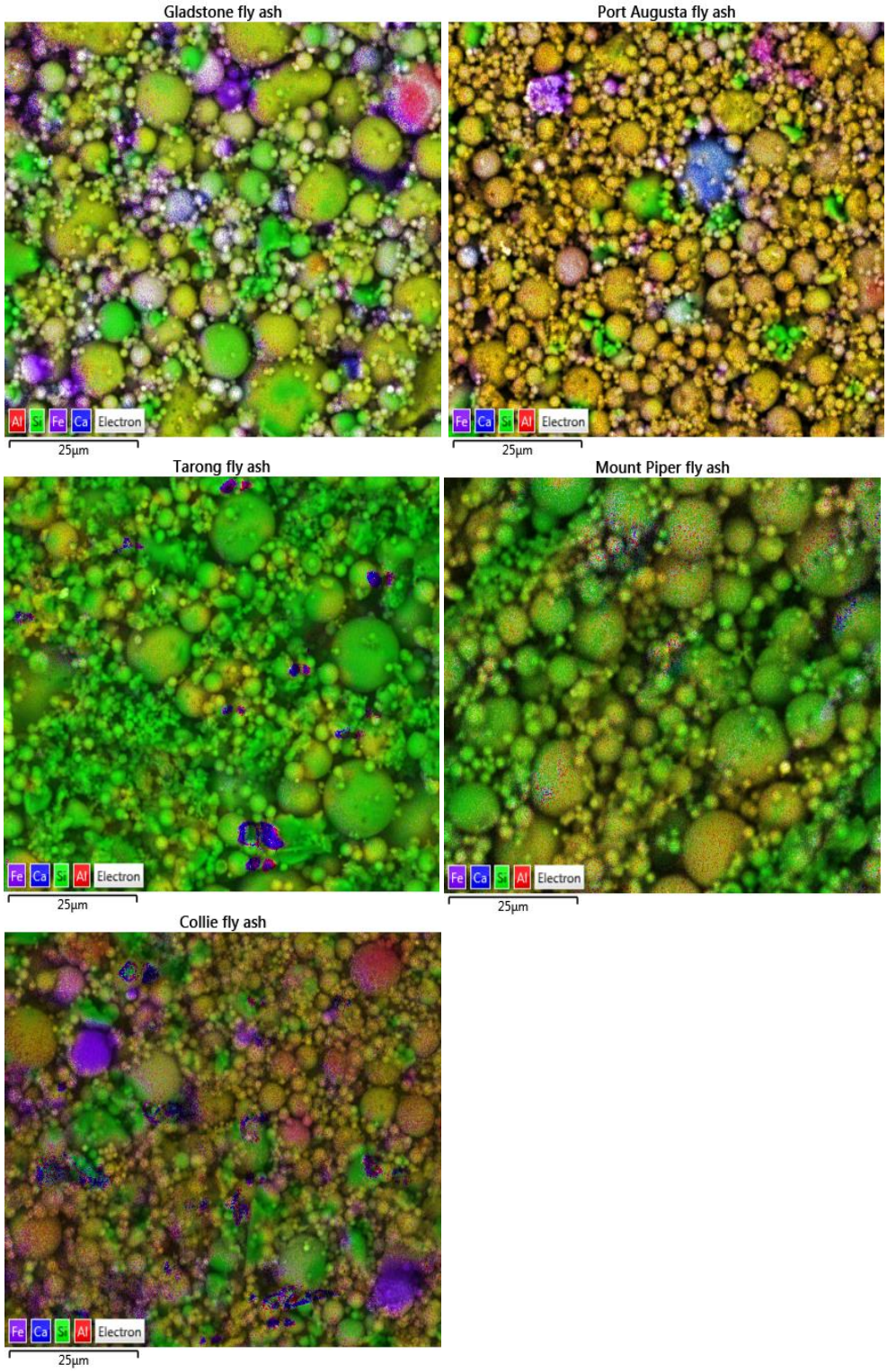

Figure 5.2 Overlay of element distribution

In this study, element overlay maps of Gladstone and Pt.Augusta precursor fly ash show a uniform and homogeneous distribution of Al_2O_3 and SiO_2, but have a different intensity for each element distribution. Pt.Augusta has higher Al_2O_3 and less SiO_2 than Gladstone fly ash as shown in Figure 5.1. While a small quantity of pure silicon-rich grains are observed in both precursors, it is dominant in the Gladstone fly ash. Randomly distributed small quantities of Ca and Fe oxides can be seen in both fly ash precursors.

The element overlay image of Collie fly ash shows a significant difference compared to the Gladstone and Pt.Augusta fly ash with a higher distribution of SiO_2 and Al_2O_3 over the fly ash grains. It further shows less uniformity and homogeneity in SiO_2 and Al_2O_3 distribution than the Gladstone fly ash. An unevenly distributed, flocked Si rich phases can also be seen in addition to the randomly distributed Fe_2O_3. While the total SiO_2 and Al_2O_3 content and SiO_2/Al_2O_3 ratio of Gladstone, Pt.Augusta and Collie fly ash varied over a relatively small range (80.7–82.3 and 1.6–1.8, respectively), their element oxide distribution shows a significant difference as shown in Figure 5.2. In contrast, the total SiO_2 and Al_2O_3 content and SiO_2/Al_2O_3 ratio of Mt.Piper and Tarong fly ash ranged between 90.5–94.6 and 2.6–3.4 respectively, showing a significant difference to the other three fly ash. Both Mt.Piper and Tarong precursors show a high availability of pure SiO_2 on their surfaces with no impurities. The Al_2O_3 are distributed randomly on a few fly ash grains, but are not homogenous. Overall the analysis shows that the five fly ash precursors have a significant variation, especially in SiO_2 and Al_2O_3 distribution and in their degree of uniformity and homogeneity.

In the geopolymer reaction, precursor fly ash reacts with alkaline activator to produce aluminosilicate gel. The gel composition depends on the extent of dissolution of silica and alumina oxides in the fly ash grains. Surface associated element oxides more easily dissolve in an aqueous environment than elements enriched in the cores of fly ash grains. The amorphous phases of fly ash, which is believed to be the phase actively involved in geopolymeric reaction (Chen-Tan et al., 2009, Chancey, 2008, Alvarez-Ayuso et al., 2008), are primarily distributed on the surface of fly ash, while the crystalline content primarily is in the inner core of the fly ash particles. Thus, the dissolution of amorphous oxides within the fly ash core is dependent on the dissolution rates of the amorphous surface layer. The results would indicate that a uniform and homogeneous distribution of SiO_2 and Al_2O_3 in the surface of precursor fly ash enables a rapid reaction with the hydroxyl ions of alkali activator, which results in the leaching of more Si^{4+} and Al^{3+}, i.e. the first phase of geopolymerization process.

Thus, better uniformity of element distribution on the surface of the particles is observed to lead to better dissolution of the Al, Si species into the aqueous solution, resulting in the formation of more aluminosilicate gel. This is in agreement with Van Jaarsveld et al. (2003) who reported that the geopolymeric reaction occurs at the surface of fly ash particles.

5.2.2 Geopolymer phases and matrix formation

Figure 5.3 identifies the different geopolymer phases created after geopolymerization of each specific fly ash. Three geopolymer phases were identified in both Gladstone and Pt.Augusta geopolymers, a single phase was observed in the Mt.Piper and Collie following geopolymerization and the Tarong geopolymer displayed two phases. Gladstone geopolymer shows well distributed geopolymeric gel. The major geopolymeric phase is a 93.6% fraction and contains aluminosilicate gel with SiO_2/Al_2O_3 ratio of 2.4. This element oxide ratio was obtained using EDS (Oxford Aztec software) analysis, which is described in Section 3.3.4-microstructural analysis. The second phase, a 5.3% fraction consists of aluminosilicate gel with SiO_2/Al_2O_3 ratio of 2.8, however, this is mixed with Fe_2O_3 impurities, the raw fly ash consists of high Fe_2O_3 content, Table 3.1. The few unreacted fly ash grains identified after geopolymerization and are observed in the third phase, a Si-rich phase containing almost no impurities.

The Pt.Augusta fly ash geopolymer has a similar microstructural (mapping) image to Gladstone, but contains randomly distributed CaO. Two out of the three geopolymer phases consists of aluminosilicate gel, but in different SiO_2/Al_2O_3 ratios. The major phase has a 89.1% fraction and contains aluminosilicate gel with SiO_2/Al_2O_3 ratio of 2.4 while the smaller phase contains aluminosilicate gel with SiO_2/Al_2O_3 ratio of 3.6. A new geopolymer phase is identified after geopolymerization of Pt.Augusta and it contains calcium-aluminosilicate gel with SiO_2/Al_2O_3 ratio of 1.4, as a 6.7% fraction.

Tarong fly ash geopolymer shows a noticeable difference compared to the Gladstone and Pt.Augusta geopolymers. Its major phase has a 94.7% fraction, aluminosilicate gel with SiO_2/Al_2O_3 ratio of 4.1, while the other phase consists of aluminosilicate gel with SiO_2/Al_2O_3 ratio of 7.4. Both the Mt.Piper and Collie geopolymers have one phase which contains aluminosilicate gel with SiO_2/Al_2O_3 ratio of 4.1 and 3.1, respectively.

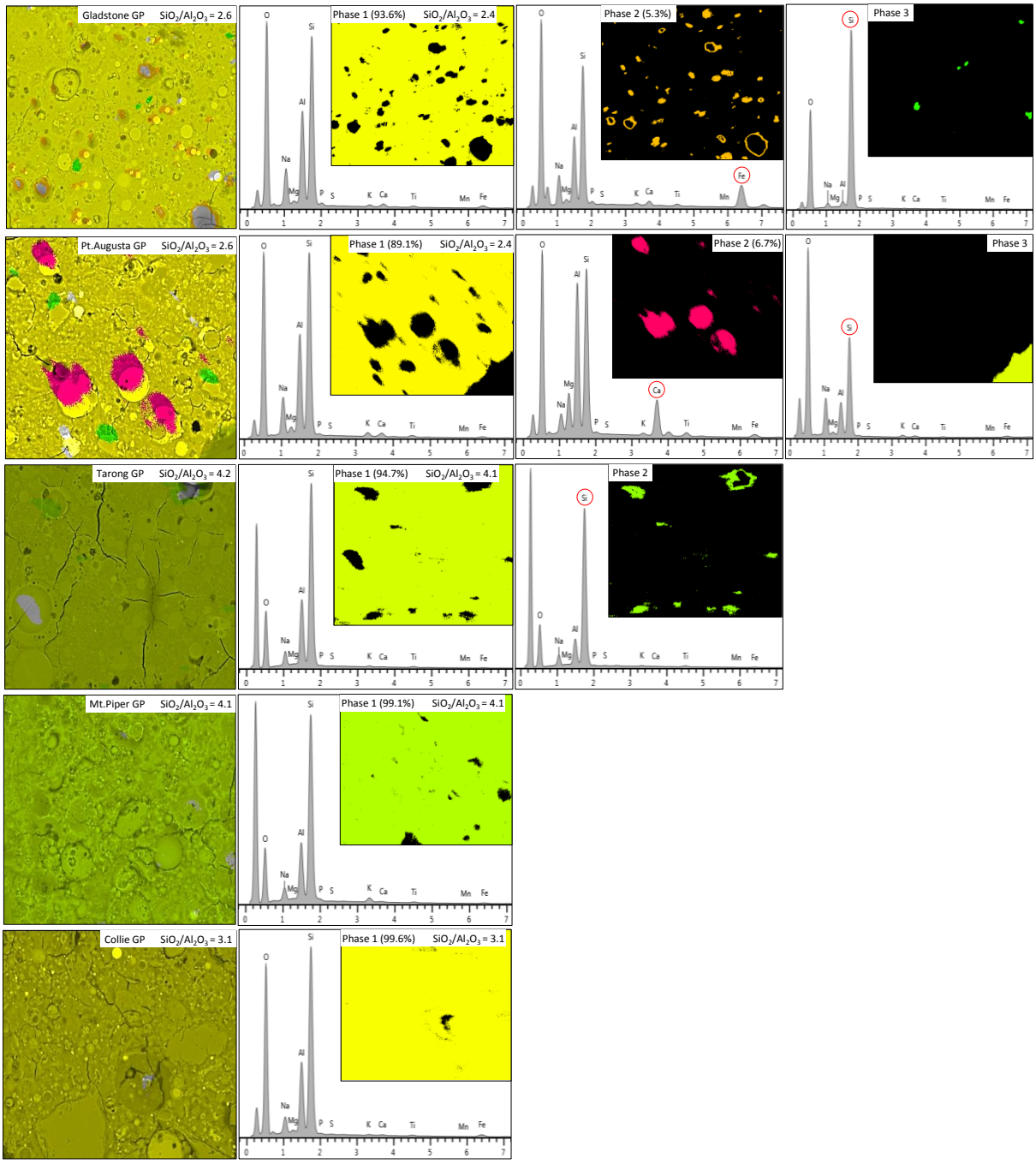

Figure 5.3 X-ray mapping of geopolymer phases

Davidovits (2005) reported that the structure of a geopolymer matrix is determined by the atomic per cent ratio of Si/Al during the geopolymerization process. Here, the observed SiO_2/Al_2O_3 weight per cent ratio and Si/Al atomic per cent ratio are almost equal, thus the SiO_2/Al_2O_3 weight per cent ratio is used to identify the matrix formed during geopolymerization in specific fly ash. The matrix formed in the major geopolymer phase (phase one in all geopolymers) is the significant phase when determining the compressive

strength. The major geopolymer phase is believed to consist of pure aluminosilicate gel without the presence of other oxide impurities. The Gladstone and Pt.Augusta fly ash geopolymers showed an identical SiO_2/Al_2O_3 ratio (2.4) in their major geopolymer phase, thus the predominant form of the geopolymeric gel is identified as polysialate-siloxo (Si-O-Al-O-Si). In contrast, Tarong and Mt.Piper fly ash geopolymers had higher Si and lower Al oxide content in the geopolymeric gel, and hence resulted in higher SiO_2/Al_2O_3 ratio (4.1) in their major geopolymer phase. The geopolymer matrix formed in the both geopolymers is hypothesised as a combination of polysialate-disiloxo (Si-O-Al-O-Si-O-Si-O) with complex sialate links. The Collie fly ash geopolymer had a SiO_2/Al_2O_3 ratio of 3.1 in the major phase and the matrix is identified as polysialate-disiloxo.

Overall, there is a good correlation between gel composition (i.e. SiO_2/Al_2O_3 ratio), geopolymer matrix and compressive strength. Both Gladstone and Pt.Augusta have a mean SiO_2/Al_2O_3 ratio of 2.6, however in Gladstone the predominant phase has a slightly lower value (2.4) and displayed higher compressive strength at 28 days. It has been reported that a SiO_2/Al_2O_3 ratio less than 2.4 results in higher compressive strength (Tennakoon et al., 2014b). The data from this study would support that observation, indicating a SiO_2/Al_2O_3 of 2.4 is a good indication of high strength. Although the Pt.Augusta contains similar quantities of aluminosilicate as Gladstone as shown in Table 1, it has a lower percentage of aluminosilicate gel of the 2.4 SiO_2/Al_2O_3 phase and a lower compressive strength than Gladstone. This is attributed to the lower uniformity of elemental distribution than observed in the Gladstone fly ash.

In contrast, Collie geopolymer has SiO_2/Al_2O_3 ratio of 3.1 and gave the lowest compressive strengths. De Silva et.al (2007) reported the polysialate-siloxo and polysialate-disiloxo gel structures to be rigid and stable 3D matrices. However, the present study shows that aluminosilicate gel with a polysialate-siloxo 3D structure, as displayed by Gladstone and Pt.Augusta ash, leads to a higher compressive strength than the polysialate-disiloxo gel structure, observed in the Collie ash. The formation of polysialate-siloxo gel during geopolymerization is hypothesized as producing high rigidity and stability, thus, resulting in higher compressive strength. Both Mt.Piper and Tarong geopolymers had a very high SiO_2/Al_2O_3 ratio (i.e. greater than 4) and produced 3D polymeric gel structures with mixed polysialate-disiloxo and silicate links. The Mt.Piper produced lowest compressive strength, as

would be expected given the gel structure. However, the Tarong gave a higher compressive strength, comparable to the Pt.Augusta.

5.2.3 Effect of element oxide ratios

The matrix formed in the major geopolymer phase is determined by the SiO_2/Al_2O_3 ratio of geopolymer mortar. The incorporation of Si^{4+}, Al^{3+}, Na^+ ions in the aluminosilicate gel can be determined by analysing SiO_2/Al_2O_3, Al_2O_3/Na_2O and SiO_2/Na_2O ratios between the initial geopolymer mix (before subjected to heat curing, Appendix B2) and resultant geopolymer mortar as shown in Figure 5.4. The variation in the major aluminosilicate gel phase between Gladstone and Tarong geopolymers is attributed to the amount of Na^+ and Si^{4+} ions enriched in the geopolymeric gel. Tarong geopolymer shows a higher SiO_2/Na_2O and Al_2O_3/Na_2O ratio in its initial geopolymer mix, compared to the Gladstone. This indicates a higher concentration of Na^+ ions in the aluminosilicate gel phase of the Gladstone geopolymer compared to the Tarong. The Na^+ ions act as a structure forming element. The structure of the aluminosilicate gel contains Si and Al tetrahedrons randomly distributed along the polymeric chains that are cross-linked so as to provide cavities of sufficient size to accommodate the charge balancing hydrated Na^+ ions. Both the Collie and Mt.Piper fly ash geopolymers displayed less incorporation of Al^{3+} ions in their main geopolymeric phase, confirmed by the lower Al_2O_3/Na_2O ratio and higher SiO_2/Al_2O_3 ratio of the resultant geopolymer mortar.

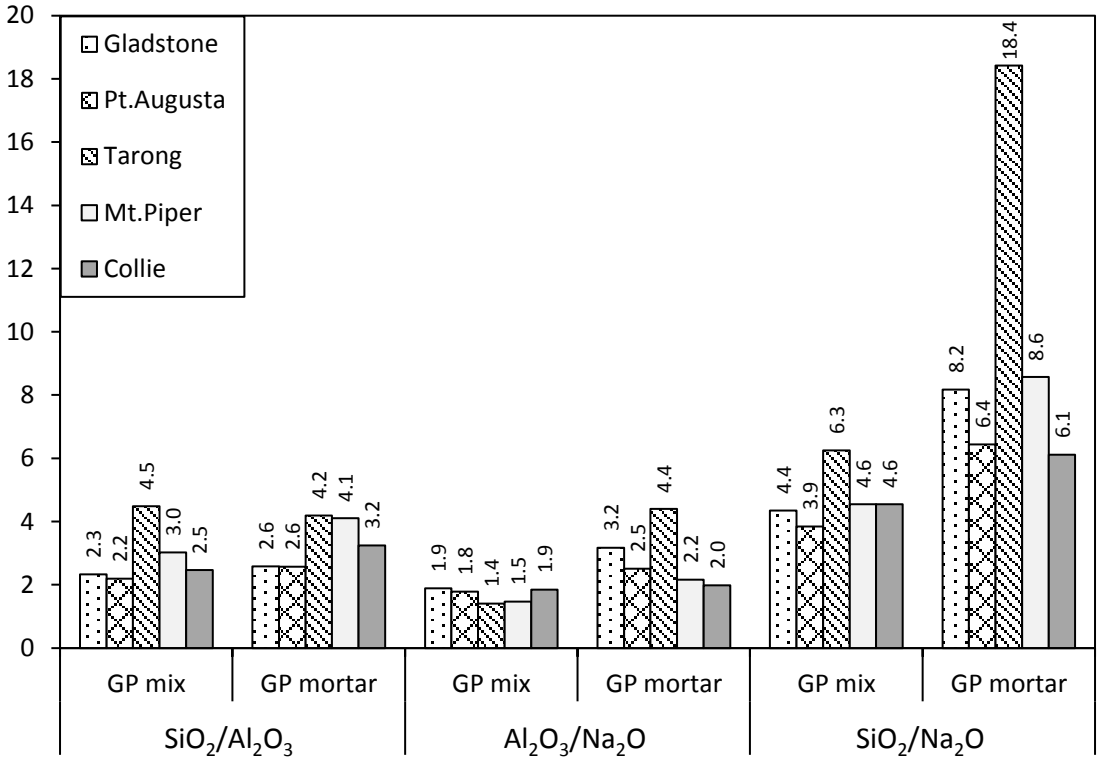

Figure 5.4 SiO_2/Al_2O_3, Al_2O_3/Na_2O and SiO_2/Na_2O ratios between geopolymer mix and mortar

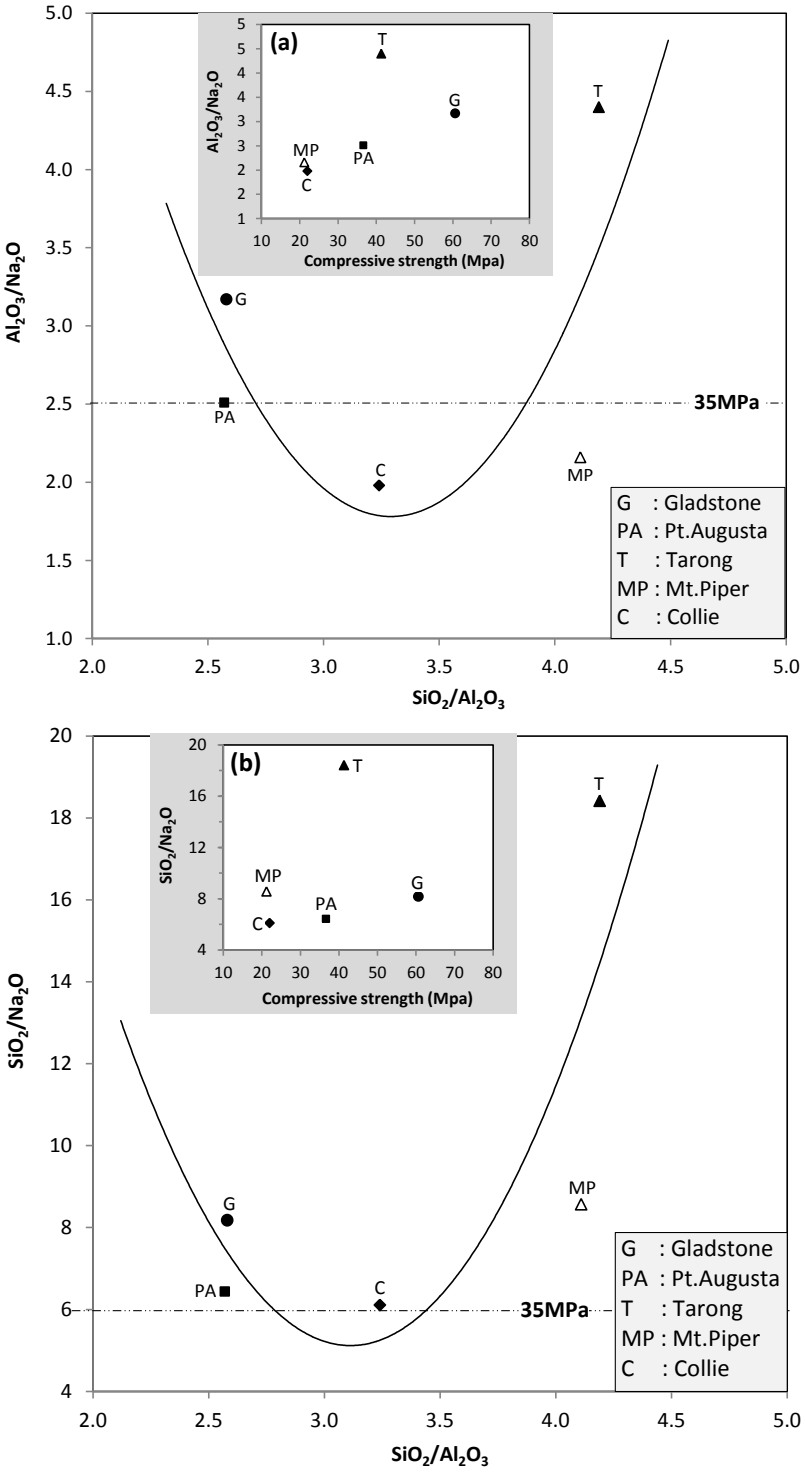

Figure 5.5 The Al_2O_3/Na_2O and SiO_2/Na_2O ratios vs. SiO_2/Al_2O_3 ratio: (a) Al_2O_3/Na_2O and (b) SiO_2/Na_2O ratio vs. compressive strength.

Figure 5.5 shows the compressive strength changes with the varying of Al_2O_3/Na_2O and SiO_2/Na_2O ratios. The compressive strength of all fly ash geopolymer mortar increased with an increase of Al_2O_3/Na_2O ratio, Figure 5.5(a). Hence, both Al_2O_3/Na_2O and SiO_2/Na_2O ratios have a positive effect on compressive strength, i.e. geopolymers with higher strengths

are more likely to be achieved with fly ash having higher Al_2O_3/Na_2O and SiO_2/Na_2O ratios. Similar behaviour has been reported by other researchers (Tennakoon et al., 2014b, Songpiriyakij et al., 2010). The results of the present study suggest that a combination of the Al_2O_3/Na_2O and SiO_2/Na_2O ratios influence compressive strength. When both Al_2O_3/Na_2O and SiO_2/Na_2O ratios exceed 2.5 and 6 respectively, 35MPa or higher compressive strength is observed at 28 days. Hence, the data would indicate that regardless of the geopolymer matrix formed, threshold values for Al_2O_3/Na_2O and SiO_2/Na_2O ratios are required to achieve a specific compressive strength.

5.3 Degree of geopolymerization of mortar

5.3.1 FT-IR analysis

In addition to the structure of the geopolymer matrix formed in geopolymerization, the presence of aluminium-silicate bonds and the degree of aluminium incorporation in the gel matrix after the geopolymerization are significant factors in strength development. The FT-IR spectrum identifies the wave lengths of Si-O and Al-O bonds in the precursor fly ash and their corresponding geopolymers, Figure 5.6. This band corresponds to the region from 1500 cm^{-1} to 500 cm^{-1}.

Previous studies (Valcke et al., 2014, Zhang et al., 2012) reported that the aluminium-silicates of both fly ash and geopolymer precursors relate to the peaks ranged from 1300 to 800 cm^{-1}, with the higher wavenumber (1000–1300 cm^{-1}) to peaks of glassy aluminium (low)-silicates, the lower wavenumber (800–900 cm^{-1}) to peaks of aluminium (high)-silicates, and in between, (900–1,000 cm^{-1}) to peaks of glassy aluminium (medium)-silicates. Further, Zang et al. (2012) showed that the presence of active bonds from the aluminium-silicates can react with alkali activator and inactive bonds from the aluminium-silicates cannot react with alkali activator. The presence of active bonds from the alkali-aluminium-silicates is dominant when wavenumbers range from 900 to 1000 cm^{-1}. In the higher (1000–1300 cm^{-1}) and lower bands (800–900 cm^{-1}), both active bonds of low aluminium-silicates and high aluminium-silicates, as well as inactive bonds of quartz and mullite occur. In addition, the peaks produced by geopolymerization gradually shift toward lower frequencies with silicates relatively rich in aluminium (Phair and Van Deventer, 2002).

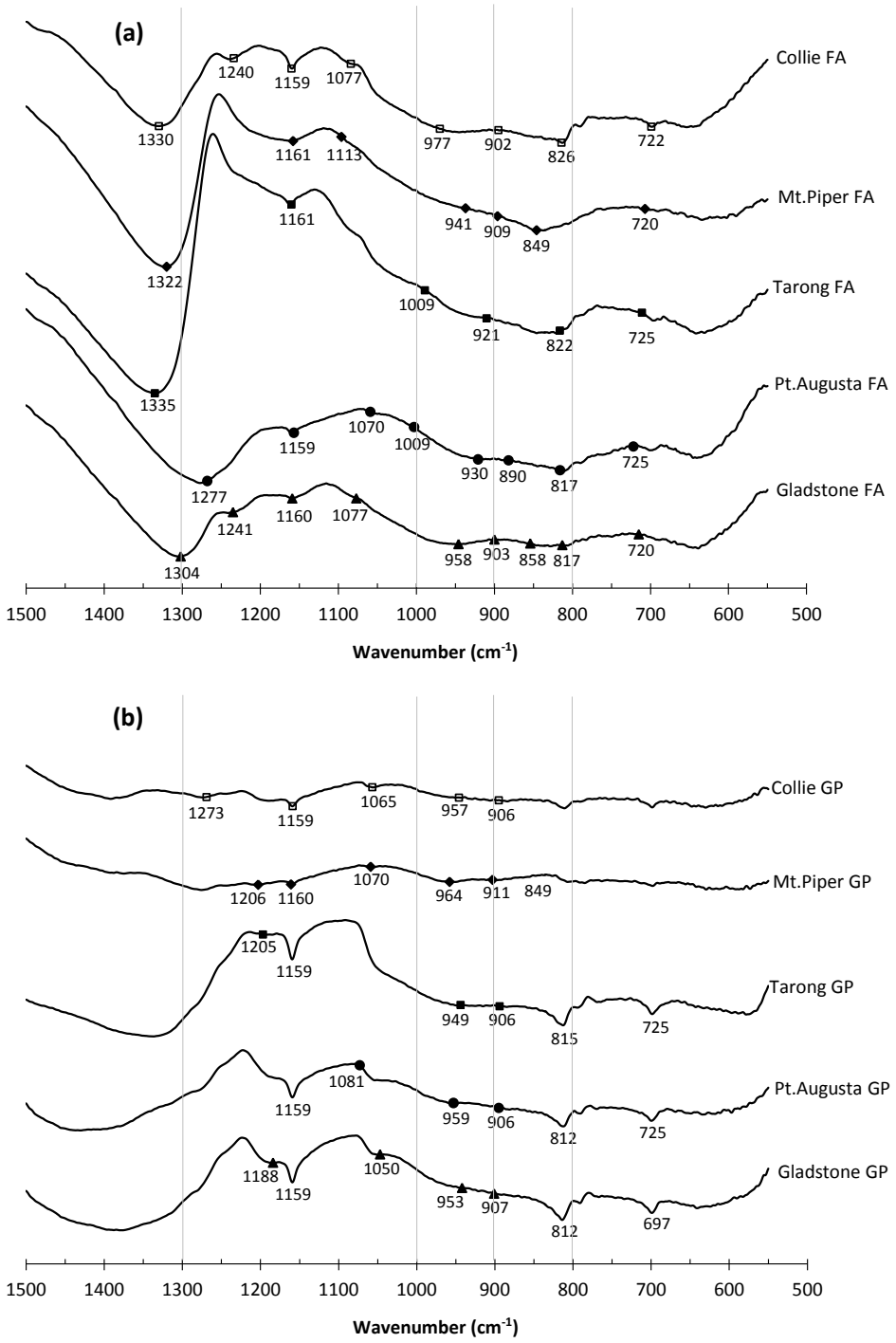

Figure 5.6 FT-IR spectra: (a) precursor fly ash (FA) and (b) their corresponding geopolymers (GP)

In this study, for the all precursor fly ash, a broad peak occurs around ~1300 cm^{-1}, with a small hump at lower wavelengths around ~1150 cm^{-1}. The Gladstone fly ash has the highest amount of active T-O-Si (T=Si or Al) bonds while the Mt.Piper fly ash has the lowest in the range from 900 to 1000 cm^{-1}. Pt.Augusta, Tarong and Collie fly ash show a similar quantity of active T-O-Si bonds. After geopolymerization, the main characteristics in geopolymers is

that the band associated with stretching vibrations of Si-O-Si (~1300 cm^{-1}) as noted in the Gladstone, Pt.Augusta and Tarong precursor fly ash shifts to values around ~800 cm^{-1} and becomes sharper. In other words, in these three fly ash the peaks of the aluminium (low)-silicates tend to broaden and display a lower peak height after geopolymerization, while those of the aluminium (medium)-silicates and aluminium (high)-silicates and tend to become sharper and increase in peak height. Mt.Piper and Collie geopolymers did not display such clearly visible sharp peaks in the range, 1000–800 cm^{-1}.

The substitution of Si^{4+} for Al^{3+} involves a reduction of the T-O-T angle and therefore the appearance of the signal at a lower wavenumber is due to a smaller bonding force. The Al-O bond is longer than the Si-O bond, and the bond force constant for the modal Al-O-Si is smaller than for the mode of the Si-O-Si bond (Phair and Van Deventer, 2002). Hence, the shifting of the peaks to lower wavenumbers Figure 5.6(b), confirms the incorporation of aluminium into the silicate backbone during the geopolymerization process for Gladstone, Pt.Augusta and Tarong. The incorporation of the aluminium is evidence of a greater degree of geopolymerization, which subsequently results in the higher compressive strengths observed for the geopolymer concrete produced. In contrast, the lack of aluminium amalgamation with silicates in both the Mt.Piper and Collie fly ash geopolymers indicates a lower degree of geopolymerization compared to other geopolymers. These results support the findings of Tennakoon et al. (2014a) who identified the rate of release of aluminium in the activation process as being critical with the rapid release of aluminium producing gels with uniform composition and structure, leading to geopolymer networks with higher strength development. Overall the results indicate that the peaks in the range, 1000–800 $cm^{-1}$are a clear indication of a high degree of geopolymerisation, and can be related to the compressive strength expected to be achieved.

5.3.2 Solid state ^{27}Al MAS–NMR analysis

The ^{27}Al MAS-NMR can provide further additional information of the geopolymer formation process. Figure 5.7 and Figure 5.8 display the ^{27}Al MAS–NMR spectra for the raw fly ash and geopolymer mortar samples. Generally, the alumina–silicate materials contain three types of coordinated aluminium atoms, such as AlO_4, AlO_5, and AlO_6, denoted Al^{IV}, Al^{V} and Al^{VI} respectively. The chemical shift is ranged for Al^{IV} at ~52 to 68 ppm, for Al^{V} at ~26 to 38 ppm and for Al^{VI} at ~6 to 15 ppm (MacKenzie and Smith, 2002). Duxson et al. (2007a) further

reported that the Al^{IV} and Al^{V} peaks overlap at ~50 ppm in the raw fly ash, and the Al^{VI} is shown at ~0 ppm, whereas the geopolymers contain relatively strong and sharp Al^{IV} peaks at ~60 ppm.

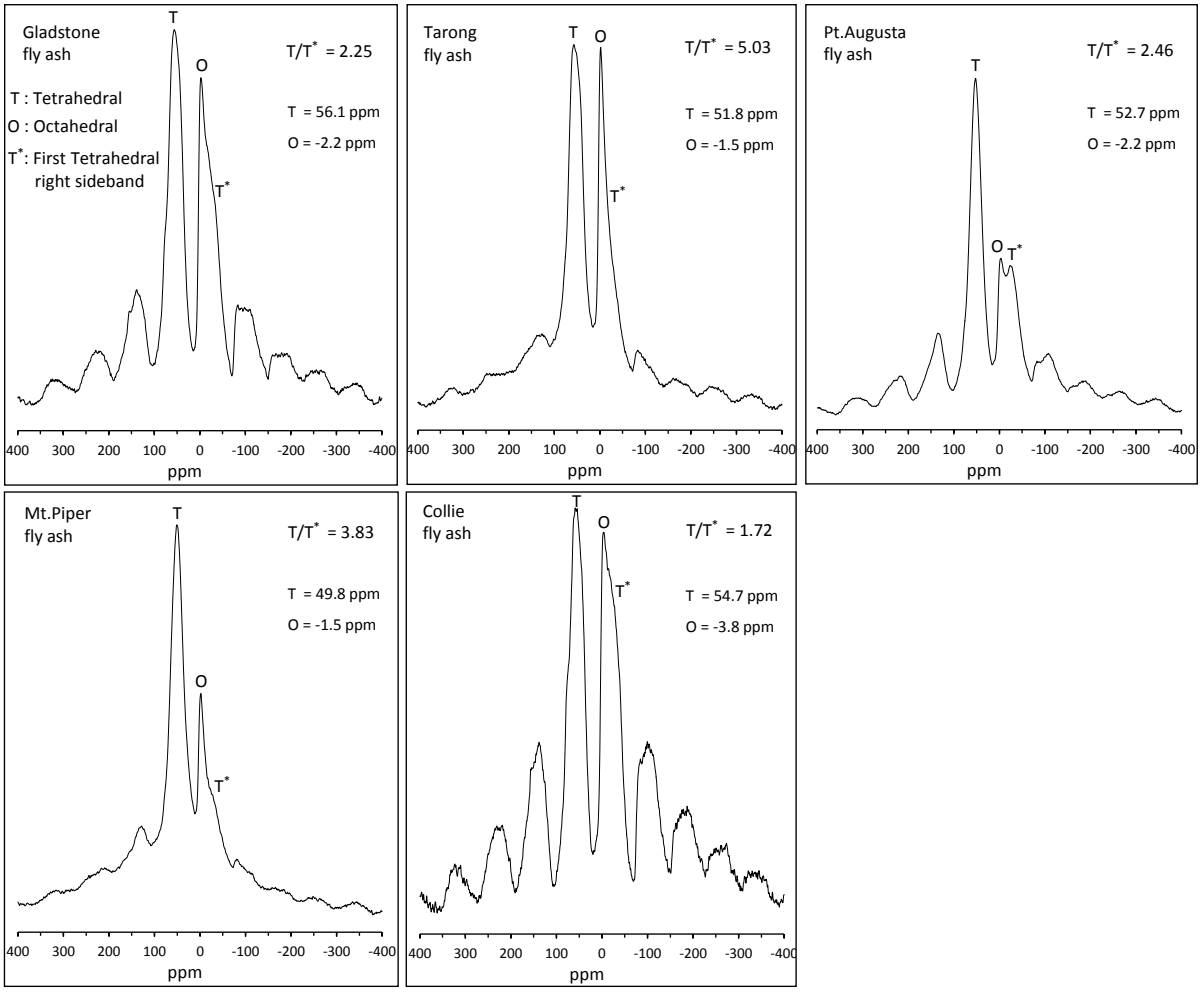

Figure 5.7 The ^{27}Al MAS–NMR spectra for raw fly ash

The Gladstone, Tarong, Pt.Augusta and Collie fly ash showed an intense and distinct peak at 56.1, 51.8, 52.7 and 54.7 ppm respectively, indicative of a large quantity of aluminium atoms tetrahedrally (Al^{IV}) coordinated. The Mt.Piper fly ash however presented an intense peak at 49.8 ppm and is suggestive of an overlap of Al^{IV} and Al^{V} peaks. All the geopolymer samples shown in Fig. 10, displayed relatively intense and distinct aluminium tetrahedral peaks in the 54.4 to 56.1 ppm range. The octahedrally (Al^{VI}) coordinated aluminium in the fly ash ranged from –1.5 to –3.8 ppm, which varied within a slightly narrow range (–0.6 to –1.5) in the resultant geopolymers.

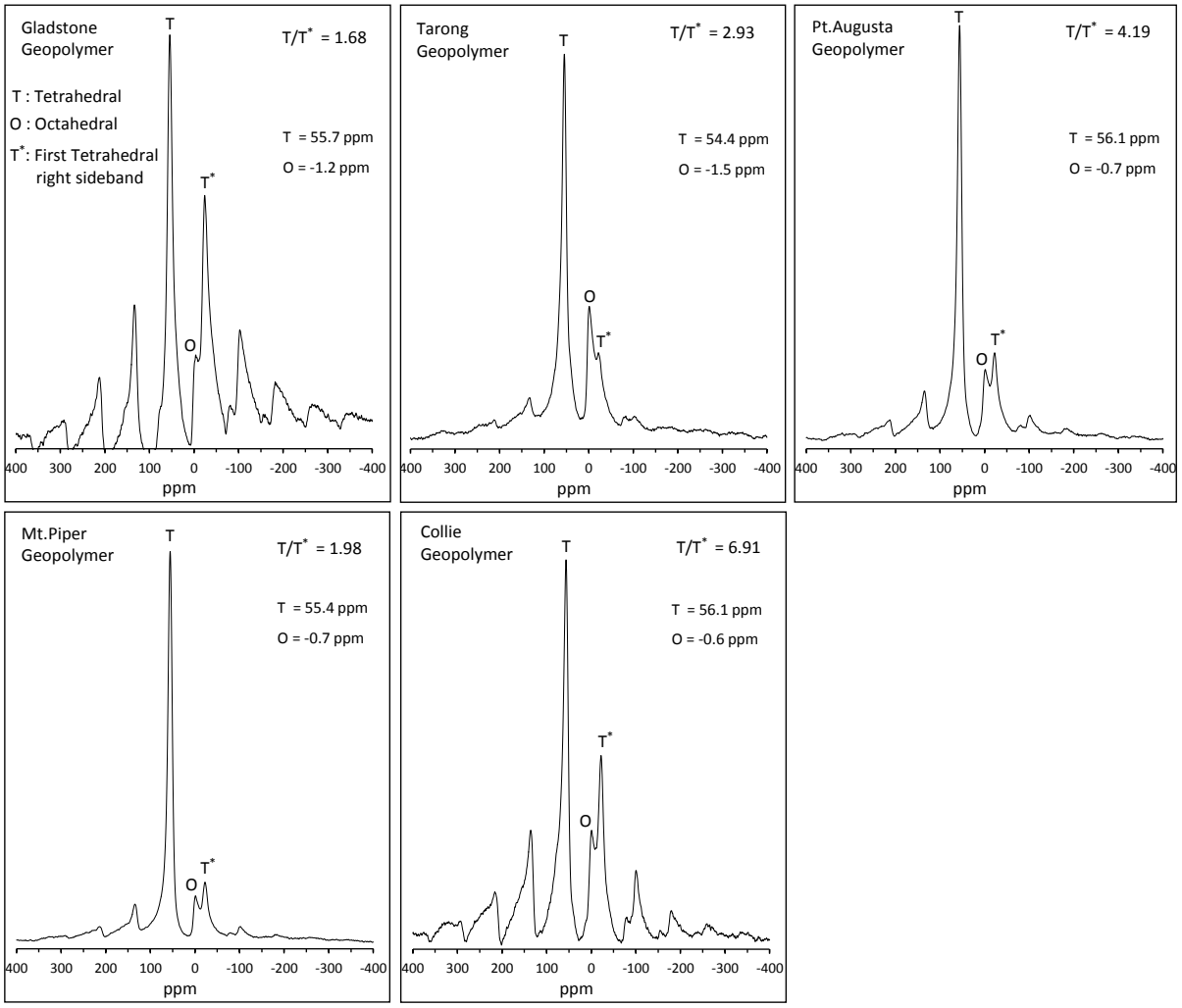

Figure 5.8 The ^{27}Al MAS–NMR spectra for fly ash based geopolymers

The chemical shift anisotropy, which is revealed by multiple spinning sidebands, is observed in both fly ash and geopolymer spectra. The shape and intensities of these spinning sidebands is semi–symmetrical, but weighted towards right side in the spectrum. This fact reflects the asymmetry in the aluminium sites in both fly ash precursor and geopolymer.

Table 5.1 Percentage of Al^{IV} and Al^{VI} coordination

Al Coordination	Fly ash type				
	Gladstone	Tarong	Pt.Augusta	Collie	Mt.Piper
Tetrahedral (Al^{IV})	54.3	57.8	59.8	50.7	71.8
Octahedral (Al^{VI})	45.7	42.2	40.2	49.3	28.2
	Geopolymer type				
	Gladstone	Tarong	Pt.Augusta	Collie	Mt.Piper
Tetrahedral (Al^{IV})	86.1	65.4	85	76.5	89.9
Octahedral (Al^{VI})	13.9	34.6	15	23.5	10.1

The integrated areas of the tetrahedral and octahedral peaks of four fly ash, excluding Mt.Piper, indicate that about ~50 to 60% of aluminium is in tetrahedrally coordinated and the balance is octahedrally coordinated, Table 5.1. Mt.Piper has a very high percentage of aluminium in tetrahedral form (~72%) and the remainder with octahedral coordination (~28%). In the alkali-fly ash reaction, octahedrally coordinated aluminium in fly ash is converted to the tetrahedral form. This conversion occurs within the dissolution/gel formation process with the alumina being incorporated into the silicon backbone. The conversion will not be total as some octahedrally coordinated aluminium will remain due to the presence of mullite in the raw fly ash, Table 3.3. Mullite does not take part in the geopolymerization reaction so the octahedrally coordinated aluminium in the mullite is expected to stay constant in the NMR spectra.

The integrated areas of the tetrahedral and octahedral peaks of the Gladstone geopolymer indicate that 86.1% of aluminum is tetrahedrally coordinated while 13.9% is octahedrally coordinated. In Pt.Augusta geopolymer, this is 85% tetrahedral and 15% octahedral. In this study, both fly ash had ~40-45% of aluminium in octahedral coordination with similar quantities converted to the tetrahedral coordination during geopolymerization ~25-30%, Table 5.1. This variation of ~5% corresponded to a significant difference in terms of compressive strength ~25 MPa. While the variation in the quantity of tetrahedrally coordinated aluminium converted to the octahedrally coordinated aluminium is similar, Gladstone showed a significantly smaller chemical shift after activation, 0.3 ppm, compared to Pt.Augusta which had a shift corresponding to 3.3 ppm. The large chemical shift change represents rapid reaction taking place during geopolymerization. This means that less structural changes can occur due to the short reaction period, the result of which is the formation of less non-uniform and more loosely packed gel structure.

In the NMR spectrum, the Gladstone fly ash also displays less asymmetry at the aluminium sites than Pt.Augusta. This is shown by a lower T/T^*ratio. T represents the tetrahedral intensity while T^* is the intensity of the first spinning side band, immediately next to the octahedral peak as shown in Figure 5.7. After geopolymerization, the T/T^* ratio of Gladstone is less than the precursor fly ash as shown in Figure 5.8, displaying higher level of symmetry in the geopolymeric gel. However, the Pt.Augusta geopolymer displayed a very high T/T^*ratio compared to the precursor fly ash, as indicated by a higher asymmetry in the aluminium in the geopolymeric gel. Overall, the relatively high symmetrical aluminium

distribution coupled with the formation of a uniform and well compacted gel structure is identified as the reason for the high compressive strength achieved by Gladstone compared to Pt.Augusta, despite their similar chemical composition.

The Mt.Piper geopolymer had a highest percentage of tetrahedrally coordinated and lowest percentage of octahedrally coordinated aluminium, 89.9% and 10.1% respectively. In addition Mt.Piper fly ash had a non–uniform aluminium distribution, as such it would be anticipated that a large quantity of tetrahedrally coordinated aluminium will undergo rapid dissolution in the initial geopolymerization process, rather than a stable conversion of the small quantity of the octahedral units into the tetrahedral form. This is supported by the high tetrahedral chemical shift change between fly ash and geopolymer, 5.6 ppm. In addition, Mt.Piper geopolymer displayed the highest T/T^*ratio, which would indicate a high level of asymmetry in the average aluminium site. Hence, a high quantity of disordered aluminium is expected to available in the initial geopolymeric gel. It is hypothesized that this rapid change results into the formation of a non-homogenous and loosely packed gel structure, leading to the low compressive strength observed. The low strength of Mt.Piper geopolymer would imply that aluminium (medium)–silicate phases are optimum for geopolymer formation as they dissolve readily due to the fact that they do not contain too much aluminium in tetrahedral coordination, and contain sufficient aluminium in octahedral coordination to form a stable homogeneous 3-D aluminosilicate gel network.

The Tarong fly ash composition differed significantly from the other fly ash in that it had the highest asymmetry, indicated by the highest T/T^*ratio. It was noted that this ratio significantly decreased after the geopolymerization as shown in Figure 5.8, confirming the high symmetrical distribution of aluminium in the gel structure. It further displayed a lower chemical shift, 2.6 ppm, in the geopolymer than Pt.Augusta, 3.3 ppm. Hence, the relatively more stable conversion of octahedral aluminium into tetrahedral coordination and their high level of symmetrical distribution in the geopolymeric gel resulted in a higher compressive strength than Pt.Augusta.

The Collie geopolymer had the lowest compressive strength. Although having a similar composition to the Mt.Piper, it had a different aluminium coordination to the Mt.Piper: 76.5% of aluminium was tetrahedrally coordinated and 23.5% octahedrally coordinated. It further had a lower chemical shift, 1.3 ppm, when converted into geopolymer, and displayed

the lower asymmetry. The Collie fly ash also had a non-uniform aluminium and silicon oxide distribution, contained a higher percentage of coarse particles and had the lowest surface area. These factors are expected to contribute to a slow dissolution of the fly ash in the alkali. The slow dissolution results in the production of a non-homogeneous gel structure, which leads to the low strength of the geopolymer.

Previous research by Tennakoon et al. (2014a) recently reported that the rate of release of aluminium in the activation process as being critical, with the rapid release of aluminium producing gels with uniform composition and structure, leading to geopolymer networks with higher strength development. However, Fernandez-Jimenez et al. (2006b) have noted that a high quantity of available aluminium increases the rate of gelation and formation of aluminosilicate gel to such a degree that precipitation on the source material slows down the further dissolution, which may lead to geopolymers with lower mechanical performance. The results in this study would indicate that a stable conversion of the aluminium from octahedral to tetrahedral coordination is required to produce a high strength geopolymer, rather than the rate of dissolution alone that influences the mechanical performance. Overall a homogeneous distribution of the aluminium on the surface of the fly ash particle is required, together with a sufficient quantity of the octahedrally coordinated aluminium in the precursor fly ash.

5.4 Pore–structure of geopolymer mortar

The quantity of the aluminosilicate gel formed is dependent on the degree of geopolymerization. This gel fills the cavities between unreacted fly ash particles and pore spaces, thus refining the size of these pores. In order to identify the pore-structural changes after geopolymerization, mercury intrusion porosimetry, based on the Washburn equation that assumes cylindrical pore geometry, was used. The pore sizes measured ranged between 3 nm and 100,000 nm. Figure 5.9(a) shows the differential pore size distribution of the five different fly ash geopolymers. All showed a bimodal pore size distribution, i.e. two peaks in specific differential curve. The pores can be divided into three groups based on the pore diameter as micro-pores (0–2 nm), meso-pores (2–50 nm) and macro-pores (ϕ>50 nm) (Sing, 1985). The meso-pores are typical pores between geopolymer phases, while micro-pores exist within the gel network. However, the macro-pores in geopolymers represent the gaps between unreacted fly ash particles (Zheng et al., 2010). My work focused on meso and macro-pore regions in five different geopolymers.

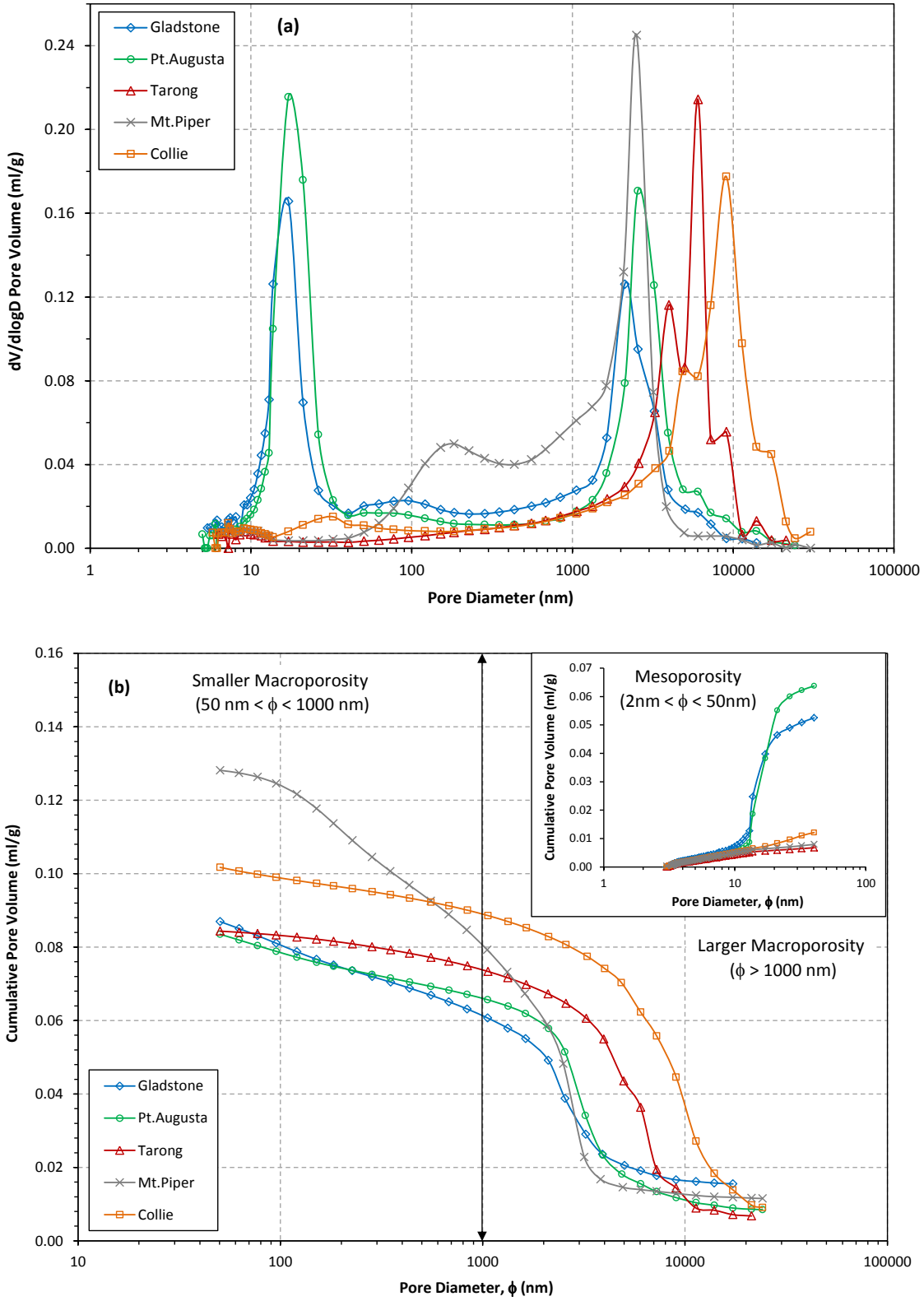

Figure 5.9 Pore diameter (ϕ) vs. (a) dV/dlogD pore volume and (b) Cumulative pore volume

Two sharp peaks can be observed in Gladstone and Pt. Augusta fly ash geopolymers with the tallest peak located in the meso-pores, 17.1nm, while the other is located in the macro-pores,

2110.89 and 2549.62nm, respectively. Pt.Augusta has a higher pore volume than Gladstone for both sharp peaks, confirming a higher porosity in its microstructure, reflected in the lower compressive strength of the Pt Augusta compared to the Gladstone. Mt.Piper and Collie fly ash geopolymers also show a bimodal pore size distribution, however, one of their peaks is characterised as a broad peak and the other one as a sharp peak. In Mt. Piper, its two peaks are observed at 2501.7nm and 183.2nm, the latter one is characterized as a broad peak. The Collie geopolymer shows similar behaviour, but a sharp peak is assigned to macro-pores, 9041.3nm, while the broad peak is located in the meso-pores, 32.1nm. The differential pore size distribution of Tarong shows a considerable difference compared to the other four geopolymers. Although it has two sharp peaks, both peaks are assigned as macro-pores as 6034.6nm and 3973.5nm. This suggests that while the Tarong has a SiO_2/Al_2O_3 ratio greater than 4 the 3D polymeric gel has significantly different structure, which may account for the relatively high compressive strength observed compared to the Mt Piper, which has a similar SiO_2/Al_2O_3 ratio.

In the hardening mechanism of the geopolymerization process the pores are created in the voids left by the expelled water and thus, the pore volume naturally increases with a higher degree of geopolymerization in fly ash based geopolymers (Ryu et al., 2013). Figure 5.9(b) displays the cumulative pore volume changes between meso-pore and macro-pore regions. Two major zones can be identified in the macro-pores region, i.e. pore diameter of 50-1000nm (smaller macro-pores) and above 1000nm (larger macro-pores). When pore size is below 1000nm, both Gladstone and Pt.Augusta geopolymers had the highest cumulative pore volume (0.090 and 0.070 ml/g, respectively), Table 5.2. Moreover, the shifting of the sharp peak in the larger macro-pore region and the appearance of a new sharp peak in the meso-pore region is believed to be due to the formation of larger quantities of aluminosilicate gel during the geopolymerization process. This corresponds to a reduction in the space between unreacted fly ash grains due to continuous dissolution and gel formation, which leads to an increase in the pores between new phases created during the geopolymerization. Thus the presence of a sharp peak in the meso-pore region of pore size distribution is a further indicator of the higher degree of geopolymerization in Gladstone and Pt.Augusta, correlating with the FT-IR data.

Table 5.2 Quantitative analysis of cumulative pore volume for fly ash geopolymers

Pore diameter (ϕ)		Cumulative pore volume (ml/g)				
		Gladstone	Pt.Augusta	Tarong	Collie	Mt.Piper
Meso-pores (2 nm < ϕ < 50 nm)		0.064	0.052	0.007	0.012	0.008
Macro-pores	50 nm < ϕ < 1000 nm	0.026	0.018	0.011	0.013	0.049
	ϕ > 1000 nm	0.061	0.066	0.073	0.089	0.079
Cumulative pores (2 nm < ϕ < 1000 nm)		0.090	0.070	0.018	0.025	0.057

In contrast, Mt.Piper and Collie geopolymers have lower cumulative pore volume when considering pore sizes below 1000nm (0.057 and 0.025 ml/g, respectively). They also display no sharp peak in the meso-pore region, confirming a lower degree of geopolymerization, again supporting the FT-IR data. Tarong geopolymer, however, had a significantly different distribution to the other geopolymers having the lowest cumulative pore volume of 0.018 ml/g below 1000nm, while also having the least meso-pores.

Overall the combination of element distribution, FT-IR and porosimetry data indicates the uniform and homogeneous distribution of SiO_2 and Al_2O_3 in the surface of Gladstone and Pt.Augusta fly ash leads to rapid dissolution of the alumina-silicates, leading to a high quantity of geopolymeric gel, incorporation of the Al in the matrix, creation of meso-pores and resulting in high compressive strengths. In contrast, Collie and Mt.Piper fly ash showed a less uniform, scattered distribution of SiO_2 and Al_2O_3, hence less release of Al and incorporation in the geopolymerization, creating larger macro-pores due to more unreacted particles and resulting in low compressive strengths. While Tarong fly ash has a high intensity of SiO_2, it also releases Al to a greater extent during activation in the alkaline media. The result of this leads to a high quantity of Al incorporated into the matrix of the gel. Hence, a comparable strength with the Pt.Augusta was achieved.

5.5 Conclusions in Chapter 5

Five types of geopolymers were synthesized in this study from different Australian fly ash. The microstructural and pore-structural changes with the degree of geopolymerization is assessed deeply and correlated with the compressive strength of final geopolymer systems. Overall, following conclusions can be made from the research presented in this chapter:

- The degree of uniformity and homogeneity of SiO_2 and Al_2O_3 distribution in fly ash directly influence the dissolution of amorphous surface layer. The extent of dissolution controls the geopolymeric gel formation and aluminium incorporation in the gel matrix.

- Combination of aluminium into the silicate backbone during geopolymerization leads to higher compressive strength. In contrast, the lack of aluminium amalgamation with silicates results in a lower degree of geopolymerization and hence lower compressive strength. In addition, the presence of reactive aluminium-silicate bonds in the 1000–800 cm-1 range after geopolymerization is a clear indication of a high degree of geopolymerization.

- A high quantity of aluminium present in octahedral coordination in the precursor fly ash, and conversion of this into tetrahedral units during alkali dissolution is required to obtain high compressive strength. However, the stable and relaxed conversion of aluminium from octahedral to tetrahedral coordination is more significant than the total quantity of octahedral coordinated aluminuim in the formation of homogeneous, well compacted geopolymeric gel and the production of high compressive strength geopolymer mortar.

- Minimum Al_2O_3/Na_2O and SiO_2/Na_2O ratios are required to achieve specific compressive strengths. If the Al_2O_3/Na_2O and SiO_2/Na_2O ratios exceed 2.5 and 6 respectively, 35MPa or higher compressive strength can be obtained at 28 days irrespective of the fly ash source.

- The aluminosilicate gel with a three dimensional (3-D) polysialate-siloxo (Si-O-Al-O-Si) polymeric structure provides high rigidity and stability in the final geopolymer, and contributes to a higher compressive strength. In contrast, gel structure consisting of polysialate-disiloxo and silicate links produces lower strength.

- The meso-porosity of fly ash based geopolymer increases with its degree of geopolymerization. Total pore volume below 1000nm in pore size, rather than overall total pore volume, is a good indicator to the degree of geopolymerization.

6 MECHANICAL PROPERTIES OF GEOPOLYMER CONCRETE

6.1 Overview

This chapter presents the test results and discussion related to the **Phase 2** of the comprehensive experimental study as shown in Figure 3.3, based on geopolymer concrete. The first section reports the compressive strength of five different fly ash geopolymer concrete mixes over a range of activator modulus at a fixed Na_2O dosage in order to optimise the best mix design for the specific fly ash. In the second section the optimum mix design for each fly ash geopolymer concrete was used to investigate the long term mechanical properties; compressive strength, flexural strength, splitting tensile strength, elastic modulus and Poisson's ratio for four fly ash geopolymer concrete. The variation of long term mechanical properties in four geopolymer concrete are discussed with regard to comprehensive microstructural analysis and the influential properties identified in Chapter 4. In the final section, the applicability of current relationships between compressive strength and the mechanical properties based on standards derived for PC concrete is been examined for the fly ash geopolymer concrete. The models derived are verified using data reported in the literature for similar geopolymer concrete.

6.2 Optimize mix design

The variation in compressive strength with AM of five different fly ash geopolymer concrete between 3 and 28 days is presented in Table 6.1. All reported strengths were mean value of three tested concrete cubes at specific period (Appendix C1). Similar to the mix optimization based on geopolymer mortar specimens in Chapter 3 Section 3.2.2.1, the AM is selected to optimize the best mix design for each geopolymer concrete. The partially reacted fly ash spheres in each mix negatively affect the compressive strength and other mechanical properties of the concrete, in particular at the interface between them and the geopolymer matrix (Steveson and Sagoe-Crentsil, 2005). Thus, an optimized geopolymer matrix of each fly ash is expected to have least number of partially reacted particles in their geopolymer gel matrices.

Table 6.1 Changing compressive strength with Activator Modulus (AM)

Geopolymer (GP)	GP mix	Compressive Strength (MPa)		
		3 days	7 days	28 days
GFA	G1.125	34.2	32.1	39.8
	*G1.25	42.6	42.2	47.9
	G1.375	41.5	43.2	48.7
	G1.5	40.7	40.7	36.5
PAFA	PA1.125	33.3	37.6	35.3
	*PA1.25	30.7	31.9	33.1
	PA1.375	35.3	42.1	42.9
	PA1.5	32.1	33.8	42.0
CFA	C1.0	14.4	18.7	17.7
	C1.125	22.5	23.5	24.3
	C1.25	21.8	21.1	22.0
	*C1.375	16.5	16.2	19.3
	C1.5	13.6	15.5	15.0
MPFA	MP0.625	14.9	13.2	16.2
	*MP0.75	20.5	22.6	24.1
	MP1.0	22.7	21.2	22.5
TFA	T1.5	27.8	28.3	31.2
	*T1.625	30.9	32.2	33.1
	T1.75	24.3	25.7	25.7

*Optimum mix design based on geopolymer mortar specimens (Section 3.2.2.1)

The mix design in each fly ash geopolymer concrete was initially selected, based on previous tests on mortar specimens, Chapter 3 Section 3.2.2.1. Additional testing was then undertaken in 0.125 increments, starting from the optimum mix design of the geopolymer mortar as shown in Table 3.12, to determine the optimum compressive strength at 28 days for each fly ash geopolymer concrete. The 28-day compressive strength vs. AM of five different fly ash geopolymer concrete is shown in Table 6.2.

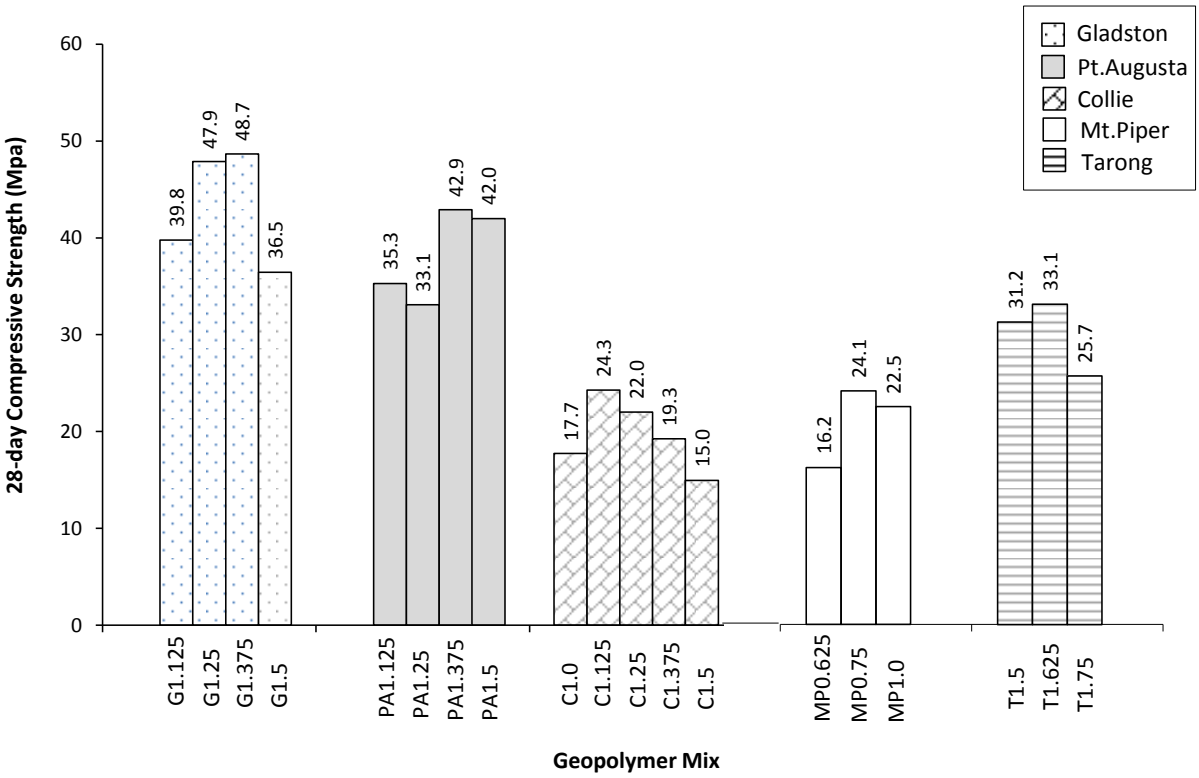

Figure 6.1 The 28-day compressive strength vs. AM

The 28-day strength of Gladstone mixes varied between 36.5 and 48.7 MPa while Pt.Augusta mixes were in the range 33.1 to 42.9 MPa. All Gladstone and Pt.Augusta concrete mixes show higher compressive strength compared to other three fly ash geopolymer concrete. Both Collie and Mt.Piper geopolymer showed the lowest compressive strength in all cases irrespective of the mix design. The strength of Collie mixes varied between 15 and 24.3 MPa while Mt.Piper mixes were between 16.2 to 24.1 MPa.

The optimum compressive strength of Gladstone, Pt.Augusta, Tarong, Collie and Mt.Piper geopolymer concrete at 28 days are 48.7, 42.9, 33.1, 24.3 and 24.1 MPa respectively as shown in Table 6.2. It was observed that the optimum strengths occur at a range of different AM. Hence, the results show no direct correlation between the AM and the compressive

strength, though the lowest AM did give the lowest strength. The optimum compressive strength of both Gladstone and Pt.Augusta were obtained at AM of 1.375, while Collie was obtained at AM 1.125 and the Mt.Piper at 0.75 and Tarong at 1.625. From the previous tests on mortar specimens reported in Chapter 4 Section 4.2, Gladstone, Pt.Augusta and Collie obtained their optimum 28-day compressive strength at AM of 1.25, 1.25 and 1.375, respectively. Thus, the conversion of geopolymer mortar into geopolymer concrete by introducing coarse aggregates had slightly changed the optimum AM. However, both Mt.Piper and Tarong geopolymers obtained their optimum compressive strength at the same AM for both the mortar and concrete. The optimum mix design for each fly ash was then used to investigate the long term performance of geopolymer concrete, in terms of both the mechanical and durability behaviour. This chapter reports the long term mechanical properties. The long term durability aspects will be discussed in Chapter 7.

6.3 Workability

Generally, geopolymer concrete mixes have "collapse" slump due to its sticky and viscous nature in fresh state. The spherical shape of the fly ash particles combined with the lubricating effect of sodium silicate solution increase the flowability and leads to the collapse of the fresh geopolymer concrete. Use of the sodium silicate and sodium hydroxide solutions, which are more viscous than water, usually makes geopolymer concrete more cohesive and sticky than PC concrete. However, a higher slump of geopolymer concrete indicates a less adhesive and highly workable mixture.

In this study, all fly ash geopolymer concrete, except Mt.Piper, displayed a very high, collapsed slump, thus workability is represented by the average diameter of slump flow, similar to that observed for self-compacted concrete (Demie et al., 2013). The measured mean slump flow (diameter) values of Gladstone, Pt.Augusta, Tarong and Collie geopolymer concrete are 735, 550,450 and 350 mm, respectively. However, the Mt.Piper resulted in very stiff mix and experienced difficulties in obtaining uniform mixing and compaction. The Mt.Piper gave a zero slump flow and in a conventional slump test gave a slump height of 40mm. Given the poor workability Mt.Piper geopolymer concrete was not used for the long term mechanical investigation due to its very stiff and non-uniform mix, and difficulties with the manufacture and compaction in large scale specimens.

6.4 Density

Table 6.2 and Figure 6.2 display the long term density development of the four different fly ash based geopolymer concrete. All reported density values were mean value of three tested concrete cylinders at specific period (Appendix C6). All geopolymer concrete display an increase of density with time. The values ranged between 2074 and 2205 kg/m^3. This is in agreement with the literature (Diaz-Loya et al., 2011, Wardhono, 2015) though displaying lower densities than PC concrete which is characteristically cited as 2400 kg/m^3 (AS, 2009).

Table 6.2 Long term density development

Geopolymer	Dry density (MPa)			*Density development (%)
	28 days	90 days	365 days	
GFA	2185	2195	2205	0.91
PAFA	2119	2145	2167	2.27
TFA	2117	2131	2187	3.31
CFA	2074	2081	2093	0.91

*Density increment at 365 days with compared to 28 day value

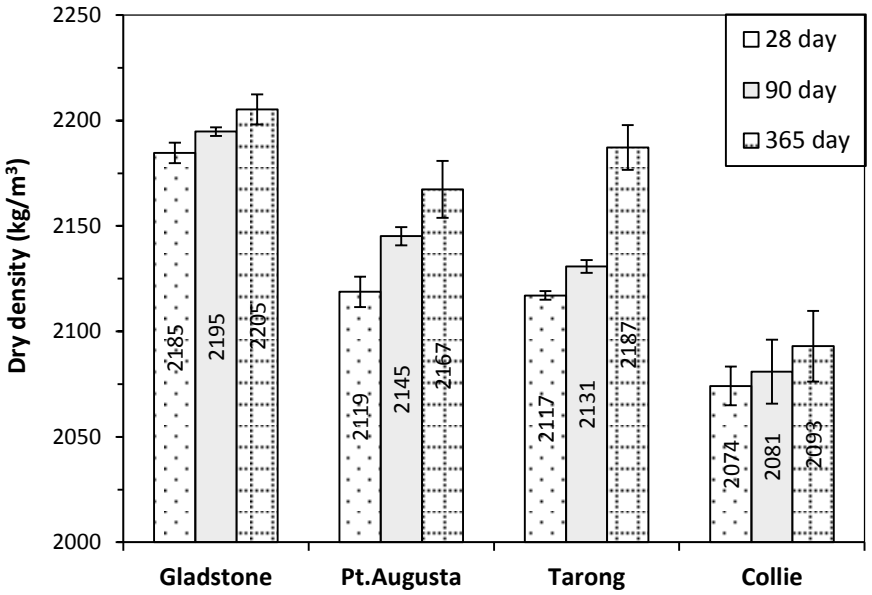

Figure 6.2 Long term density development

Gladstone geopolymer gave the highest density while Collie obtained the lowest at all ages, the density of Pt.Augusta and Tarong geopolymers were between the two. Tarong geopolymer showed the highest density development (3.31%) at 365 days compared to the 28-day density and Pt.Augusta demonstrated the next highest (2.27%) increase in density.

Collie geopolymer had the lowest density development (0.92%) and had the lowest density in all ages. Gladstone gave the highest density values irrespective of age but had an identical density development to that of the Collie.

6.5 Long term mechanical properties

6.5.1 Compressive strength

Table 6.3 and Figure 6.3 show long term compressive strength development of the four fly ash geopolymer concrete. It is observed that the compressive strength of all geopolymers tended to increase with time, but in different increment ratios, depending on the fly ash properties. Gladstone geopolymer obtained the highest strength while Collie the lowest at all ages, the strength of Pt.Augusta and Tarong geopolymers were once more between the two.

Table 6.3 Long term compressive strength development

Geopolymer	Dry density (MPa)			*Strength development (%)
	28 days	90 days	365 days	
GFA	82.5	86.5	87.4	5.9
PAFA	36.9	45.6	47.0	27.4
TFA	29.6	36.5	42.8	44.6
CFA	24.9	27.7	28.7	15.3

*Compressive strength increment at 365 days with compared to 28 day value

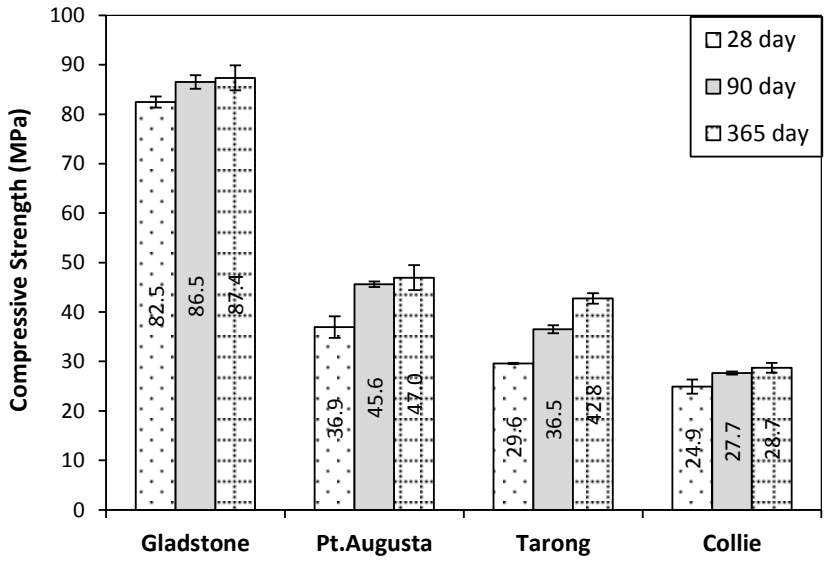

Figure 6.3 Long term compressive strength development

The compressive strength of Gladstone geopolymer ranged from 82.5 to 87.4 MPa while the Collie varied from 24.9 to 28.7 MPa between 28 and 365 days. It was noted that Gladstone obtained 95% of its ultimate strength in first 28 days, showing the lowest percentage increase in strength between 28 and 365 days. Collie geopolymer demonstrated a higher strength gain, 15.3% between 28 and 365 days. However, the actual increase in strength is only by 3.8 MPa which is lower than the 4.9 MPa increase observed for Gladstone. Tarong and Pt.Augusta geopolymer concrete displayed a high compressive strength development, 44.6% (13.2 MPa) and 27.4% (10.1 MPa) respectively, between 28 and 365 days. Pt.Augusta had significant strength development (8.7 MPa) by 90 days, but little further increase (1.4 MPa) in the period between 90 and 365 days. Tarong geopolymer however had a similar increase both from 28 to 90 days (6.9 MPa) and from 90 to 365 days (6.3 MPa). These results demonstrate that there is a strength development over time even though heat curing has been observed to enhance the initial geopolymerization process (Bakharev, 2005a, Palomo et al., 1999). Ryu et al. (2013) investigated compressive strength of geopolymer mortar up to 90 days using a fly ash obtained from a Korean power plant with different mix proportions. The compressive strength development between 28 and 90 days is in the range of 13.1 to 47.5 MPa. Thus the data showed that compressive strength increased by a ratio ranged between 5.7 and 9.7% in this time period. The order of the strength gain is observed to be strongly dependent on the degree of reactivity of fly ash in alkaline media.

6.5.2 Tensile strength

6.5.2.1 Flexural strength

Table 6.4 and Figure 6.4 show the long term flexural strength development of the four fly ash geopolymer concrete. All reported flexural strengths were mean value of three tested concrete beams at specific period (Appendix C2). The flexural strength ranged from 3.36 to 6.30 MPa between 28 and 365 days. Similar to the compressive strength development, the flexural strength of all concrete tended to increase with time. The highest and lowest flexural strengths were displayed by Gladstone and Collie geopolymers, while the Pt.Augusta and Tarong were again in between.

Table 6.4 Long term flexural strength development

Geopolymer	Flexural strength (MPa)			*Strength development (%)
	28 days	90 days	365 days	
GFA	5.44	6.11	6.30	15.8
PAFA	3.57	4.30	5.55	55.5
TFA	3.75	4.52	6.11	62.9
CFA	3.36	3.73	3.92	16.6

*Flexural strength increment at 365 days with compared to 28 day value

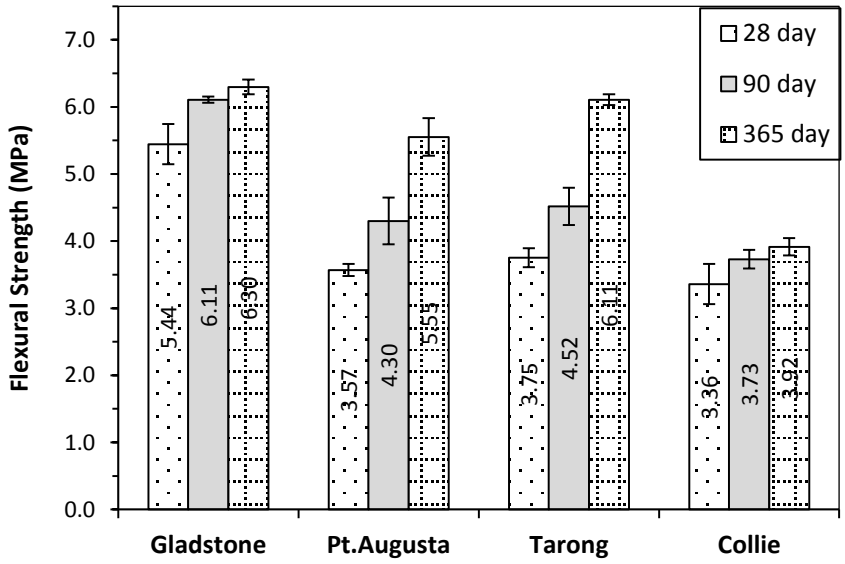

Figure 6.4 Long term flexural strength development

Whilst Tarong geopolymer showed a lower compressive strength, it achieved a slightly higher flexural strength than Pt.Augusta. The flexural strength of the specimens ranged from 7 to 14% of the compressive strength, compared to a range of 9 to 12% typically cited for PC concrete. Diaz-Loya et al. (2011) reported a similar trend but over a wider range, such that the flexural strength ranged between 9 and 26% of the compressive strength. In a comparison of the four fly ash geopolymers, Tarong achieved the highest flexural strength development (62.9%) between 28 and 365 days, followed by Pt.Augusta (55.5%). However, similar to compressive strength development, Gladstone and Collie geopolymer concrete showed the lowest flexural strength development with the age.

6.5.2.2 Splitting tensile strength

Table 6.5 and Figure 6.5 show the long term splitting tensile strength development of four fly ash geopolymer concrete. All reported splitting tensile strengths were mean value of three

tested concrete cylinders at specific period (Appendix C3). The splitting tensile strength of all geopolymer concrete increased with time. The splitting tensile strength ranged from 1.15 to 4.72 MPa between 28 and 365 days, and ranged from 4 to 8% of the compressive strength. Gladstone and Collie geopolymers achieved the highest and lowest splitting tensile strength with Pt.Augusta and Tarong geopolymers once more falling between the two. It is interesting to note that Pt.Augusta showed higher splitting tensile strength than Tarong, though it had lower flexural strength capacity.

Table 6.5 Long term splitting tensile strength development

Geopolymer	Splitting tensile strength (MPa)			*Strength development (%)
	28 days	90 days	365 days	
GFA	4.26	4.67	4.72	10.8
PAFA	2.49	3.41	3.71	49.0
TFA	1.60	2.32	2.90	81.3
CFA	1.15	1.30	1.86	61.8

*Splitting tensile strength increment at 365 days with compared to 28 day value

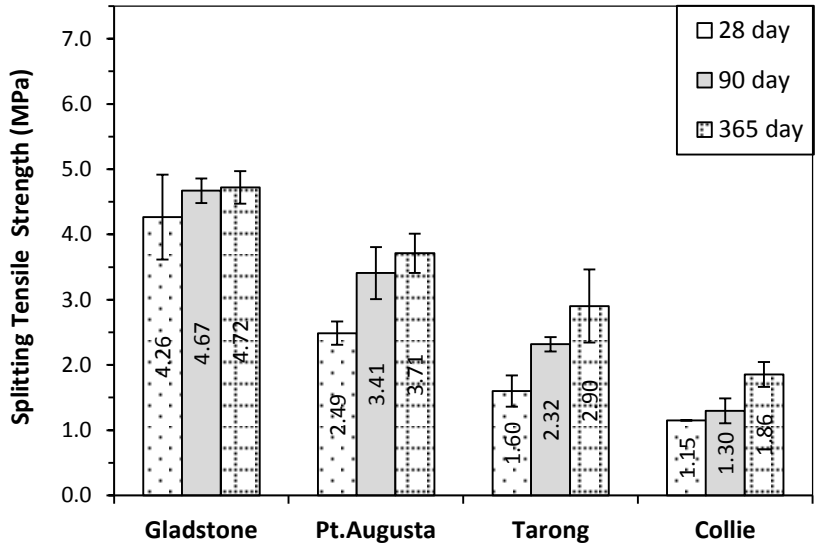

Figure 6.5 Long term splitting tensile strength development

6.5.3 Elastic modulus

The elastic modulus of concrete is defined as the stress retained to induce a unit strain within the elastic limit. The stress-strain curves shown in Figure 6.6 presents the values of elastic modulus measured in this study. As the geopolymer concrete demonstrated brittle failure (Diaz-Loya et al., 2011), the descending branch of the stress–strain curve could not be

determined in any of the tests. Each curve who shows the tangent modulus of elasticity, which varied from 8.2 to 22.7 GPa between Collie and Gladstone geopolymer at 28 days.

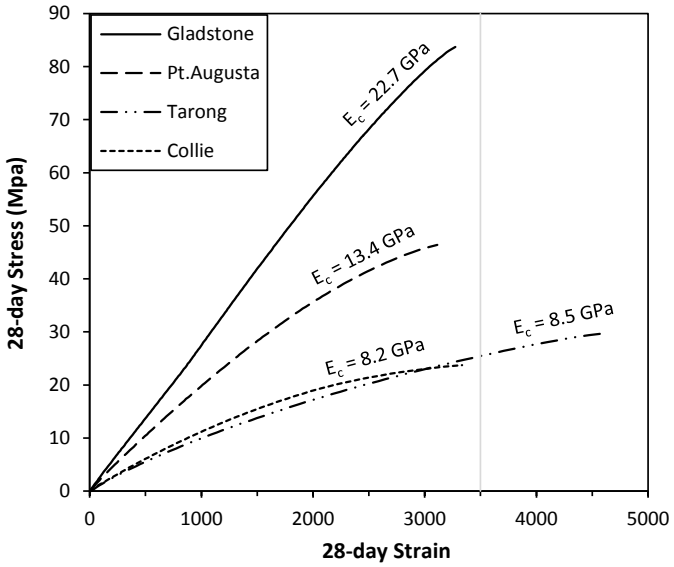

Figure 6.6 Stress–Strain relationship of geopolymer concrete

Table 6.6 and Figure 6.7 show elastic modulus development at 90 and 365 days. All reported elastic modulus values were mean value of three tested concrete cylinders at specific period (Appendix C4). Similar to the strength properties discussed, the elastic modulus also tended to increase with time in all concrete with different increment ratios. Gladstone geopolymer showed the highest value while Collie gave the lowest at all ages. In the first 90 days, Tarong had a very low elastic modulus, similar to Collie and lower than Pt.Augusta. However, by 365 days it had achieved the second highest elastic modulus, having a two-fold increase between 90 and 365 days.

Table 6.6 Long term elastic modulus development

Geopolymer	Elastic Modulus (GPa)			*Elastic modulus development (%)
	28 days	90 days	365 days	
GFA	22.7	23.3	29.0	27.8
PAFA	13.4	14.5	17	26.9
TFA	8.5	10.3	20.9	145.9
CFA	8.2	9.7	10.3	25.6

*Elasticity modulus increment at 365 days with compared to 28 day value

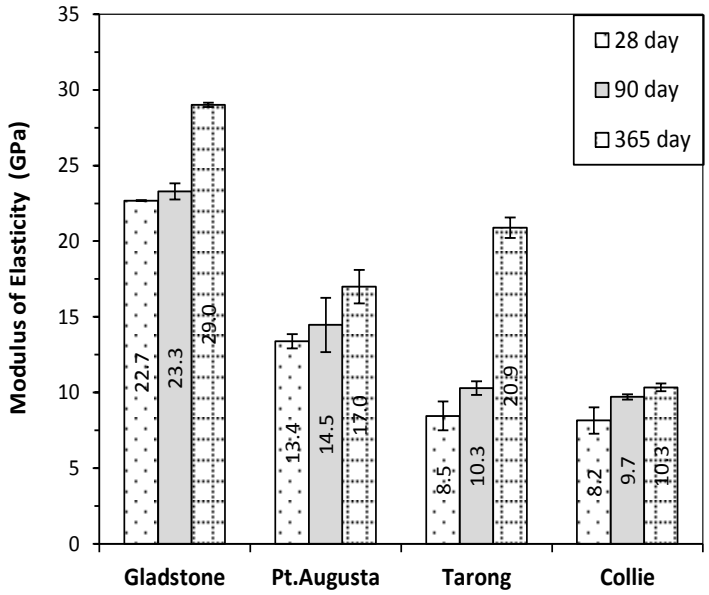

Figure 6.7 Long term elastic modulus development

6.5.4 Poisson's ratio

Figure 6.8 shows long term Poison's ratio development between the four geopolymer concrete. All reported Poison's ratio values were mean value of three tested concrete cylinders at specific period (Appendix C5). The values ranged from 0.12 to 0.28 between 28 and 365 days, and increased with the age. Warner et al. (1998) reported that Poisson's ratio values of PC concrete can range between 0.11 and 0.21, but usually fall in the range from 0.15 to 0.2. Values obtained by the four geopolymer concrete tended to populate the lower end of this range at 28 days, but three of them fall into the standard range (0.15–0.2) at 90 days. Tarong geopolymer exceeded this upper end of PC concrete and obtained a significantly high Poisson's ratio at 90 and 365 days. However, all other geopolymers fell into the standard range of 0.15–0.2 at 365 days.

Diaz-Loya et al. (2011) prepared geopolymer concrete using 13 different low calcium fly ash with a mix of 14 M sodium hydroxide and sodium silicate at a weight ratio of 1:1 cured at 60 ^{o}C for 72 hours. The observed Poisson's ratio at 28 days was ranged from 0.08 to 0.17. It is noted that most of the data points of Diaz-Loya et al.'s study (2013) also fell within the range of 0.11 to 0.20. Hence, experiment on results of this study corroborate the previously published data and provide clear evidence that Poisson's ratio of fly ash geopolymer concrete is similar to that of PC concrete.

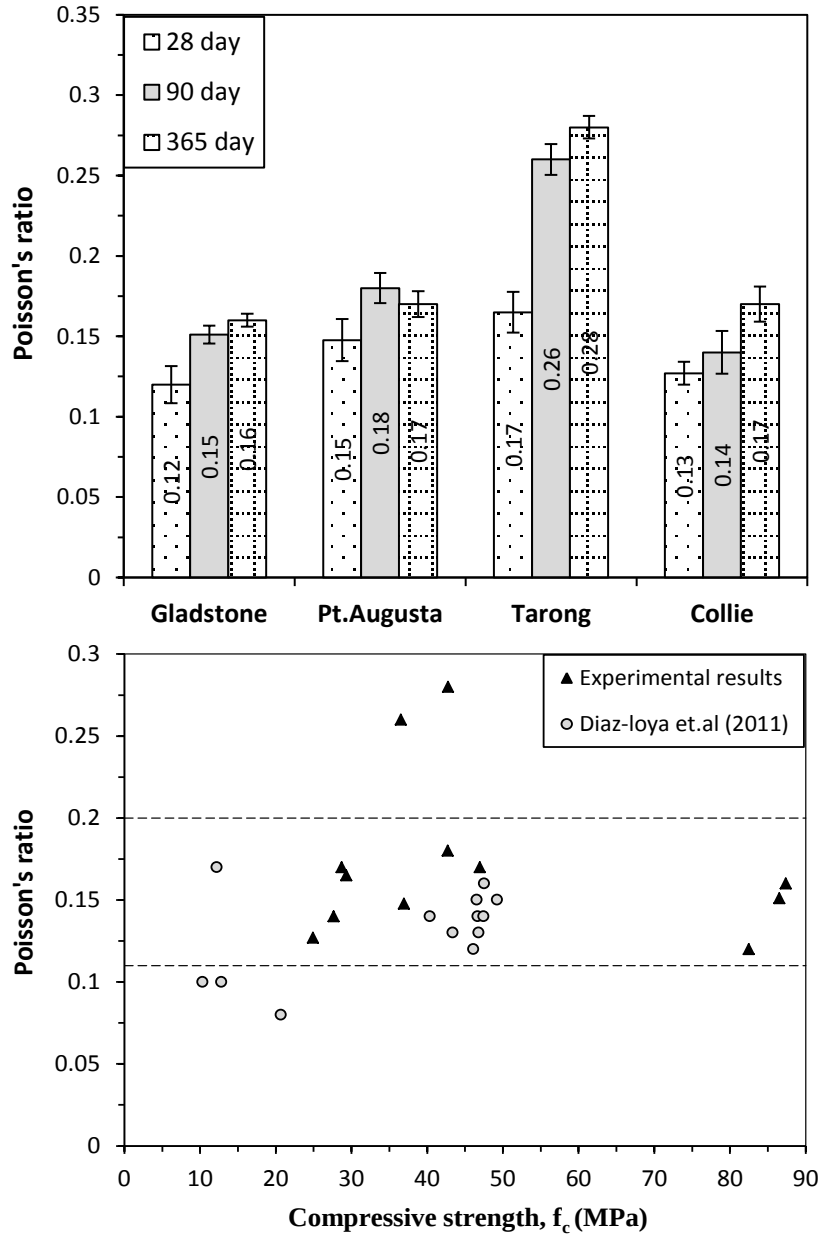

Figure 6.8 Long term Poisson's ratio development

6.6 Effect of microstructure development on mechanical properties

6.6.1 Geopolymeric gel matrix

In the geopolymerization process, alumina and silica species in fly ash rapidly react with highly alkaline activator solution and produce a three-dimensional polymeric chain and ring structure consisting of Si–O–Al–O bonds, Equation 6.1 (Palomo et al., 1999) where z is the type of bond presence (1, 2, or 3), and n is the degree of polymerization. The schematic

formation of the resultant geopolymer product is generally represented by Equation 6.2 and 6.3 (Davidovits, 1999).

$$Na_n[-(SiO_2)z-AlO_2]n\cdot wH_2O \qquad (6.1)$$

$$n(Si_2O_5,Al_2O_2) + 2nSiO_2 + 4nH_2O + NaOH \longrightarrow Na^+ + n(OH)_3-Si-O-\underset{\underset{(OH)_2}{|}}{Al^-}-O-Si-(OH)_3 \qquad (6.2)$$

(Geopolymer precursor)

$$n(OH)_3-Si-O-\underset{\underset{(OH)_2}{|}}{Al^-}-O-Si-(OH)_3 + NaOH \longrightarrow (Na^+)-(-\overset{|}{\underset{\underset{|}{\overset{|}{O}}}{Si}}-O-\overset{|}{\underset{\underset{|}{\overset{|}{O}}}{Al^-}}-\overset{|}{\underset{\underset{|}{\overset{|}{O}}}{O}}-Si-O-) + 4nH_2O \qquad (6.3)$$

(Geopolymer backbone)

The Si/Al (atomic) ratio determines the structure of the geopolymer backbone. In this study, it ranged between 2.69–2.84, 2.55–2.64 and 2.48–2.58 for, Gladstone, Pt.Augusta and Collie, at 28, 90 and 365 days respectively. As such, the geopolymer structure was inferred to be polysialate–siloxo (Si–O–Al–O–Si–O). In Tarong geopolymer, the Si/Al ratio was 4.05–3.65, and the corresponding gel structure is identified as polysialate–disiloxo (Si–O–Al–O–Si–O–Si–O). In all geopolymers, the Si/Al ratio decreased with age. This indicates an on-going geopolymerization process, with continuous gel formation along with incorporation of alumina into the silicate backbone. The Si/Al ratio of all geopolymer concrete, other than Tarong, varied over a small range, but their mechanical properties differed significantly. Hence, although the Si/Al ratio indicated that the geopolymer bond structure should be similar, the nature of the geopolymer gel matrix formed, in terms of uniformity and compactness, would appear to be significantly different, which is hypothesized as the reason for the mechanical properties observed.

The matrix formed and its development with the time in Gladstone and Collie geopolymer concrete are displayed in Figure 6.9. Gladstone produced a uniformly distributed geopolymeric gel–microstructure at all ages. The degree of reactivity of fly ash governs the dissolution, coagulation and gel formation, which is itself dependent on the properties of source material.

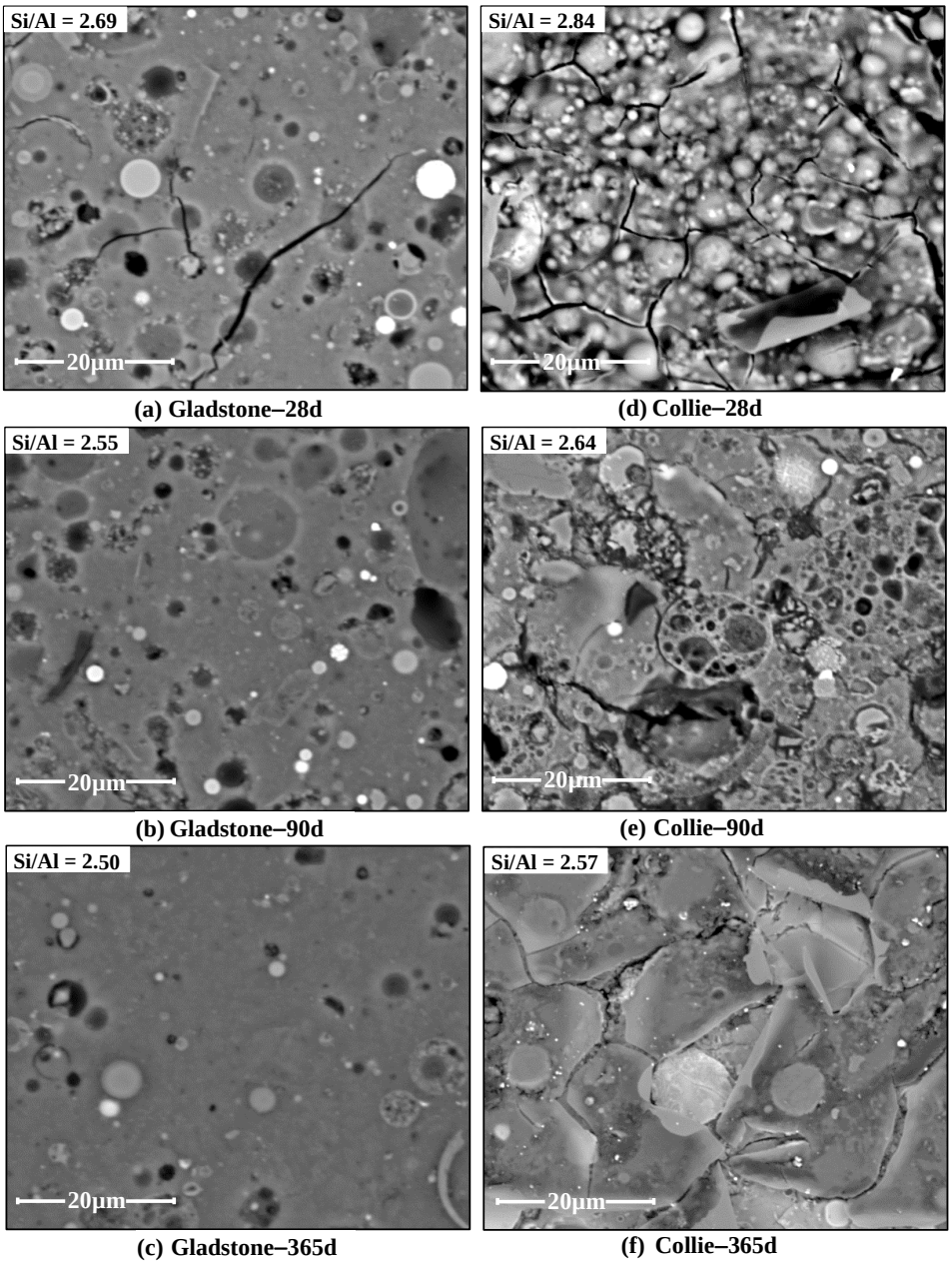

Figure 6.9 SEM images of gel–microstructure in (a–c) Gladstone and (d–f) Collie geopolymers

In Chapter 4, it is reported that higher quantity of fly ash particles with the range of 10 and 20µm size coupled with a larger surface area increased the fly ash reactivity. Gladstone fly ash has the highest surface area with a large amount of finer particles, especially a higher percentage passing at 10, 20 and 45 micron sieves. It also consists of a high amount of reactive alumina–silica amorphous phase. The very fine particles of amorphous phase in Gladstone thus rapidly react with the alkali activator and precipitates geopolymeric gel on to the surface of the fly ash particles. This is because alumina–silica species are primarily leached by dissolution of the amorphous phase, not the crystalline phases of fly ash

(Hanjitsuwan et al., 2014), with the significant part of the alkali–fly ash reaction occurring at the particle–liquid interface (Diaz et al., 2010). This gel then diffuses through the surface covering and coalescing unreacted fly ash spheres together. Continuous gel precipitation further fills up the interior spaces and forms a uniform, strongly compacted and well condensed gel–microstructure.

The Gladstone fly ash also contains a high CaO percentage. The CaO reacts with the alkali activator and produces calcium–aluminosilicate gel (C–A–S–H), Figure 6.10(a). The C–A–S–H gel coupled with the sodium–aluminosilicate (N–A–S–H) gel provides additional rigidity to the geopolymer backbone. The combination of the C–A–S–H and N–A–S–H gels result in the dense microstructure observed for the Gladstone geopolymer. This dense microstructure in turn results in the high compressive strength at 28 days and beyond. Due to high reactivity of the material, little fly ash remains available for subsequent geopolymeric reaction, and hence the minimal strength development observed between 28 and 365 days.

Collie geopolymer displayed a significantly different microstructure compared to that of Gladstone. A large number of unreacted fly ash particles were observed in the microstructure at 28 days, Figure 6.9(d). These comprised a number of unreacted fly ash particles that were separated from the geopolymeric binder, indicating weak adhesion between the gel and the particles. Other unreacted spheres were partially embedded in the precipitated gel. Collie fly ash has the lowest surface area and a higher fraction of coarser particles, i.e. very low level of particles passing at 10, 20 and 45 micron sieves. Although it contains the highest percentage of reactive amorphous phase the reactivity and dissolution of coarser fly ash particles in alkali activator and subsequent geopolymeric gel formation is observed to be much lower, as evidenced by the large number of unreacted particles. This resulted in the low compressive strength for geopolymer concrete produced using Collie fly ash. On the other hand, the microstructure does show a decrease in the number of unreacted particles at 365 days, indicating that there has been some additional geopolymerization and gel formation, as reflected by the increase in strength observed. This excess gel however is distributed unevenly over the matrix. This resulted in forming non-homogeneous small gel units as displayed in Figure 6.9(f) rather than forming an interconnected uniform gel matrix. Hence, this would indicate that the compressive strength of geopolymer concrete does not only rely on the quantity of gel formation, but also on uniform distribution of gel and compactness, the

combination of which leads to the dense microstructure observed. This is hypothesised as the reason that the Collie geopolymer had a low compressive strength even after 365 days.

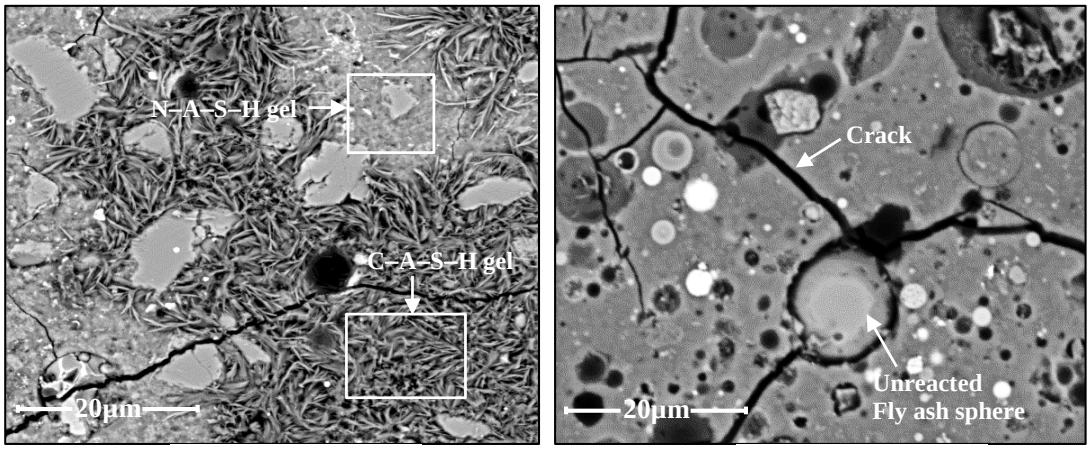

(a) Gladstone–28d **(b) Tarong–365d**

Figure 6.10 SEM images of (a) different aluminosilicate gel and (b) crack pattern

Both Pt.Augusta and Tarong had what could be regarded as moderate compressive strength between ~30 and ~48 MPa. The microstructure of both geopolymer concrete are shown in Figure 6.11. The gel matrices of both are heterogeneous, having a number of unreacted/partially reacted fly ash particles. Both geopolymers had micro–cracks on their surface, but with Tarong displaying more micro-cracks and a greater crack width than the Pt.Augusta. Similar to Gladstone, both Pt.Augusta and Tarong contained a large amount of fine particles, but they had a lower surface area and amorphous content. These material differences are hypothesised as negatively affecting their degree of alkali reactivity resulting in the non-uniform, heterogeneous geopolymer matrix observed for both concrete. The unreacted/partially reacted fly ash particles behave as composites. These composites and the interface between them and geopolymer matrix is hypothesized as an area of weakness and thus has a significant bearing on the overall strength of the concrete (Steveson and Sagoe-Crentsil, 2005), resulting in the lower compressive strength achieved compared to the Gladstone geopolymer concrete.

Pt.Augusta fly ash has the highest CaO content while Tarong has the lowest. The C–A–S–H gel produced by this additional CaO in the Pt.Augusta is identified as one reason for the higher strength observed compared to the Tarong, although it has a lower surface area. Tarong fly ash contains more unburnt carbon content. This acts as an inert particulate in the gel matrix, thus may cause a spread of micro cracks. Both geopolymers however showed a

significant strength development between 28 and 365 days. It is hypothesised that the relatively low surface area of the two fly ash led to a lower initial dissolution of alumina-silicate species. This dissolution continued over time and produced more geopolymer gel, which lead to the increase in the homogeneity observed and resulted in the strength development observed for both Pt.Augusta and Tarong.

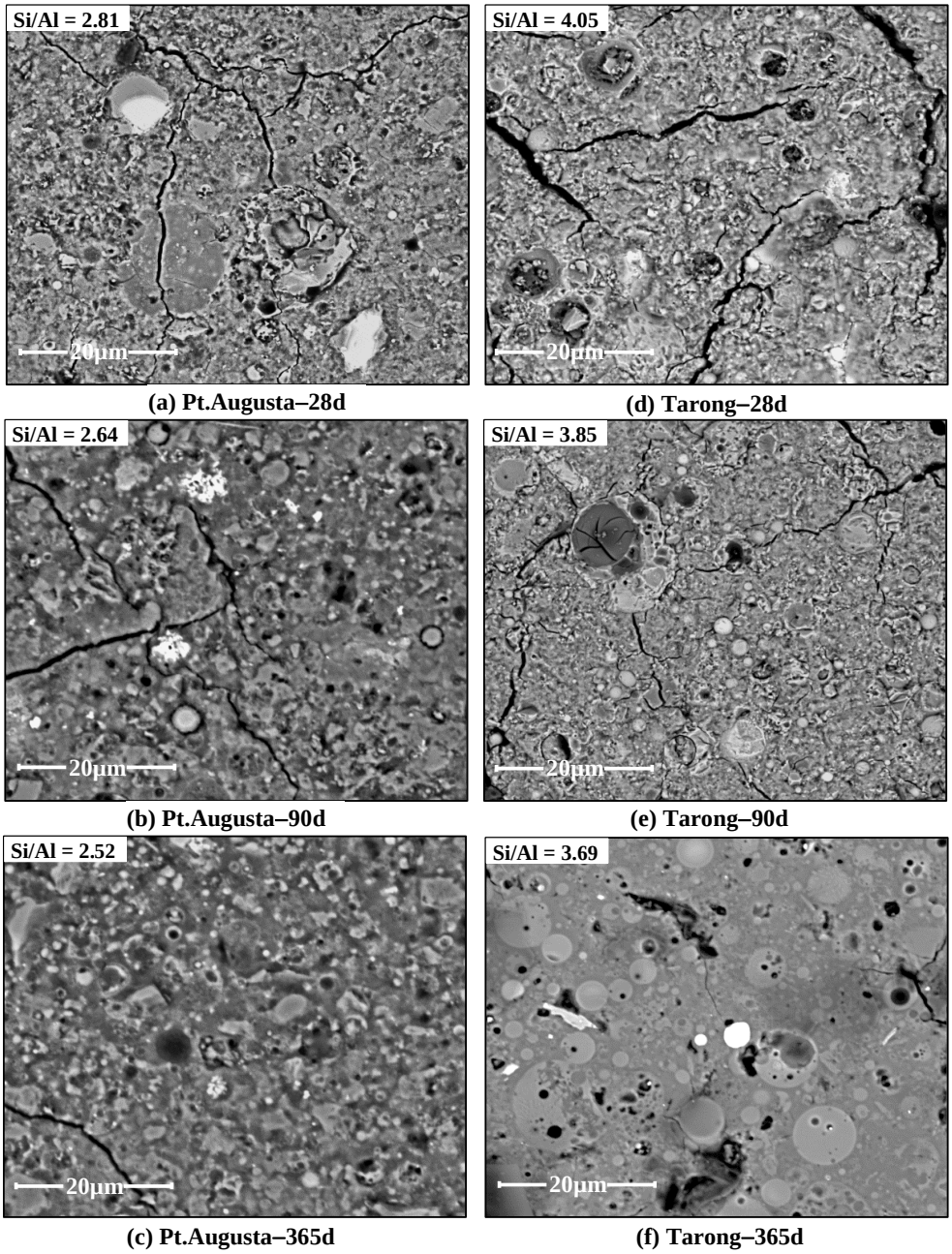

Figure 6.11 SEM images of microstructure in (a-c) Pt.Augusta and (d-f) Tarong geopolymer

6.6.2 Interfacial Transition Zone (ITZ)

In addition to the nature of the geopolymer matrix formed, the ITZ of geopolymer concrete plays a crucial role in the concrete performance. In PC concrete, coarse aggregate has an ITZ of about 100µm depth with two layers; one is a duplex film (1µm) at the surface of the aggregate and other one is the porous transition zone of 20−100µm deep (Demie et al., 2013). However, Demie et al. (2013) noted that ITZ in fly ash geopolymer concrete is formed by combining these two layers, and is defined as the interface between aggregate and geopolymer paste. The flexural strength and splitting tensile strength of fly ash geopolymer concrete are strongly dependent on this geopolymer gel−aggregate bond strength. Figure 6.12 shows a comparison of ITZ with the bulk geopolymer gel matrix in four different concrete.

The ITZ is critical because it is known to have a different microstructure from the bulk of hardened geopolymer paste and the interface is also considered as the specific location of early cracking. Literature (Scrivener et al., 2004, Cwirzen and Penttala, 2005) reported that ITZ in PC concrete is caused by the disorder of packing the anhydrous cement grains in the transition zone. In geopolymer concrete, ITZ is caused by incomplete packing of unreacted fly ash microsphere particles in the transition between the geopolymer paste and coarse aggregates as the aluminosilicate gel formation is strongly dependent on the degree of reactivity of fly ash. This phenomenon is due to the incomplete dissolution of a large proportion of fly ash and the existence of differing composition and size of unreacted fly ash particles. The ITZ is a region of transition which is highly heterogeneous, non-uniform and varying from point to point along each aggregate particle. In this study, Gladstone showed a denser ITZ between aggregates and geopolymer matrix as shown in Figure 6.12(a-b). There is no obvious difference noted between the microstructure of the ITZ and the bulk geopolymer matrix. Sarker et al. (2013) showed the fracture plane in the PC concrete passed predominantly around the aggregates and those in the geopolymer concrete generally passed predominantly through the aggregates. This behaviour was observed in Gladstone geopolymer in the tensile testing. The high bond strength at the interface of the geopolymer binder and the aggregates lead to the fracture plane passing predominantly through the aggregates instead of following the interface. The strong ITZ observed in Gladstone geopolymer is identified as the reason for the high flexural and splitting tensile strengths observed at all ages.

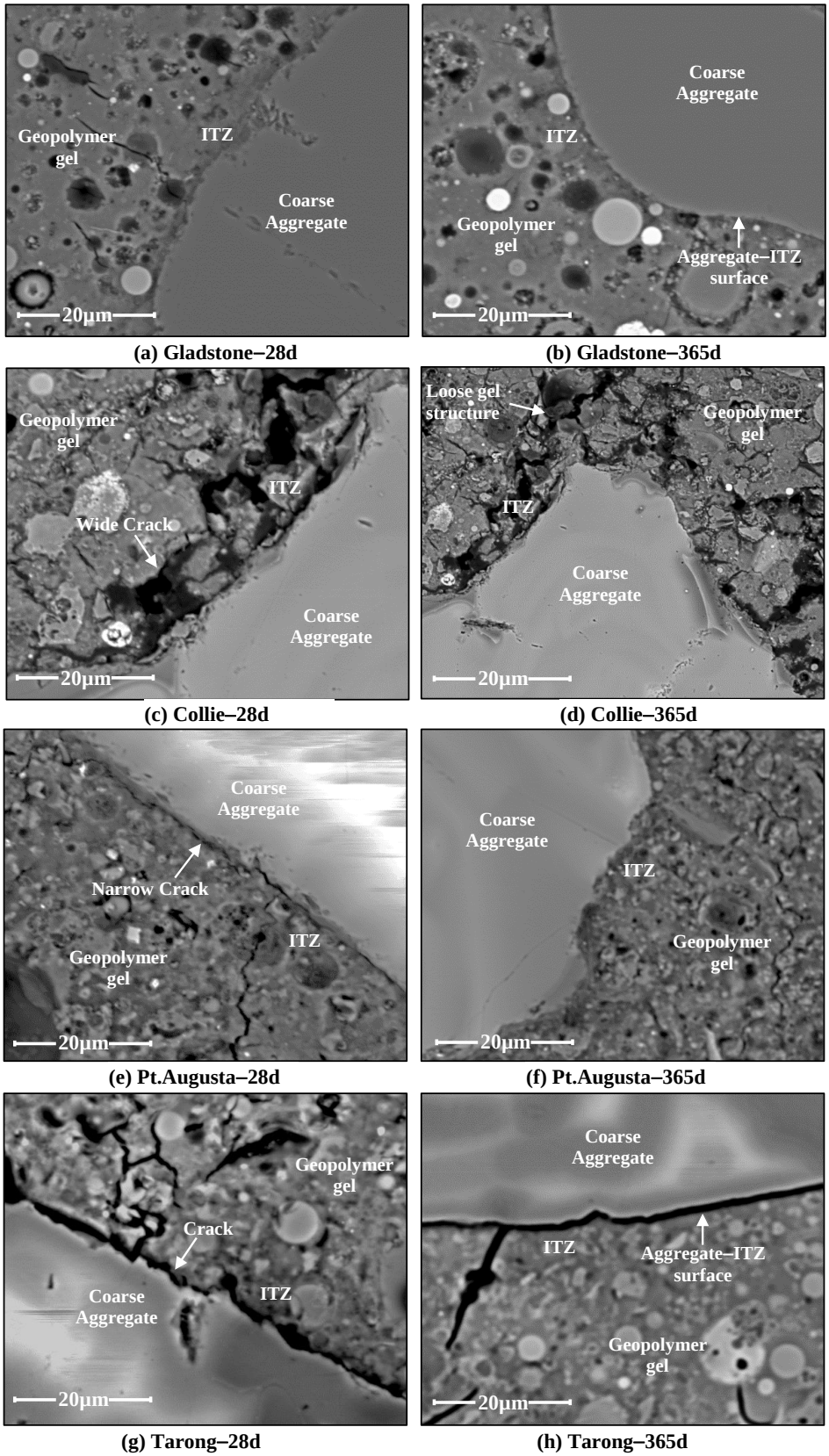

Figure 6.12 SEM images of ITZ in different fly ash geopolymer concrete

Collie showed a highly heterogeneous and non-uniform ITZ, Figure 6.12(c-d). The unreacted, partially reacted fly ash spheres in Collie geopolymer concrete in the aggregate interface produced a loose and porous interfacial zone. The propagated micro-cracks further took away the interconnection between aggregate and geopolymer binder, and hence produced a weak aggregate-gel bond strength. The experimental observations further revealed that the fracture plane of the Collie geopolymer concrete specimen passed predominantly around the aggregate, rather than through the aggregates. This explains the low flexural and tensile strength reported in Collie geopolymer concrete at 28 days. As the geopolymerization progresses, the space between the aggregate and the geopolymer paste was gradually replaced by some additional geopolymer gel as the polymerization continued. However, due to the low degree of reactivity of Collie fly ash the gel formation is expected to be relatively small. The SEM image shows a relatively porous and loose interface at 365 days confirming this expectation. This resulted in the minimal tensile strength development observed in Collie geopolymer concrete.

Pt.Augusta does not show any discernible difference between the microstructure of ITZ and the bulk geopolymer matrix. Narrow micro-cracks are observed in the aggregate-gel interface at 28 days, but not at 365 days, which appears as a strong aggregate-gel interface. The continuous geopolymerization process and gel formation thus densify (refine) the ITZ filling spaces between aggregate-gel interface. This resulted in the high splitting tensile strength development achieved by Pt.Augusta between 28 and 365 days. SEM showed that Tarong had a weak aggregate-gel interface compared to Pt.Augusta. Tarong, however, did display progressive geopolymer gel formation with age, Figure 6.12(d-f), but this gel refined the bulk gel-microstructure rather than the ITZ. This resulted in a weak aggregate-gel interface even at 365 days. The high unburnt carbon in Tarong is understood to weaken the bonding with aggregates. It further contains high amorphous SiO_2 content, which is expected to result in more Si^{+4} being leached into the activator. The optimum Tarong geopolymer mix also required a higher sodium silicate concentration than other mixes. Fernandez-Jimenez et.al (2006a) has reported that the presence of excess Si^{+4} in the alkaline activator solution has a substantial negative effect on the gel-aggregate bond. The combination of these factors appeared to negatively affect the gel-aggregate bond in Tarong geopolymer concrete. This is supported by the lower splitting tensile strength observed compared to the Pt.Augusta.

It was noted that the Tarong had a higher flexural strength than Pt.Augusta at all ages. Sarker et al. (2013) stated that the higher tensile and bond strengths of geopolymer concrete increased its critical stress intensity factor which resulted in less tortuosity of the fracture plane and relatively more brittle type of failure than in the PC concrete. Both Tarong and Pt.Augusta geopolymers followed a similar trend, but Tarong showed a significantly higher failure strain than Pt.Augusta, Figure 6.6, thus improving the ductility of the material. The maximum fibre stress reached in the flexural strength test is higher than the splitting strength because the propagation of a crack is blocked by less stressed material near to the neutral axis. The high strain capacity of Tarong assists in re-distribution of stresses. This is hypothesised as the reason for higher resistance to the flexural failure in Tarong than Pt.Augusta concrete.

All geopolymer concrete in this study showed a much lower elastic modulus than PC concrete for similar compressive strengths (AS, 2009). Liu et al. (2014) reported that the pore volume and elastic modulus have a linear relationship, as the density of the geopolymer concrete increases the elastic modulus also increases. Puertas et al. (2011) reported that elastic modulus of concrete is dependent on the porosity and packing efficiency, i.e. the higher the packing density the higher the modulus of elasticity. This study showed all fly ash geopolymer concrete had a lower density than PC concrete. The water content in the geopolymer mix does not participate in the geopolymer reaction, Equation 3, and is expected to evaporate during the high temperature curing. This may lead to more air voids in the geopolymer matrix and is believed to increase the porosity of the geopolymer concrete compared with PC concrete. In addition, the micro-cracks induced on the surface of geopolymer matrix due to high temperature curing can easily spread through these air voids into the geopolymer matrix. The increase of porosity and crack propagation would negatively influence the packing density of the geopolymer gel-microstructure. This is hypothesised as the reason for the reported lower elastic modulus compared to PC concrete.

Similar to the aforementioned mechanical properties discussed, the Gladstone geopolymer showed the highest elastic modulus while Collie had the lowest. The literature (Williams et al., 2011, Kirschner and Harmuth, 2004) reports that the elastic modulus of geopolymer concrete is dependent on the degree of geopolymerisation. Duxson et al. (2007b) further noted that the elastic modulus is influenced by the alkali-activated metakaolin microstructure rather than by the chemical composition. The Gladstone geopolymer had a densely packed,

uniform gel-microstructure with the least amount of partially dissolved fly ash grains and surface micro-cracks. It further showed a high level of interconnectivity between geopolymer gel and aggregates, especially at the aggregate interface. This would account for the high elastic modulus achieved by Gladstone geopolymer. In contrast, Collie had a very heterogeneous and non-uniform microstructure with many unreacted particles and an interconnected micro-crack network, showing a higher discontinuity and looser microstructure resulting in the low elastic modulus observed. The differences in the elastic modulus of Pt.Augusta and Tarong geopolymers also correlate well with their respective geopolymer matrices. Pt.Augusta had a less dense gel matrix with partially dissolved fly ash grains and voids. There is no clear difference of microstructure observed with the age. Hence, this would explain the low elastic modulus of Pt.Augusta compared with Gladstone at all ages. Tarong had a less compacted heterogeneous microstructure up to 90 days. However, beyond 90 days the microstructure was significantly denser, consistent with continuing dissolution and gel formation. The improvement in compactness and packing density of the gel-microstructure is hypothesised as the reason for the observed improved elastic modulus development in Tarong after 90 days.

6.7 Relationship between mechanical properties

Correlations between mechanical properties were derived using statistical regression analysis based on the aforementioned long term experimental data. Linear regression lines were obtained using the least−squares technique, to drive the relationships, which best fit the experimental data after analysing residuals and adjusted R^2 values of several different regression models. Moreover, the confidence and prediction interval bands for the each regression line were calculated and plotted together with the relevant best fit line. The confidence interval focuses on the prediction lines, while the prediction interval focuses on the specific data point. The points on each interval were obtained by subtracting from, and adding to, the product of its estimated statistic, t_s, and standard error, S_e (Altman and Gardner, 1988).

The confidence interval means that there is a 95% probability that the true linear regression line of the population will lie within the confidence interval of the regression line calculated from the sample data, Equation 6.4 (Brown, 2001). The prediction interval means that for a

specific value X_0, there is a 95% probability that the real value of Y (in the population) corresponding to X_0 is located within this interval, Equation 6.5 (Brown, 2001).

$$Y_{pred.} \pm t_{0.05}\sqrt{\frac{\sum(Y-Y_{pred.})^2}{n-2}} \cdot \sqrt{\frac{1}{n}+\frac{(X-\bar{X})^2}{SS_x}} \quad (6.4)$$

$$Y_{pred.} \pm t_{0.05}\left(1+\sqrt{\frac{\sum(Y-Y_{pred.})^2}{n-2}}\right) \cdot \sqrt{1+\frac{1}{n}+\frac{(X-\bar{X})^2}{SS_x}} \quad (6.5)$$

where $Y_{pred.}$ is the prediction of Y values, $t_{0.05}$ is the *t* critical value for 95% interval, n is the number of data points used to establish regression line, X is the true value while $\bar{X}$ is the mean of sample and SS_x is the sum of the squares of standard error of X values.

6.7.1 Compressive strength vs. Workability

Figure 6.13 displays a strong correlation between compressive strength and workability. That is, compressive strength increases with an increase in workability in accordance to the relationship derived using the results of the present study, $f_c=0.15\phi-31$, whereas f_c and ϕ represent compressive strength (MPa) and slump flow diameter (mm), respectively. Demie et al. (2013) prepared self-compacting geopolymer concrete using a low calcium fly ash, and observed an increase of compressive strength with an increase of workability. The compressive strengths range was 40.85–53.08 MPa from 1 to 28 days, and corresponding slump flow values lay between 625 and 710mm. It is noted that the experimental data reported by Demie et al. (2013) well support the proposed equation. This would demonstrate that the workability does have an influence on the compressive strength, but a broader study is required to identify the acceptable range of slump flow for the fly ash geopolymer concrete.

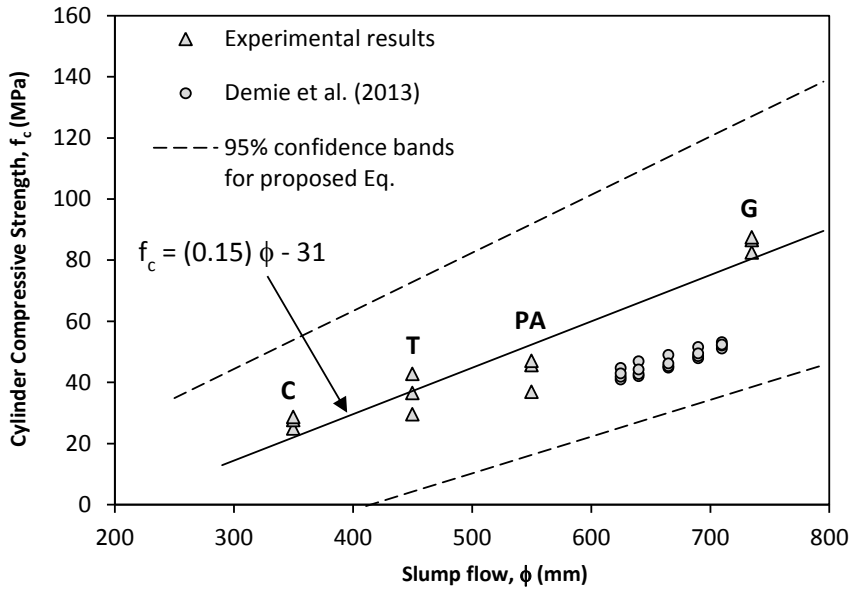

Figure 6.13 Compressive strength vs. slump flow

6.7.2 Compressive strength vs. Density

Figure 6.14 displays a good correlation between compressive strength and density based on the current experimental results, which yielded the relationship as $f_c = 0.44\rho–900$, whereas ρ and f_c represent density (kg/m^3) and compressive strength (MPa), respectively. Diaz-Loya et al. (2011) prepared a series of geopolymer concrete specimens using 13 different low calcium (class F) fly ash. The measured dry density of those specimens ranged from 1890 to 2371 kg/m^3, and included in Figure 6.14 for comparison with the present experimental results. These density values did not directly follow the proposed relationship derived based on the present study. However, a good relationship can be seen between compressive strength and density if Gladstone geopolymer concrete results are excluded from the experimental data reported by the author and who Diaz-Loya et al. (2011) (refer Figure 6.14–A).

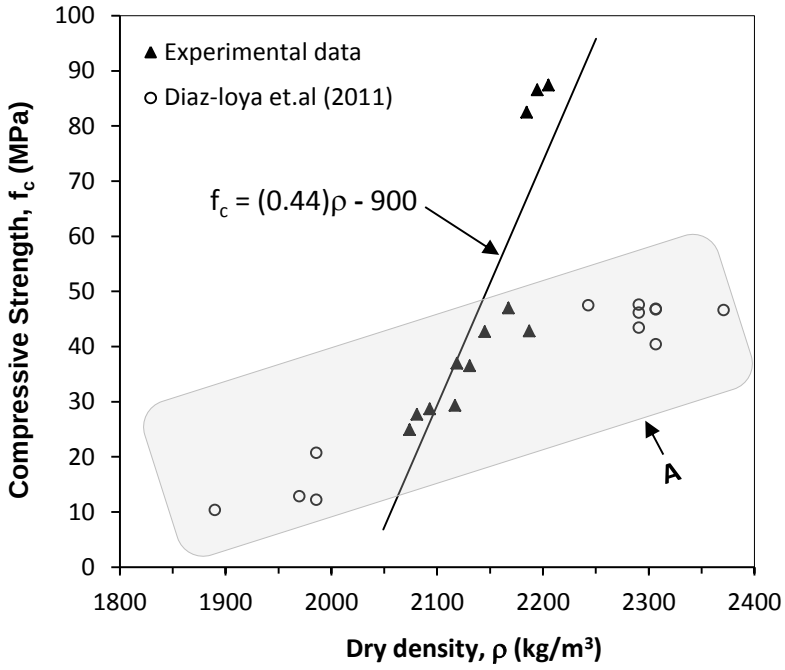

Figure 6.14 Compressive strength vs. density

6.7.3 Compressive strength vs. Flexural strength

Figure 6.15 shows a scatter plot of the flexural versus the compressive strength and a linear regression line representing the relationship between the two variables. The proposed regression model is as given below in Equation 6.6, whereas $f_{ct.f}$ is the mean flexural strength and f_c is the mean compressive strength.

$$f_{ct.f} = 0.7\sqrt{f_c} \text{ MPa} \quad (6.6)$$

Both the 95% confidence and prediction intervals for the Equation 6.6 were also calculated and plotted in Figure 6.15. That is, there is a 95% probability that the any best fit line for the low calcium (class F) fly ash geopolymer concrete population lies within the confidence intervals of the Eq. 6. On the other hand, there is a 95% probability that the flexural strength of low calcium fly ash geopolymer concrete population, corresponding to the specific compressive strength, is located within the prediction intervals of Equation 6.6.

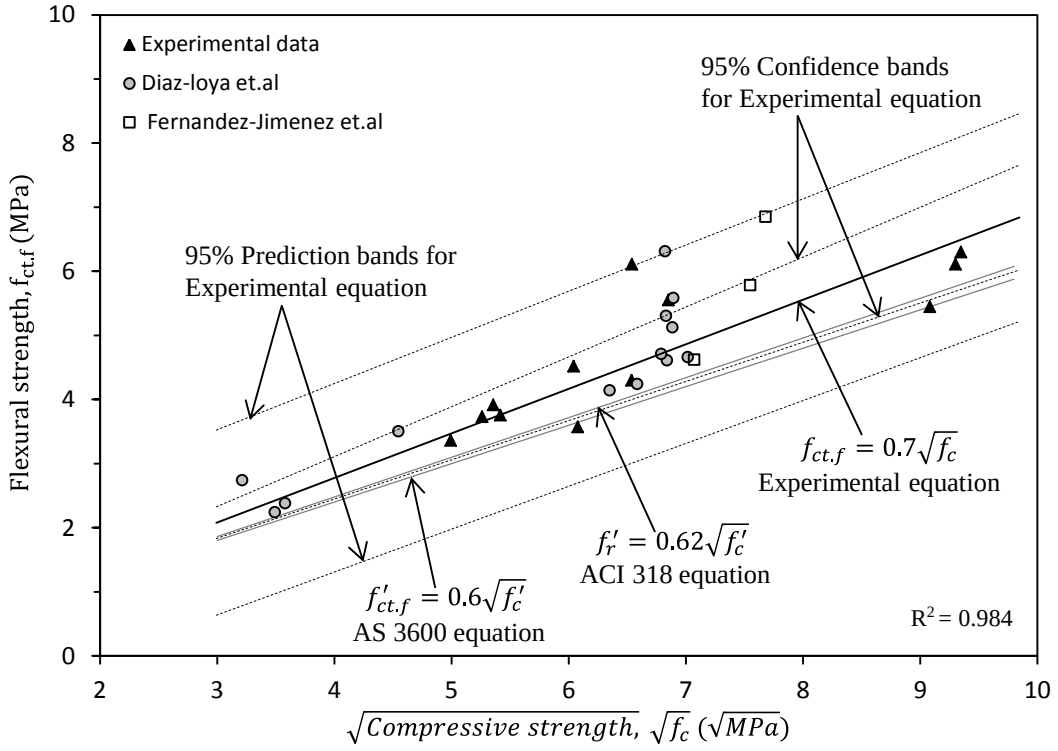

Figure 6.15 Flexural strength vs. compressive strength

To cross check the model, data reported by Diaz-Loya et al. (2011) and Fernandez-Jimenez et al. (2006a) were also included. Diaz-Loya et al. (2011) prepared geopolymer concrete using 13 different fly ash (class F) with a 14M sodium hydroxide and sodium silicate activator at a weight ratio of 1:1 cured at 60 ^{o}C for 72 hours. The observed compressive and flexural strengths ranged from 10.34 to 49.24 MPa and 2.24 to 4.71 MPa, respectively. Fernandez-Jimenez et al. (2006a) reported a range of compressive and flexural strengths working with single type of fly ash, which was activated with a 12.5M sodium hydroxide and sodium silicate activator solution and cured at 85 ^{o}C for 20 hours. It can also be appreciated that almost all these data points (Diaz-Loya et al., 2011, Fernández-Jiménez et al., 2006a) fall within the prediction bands of Equation 6.7, which increased the reliability of this proposed design equation.

Both the Australian standard, AS 3600 section 3.1.1.3 (2009) and American Concrete Institute, ACI 318 section 8.5.2.3 (2008) provide equations to estimate the flexural strength for use in calculating deflections in PC concrete (Equation 6.7 and Equation 6.8, respectively). It is worth noting that derived regression equation for fly ash geopolymer concrete (Equation 6.6) followed a similar pattern to Equation 6.7 and Equation 6.8.

$$f'_{ct.f} = 0.6\sqrt{f'_c} \text{ MPa} \quad (6.7)$$

$$f'_r = 0.62\sqrt{f'_c} \text{ MPa} \quad (6.8)$$

where both $f'_{ct.f}$ and f'_r represent the characteristic flexural strength and f'_c is the characteristic compressive strength.

It can be inferred from Equation 6.6 that as the compressive strength increases so does the flexural strength; however, the ratio of flexural to compressive strength decreases as the compressive strength increases. On the other hand, both the AS 3600 (2009) and ACI 318 (2008) equations lie below the lower confidence interval of Equation 6.6. That means, the design equations provided by both standards for PC concrete underestimate the flexural strength for geopolymer concrete. Hence, application of current codes of PC concrete would provide a conservative design of geopolymer concrete structures in terms of flexural strength.

6.7.4 Compressive strength vs. splitting tensile strength

The splitting tensile strength of the four different fly ash geopolymers ranged from 1.15–4.26 MPa, 1.30–4.67 MPa and 1.86–4.72 MPa at 28, 90 and 365 days, respectively. Figure 6.16 shows a scatter plot of the splitting tensile versus the compressive strength. The proposed linear regression line, Equation 6.9, representing the relationship between the two variables in fly ash geopolymer concrete, whereas $f_{ct.sp}$ is the mean splitting tensile strength and f_c is the mean compressive strength.

$$f_{ct.sp} = 0.45\sqrt{f_c} \text{ MPa} \quad (6.9)$$

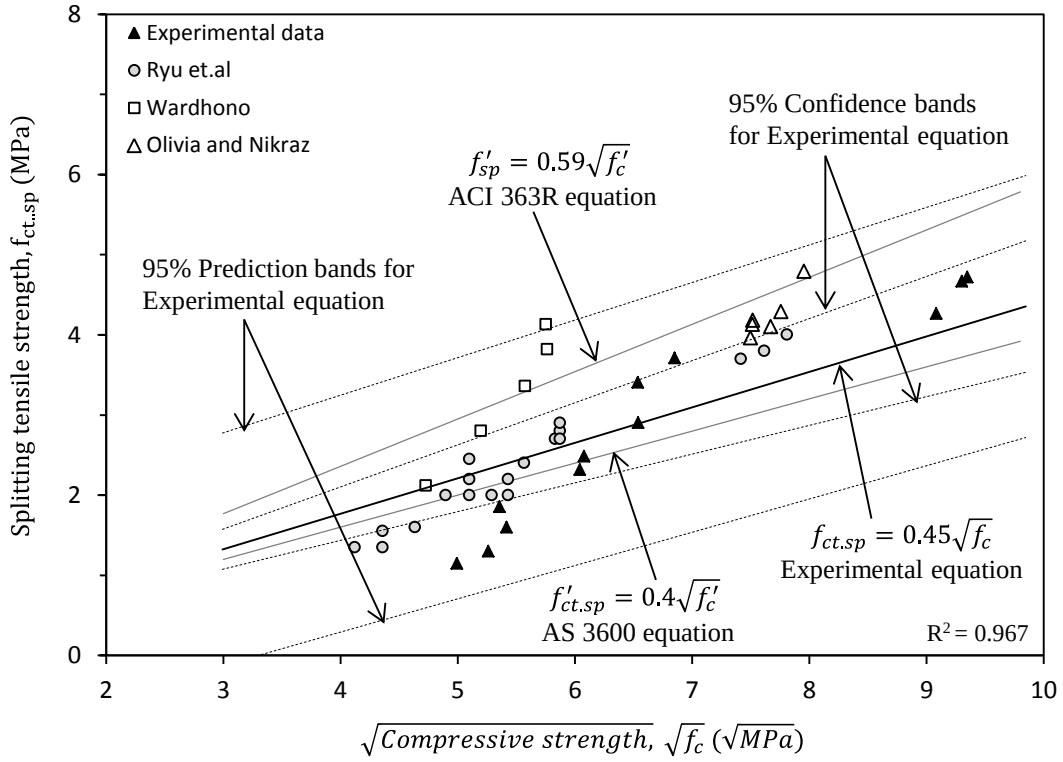

Figure 6.16 Splitting tensile strength vs. compressive strength

To validate of the regression equation, data reported by Olivia and Nikraz (2012), Ryu et al. (2013) and Wardhono et al. (2015) are included. Olivia and Nikraz (2012) produced fly ash geopolymer concrete using Taguchi method, and determined the compressive and splitting tensile strengths. The reported values ranged from 56.24 to 63.29 and 3.96 to 4.79 MPa for the compressive and splitting tensile strengths. Ryu et al. (2013) produced geopolymer concrete using a low calcium fly ash with 9 M sodium hydroxide and sodium silicate at a mass ratio of 50:50 cured at 60 C for 24 hours. The compressive strengths ranged from 17.5 to 61.5 MPa while splitting strength values were between 1.35 and 4.05 MPa. Wardhono (2015) produced geopolymer concrete using low calcium fly ash and observed the range of compressive and splitting tensile strength. It was noted that almost all these data points (Wardhono, 2015, Ryu et al., 2013, Olivia and Nikraz, 2012) are within the prediction bands of Eq. 9, which enhanced the reliability of this proposed design equation.

The Australian standards, AS 3600 (2009) and American Concrete Institute, ACI 363R (1992) provide models, Equation 6.10 and Equation 6.11, to describe the relationship between the splitting tensile and compressive strength for PC concrete.

$$f'_{ct.sp} = 0.4\sqrt{f'_c} \ \text{MPa} \qquad (6.10)$$

$$f'_{sp} = 0.59\sqrt{f'_c} \text{ MPa} \quad (6.11)$$

where both $f'_{ct.sp}$ and f'_{sp} represent the characteristic splitting tensile strength and f'_c is the characteristic compressive strength.

It can be seen that while the equation cited in AS 3600 (2009) falls within the confidence intervals of Equation 6.9, the design equation cited by ACI 363R (1992) is above the upper confidence interval. In other words, the splitting tensile strength of fly ash geopolymer concrete in the present study is lower than that provided by the formulae given in ACI 363R (1992) for the PC concrete of similar strength. However, it is worth noting that, when compressive strength is below 40 MPa, the corresponding splitting tensile strengths of fly ash geopolymers are overestimated by the equation stated in AS 3600 (2009) as shown in Figure 6.16. In this situation, the application of the current AS 3600 (2009) for PC concrete would not provide a conservative estimate but rather would lead to an overestimate of the strength, which could have serious consequences with regard to the performance of geopolymer concrete in structures.

6.7.5 Splitting tensile vs. Flexural strength

Figure 6.17 shows a scatter plot of the splitting tensile versus the flexural strengths, and the linear regression line representing the relationship between the two variables. The proposed regression model is as follows, Equation 6.12, whereas $f_{ct.f}$ is the mean flexural strength and $f_{ct.sp}$ is the mean splitting tensile strength.

$$f_{ct.sp} = 0.62 f_{ct.f} \text{ MPa} \quad (6.12)$$

To support the validity of the model, data reported by Olivia and Nikraz (2012) and Wardhono (2015) are also included. All these data points are fallen between prediction intervals of Equation 6.12.

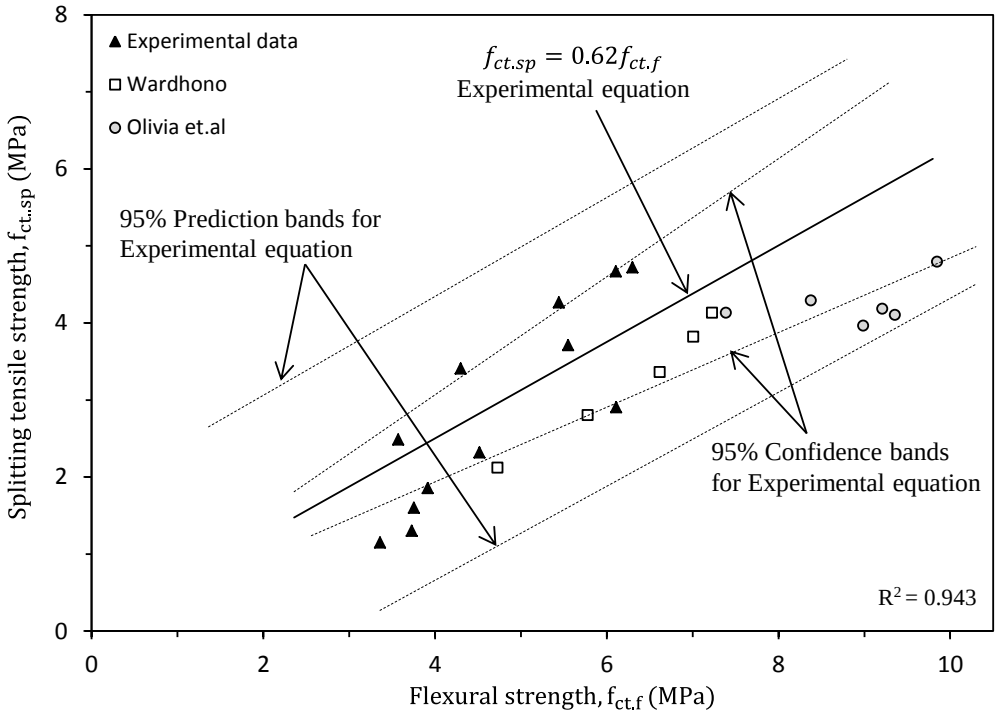

Figure 6.17 Splitting tensile strength vs. flexural strength

Neville (1996) reported that flexural strength of PC concrete overestimates the tensile strength of concrete, and Raphael (1984) showed that the value of tensile strength is approximately 0.75 of the flexural strength. The mechanism behind this variation can be explained by the influence of the loading arrangement on the tensile stress distribution. The splitting tensile test produces biaxial stress, but a significantly greater volume of the specimen is subjected to tensile stress which is dependent on the gel–aggregate bond. The remaining volume is under horizontal compressive stress. As such, the maximum fibre stress reached in the flexural strength test is higher than the splitting test, because the propagation of a crack is blocked by lower stressed material near to the neutral axis. Thus the energy available is less than that necessary for the formation of new crack surfaces, resulting higher resistance to tensile failure.

The present study follows this trend and is reflected by the splitting data which gave the most conservative estimates for the tensile strength. Thus adopting the splitting test would provide more confidence in designing structures and as such would be recommended as the most appropriate test for the fly ash geopolymer concrete. Overall the data shows that the flexural strength of fly ash geopolymer concrete is higher than that of PC concrete, as denoted in Equation 6.6. Based on the data the linear regression model presented in Equation 6.12 predicts that the splitting tensile strength of fly ash geopolymer concrete is approximately

0.62 times the flexural strength, not the 0.75 times suggested by Raphael (1984) for PC concrete.

6.7.6 Prediction of tensile strength

6.7.6.1 Uniaxial tensile strength

The uniaxial tensile strength is the maximum stress that concrete can withstand when subjected to uniaxial tension. In this study, the uniaxial tensile strength of the four fly ash geopolymer concrete, Table 6.7, was calculated in accordance with AS 3600 (2009) using measured splitting and flexural tensile strength test results and compressive strength. Applying AS 3600 (2009) to predict the long term performance found that the predicted uniaxial tensile strength follows a positive linear relationship with the increase of compressive strength with time. This behaviour is similar to that of PC concrete.

In Gladstone and Pt.Augusta geopolymers, the uniaxial tensile strength calculated from splitting tensile strength values is significantly higher than the tensile strength obtained from flexural strength test. Conversely, both the Tarong and Collie geopolymer concrete showed significantly less uniaxial tensile strength based on the splitting tensile test than flexural strength values. Thus the choice of the test on which to base the uniaxial tensile strength is a critical factor for the fly ash geopolymer concrete. Neville (1996) reported that the splitting test is both simple to perform and gives more uniform results than flexural strength test in PC concrete. However, only the Tarong and Collie geopolymers showed a conservative estimate for the uniaxial tensile strength based on splitting tensile test. Hence, this would illustrates the universal equation cannot be used to calculate the uniaxial tensile strength of different fly ash geopolymer concrete.

Table 6.7 Uniaxial tensile strength based on AS 3600 (2009)

Testing period	GP	Uniaxial tensile strength (f_{ct}), MPa		
		based on Splitting tensile strength $f_{ct} = 0.9f_{ct.sp}$	based on Flexural tensile strength $f_{ct} = 0.6f_{ct.f}$	Based on Compressive strength $f_{ct} = 1.4 \text{ x } 0.36\sqrt{f_c}$
28 days	GFA	3.83	3.26	4.58
	PAFA	2.24	2.17	3.07
	TFA	1.44	2.25	2.74
	CFA	1.04	2.02	2.52
90 days	GFA	4.2	3.67	4.69
	PAFA	3.07	2.58	3.40
	TFA	2.09	2.71	3.04
	CFA	1.17	2.24	2.65
365 days	GFA	4.25	3.78	4.72
	PAFA	3.34	3.33	3.46
	TFA	2.61	3.67	3.30
	CFA	1.67	2.35	2.70

6.7.6.2 Flexural and splitting tensile strengths

According to the AS 3600 (2009), both the flexural and splitting tensile strengths can be determined from the measured compressive strength values as shown in Table 6.8.

Table 6.8 Predicted flexural and splitting tensile strengths

Testing period	GP	*Predicted tensile strength (MPa)	
		Flexural strength $f_{ct.f} = 1.4 \text{ x } 0.6\sqrt{f_c}$	Splitting tensile strength $f_{ct.sp} = 1.4 \text{ x } 0.4\sqrt{f_c}$
28 days	GFA	7.63	5.09
	PAFA	5.10	3.40
	TFA	4.57	3.05
	CFA	4.19	2.79
90 days	GFA	7.81	5.21
	PAFA	5.67	3.78
	TFA	5.07	3.38
	CFA	4.42	2.95
365 days	GFA	7.85	5.24
	PAFA	5.76	3.84
	TFA	5.50	3.66
	CFA	4.50	3.00

*based on measured compressive strength with regards to (AS, 2009)

In order to understand the application of the equations stated in AS 3600 (2009) for the different fly ash geopolymer concrete, the measured and predicted tensile strengths, in term of flexural and splitting tensile strengths have been compared in Figure 6.18(a–b).

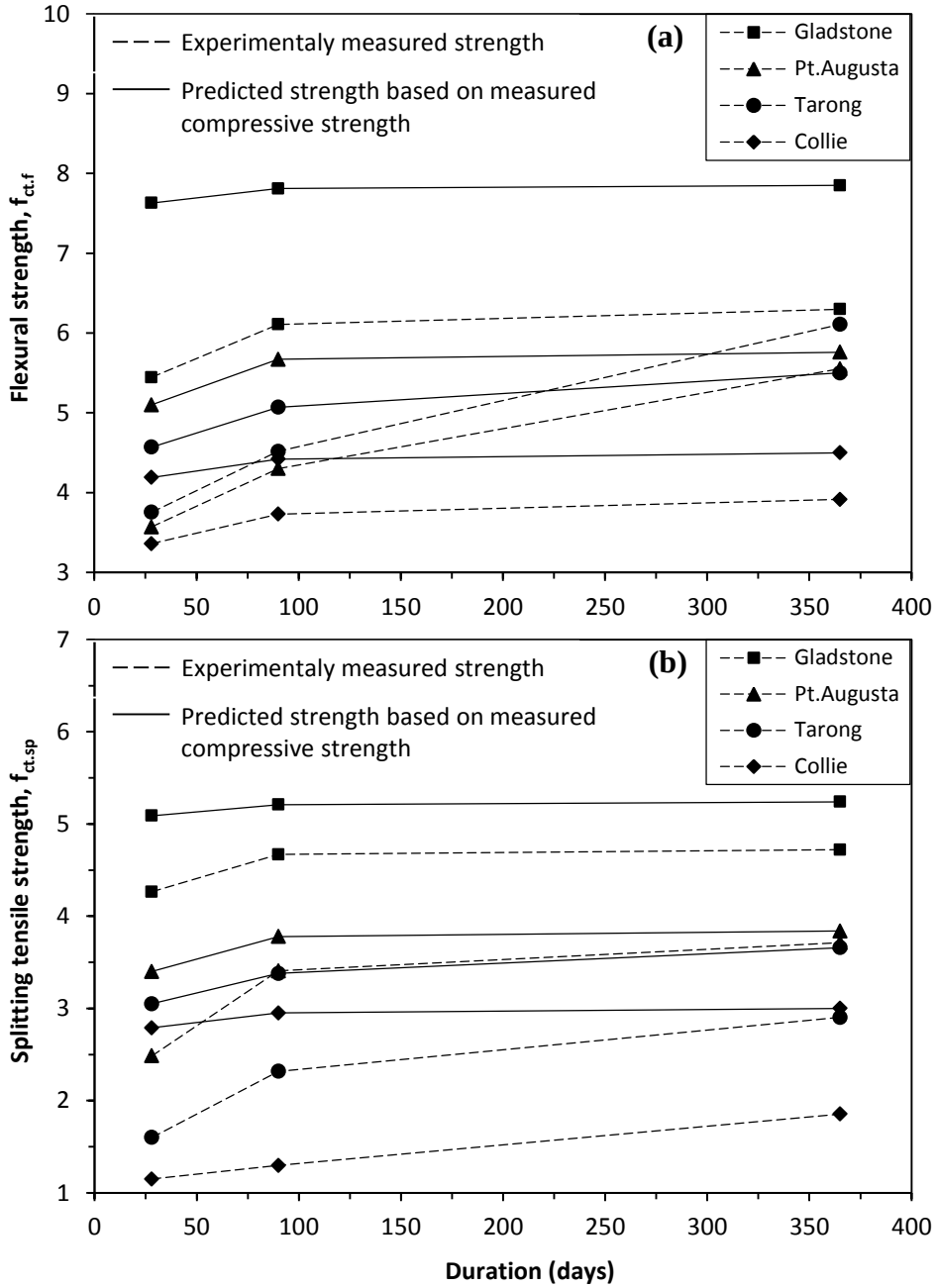

Figure 6.18 Measured vs. predicted tensile strengths; (a) flexural & (b) splitting tensile strength

The comparison clearly showed that the measured flexural strength and splitting tensile strength of all fly ash geopolymer concrete are lower than that predicted by AS 3600 (2009). This indicates that the use of AS 3600 (2009) equations based on compressive strength to

predict the flexural and splitting tensile strengths of fly ash geopolymer concrete would not be conservative.

6.7.7 Compressive strength vs. Elastic modulus

A linear regression model representing the correlation between elastic modulus and compressive strength is presented in Figure 6.19. The equation obtained from the regression analysis is given in Equation 6.13, where E_c is the elastic modulus, p is the average dry density in kg/m^3 and f_c is the mean compressive strength.

$$E_c = 0.024\, p^{1.5}\sqrt{f_c} \qquad \text{MPa} \tag{6.13}$$

The plot also includes the confidence and prediction bands for the proposed linear regression model. The applicability of the model was supported by including data previously reported Olivia and Nikraz (2012), Hardjito and Rangan (2005), Diaz–loya et al. (2011) and Wardhono (2015).

ACI 318 (2008) gives the elastic modulus as a direct function of the compressive strength for PC concrete, Equation 6.14.

$$E_c = 4733\sqrt{f_c'} \qquad \text{MPa} \tag{6.14}$$

Given that the fly ash geopolymer concrete samples exhibited a wide range of density values, Table 6.2, the regression model was derived using the interaction between compressive strength and density of the geopolymer concrete as a predictor of the elastic modulus. The regression model represented in Equation 6.13 has an R^2 value of 97%, suggesting that the inclusion of density in the prediction model helps in capturing the variability in the elastic modulus of fly ash geopolymer concrete. The applicability of this model was again validated using the data previously reported Olivia and Nikraz (2012), Hardjito and Rangan (2005), Diaz–Loya et al. (2011) and Wardhono (2015).

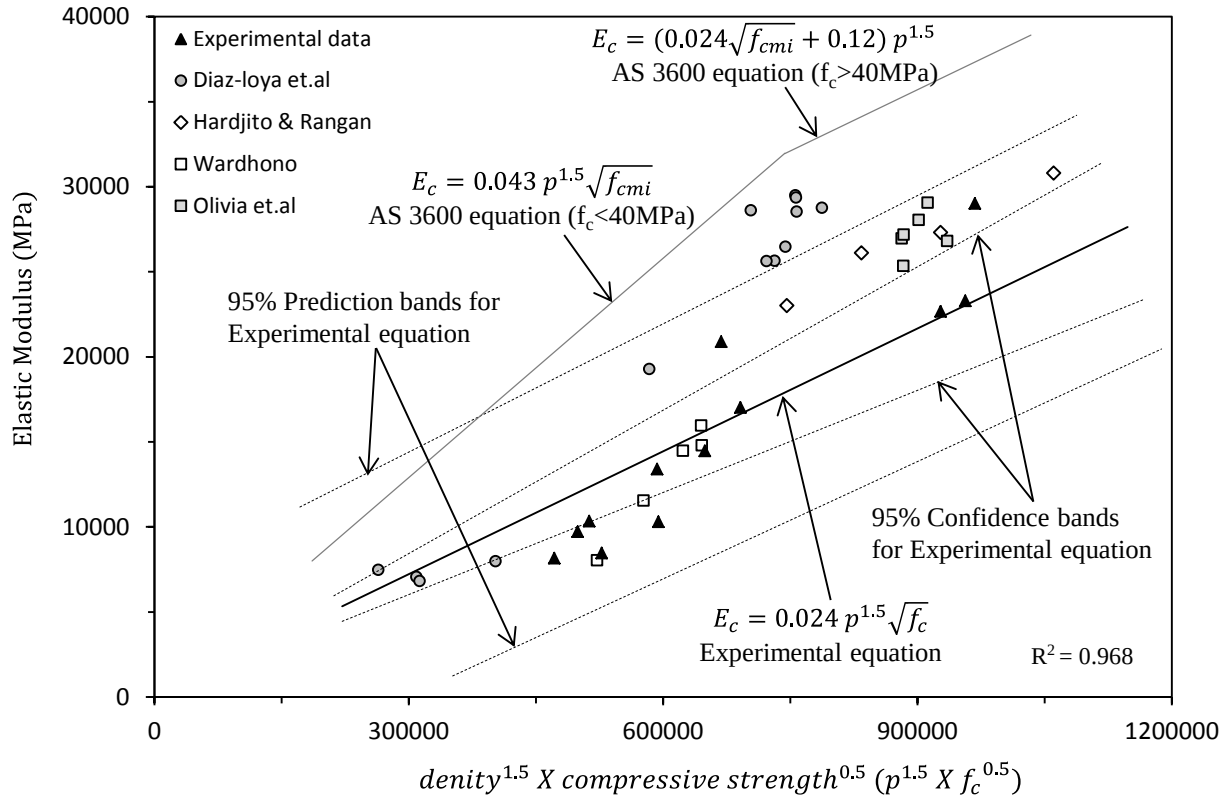

Figure 6.19 Relationship between elastic modulus, density and compressive strength

The AS 3600 section 3.1.1.4 (2009) provides a similar design equation with the inclusion of density. AS 3600 states that the mean elastic modulus of PC concrete shall be either taken as equal to Eq. 15 or 16, depending on the mean compressive strength value.

$$E_c = 0.043\, p^{1.5}\sqrt{f_{cmi}} \quad \text{MPa} \qquad ;\text{when } f_{cmi} \leq 40 \text{ MPa} \tag{6.15}$$

$$E_c = \left(0.024\sqrt{f_{cmi}} + 0.12\right) p^{1.5} \quad \text{MPa} \qquad ;\text{when } f_{cmi} > 40 \text{ MPa} \tag{6.16}$$

ACI 318 section 8.5.1 (2008) also gives a similar equation (Equation 6.15) for the PC concrete derived from short-term tests ranging in density from 1440 to 2485 kg/m^3.

It is noted that AS3600 (2009) line is furthest away from the confidence and prediction intervals of the proposed regression line for fly ash geopolymer concrete. The data points obtained from this study and previous studies, based on wide range of fly ash geopolymer concrete, were located below the AS3600 (2009) equation. The results show that the equations derived for PC concrete overestimate the elastic modulus of fly ash geopolymer concrete. Again the application of current codes for PC concrete to geopolymer concrete in

terms of elastic modulus could have serious consequences with regard to the performance of geopolymer concrete in structures.

6.8 Conclusions in Chapter 6

Based on the results of the experimental study, the following conclusions can be drawn:

- The 365-day compressive strength of four different fly ash based geopolymer concrete ranged between 28 and 88 MPa. The compressive strength increased with time for all geopolymer concrete. The rate of increase was different for each, depending on the properties of the precursor fly ash.

- The combination of C-A-S-H gel, which is formed by CaO in fly ash, with the N–A–S–H (main) gel provides additional rigidity to the geopolymer backbone. The presence of a high quantity of CaO leads to a densely packed microstructure at an early age, giving high early compressive strength.

- The 365-day flexural and splitting tensile strengths, of the four different fly ash geopolymer concrete ranged between 3.92 to 6.3 MPa and 1.86 to 4.72 MPa, respectively. The nature of the ITZ formed between aggregates and aluminosilicate gel matrix were shown to cause the tensile strength variation among the four geopolymers.

- Gladstone had a well compacted dense ITZ, where no obvious difference was noted with the bulk geopolymer matrix. In contrast, Collie produced a porous ITZ. The unreacted/partially reacted fly ash particles were loosely packed in this zone. The density of the ITZ was the key factor in determining the tensile strength of the geopolymer concrete.

- The 365-day elastic modulus and Poisson's ratio of four different geopolymer concrete ranged from 10.3 to 29 GPa and 0.16 to 0.28 respectively. The packing density of the aluminosilicate gel matrix influences elastic modulus development. An increase in porosity and micro cracks negatively affects the compactness of the gel matrix, which in turn affects the elastic modulus.
- The correlations between key mechanical properties of 100% fly ash based geopolymer concrete made with a wide range of low calcium (class F) fly ash have been studied, and then compared with the design equations available for the PC concrete in Australian standards and American Concrete Institute.

- The AS 3600 and ACI 318 specified relationships for flexural strength underestimates the flexural strength of geopolymer concrete, whereas the AS 3600 specified relationship for splitting tensile strength gives a reasonable prediction for geopolymer concrete. However, the ACI 363R stated equation significantly overestimates the splitting tensile strength of geopolymers.

- The splitting tensile strength of fly ash geopolymer concrete is approximately 0.62 times the flexural strength, lower than the ratio (0.75 times) suggested for PC concrete.

- The AS 3600 stated design equation highly overvalues the elastic modulus for geopolymer concrete, and this overestimation is higher when compressive strength is below 40 MPa. Similar behaviour was noted with respect to the splitting tensile strength prediction using AS 3600.

7 INITIAL STUDY ON DURABILITY OF GEOPOLYMER CONCRETE

7.1 Overview

This chapter presents the test results and discussion related to the **Phase 2** of the comprehensive experimental study shown in Figure 3.3 for geopolymer concrete. The identified optimum mix design for each fly ash geopolymer concrete in Chapter 6 has been used to investigate the long term durability properties, such as water absorption, water permeability, air permeability, chloride diffusivity, resistivity, ultrasonic pulse velocity and Schmidt rebound hammer test for four different fly ash geopolymer concrete.

The data was collected at set points over a one year period for all the aforementioned durability tests, and includes four different sources of fly ash used in manufacturing of geopolymer concrete. The Section 7.2 presents test results and development of specific durability characteristics with the increase of age of concrete. Meantime, Section 7.3 presents the pore structure and microstructure changes of different fly ash geopolymer concrete, which have been examined by using mercury intrusion porosimetry (MIP), and scanning electron microscopic (SEM) analysis, respectively up to one year. Lastly, Section 7.4 discusses the variation of durability properties with time in conjunction with the MIP and SEM analysis.

7.2 Long term durability properties

7.2.1 Ultrasonic Pulse Velocity

The ultrasonic pulse velocity (UPV) test is a common technique employed for analysing the uniformity and relative quality of concrete to indicate the presence defects, such as voids and cracks (Yap et al., 2013). Table 7.1 and Figure 7.1 show the varying UPV with time in four different fly ash geopolymer concrete. All reported UPV values were mean value of three tested concrete slabs at specific period (Appendix D1). The Gladstone and Collie geopolymer concrete displayed the highest and the lowest UPV values, which correspond with the highest and lowest compressive strengths, Table 6.3. The UPV of Pt.Augusta and Tarong geopolymer concrete fell between the Gladstone and Collie geopolymers.

Table 7.1 UPV variation in different fly ash geopolymers

Geopolymer	UPV (km/s)			*UPV development (%)
	28 days	90 days	365 days	
GFA	3.61	3.68	3.91	8.3
PAFA	3.14	3.18	3.21	2.2
TFA	3.02	3.16	3.69	22.2
CFA	2.71	2.71	2.91	7.4

*UPV increment at 365 days with compared to 28 day value

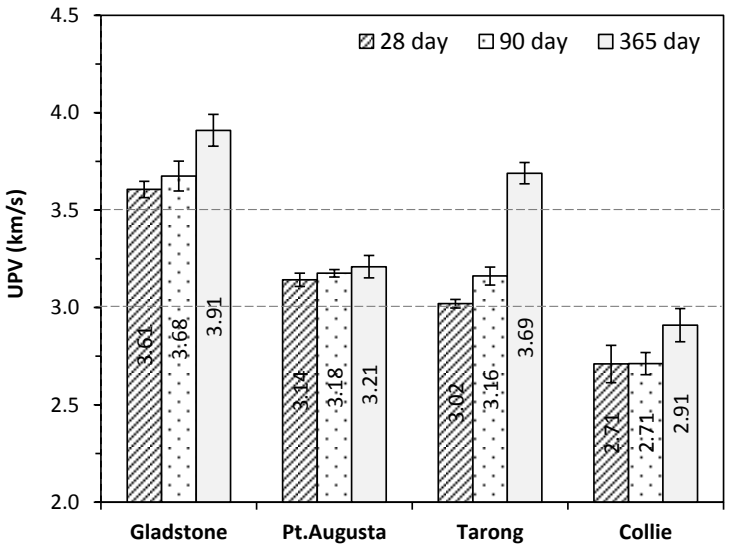

Figure 7.1 UPV variations in different geopolymers

The standard pulse velocity of PC concrete is generally in the range 3.5 to 4.5 km/s (Garbacz and Garboczi, 2003), categorized as being in good condition, which implies that the concrete is free from any large voids or cracks that may affect its long term structural reliability. In this study, only the Gladstone geopolymer concrete falls in to this UPV range at all ages, and is classified as comparable to PC concrete. Since the ultrasonic pulse will propagate more easily through the solid phase than that of empty space, the high UPV of Gladstone geopolymer concrete would indicate a high solid volume fraction/density and a low porosity of the specimens (Karakurt et al., 2010).

Pt.Augusta geopolymer displayed the lowest UPV increase with age of all the geopolymer concrete, falling between 3 and 3.5 km/s at all ages, which is slightly lower than the general range of PC concrete (Garbacz and Garboczi, 2003). Tarong geopolymer had a similar UPV variation to the Pt.Augusta up to 90 days, however, displayed a significant UPV increase (Table 7.1) and was comparable with the PC concrete at 365 days. The Collie geopolymer concrete, however, is identified as poor quality concrete with UPV values below 3 km/s (Browne et al., 1983). Khatib and Bayomy (Khatib and Bayomy, 1999) noted that the presence of micro cracks in concrete will cause a reduction in compressive strength, which consequently reduces the UPV. The variation in the UPV of four geopolymer concrete with the age is further discussed in Section 7.3 parallel to the microstructure changes and pore size distribution.

The relationship between UPV, density (Table 6.2) and compressive strength (Table 6.3) is illustrated in Figure 7.2. The correlation coefficient, R^2, of the linear relationship between density and UPV is 0.94, and between density and compressive strength is 0.74. This indicated that there is a strong relationship between density and UPV of fly ash geopolymer concrete, similar to PC concrete, and could be successfully used to get an indication of the solid volume fraction, which in turn demonstrates the quality of concrete.

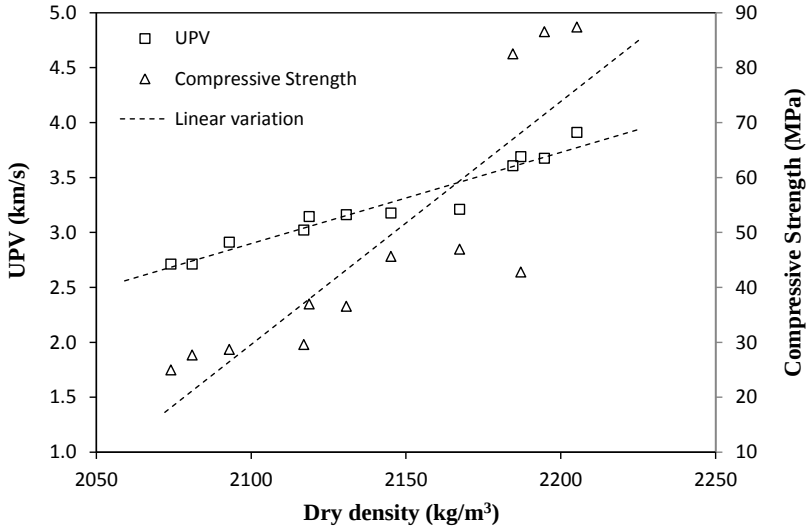

Figure 7.2 Correlation between UPV, Compressive strength and Density

7.2.2 Water absorption

A comparison of the water absorption of the four different fly ash geopolymer concrete between 28 and 365 days is shown in Table 7.2, Figure 7.3. All reported water absorption results were mean value of tested concrete cylinders at specific period (Appendix D2). Water absorption can be used as a representation of the open nature of the porosity of the geopolymer gel paste. The measurement is taken by calculating the difference in specimen weight under oven-dried and fully saturated conditions (AS, 1999b). The water absorption in geopolymer concrete varied in the range of 1.76% to 6.22% between 28 and 365 days. Collie geopolymer showed the highest water absorption and Tarong the lowest at all ages. The water absorption of Gladstone and Pt.Augusta geopolymers fall between the other two geopolymers throughout.

In PC concrete, a water absorption greater than 5% is classified as high permeable concrete, while less than 3% is classified as low permeable concrete (Rendell et al., 2002). Other than Tarong, all the geopolymer concrete exceeded this upper limit and at 28 days exhibit the behaviour of a high permeable concrete, which in turn is indicative of having of a highly porous external surface. Both Gladstone and Pt.Augusta displayed significant improvement with the age, Table 7.2. Gladstone was well below the upper limit after 365 days, but Pt.Augusta was almost equal to 5% and Collie remained above the 5% threshold. Tarong displayed significantly lower water absorption, i.e. less than 2%, and is categorised as a low permeable concrete.

Table 7.2 Water absorption in different fly ash geopolymers

Geopolymer	Water absorption (%)			*Water absorption reduction (%)
	28 days	90 days	365 days	
GFA	5.57	5.11	4.63	16.9
PAFA	6.00	5.84	5.04	16.0
TFA	2.04	1.96	1.76	13.7
CFA	6.22	6.15	6.07	2.4

*Water absorption decrement at 365 days with compared to 28 day value

Note: Water absorption > 5%: High permeable concrete; Water absorption < 3%: Low permeable concrete (Rendell et al., 2002)

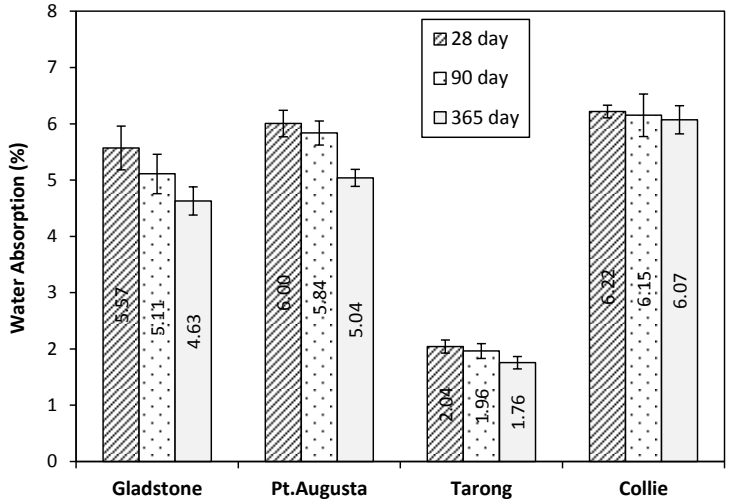

Figure 7.3 Water absorption in different fly ash geopolymers

7.2.3 Apparent Volume of Permeable Voids

The Apparent Volume of Permeable Voids (AVPV), or closed porosity, is a percentage of pore space measured by boiling the saturated concrete (AS, 1999b). The permeable voids indicate the interconnected void space as capillary pores, gel pores and air voids within the geopolymer concrete. A comparison of the AVPV of the four different fly ash geopolymer concrete between 28 and 365 days is shown in Table 7.3, Figure 7.4.

The trends observed were similar to water absorption with all the geopolymer concrete displaying a decrease in AVPV with time. The AVPV of the four geopolymer concrete again varied over a wide range. Tarong once more has the lowest value, 7.40% and the Collie the highest value, 19.11%. In PC concrete an AVPV less than 13% is classified as good quality concrete, while greater than 18% is classified as poor quality concrete (VicRoads, 2007).

Gladstone and Tarong geopolymer concrete were below this lower limit at all ages, indicating limited pore interconnectivity in their pore structure. It is worth noting that Tarong is significantly the best performing geopolymer with regard to water absorption and AVPV, in contrast to the compressive strength and UPV data. Both Pt.Augusta and Collie geopolymers had very high AVPV percentages at early age, but significant reduction was noted between 90 and 365 days period, with an AVPV approaching 14% at one year.

Table 7.3 AVPV of different fly ash geopolymers

Geopolymer	AVPV (%)			*AVPV reduction (%)
	28 days	90 days	365 days	
GFA	13.54	12.86	12.29	9.2
PAFA	18.12	17.59	14.68	19.0
TFA	8.38	8.38	7.40	11.7
CFA	19.11	18.20	14.22	25.6

*AVPV decrement at 365 days with compared to 28 day value

Note: AVPV < 14%: Good quality concrete; AVPV > 16%: Poor quality concrete (VicRoads, 2007)

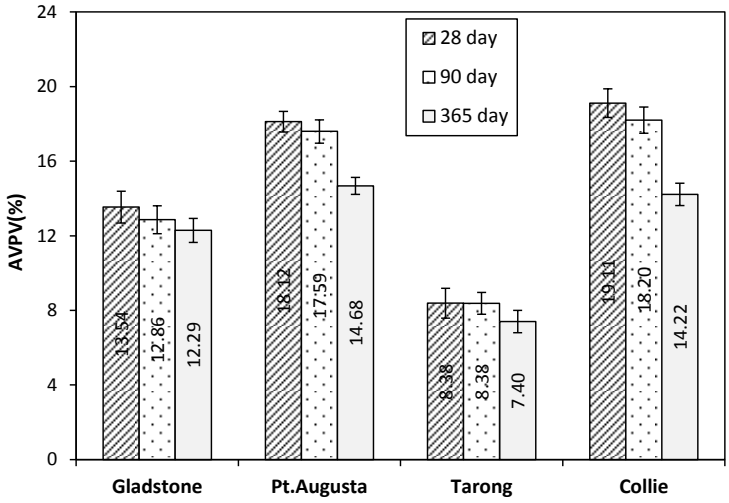

Figure 7.4 AVPV of different fly ash geopolymers

7.2.4 Water permeability

The water permeability curves of the four fly ash geopolymer concrete between 28 and 365 days are shown in Figure 7.5. All reported water permeability results were mean value of three tested concrete slabs at specific period (Appendix D3). The slope of the linear regression curve between water flow and square root of time displays the corresponding water permeability index, WPI, (Basheer et al., 1995) for each geopolymer concrete, Table 7.4. In the water permeability test, both capillary absorption and the applied pressure contribute to the rate of water flow. In all geopolymer concrete, water permeability decreases with time, Figure 7.5. The Gladstone and Pt.Augusta geopolymer concrete had the lowest WPI at all ages, and are classified as low water permeable concrete as the WPI did not exceed $1.3x10^{-7}$ $m^3/\sqrt{min}$ (Autoclam, 1995).

Collie geopolymer had the highest permeability at all testing points with the corresponding WPI exceeding $2.6x10^{-7}$ $m^3/\sqrt{min}$ and is thus categorized as a high water permeable concrete (Autoclam, 1995). In contrast, Tarong geopolymer concrete displayed the second highest volume of water penetration and WPI, after Collie, at 28 days but had significantly decreased to less than $1.3x10^{-7}$ $m^3/\sqrt{min}$ at 90 and 365 days. This is again consistent with on-going geopolymerization, in agreement with the corresponding UPV and strength data.

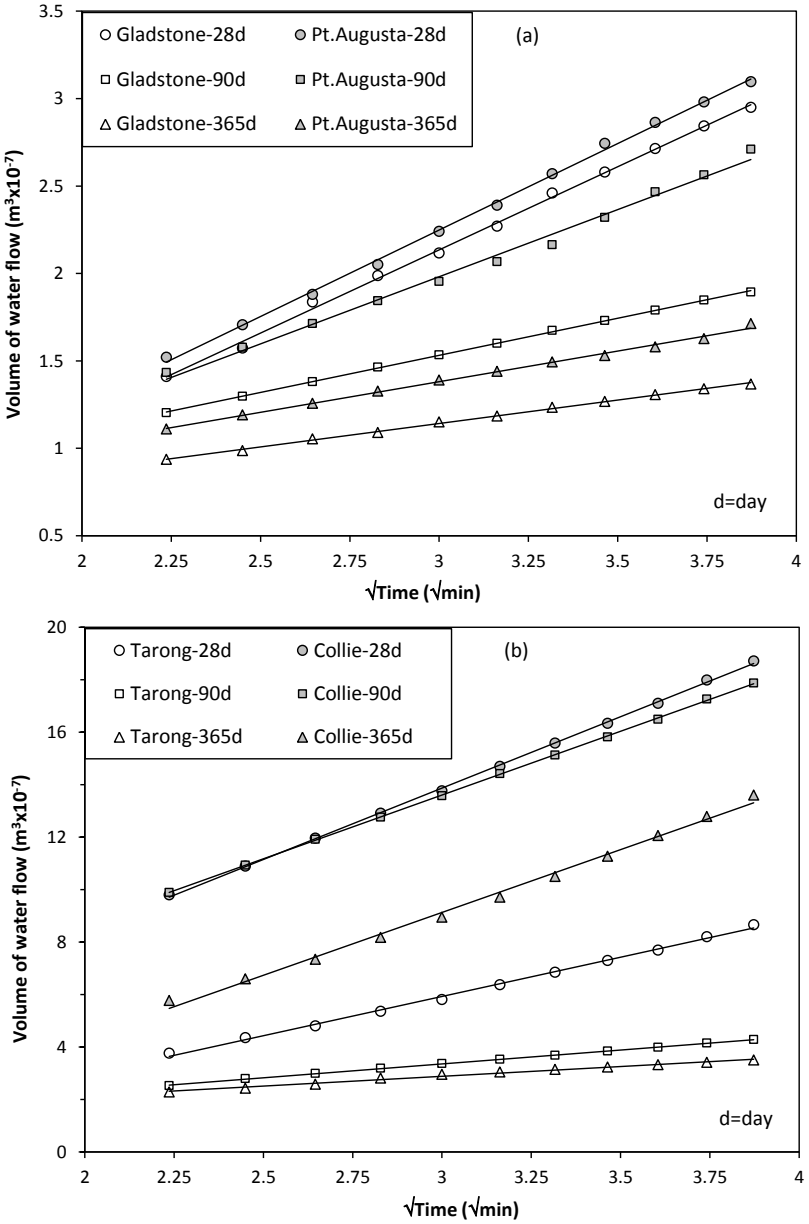

Figure 7.5 Water permeability of fly ash geopolymer concrete

Table 7.4 Water permeability indices (*WPI x 10^{-7} $m^3/\sqrt{min}$)

Geopolymer	28 days		90 days		365 days	
	*WPI	R^2	*WPI	R^2	*WPI	R^2
Gladstone	0.951	0.998	0.424	0.999	0.268	0.998
Pt.Augusta	0.989	0.998	0.768	0.993	0.350	0.996
Tarong	2.990	0.998	1.058	0.999	0.750	0.989
Collie	5.440	0.999	4.861	0.999	4.790	0.995

Note: *WPI<1.3: High quality concrete, *WPI>2.6: Poor quality concrete (Autoclam, 1995)

7.2.5 Air permeability

The air permeability curves of the geopolymer concrete between 28 and 365 days are given in Figure 7.6. All reported air permeability results were mean value of three tested concrete slabs at specific period (Appendix D4). A plot of natural logarithm of air pressure against time shows a linearity that is confirmed by the correlation coefficients, R^2, which exceed 0.98 of all the air permeability data. The slope of this linear regression curve gives the air permeability index, API (Basheer et al., 1995), Table 7.5. The API of all the geopolymer concrete reduced with time. Similar to the water permeability variation, the Gladstone and Pt.Augusta geopolymers presented the lowest API at all ages. Both geopolymers had API less than 0.1 Ln(mbar)/min, which classifies them as low air permeable, high quality concrete (Autoclam, 1995).

In Collie the pressure fell to zero within a few minutes which would indicate an extensively more porous microstructure. While the API did reduce with time from 1.144 to 0.2 Ln(mbar)/min between 28 and 365 days, it would classify the material as high air permeability concrete. Once more, Tarong differed compared to the other geopolymers. The corresponding API was above the 0.1 Ln(mbar)/min threshold at 90 days, but significantly decreased with time and was below the threshold value, confirming low air permeability at 365 days. It is notable that Tarong is the best performing geopolymer concrete with respect to water absorption and AVPV but is not when considering the compressive strength, UPV, water and air permeability, which all show similar performance characteristics.

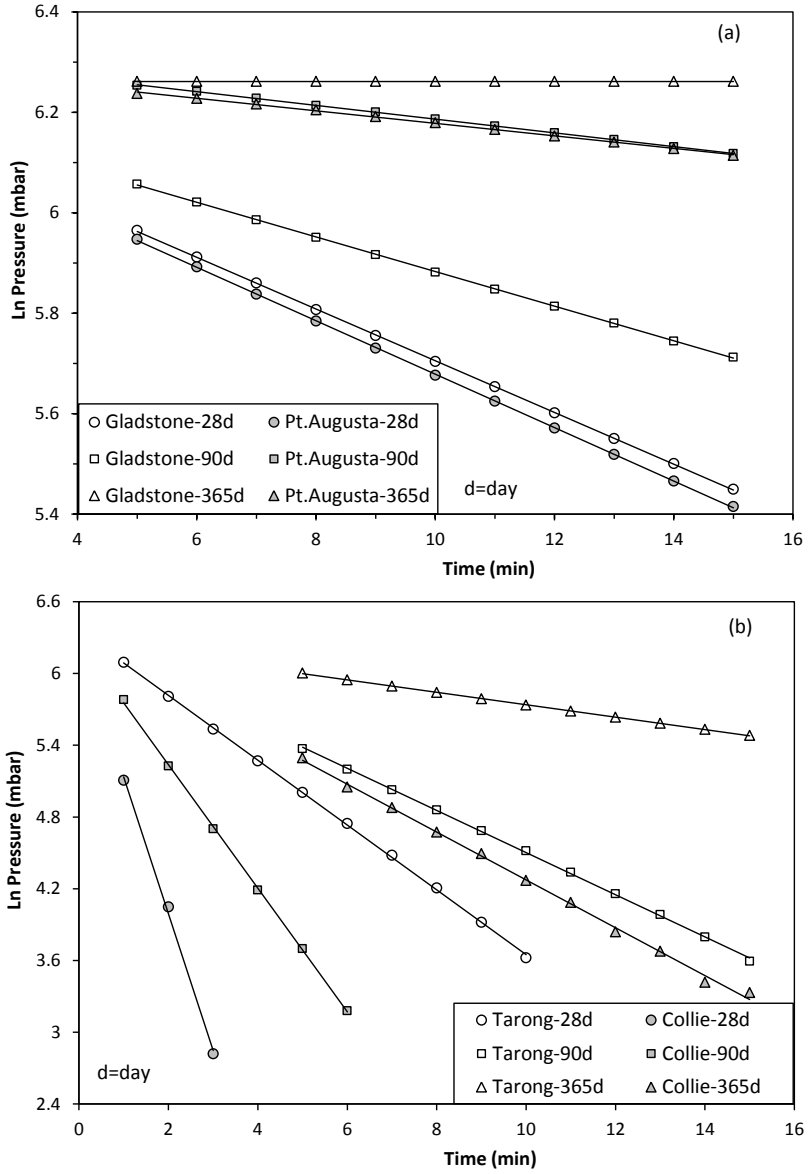

Figure 7.6 Air permeability of fly ash geopolymer concrete

Table 7.5 Air permeability Indices [Ln(mbar)/min]

Geopolymer	28 days		90 days		365 days	
	API	R^2	API	R^2	API	R^2
Gladstone	0.052	0.999	0.035	0.999	0.000	1.000
Pt.Augusta	0.053	0.999	0.014	0.999	0.013	0.999
Tarong	0.271	0.999	0.176	0.999	0.052	0.999
Collie	1.144	0.998	0.517	0.999	0.200	0.998

Note: API<0.1: High quality concrete, API>0.5: Poor quality concrete (Autoclam, 1995)

7.2.6 Resistivity

The electrical resistivity of concrete is an important factor considering the rate of corrosion of the reinforcing steel once the process has been initiated. Hence, the electrical resistivity of concrete is an effective parameter to evaluate the risk of reinforcing steel corrosion when corrosion is induced by chloride attack (Morris et al., 2002). A concrete material with high resistivity will show a lower corrosion rate compared to a concrete with a low resistivity. The resistivity test results are shown in Table 7.6. All reported resistivity results were mean value of three tested concrete slabs at specific period (Appendix D5).

Table 7.6 Resistivity of different fly ash geopolymers

Geopolymer	Resistivity (kΩ.cm)		
	28 days	90 days	365 days
GFA	5.8	14.4	79.2
PAFA	3.0	6.1	76.8
TFA	2.0	5.2	78.4
CFA	3.6	7.1	14.6

In this study, all fly ash geopolymer concrete displayed low concrete resistivity at 28 days, Figure 7.7. This would indicate the potential to have a high corrosion rate if corrosion is initiated (Bungey et al., 2006). Although, the resistivity of Gladstone increased into the 10 and 20 kΩ.cm range, low corrosion risk, all other geopolymers still predicted the likelihood of a high corrosion rate at 90 days. At 365 days all the geopolymer concrete, other than Collie, displayed very high resistivity, no corrosion risk, Collie being classified as low corrosion risk.

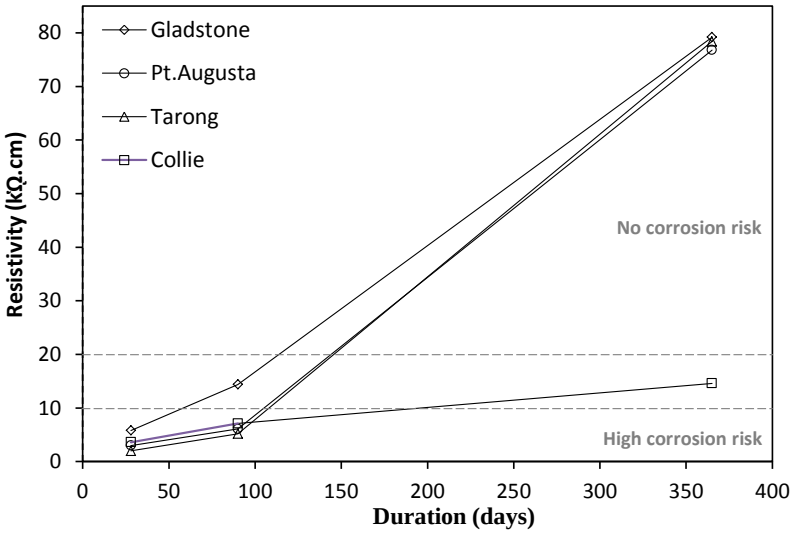

Figure 7.7 Resistivity of fly ash geopolymer concrete

The electrical conductivity of PC concrete is affected by the extent of connected capillary pores and ionic concentration in the pore structure (McCarter et al., 2000). This study used high Na_2O dosage to activate the fly ash. The low resistivity at 28 days would indicate a high ionic concentration in the pore solution, which is attributed to the use of the high Na_2O activator. The rise in resistivity would indicate that the ionic activity in the pore solution is decreasing with time. This would be consistent with continuing geopolymerisation which would reduce the ionic species in the pore solution.

While resistivity is a useful parameter in assessing the corrosion tendency of steel in PC concrete, it is influenced by a wide range of factors. The factors such as degree of hydration, cement mix, temperature and humidity play an important role in influencing PC concrete resistivity. Thus, drying in the laboratory atmosphere may also be a factor in the high resistivity values obtained by all geopolymers, except Collie, at one year.

7.2.7 Chloride diffusion

The salt ponding test is a long term test and can be used to measure the actual penetration of chloride ions into the geopolymer concrete. The apparent diffusion coefficient (D_a) and surface concentration (C_s), tabulated in Table 7.7 were calculated by plotting the chloride profiles as shown in Figure 7.8 and determining the best flitted curve using Fick's 2nd law of diffusion (Crank, 1975).

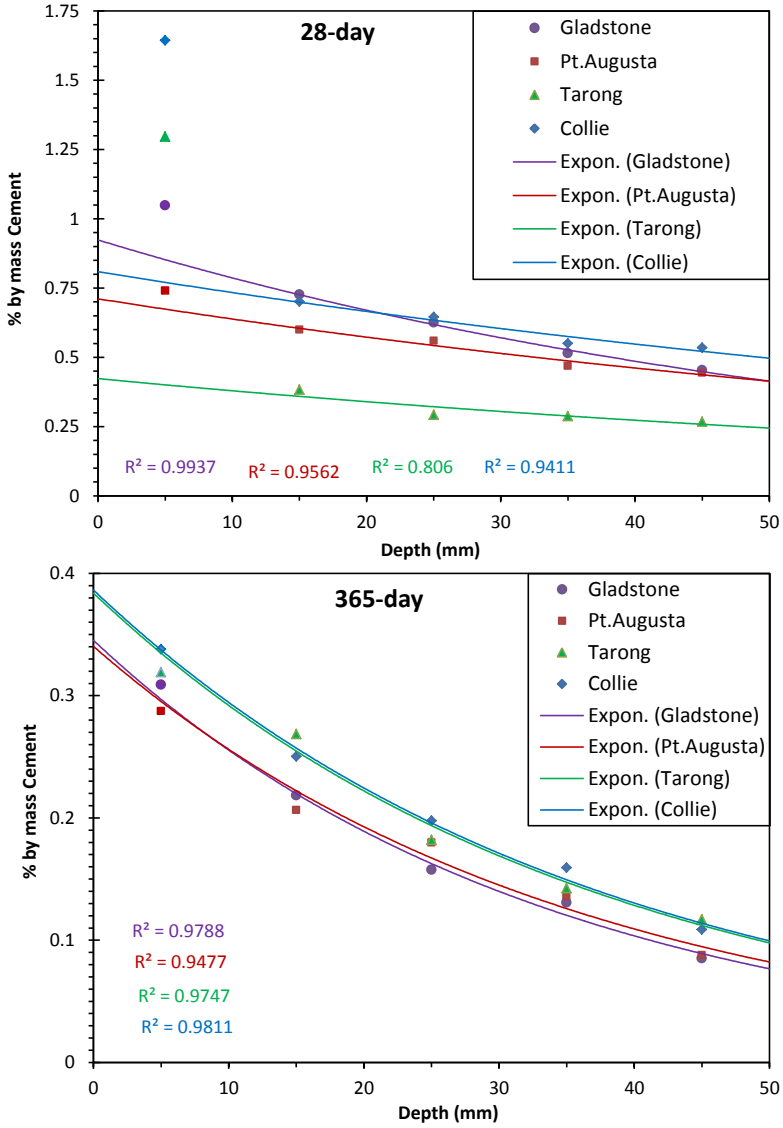

Figure 7.8 Chloride penetration profiles of fly ash geopolymer concrete

Table 7.7 Chloride diffusion coefficient and maturity factor

Geopolymer	28 day		365 day		Maturity factor (m)
	C_s (% concrete)	D_a x 10^{-11} (m^2/s)	C_s (% concrete)	D_a x 10^{-11} (m^2/s)	
Gladstone	0.925	15.8	0.345	7.9	- 0.234
Pt.Augusta	0.725	18.9	0.340	8.5	- 0.309
Tarong	0.425	19.5	0.380	9.6	- 0.294
Collie	0.825	21.5	0.385	9.9	- 0.344

Note: PC (m= -0.264), PC+fly ash (m= -0.699), PC+slag (m= -0.621) concrete (Bamforth, 1999)
PC+slag (m= -0.833), PC+slag+silica fume (m= -0.527) concrete (Hong and Hooton, 1999)

The Gladstone, Pt.Augusta and Collie geopolymer concrete showed high surface chloride concentration at early age, and was significantly higher than that reported for PC and blended cement concrete (Adam, 2009, Bamforth, 1999). Tarong geopolymer concrete however displayed low surface chloride concentration at 28 days, comparable with PC and blended cement concrete (Hong and Hooton, 1999, Bamforth, 1999). Surface chloride concentration of all geopolymer concrete decreased with the age of the concrete and varied between 0.34 and 0.39 at one year.

The apparent diffusion coefficient of four geopolymer concrete was between 15.8 x 10^{-11} and 21.5 x 10^{-11} m^2/s at 28 days. These values are slightly higher than the value observed by Adam (2009) for 28 day PC concrete. However, the diffusion coefficient of all geopolymer concrete decreased with age. In PC and blended cement concrete, this is represented as the maturity factor, m (Bamforth and Pocock, 2000), which takes into account changes (i.e. reduction) in the diffusion coefficient with time. This improved performance of the PC and blended cement concrete is attributed to their on-going hydration with time.

All geopolymer concrete displayed continuing geopolymerization beyond 90 days. Due to concurrent gel formation thus densified the geopolymer microstructure and pore-structure over the one year period, resulted in lower diffusion coefficient at 365 days. The maturity factor for all geopolymer concrete were calculated between 28 and 365 day period, Table 7.7, and compared with the PC concrete. The calculated maturity factor in the four geopolymers are similar and correspond well with those reported for PC concrete (Bamforth, 1999), although lower than the values (m) reported for blended cement concrete (Hong and Hooton, 1999, Bamforth, 1999).

7.2.8 Schmidt surface hardness

The Schmidt surface hardness (Rebound hammer) test is one of the oldest non-destructive methods. The surface hardness of the four fly ash geopolymer concrete is illustrated in Figure 7.9. All reported rebound hammer values were mean value of three tested concrete slabs at specific period (Appendix D6). The highest and lowest compressive strength (Table 6.3) concrete, Gladstone and Collie, corresponded to the highest and lowest rebound values for all ages. However, while Tarong gave a higher surface hardness than Pt.Augusta, their compressive strength behaviour is the opposite.

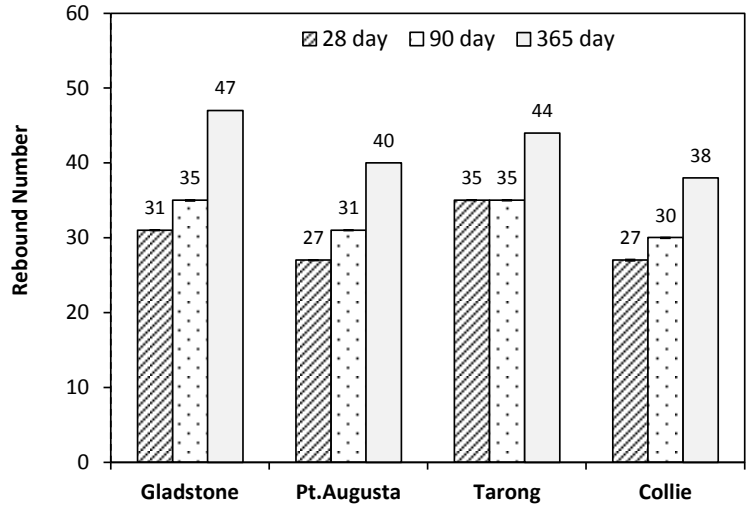

Figure 7.9 Schmidt surface hardness of fly ash geopolymer concrete

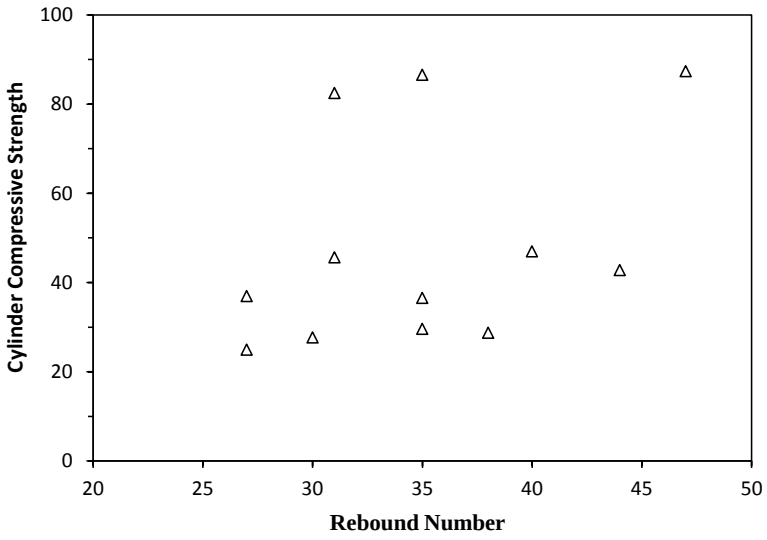

Figure 7.10 Schmidt surface hardness of fly ash geopolymer concrete

Schmidt rebound hammer is useful in assessing concrete uniformity and in comparing one concrete against another, but can only be used as a rough indication of concrete strength in absolute terms. The relationship between compressive strength and surface hardness of different fly ash geopolymer concrete are shown in Figure 7.10. However, analysis of the data indicates the correlation between these factors was not strong. The microstructure investigation (Chapter 6) showed that each fly ash geopolymer concrete has a different geopolymer matrix, depending on the Si/Al ratio of the final gel product. It further observed that compressive strength is dependent on the nature of the gel matrix formed after geopolymerization. Hence each fly ash geopolymer is believed to have a different Schmidt hammer response, unique to that material. This experimental data would suggest that a

universal correlation factor cannot be used, thus each fly ash based geopolymer should have its own correlation curve based on Schmidt hammer and compressive strength values.

7.3 Geopolymer pore-structure and microstructure

7.3.1 Pore-structure

Figure 7.11 displays incremental (dV/dlogD) pore size distribution of the four fly ash geopolymers at 28 and 365 days. Each incremental curve displays bimodal pore distribution, and two major regions are identified based on the pore size (ϕ), as the ϕ<50nm, meso-pores, and ϕ>1000nm (1µm), macro-pores. The meso-pores typically represents the pores within the geopolymeric gel phase, while the macro-pores the voids between unreacted fly ash composites (Zheng et al., 2010).

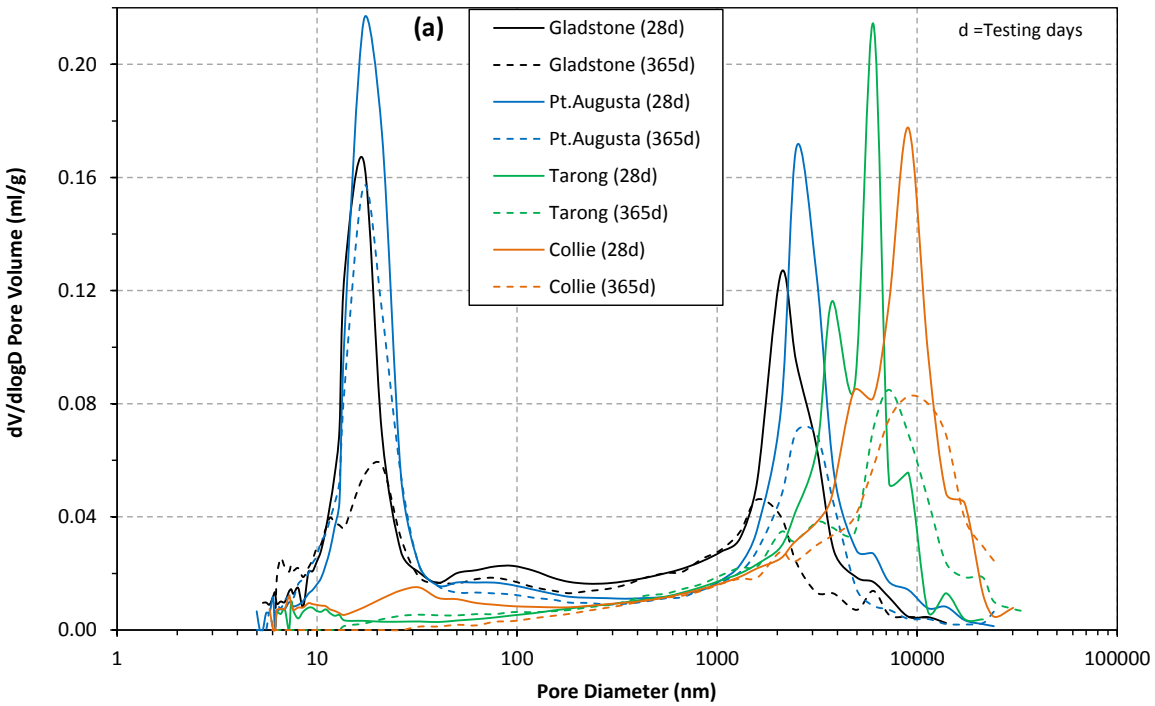

Figure 7.11 Incremental (dV/dlogD) pore distributions of different geopolymers

Two sharp peaks can be observed in Gladstone and Pt.Augusta fly ash geopolymers at both 28 and 365 days. At each point the highest peak is located in the meso-pores, while the second peak is located in the macro-pore (ϕ>1µm) region. Collie and Tarong fly ash geopolymers also show a bimodal pore size distribution at 28 days. Collie displayed a sharp peak in the macro-pore (ϕ>1µm) region while a small broad peak is located in the meso-pores region. Tarong geopolymer once more differed to the other geopolymers, and displayed two

peaks in the macro-pore (ϕ>1μm) region. It is worth noting that both Collie and Tarong geopolymers had only one peak at 365 days, both peaks are assigned as macro-pores with no peak appearing in the meso-pores region. Overall, the incremental curve shows a decrease of peak height for all geopolymers with time.

Figure 7.12 displays cumulative pore volume of the four geopolymers with respect to the pore size at 28 and 365 days. Moreover, the quantity of total meso and macro pores of four geopolymers at two time intervals is tabulated in Table 7.8.

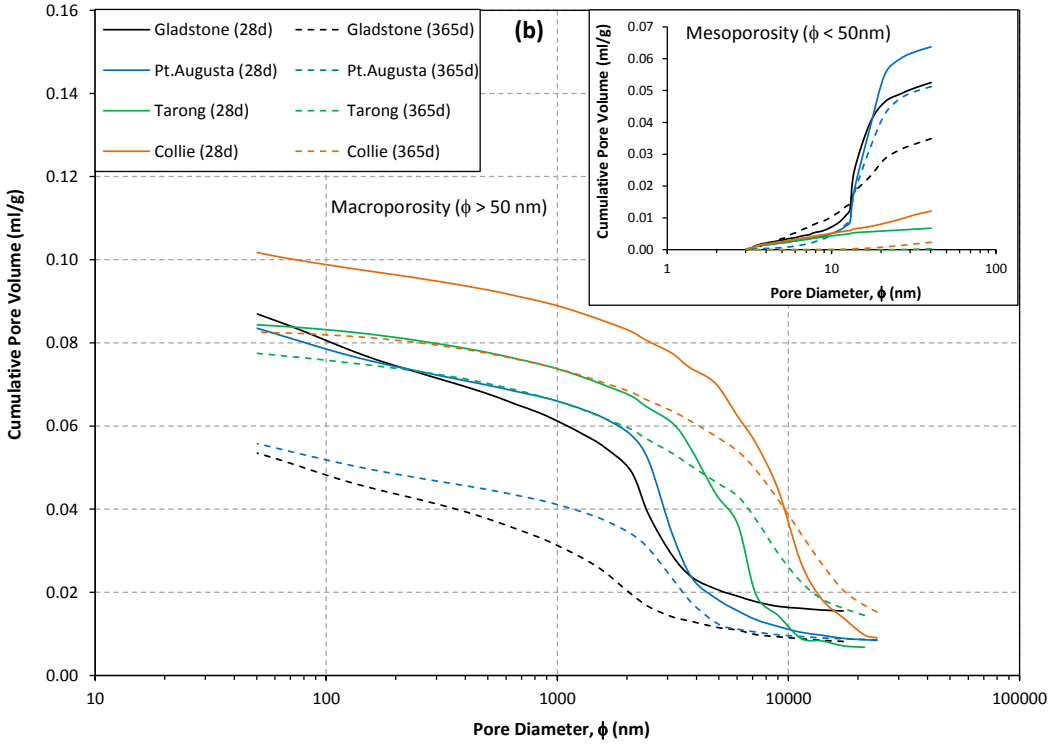

Figure 7.12 Cumulative pore distributions of different geopolymers

Table 7.8 Total porosity of fly ash geopolymers (ml/g)

Geopolymer	Meso-pores (ϕ < 50 nm)		Macro-pores (ϕ > 1μm)	
	28 day	365 day	28 day	365 day
Gladstone	0.05439	0.03643	0.06068	0.03076
Pt.Augusta	0.06531	0.05246	0.06566	0.04079
Tarong	0.00706	0.00044	0.07336	0.06559
Collie	0.01315	0.00283	0.08858	0.07348

The Pt.Augusta geopolymer displayed the highest meso-porosity, followed by Gladstone while Tarong and Collie had the lowest. The meso-porosity of all geopolymers however

decreased with the age of concrete, corresponding to filling of the pores and refinement of the pore sizes due to the on-going geopolymerization and gel production.

In the macro-pore (ϕ>1µm) region, Collie geopolymer showed the highest cumulative pore volume, followed by Tarong geopolymer at both 28 and 365 days. Both Gladstone and Pt.Augusta had a low macro-porosity compared to Collie, and both materials showed a large reduction in macro-pores between 28 and 365 days. While the other two geopolymers showed macro-porosity decrease with time, their reduction percentage is much lower than Gladstone. The unreacted fly ash particles react with alkali and produce aluminosilicate gel over time, which fills the voids and cavities in both the gel matrix and gel-aggregate zone. This results in the decreased macro-porosity observed in all geopolymers with time.

The porosity of geopolymer is affected by the fineness of fly ash, with a higher fineness of material filling the cracks between the aggregates and leading to a lower porosity (Sinsiri et al., 2010). It is hypothesised that the high quantity of coarse particles in Collie fly ash causes an uneven gel distribution reducing the ability to fill the cracks and voids in geopolymer pastes and the aggregates and leads to the highest macro-porosity in this concrete compared with the other geopolymer concrete.

7.3.2 Microstructure

The microstructure development of the four different fly ash based geopolymer concrete is broadly discussed in Chapter 6 Section 6.6. The nature of the gel matrix formed and packing density of gel-aggregate zone in the four geopolymer concrete is briefly summarized and presented here.

Gladstone geopolymer produced a uniformly distributed geopolymeric gel–microstructure at all ages. The on-going geopolymerization and continuous gel production filled the interior spaces and formed a uniform, strongly compacted and well condensed gel–microstructure. There was a strong bond between coarse aggregates and gel matrix with almost no micro–crack propagation such that it displayed no difference between bulk gel matrix and gel–aggregate zone.

The Pt.Augusta geopolymer had a heterogeneous microstructure and a number of partially reacted fly ash particles with induced micro-cracks in the gel matrix. Similar to Gladstone, there is no difference observed in gel–aggregate zone compared to the rest of the gel matrix.

The number of micro-cracks decreased with age, almost no cracks were observed at one year. At 365 days the concrete also had a more highly compacted and dense microstructure than at 28 days.

At 28 days Tarong had a heterogeneous microstructure, with a higher quantity and wider micro-cracks in the gel matrix compared to Pt.Augusta. Additionally these micro-cracks were evident in the gel-aggregate zone. Tarong displayed significant microstructure development at 365 days and the bulk gel-microstructure was similar in appearance to the Pt.Augusta geopolymer, with a dense gel matrix but with a high number of micro-cracks.

A loosely packed, less solid gel matrix was observed in Collie geopolymer concrete at all ages, indicating very weak adhesion between aggregates and gel matrix. It further displayed a large number of cracks which were visibly larger than those in the other geopolymer concrete. This resulted in the separation of the microstructure into small sections with discontinuities within the gel matrix. The cracks extended to the gel-aggregate zone and formed large cavities between aggregates and gel matrix.

7.4 Effect of pore-structure and microstructure development on durability

An improvement in the durability properties are observed for all four geopolymer concrete with time. The Collie fly ash performs worst for all parameters studied at each age, while the Gladstone performs the best for all parameters other than the water absorption and AVPV. The improvement in all the durability characteristics would indicate that all of the geopolymers undergo further geopolymerisation following heat curing and that this continues beyond 90 days. This is supported by microstructural and MIP data which show distinct changes between 28 and 365 days. The relative quantities of meso and macro pores present in the specific fly ash geopolymer concrete coupled with the uniformity and compactness of the gel matrix correlate well with the durability characteristics observed in Section 7.2.

The water/solid ratio and paste volume fraction of the four geopolymer concrete were similar, thus the reaction products and the packing density are crucial in determining the water absorption. Gladstone and Pt.Augusta geopolymer concrete showed high water absorption, and MIP data showed both geopolymers contained a high meso-porosity. Water absorption is primarily governed by the capillary suction. Capillary suction is governed by the connectivity of the concrete surface to the bulk concrete via the meso-pores in the gel paste. These two

concrete also displayed a high AVPV percentage, which is also dependent on the interconnectivity of the capillaries in the concrete. Thus the high meso-pore content in Gladstone and Pt Augusta would account for the high water absorption and AVPV values displayed.

In contrast both geopolymer concrete based on the air and water permeability data are classified as low permeable concrete. In the permeability test, the applied pressure is the principal driver of water ingress rather than capillary suction. The permeability data is is determined by the overall porosity of the concrete. Gladstone and Pt.Augusta geopolymers showed low macro-porosity, even though both concrete had a high volume of interconnected gel pores. Moreover, Gladstone and Pt.Augusta fly ash contain a high percentage of CaO, which produces calcium-aluminosilicate gel. The presence of this type gel is expected to provide additional pore-filling and result in a denser the pore structure, as observed in the SEM analysis, Chapter 6 Section 6.6 and indicated by the UPV and density data (Karakurt et al., 2010). Hence, the low macro-porosity would account for the low water and air permeability observed in these materials. Collie, however, has a high macro-porosity and a loosely compacted and non-homogeneous microstructure with a large number of cracks. The combination of this would account for the high water absorption and permeability of Collie fly ash geopolymer concrete.

Tarong geopolymer displayed significantly different characteristics to the other geopolymer concrete. It displayed high air and water permeability characteristics at 90 days, but a low water absorption and AVPV. However by 365 days both the air and water permeability had significantly reduced. The low initial water absorption and AVPV is attributed to the low meso-porosity, which has been observed to influence the capillary suction, on which these parameters are dependent. The reduction in air and water permeability is then due to the reduction in the macro-pores, which influence the overall permeability, observed between the initial period and the 365 day data.

The high surface chloride concentration observed in the Gladstone, Pt.Augusta and Collie geopolymer concrete at early age is in line with the water absorption and water permeability data. The high surface water absorption would indicate a permeable surface layer enabling capillary suction to occur resulting in a high surface concentration of chloride ions. However, the low water permeability data would indicate a dense, impermeable concrete matrix,

reflected in the low chloride diffusion coefficients determined. This is further supported by the Tarong geopolymer, which had lower water absorption and lower surface chloride concentration. A reduction in both the chloride diffusion coefficient and the surface chloride concentration was noted in all geopolymer concrete at one year, again consistent with the previous data. The fall in the surface chloride is attributed to the formation of aluminosilicate gel in the surface layer reducing the pore volume. This in turn leads to a reduction in solution in the surface layer and the free chloride ions which are present in this pore solution.

In PC and blended cement concrete, a part of the chloride ion ingress is retained and bound by the hydration products, mainly by the calcium silicate hydrate (C-S-H) gel (Kayali et al., 2012). The free chloride ions that are not bound by C-S-H gel are only able to travel through the pore solution and induce corrosion on the reinforcing bars. Chindaprasirt and Chalee (2014) reported that diffused chloride ions in Geopolymer concrete is bound by the calcium oxide and sodium hydroxide. This is similar to the chloride binding process of PC concrete. The high sodium hydroxide in geopolymer concrete bound chloride ions whereas a high content of calcium oxide reacted with silicate compounds and produces calcium aluminosilicate (C-A-S-H) gel which also leads to an additional chloride binding. The high calcium oxide in Gladstone and Pt.Augusta is expected to be bound more chlorides with the production of higher amount of C-A-S-H gel at the geopolymerization process than other two geopolymers.

The effect of binding compared to geopolymer is that PC and blended cements may well have more binding capacity, hence can sustain higher total chloride prior to corrosion being initiated, that is a higher critical chloride threshold. Also the C-S-H gel and $Ca(OH)_2$ in PC and blended cement concrete give a high pH and a buffer while geopolymer concrete may have a lower pH and no buffering so as OH^-/Cl^- ion ratio is critical the OH^- may be less, so a lower Cl^- is required.

The long term durability of fly ash geopolymer concrete is dependent upon the permeability characteristics of concrete which is associated with the ability of the surface layer to resist the penetration of water, air and water-borne chlorides into the geopolymer concrete and initiate reinforcement corrosion. The rate of this is a function of the packing density of aluminosilicate gel matrix, the porosity and the connectivity of the pore structure. The data obtained suggests that all fly ash geopolymer concrete, other than Collie, have low air and

water permeability, which improves with age due to on-going geopolymerization and give a performance comparable with PC and blended cement concrete.

7.5 Conclusions in Chapter 7

Based on the results of the experimental study, the following conclusions can be made:

- An improvement in the durability properties are observed for all four geopolymer concrete with time. The improvement in all the durability characteristics would indicate that all of the geopolymers undergo further geopolymerisation following heat curing and that this continues beyond 90 days.

- There is a strong relationship between density and UPV of fly ash based geopolymer concrete, similar to PC concrete. This could be successfully used to provide an indication of the solid volume fraction and the quality of geopolymer concrete, free from large voids and cracks.

- Each fly ash geopolymer concrete is believed to have a different Schmidt hammer response, unique to that of geopolymer material. Thus, each fly ash based geopolymer concrete requires its own correlation curve based on Schmidt hammer and compressive strength values.

- The quantity of meso-pores (ϕ<50 nm) governs the water absorption of geopolymer concrete. This is due to the concrete surface being connected to the bulk concrete by capillary vessels via meso-pores in the aluminosilicate gel paste.

- A high quantity of coarse particles in the precursor fly ash causes an uneven material distribution which leads to a high macro-porosity. Collie, has a high macro-porosity (ϕ>1 µm) and a loosely compacted and non-homogeneous microstructure with a large number of cracks. The combination of this would account for the high water absorption and water and air permeability.

- Tarong behaved differently to the other geopolymer concrete, in terms of long term durability. While it had a low water absorption and AVPV throughout, it displayed high air and water permeability at 90 days, but thereafter these decreased and were significantly lower at one year.

- The lowest water absorption and AVPV of Tarong geopolymer is attributed to the low meso-porosity, which has been observed to influence the capillary suction, on which these parameters are dependent. The reduction in air and water permeability is then due to the continuing geopolymerization and refine pore-structure reducing macro-pores, which influence the overall permeability.
- The high surface chloride concentration observed in the Gladstone, Pt.Augusta and Collie geopolymer concrete at early age is in line with the water absorption and water permeability data. The high surface water absorption would indicate a permeable surface layer enabling capillary suction to occur resulting in a high surface concentration of chloride ions.

- A reduction in both the chloride diffusion coefficient and the surface chloride concentration was noted in all geopolymer concrete at one year. The fall in the surface chloride is attributed to the formation of aluminosilicate gel in the surface layer due to continuing geopolymerization reducing the pore volume. This in turn leads to a reduction in solution in the surface layer and the free chloride ions which are present in this pore solution.

- The diffusion coefficients of the fly ash based geopolymer concrete decreased with time and are comparable to the PC concrete in their long term performance.

8 Conclusions and Recommendations

8.1 Overview

This chapter presents the summary and the main conclusions which can be drawn from the investigation of the influence of properties of fly ash from different sources on the mix design and performance of geopolymer concrete.

8.2 Summary and Conclusion

8.2.1 Mix design and compressive strength

Low calcium, class F precursor fly ash from five different coal power stations in Australia has been investigated. The compressive strength of fly ash geopolymer mixes was examined over a range of activator modulus at a fixed Na_2O dosage in order to optimize the mix design of both geopolymer mortar and concrete for each specific fly ash. A series of tests have been conducted on geopolymer mortar as the first phase of the research. The microstructural and pore-structural changes with the degree of geopolymerization is assessed in depth and correlated with the compressive strength of final geopolymer systems. In conclusion, all the data has been analysed to explain the effects of the chemical, physical and mineralogical properties of precursor fly ash on the compressive strength of the geopolymer mortars.

Overall, following main conclusions can be made from the first phase of the research:

- The optimum activator modulus (SiO_2/Na_2O in alkaline activator) for compressive strength of geopolymer mortar is dependent on the chemical composition of the precursor fly ash. In this study, the activator modulus ranged between 0.75 for Mt.Piper fly ash to 1.625 for Tarong fly ash.

- Both the effective activator modulus (SiO_2/Na_2O in alkaline activator and fly ash) and SiO_2/Al_2O_3 ratio of resultant geopolymer mortar do not appear to show a direct correlation with the compressive strength of geopolymer mortar.

- The amount of unburnt carbon (loss on ignition) in fly ash demonstrates an inverse correlation with the compressive strength. This is hypothesised as being due to the absorption of activator solution by unburnt carbon, which reduces the activator available for geopolymerization and workability.

- Workability is a key factor contributing to compressive strength of low calcium fly ash geopolymer and a flow in the range 110 ± 5% to 140 ± 5% is required for optimum performance. In contrast, the workability correlates well with the shear thinning exponent, m, in $(\eta/\eta_{max}) \sim (\dot{\gamma}/\dot{\gamma}_{max})^{-m}$ which depends on the particle size distribution, particularly the fineness, with the quantity of particles passing at the 10, 20 and 45μm sieve sizes.

- The specific surface area of precursor fly ash coupled with the quantity of particles passing at the 10 and 20μm sieve size is the key factor in the dissolution, coagulation and gel formation of geopolymers. The higher the surface area and the greater the particles smaller than 20μm, the better the gel formation.

- When fly ash geopolymer mortars are within the specified flow range, the amorphous content of particles in the 10 to 20μm range was identified as being critical to the strength development, rather than the total amorphous content. Moreover, the degree of uniformity and homogeneity of SiO_2 and Al_2O_3 distribution in the fly ash directly influence the dissolution of this amorphous surface layer. The extent of fly ash dissolution controls the geopolymeric gel formation and aluminium incorporation in the gel matrix.

- The combination of aluminium into the silicate backbone during geopolymerization leads to higher compressive strength. In contrast, the lack of aluminium amalgamation with silicates results in a lower degree of geopolymerization and hence lower compressive strength. In addition, the presence of reactive aluminium-silicate bonds in the 800–1000 cm^{-1} range after geopolymerization is a clear indication of a high degree of geopolymerization.

- A high quantity of aluminium present in octahedral coordination in the precursor fly ash, and conversion of this into tetrahedral units during alkali dissolution is required to obtain high compressive strength. In addition, the stable and relaxed conversion of aluminium from octahedral to tetrahedral coordination is more significant than the total quantity of octahedral coordinated aluminium in the formation of homogeneous, well compacted geopolymeric gel and the production of high compressive strength geopolymer mortar.

- The aluminosilicate gel with a three dimensional (3-D) polysialate-siloxo (Si-O-Al-O-Si) polymeric structure provides high rigidity and stability in the final geopolymer, and contributes to a higher compressive strength. In contrast, a gel structure consisting of polysialate-disiloxo and silicate links produces lower strength.

- The meso-porosity of fly ash based geopolymer increases with its degree of geopolymerization. Total pore volume below 1000nm in pore size, rather than overall total pore volume, is a good indicator to the degree of geopolymerization.

- A good correlation is observed between the zeta potential of the raw fly ash and the CaO percentage, with a high CaO content leading to negative zeta potential. The larger the negative zeta potential of the fly ash the higher the compressive strength of the resultant geopolymer. However, a smaller negative zeta potential of the geopolymer is an indication of more gel formation and hence a high compressive strength.

8.2.2 Long term material performance

The long term performance of mechanical and durability properties of four different fly ash geopolymer concrete were investigated in the second phase of research. The investigated mechanical properties were compressive strength, flexural strength, splitting tensile strength, elastic modulus and Poisson's ratio whereas the durability properties were water absorption, water permeability, air permeability, resistivity, chloride diffusivity, ultrasonic pulse velocity and surface hardness. The influence of the properties of precursor fly ash on these material properties in the long term were examined in depth through comprehensive microstructural and pore-size distribution analysis. Finally, the applicability of current relationships between compressive strength and the mechanical properties based on standards derived for Portland cement (PC) concrete have been critically examined for fly ash geopolymer concrete.

Overall, the following conclusions can be made from the second phase of the research:

- The compressive strength of four different fly ash based geopolymer concrete at one year ranged between 28 and 88 MPa. There is an on-going geopolymerization which increased compressive strength with time, even beyond 90 days, for all geopolymer concrete. The rate of compressive strength increase was different for each, depending on the properties of the precursor fly ash.

- The combination of calcium aluminosilicate (C–A–S–H) gel, which is formed by CaO in precursor fly ash, with the sodium aluminosilicate (N–A–S–H) main gel provides additional rigidity to the geopolymer backbone. Hence, the presence of a high quantity of

CaO leads to a densely packed microstructure at an early age, giving high early compressive strength to the geopolymer concrete.

- The flexural and splitting tensile strengths of the four different fly ash geopolymer concrete at one year ranged between 3.92 to 6.3 MPa and 1.86 to 4.72 MPa, respectively. Tensile strength of geopolymer concrete is governed by the gel-aggregate bond. Hence the nature of the interfacial transition zone (ITZ) formed between aggregates and aluminosilicate gel matrix was shown to cause the tensile strength variation among the four geopolymer concrete.

- Gladstone geopolymer concrete had a well compacted dense ITZ, and no obvious difference noted between the ITZ and the bulk geopolymer matrix. In contrast, Collie geopolymer concrete produced a porous ITZ. The unreacted/partially reacted fly ash particles were loosely packed in this zone. The density of the ITZ was the key factor in determining the tensile strength of the geopolymer concrete.

- The elastic modulus and Poisson's ratio of four different geopolymer concrete at one year ranged from 10.3 to 29 GPa and 0.16 to 0.28. The packing density of the aluminosilicate gel matrix influences elastic modulus development. An increase in porosity and micro cracks negatively affects the compactness of the gel matrix, which in turn affects the elastic modulus.

- Water absorption of concrete is governed by capillary suction whereas the applied pressure is the principle driving force in water permeability. The quantity of meso-pores (ϕ<50 nm) governs the water absorption of geopolymer concrete. The concrete surface is simply connected to the bulk concrete by capillary vessels via meso-pores in the aluminosilicate gel paste. In contrast, the quantity of macro-pores (ϕ>1 µm) governs the water and air permeability of geopolymer concrete. A high quantity of coarse particles in fly ash causes an uneven material distribution which leads to a high macro-porosity.

- The on-going geopolymerization and concurrent gel formation in the surface layer reduces the pore volume over time. This in turn leads to a reduction in chloride ions in the surface layer and the free chloride ions which are present in this pore solution. Moreover,

the diffusion coefficient of geopolymer concrete decreases with the age of concrete at a rate comparable to PC and blended cements concrete.

- The long term performance of Tarong geopolymer concrete differed from other geopolymer concrete. In particular, it displayed a significant improvement of material properties after 90 days due to on-going geopolymerization. The continuous gel production fills cracks and voids in the bulk gel matrix while refining the pore sizes, which resulted in a dense pore-structure after one year.

- The correlations between key mechanical properties of fly ash based geopolymer concrete and compressive strength have been studied, and then compared with the design equations available for PC concrete in Australian standards (AS) and American Concrete Institute (ACI). The AS 3600 and ACI 318 specified relations for flexural strength gives an underestimate prediction for geopolymer concrete.

- The AS 3600 specified relation for splitting tensile strength gives a reasonable prediction for geopolymer concrete. However, the ACI 363R stated equation significantly overestimates the splitting tensile strength of geopolymer concrete. In contrast, the AS 3600 stated design equation considerably overvalues the elastic modulus for geopolymer concrete. This overestimation is higher when compressive strength is below 40 MPa.

- There is a strong relationship between density and ultrasonic pulse velocity of fly ash based geopolymer concrete, similar to the PC concrete. This can be successfully used to get an indication of the solid volume fraction which in turn relates to the quality of geopolymer concrete. On the other hand, there is no unique correlation curve for different fly ash based geopolymer concrete based on Schmidt (rebound) hammer and compressive strength values. Hence, each fly ash based geopolymer concrete should have its own correlation curve and a universal correlation factor cannot be used.

8.2.3 Overview of Engineering properties

The key steps towards producing a geopolymer concrete using a wide range of fly ash revolve around the design of an appropriate combination of binder, aggregates and admixtures which will give performance such as rheology, mechanical performance and

durability which is fit for purpose in the desired application. The broad engineering properties tested in long term considering various aspects of mechanical performance and durability can be listed briefly as follows:

- Fly ash geopolymer concrete achieves comparable compressive strength for standard site (PC) concrete at exposure classification B1, B2 as specified in Australasian standards (AS, 2009). Compressive strength increases over time in the long term are similar to that of the PC and blended cement concrete.

- Fly ash geopolymer concrete has high flexural tensile strength than PC and blended cement concrete. The splitting tensile strength of geopolymer concrete is however comparable to that of PC and blended cement concrete. Moreover, fly ash geopolymer concrete displays lower elastic modulus than Portland cement concrete for similar compressive strength.

- The elastic modulus of concrete is a very important mechanical parameter reflecting the ability of the concrete to deform elastically. For instance, in pre-stressed concrete structures, elastic shortening of pre-stressed concrete is one of the main factors contributing to pre-stress loss. In addition, in order to make full use of the compressive strength potential, the structures using high-strength concrete tend to be slimmer and require a higher elastic modulus so as to maintain its stiffness. Thus, lower elastic modulus observed in 100% fly ash based geopolymer concrete may limit its practical implementation in compression structural elements, such as columns, as higher elastic modulus in concrete can avoid excessive deformation while providing satisfactory serviceability.

- Fly ash geopolymer concrete behaves as a high durable concrete in long term, in terms of permeation and diffusion characteristics. It shows high resistance to air and water penetration into concrete. The reduction of the chloride diffusion coefficient is similar to PC cement concrete after one year.

8.3 Key findings of the research

This research has been conducted to investigate the influence of the properties of fly ash from different sources on the mix design and long term performance of geopolymer concrete. Table 8.1 presents the key findings of the research which addressed a significant gap in the research area and made a contribution to knowledge.

Table 8.1 Key findings of the research

No.	Key factors affecting compressive strength of fly ash geopolymer mortar
1	Workability (flow) in the range 110 ± 5% to 140 ± 5% is required for optimum compressive strength.
2	High surface area with high quantity of particles smaller than 20µm in fly ash leads to high compressive strength.
3	Amorphous content of particles below 20µm range is critical to the strength development, rather than the total amorphous content.
4	A high CaO content in fly ash leads to high compressive strength.
5	High degree of uniformity and homogeneity of SiO_2 and Al_2O_3 distribution of amorphous surface layer in fly ash leads to high compressive strength.
6	A high quantity of aluminium present in octahedral coordination in fly ash and stable and relaxed conversion of this into tetrahedral units during alkali dissolution leads high compressive strength.
No.	Key long term features in fly ash geopolymer concrete
1	Geopolymer concrete undergoes on-going geopolymerisation following heat curing and improves engineering properties beyond 90 days.
2	Geopolymer concrete has high flexural strength, comparable splitting tensile strength and lower elastic modulus to the PC concrete.

3	Design equations stated in standards for PC concrete cannot be used to derive elastic modulus, but can be used for the tensile strength in geopolymer concrete.
5	A high quantity of meso-pores in the gel paste increase the water absorption while high quantity of macro-pores leads to an increase in water and air permeability.
6	Chloride diffusion into concrete decreases with the age of concrete and is comparable to PC cement concrete after one year.

8.4 Recommendation for future research

Future work should be undertaken to gain a better understanding of the long term performance of different fly ash based geopolymer concrete and their practical application in structural engineering components. This is essential before fly ash geopolymer concrete can be widely adopted in commercial applications as structural components. Thus, the following recommendations provide some insights on the future research that can be undertaken to improve and optimise the findings of this thesis:

- This research found that several key parameters which affect the ultimate compressive strength of geopolymer mortar. The interrelationship between these key parameters and degree of impact of specific parameters to the final compressive strength require further study to determine their significance. Ideally this would provide a mechanism by which to select an appropriate mix design for a specific fly ash without the need for extensive trial mixes to determine the optimum design. The usage of statistical package to analyse the significance of the specific parameter to the strength while conducting additional experiments with wide range of fly ash is highly recommended.

- The setting time of fly ash geopolymer was found to be dramatically longer than that of PC concrete. It is recommended that more research be undertaken on the setting times and flowability for geopolymer mortar. Moreover, the preliminary experimental results show that the fundamental rheology properties influence the final compressive strength. In-depth investigations using geopolymer concrete and geopolymer paste with more rheological tests is thus required to further identify the relationship between rheology and compressive strength.

- While this study used much data to develop correlation between mechanical properties and compressive strength, a large data set is still needed for a more systematic statistical analysis. The equations stated in different standards for PC concrete were based on very large quantity of data points. To reduce the discreteness of the data and enhance the correlation coefficient of regression, more experimental data for the mechanical properties of geopolymer concrete produced with wide range of fly ash is required.

- One of the major area of interest is the lower modulus of elasticity observed in fly ash based geopolymer concrete. Further investigation should be undertaken to explore the possibility of improve the elastic modulus of fly ash based geopolymer concrete by incorporating coarse aggregate of higher stiffness.

- This research demonstrates that total porosity and pore size distribution directly affect to the long term permeation and diffusion characteristics of different fly ash geopolymer concrete. Further investigation of pore-structure in terms of pore size distribution of concrete at different depth intervals and their interconnectivity through hardened gel matrix is recommended to be conducted with novel techniques such as tomography analysis.

- The resistivity and chloride penetration (salt ponding) test results indicated that geopolymer concrete produced with a wide range of low calcium fly ash might have a comparable performance to PC and blended cements to chloride attack. Comprehensive research on the long term corrosion resistance performance of different fly ash based geopolymer concrete exposed to natural and forced (accelerated) environments by simulating chloride attack are recommended utilizing corrosion monitoring techniques such as half-cell potential and linear polarization techniques. This needs to address both the diffusion characteristics of the material and the critical chloride concentration required to initiate corrosion.

- Understanding reliable critical chloride concentration (C_{crit}) in fly ash geopolymer concrete is important for the design of structures and their condition assessment in long term, as the service life is often considered as the time required to reach the chloride

threshold value at the depth of the reinforcement. Moreover the examination of factors influencing C_{crit} of geopolymer is highly recommended; especially the chloride binding capacity of the geopolymer matrix and the initial pH of the pore solution as well as the long term impact on pH due to the lack of Portlandite and calcium hydroxide. Further investigation of the effect of carbonation on pH in geopolymer concrete is also essential.

- The 100% fly ash replacement with Portland cement in geopolymer concrete has been reported to have significant environmental benefits in terms of carbon dioxide emission. However, the overall environmental and cost benefit of fly ash based geopolymer concrete still remains unclear. The use of high concentration alkali and heat curing will increase the use of energy and carbon dioxide production indirectly. A detailed cost benefit analysis can be undertaken to determine the financial and environmental impact of the production of fly ash geopolymer concrete. The study can assess the potential applications of the materials and how widespread their use may be within the construction industry. The analysis should involve the suppliers and manufacturers of replacement materials and precast concrete manufactures.

REFERENCES

AASHTO T260-1997a. Standard Method of Test fo Sampling and Testing for Chloride Ion in Concrete and Concrete Raw Materials. AASHTO, USA.

AASHTO T-259-1997b. Standard Method of Test for Resistance of Concrete to Chloride Ion Penetration. AASHTO, USA.

ACI 363R-1992. State-of-the-art report on high-strength concrete. ACI Committee, American Concrete Institute.

ACI 318-2008. Building code requirements for structural concrete. ACI Committee, American Concrete Institute.

ADAM, A. A. 2009. Strength and durability properties of alkali activated slag and fly ash-based geopolymer concrete. Ph.D. Thesis, School of Civil, Environmental and Chemical Engineering, RMIT University, Melbourne, Australia.

ALTMAN, D. G. & GARDNER, M. J. 1988. Statistics in Medicine: Calculating confidence intervals for regression and correlation. British medical journal (Clinical research ed.), 296, 1238-1247.

ALVAREZ-AYUSO, E., QUEROL, X., et al. 2008. Environmental, physical and structural characterisation of geopolymer matrixes synthesised from coal combustion fly ashes. Journal of Hazardous Materials, 154, 175-183.

AS 1012.17-1997. Methods of testing concrete - Determination of the static chord modulus of elasticity and Poisson's ratio of concrete specimens. Standards Australia.

AS 1012.12.2-1998a. Methods of testing concrete - Determination of mass per unit volume of hardened concrete - Water displacement method. Standards Australia.

AS 3582.1-1998b. Supplementary cementitious materials for use with portland and blended cement, Part 1: Fly ash. Standards Australia.

AS 1012.9-1999a. Method of testing concrete, Method 9: Determination of the compressive strength of concrete specimens. Standards Australia.

AS 1012.21-1999b. Methods of testing concrete - Determination of water absorption and apparent volume of permeable voids in hardened concrete. Standards Australia.

AS 1141.5-2000a. Methods for sampling and testing aggregates, Method 5: Particle density and water absorption of fine aggregate. Standards Australia.

AS 1012.10-2000b. Methods of testing concrete - Determination of indirect tensile strength of concrete cylinders (Brasil or splitting test). Standards Australia.

AS 1012.11-2000c. Methods of testing concrete - Determination of the modulus of rupture. Standards Australia.

AS 3600-2009. Concrete structures. Standards Australia.

AS 2758.1-2014a. Aggregates and rock for engineering purposes-Concrete aggregates. Standards Australia.

AS 1012.3.1-2014b. Determination of properties related to the consistency of concrete - Slump test. Standards Australia.

ASTM C597-2009. Standard Test Method for Pulse Velocity Through Concrete. ASTM International.

ASTM C1543-2010. Standard Test Method for Determining the Penetration of Chloride Ion into Concrete by Ponding. ASTM International.

ASTM C618-2012. Standard Specification for Coal Fly Ash and Raw or Calcined Natural Pozzolan for use as a Mineral Admixture in Portland Cement Concrete. ASTM International.

ASTM C109/C109M-2013a. Standard Test Method for Compressive Strength of Hydraulic Cement Mortars (Using 2-in. or [50-mm] Cube Specimens). ASTM International.

ASTM C1437-2013b. Standard Test Method for Flow of Hydraulic Cement Mortar. ASTM International.

ASTM C805/C805M-2013c. Standard Test Method for Rebound Number of Hardened Concrete. ASTM International.

Autoclam Permeability System-1995. Operating manual. Structural Materials Research Group, Queen's University of Belfast, U.K.

BAKHAREV, T. 2005a. Geopolymeric materials prepared using Class F fly ash and elevated temperature curing. Cement and Concrete Research, 35, 1224-1232.

BAKHAREV, T. 2005b. Resistance of geopolymer materials to acid attack. Cement and Concrete Research, 35, 658-670.

BAMFORTH, P. 1999. The derivation of input data for modelling chloride ingress from eight-year UK coastal exposure trials. Magazine of Concrete Research, 51, 87-96.

BAMFORTH, P. & POCOCK, D. 2000. Design for durability of reinforced concrete exposed to chlorides. 6th international conference on deterioration and repair of reinforced concrete in the Arabian Gulf region, Bahrain.

BARBOSA, V. F., MACKENZIE, K. J., et al. 2000. Synthesis and characterisation of materials based on inorganic polymers of alumina and silica: sodium polysialate polymers. International Journal of Inorganic Materials, 2, 309-317.

BASHEER, L., KROPP, J., et al. 2001. Assessment of the durability of concrete from its permeation properties: a review. Construction and building materials, 15, 93-103.

BASHEER, M., GONÇALVES, A., et al. 2007. Non-destructive methods to measure water transport:Penetrability and thickness of the concrete cover. RILEM Technical Committee, 1-71.

BASHEER, P., MONTGOMERY, F., et al. 1995. Clam tests for measuring in-situ permeation properties of concrete. Nondestructive Testing and Evaluation, 12, 53-73.

BAWEJA, I. & NELSON, P. 1998. Supplementary Cementing Materials: Their Acceptance in Australian Specifications. ACI Special Publication, 178, 398-407.

BENHELAL, E., ZAHEDI, G., et al. 2013. Global strategies and potentials to curb CO2 emissions in cement industry. Journal of Cleaner Production, 51, 142-161.

BENTUR, A., DIAMOND, S., et al. 1997. Steel corrosion in concrete: fundamentals and civil engineering practise. E & FN Spon, London.

BERRY, M., CROSS, D., et al. 2009. Changing the environment: an alternative "Green" concrete produced without Portland cement. Proc., World of Coal Ash Conf., Lexington, KY, USA, United States.

BODEN, T., MARLAND, G., et al. 2009. Global CO2 emissions from fossil-fuel burning, cement manufacture and gas flaring. Carbon Dioxide Information Analysis Center (CDIAC) Laboratory, Oak Ridge National Laboratory, Oak Ridge, USA.

BONDAR, D., LYNSDALE, C. J., et al. 2013. Alkali-Activated Natural Pozzolan Concrete as New Construction Material. ACI Materials Journal, 110, 331-337.

BONDAR, D., LYNSDALE, C. J., et al. 2011. Effect of type, form, and dosage of activators on strength of alkali-activated natural pozzolans. Cement and Concrete Composites, 33, 251-260.

BROOMFIELD, J. P. 2006. Corrosion of steel in concrete: understanding, investigation and repair. CRC Press.

BROWN, A. M. 2001. A step-by-step guide to non-linear regression analysis of experimental data using a Microsoft Excel spreadsheet. Computer methods and programs in biomedicine, 65, 191-200.

BROWNE, R., GEOGHEGAN, M., et al. 1983. Corrosion of reinforcement in concrete construction. E & FN Spon, London.

BUNGEY, J. H., GRANTHAM, M. G., et al. 2006. Testing of concrete in structures. Crc Press.

CHANCEY, R. T. 2008. Characterization of crystalline and amorphous phases and respective reactivities in a Class F fly ash. ProQuest.

CHEN-TAN, N. W., VAN RIESSEN, A., et al. 2009. Determining the reactivity of a fly ash for production of geopolymer. Journal of the American Ceramic Society, 92, 881-887.

CHEN, C., HABERT, G., et al. 2010. Environmental impact of cement production: detail of the different processes and cement plant variability evaluation. Journal of Cleaner Production, 18, 478-485.

CHENG, T. W. & CHIU, J. P. 2003. Fire-resistant geopolymer produced by granulated blast furnace slag. Minerals Engineering, 16, 205-210.

CHINDAPRASIRT, P. & CHALEE, W. 2014. Effect of sodium hydroxide concentration on chloride penetration and steel corrosion of fly ash-based geopolymer concrete under marine site. Construction and Building Materials, 63, 303-310.

CHINDAPRASIRT, P., CHAREERAT, T., et al. 2007. Workability and strength of coarse high calcium fly ash geopolymer. Cement and Concrete Composites, 29, 224-229.

CLAISSE, P., GANJIAN, E., et al. 2003. In situ measurement of the intrinsic permeability of concrete. Magazine of concrete research, 55, 125-132.

CORBETT, D. 2014. World first earth-friendly concrete airport. Concrete in Australia 40, 7-8.

CRANK, J. 1975. The Mathematics of Diffusion: Second Edition. Clarendon Press.

CWIRZEN, A. & PENTTALA, V. 2005. Aggregate–cement paste transition zone properties affecting the salt–frost damage of high-performance concretes. Cement and Concrete Research, 35, 671-679.

CWIRZEN, A., PROVIS, J. L., et al. 2014. The effect of limestone on sodium hydroxide-activated metakaolin-based geopolymers. Construction and Building Materials, 66, 53-62.

DAVIDOVITS, J. 1991. Geopolymers. Journal of Thermal Analysis and calorimetry, 37, 1633-1656.

DAVIDOVITS, J. 1994. High-alkali cements for 21st century concretes. ACI Special Publication, 144, 383-398.

DAVIDOVITS, J. 1999. Chemistry of Geopolymeric Systems. International Geopolymer Conference, France.

DAVIDOVITS, J. 2000. Geopolymer concrete. Geopolymer congress, France.

DAVIDOVITS, J. 2005. Geopolymer chemistry and sustainable development. The poly (sialate) terminology: a very useful and simple model for the promotion and understanding of green-chemistry. Geopolymer conference, France.

DE SILVA, P., SAGOE-CRENSTIL, K., et al. 2007. Kinetics of geopolymerization: role of Al2O3 and SiO2. Cement and Concrete Research, 37, 512-518.

DEMIE, S., NURUDDIN, M. F., et al. 2013. Effects of micro-structure characteristics of interfacial transition zone on the compressive strength of self-compacting geopolymer concrete. Construction and Building Materials, 41, 91-98.

DIAZ-LOYA, E. I., ALLOUCHE, E. N., et al. 2011. Mechanical Properties of Fly-Ash-Based Geopolymer Concrete. ACI Materials Journal, 108, 300-306.

DIAZ, E. I., ALLOUCHE, E. N., et al. 2010. Factors affecting the suitability of fly ash as source material for geopolymers. Fuel, 89, 992-996.

DUXSON, P., FERNÁNDEZ-JIMÉNEZ, A., et al. 2007a. Geopolymer technology: the current state of the art. Journal of Materials Science, 42, 2917-2933.

DUXSON, P., MALLICOAT, S., et al. 2007b. The effect of alkali and Si/Al ratio on the development of mechanical properties of metakaolin-based geopolymers. Colloids and Surfaces A: Physicochemical and Engineering Aspects, 292, 8-20.

DUXSON, P., PROVIS, J. L., et al. 2005. Understanding the relationship between geopolymer composition, microstructure and mechanical properties. Colloids and Surfaces A: Physicochemical and Engineering Aspects, 269, 47-58.

ELAKNESWARAN, Y., NAWA, T., et al. 2009. Influence of surface charge on ingress of chloride ion in hardened pastes. Materials and Structures, 42, 83-93.

FAVIER, A., HABERT, G., et al. 2015. A multinuclear static NMR study of geopolymerisation. Cement and Concrete Research, 75, 104-109.

FERNÁNDEZ-JIMÉNEZ, A., M. , PALOMO, A., et al. 2006a. Engineering Properties of Alkali-Activated Fly Ash Concrete. ACI Materials Journal, 103, 106-112.

FERNANDEZ-JIMENEZ, A. & PALOMO, A. 2003. Characterisation of fly ashes. Potential reactivity as alkaline cements. Fuel, 82, 2259-2265.

FERNANDEZ-JIMENEZ, A. & PALOMO, A. 2005. Composition and microstructure of alkali activated fly ash binder: Effect of the activator. Cement and Concrete Research, 35, 1984-1992.

FERNÁNDEZ-JIMÉNEZ, A., PALOMO, A., et al. 2005. Microstructure development of alkali-activated fly ash cement: a descriptive model. Cement and Concrete Research, 35, 1204-1209.

FERNÁNDEZ-JIMÉNEZ, A., PALOMO, A., et al. 2006b. The role played by the reactive alumina content in the alkaline activation of fly ashes. Microporous and Mesoporous materials, 91, 111-119.

GALLUCCI, E., SCRIVENER, K., et al. 2007. 3D experimental investigation of the microstructure of cement pastes using synchrotron X-ray microtomography (μCT). Cement and Concrete Research, 37, 360-368.

GARBACZ, A. & GARBOCZI, E. J. 2003. Ultrasonic evaluation methods applicable to polymer concrete composites. US Department of Commerce, Technology Administration, National Institute of Standards and Technology.

GARTNER, E. 2004. Industrially interesting approaches to low-CO2 cements. Cement and Concrete Research, 34, 1489-1498.

GOURLEY, J. 2003. Geopolymers; opportunities for environmentally friendly construction materials. Conference on Adaptive materials for a modern society, Sydney, Australia.

GOURLEY, J. & JOHNSON, G. 2005. Developments in geopolymer precast concrete. World Congress of Geopolymer, Perth, Australia.

GUO, X., SHI, H., et al. 2010. Compressive strength and microstructural characteristics of class C fly ash geopolymer. Cement and Concrete Composites, 32, 142-147.

HABERT, G., D'ESPINOSE DE LACAILLERIE, J. B., et al. 2011. An environmental evaluation of geopolymer based concrete production: reviewing current research trends. Journal of Cleaner Production, 19, 1229-1238.

HANJITSUWAN, S., HUNPRATUB, S., et al. 2014. Effects of NaOH concentrations on physical and electrical properties of high calcium fly ash geopolymer paste. Cement and Concrete Composites, 45, 9-14.

HARDJITO, D. & RANGAN, B. V. 2005. Development and properties of low-calcium fly ash-based geopolymer concrete. Research Report-GC1, Curtin University of Technology, Perth, Australia, 1-103.

HARDJITO, D., WALLAH, S. E., et al. 2004. On the development of fly ash-based geopolymer concrete. ACI Materials Journal-American Concrete Institute, 101, 467-472.

HONG, K. & HOOTON, R. 1999. Effects of cyclic chloride exposure on penetration of concrete cover. Cement and Concrete Research, 29, 1379-1386.

HUNTZINGER, D. N. & EATMON, T. D. 2009. A life-cycle assessment of Portland cement manufacturing: comparing the traditional process with alternative technologies. Journal of Cleaner Production, 17, 668-675.

IYER, R. 2002. The surface chemistry of leaching coal fly ash. Journal of hazardous materials, 93, 321-329.

JENNINGS, H. M., BULLARD, J. W., et al. 2008. Characterization and Modeling of Pores and Surfaces in Cement Paste:Correlations to Processing and Properties. Journal of Advanced Concrete Technology, 6, 5-29.

JUNAID, M. T., KHENNANE, A., et al. 2015. Performance of fly ash based geopolymer concrete made using non-pelletized fly ash aggregates after exposure to high temperatures. Materials and Structures, 48, 3357-3365.

JUNAID, M. T., KHENNANE, A., et al. 2014. Aspects of the deformational behaviour of alkali activated fly ash concrete at elevated temperatures. Cement and Concrete Research, 60, 24-29.

KAPS, C. H. & BUCHWALD, A. 2002. Sustainable Cement-free Concrete. Geopolymer Conference, Melbourne, Australia.

KARAKURT, C., KURAMA, H., et al. 2010. Utilization of natural zeolite in aerated concrete production. Cement and Concrete Composites, 32, 1-8.

KAYALI, O., KHAN, M., et al. 2012. The role of hydrotalcite in chloride binding and corrosion protection in concretes with ground granulated blast furnace slag. Cement and Concrete Composites, 34, 936-945.

KHALE, D. & CHAUDHARY, R. 2007. Mechanism of geopolymerization and factors influencing its development: A review. Journal of Materials Science, 42, 729-746.

KHATIB, Z. K. & BAYOMY, F. M. 1999. Rubberized Portland cement concrete. Journal of materials in civil engineering, 11, 206-213.

KIRSCHNER, A. & HARMUTH, H. 2004. Investigation of geopolymer binders with respect to their application for building materials. Ceramics Silikáty, 48, 7-20.

KONG, D. L. Y. & SANJAYAN, J. G. 2010. Effect of elevated temperatures on geopolymer paste, mortar and concrete. Cement and Concrete Research, 40, 334-339.

KUKIER, U., ISHAK, C. F., et al. 2003. Composition and element solubility of magnetic and non-magnetic fly ash fractions. Environmental Pollution, 123, 255-266.

KUPWADE-PATIL, K. & ALLOUCHE, E. N. 2013. Examination of chloride-induced corrosion in reinforced geopolymer concretes. Journal of Materials in Civil Engineering, 25, 1465-1476.

LAW, D. W., ADAM, A. A., et al. 2014. Long term durability properties of class F fly ash geopolymer concrete. Materials and Structures, 48, 1-11.

LAWRENCE, C. D. 2003. The production of low-energy cements. Butterworth-Heinemann.

LI, C., GONG, X., et al. 2011. CO2 emissions due to cement manufacture. Materials Science Forum, 685, 181-187.

LI, X., MA, X., et al. 2013. Mechanical properties and microstructure of Class C fly ash-based geopolymer paste and mortar. Materials, 6, 1485-1495.

LIEBERMAN, R. N., GREEN, U., et al. 2015. Coal fly ash as a potential fixation reagent for radioactive wastes. Fuel, 153, 437-444.

LIN, K. L., SHIU, H. S., et al. 2014. Effects of SiO2/Na2O molar ratio on properties of TFT-LCD waste glass-metakaolin-based geopolymers. Environmental Progress & Sustainable Energy, 33, 205-212.

LIU, M. Y. J., ALENGARAM, U. J., et al. 2014. Evaluation of thermal conductivity, mechanical and transport properties of lightweight aggregate foamed geopolymer concrete. Energy and Buildings, 72, 238-245.

LLOYD, R. R., PROVIS, J. L., et al. 2010. Pore solution composition and alkali diffusion in inorganic polymer cement. Cement and Concrete Research, 40, 1386-1392.

MA, Y., HU, J., et al. 2013. The pore structure and permeability of alkali activated fly ash. Fuel, 104, 771-780.

MACKENZIE, K. J. & SMITH, M. E. 2002. Multinuclear solid-state nuclear magnetic resonance of inorganic materials. Elsevier.

MALHOTRA, V. M. 2008. Role of fly ash in reducing greenhouse gas emissions during themanufacturing of portland cement clinker. Second International Conference on Advances in Concrete Technologies in the Middle East Conference Research Papers, Dubait.

MCCARTER, W., STARRS, G., et al. 2000. Electrical conductivity, diffusion, and permeability of Portland cement-based mortars. Cement and Concrete Research, 30, 1395-1400.

MCLELLAN, B. C., WILLIAMS, R. P., et al. 2011. Costs and carbon emissions for geopolymer pastes in comparison to ordinary portland cement. Journal of Cleaner Production, 19, 1080-1090.

MEYER, C. 2009. The greening of the concrete industry. Cement and Concrete Composites, 31, 601-605.

MIRANDA, J. M., FERNÁNDEZ-JIMÉNEZ, A., et al. 2005. Corrosion resistance in activated fly ash mortars. Cement and Concrete Research, 35, 1210-1217.

MOLYNEAUX, T., LAW, D., et al. 2007. Strength of mortar containing activated slag and fly ash. 23rd Biennial Conference of the Concrete Institute of Australia: Design Materials and Construction, Adelaide, South Australia.

MORRIS, W., VICO, A., et al. 2002. Corrosion of reinforcing steel evaluated by means of concrete resistivity measurements. Corrosion Science, 44, 81-99.

MUELLER, S., LLEWELLIN, E., et al. 2009. The rheology of suspensions of solid particles. Proceedings of the Royal Society of London A: Mathematical, Physical and Engineering Sciences, London, United Kingdom.

NÄGELE, E. & SCHNEIDER, U. 1989. From cement to hardened paste-an elektrokinetic study. Cement and Concrete Research, 19, 978-986.

NAZARI, A., KHALAJ, G., et al. 2012. Prediction total specific pore volume of geopolymers produced from waste ashes by ANFIS. Ceramics International, 38, 3111-3120.

NEUPANE, K., BAWEJA, D., et al. 2012. Mechanical properties of geopolymer concrete: Applicability of relationships defined by AS 3600. Concrete In Australia, 40, 50-56.

NEUPANE, K., BAWEJA, D., et al. 2014. Mechanical properties of Geopolymer concrete: Applicability of relationships defined by AS 3600. Concrete in Australia, 40, 50-56.

NEVILLE, A. M. 1996. Properties of Concrete. Pearson Education Limited.

OH, J. E., JUN, Y., et al. 2014. Characterization of geopolymers from compositionally and physically different Class F fly ashes. Cement and Concrete Composites, 50, 16-26.

OLIVIA, M. & NIKRAZ, H. 2012. Properties of fly ash geopolymer concrete designed by Taguchi method. Materials & Design, 36, 191-198.

OLIVIA, M. & NIKRAZ, H. R. 2011. Strength and water penetrability of fly ash geopolymer concrete. Journal of Engineering and Applied Sciences, 6, 70-78.

PALOMO, A., FERNÁNDEZ-JIMÉNEZ, A., et al. 2004. "Geopolymers": same basic chemistry, different microstructures. Materiales Construccion, 54, 77-91.

PALOMO, A., GRUTZECK, M. W., et al. 1999. Alkali-activated fly ashes: A cement for the future. Cement and Concrete Research, 29, 1323-1329.

PALOMO, A. & LÓPEZ DELA FUENTE, J. I. 2003. Alkali-activated cementitous materials: Alternative matrices for the immobilisation of hazardous wastes: Part I. Stabilisation of boron. Cement and Concrete Research, 33, 281-288.

PENG, J., HUANG, L., et al. 2013. Modeling of carbon dioxide measurement on cement plants. Advanced Materials Research, 610-613, 2120-2128.

PHAIR, J. & VAN DEVENTER, J. 2002. Effect of the silicate activator pH on the microstructural characteristics of waste-based geopolymers. International Journal of Mineral Processing, 66, 121-143.

PHAIR, J. W. & VAN DEVENTER, J. S. J. 2001. Effect of silicate activator pH on the leaching and material characteristics of waste-based inorganic polymers. Minerals Engineering, 14, 289-304.

PIMRAKSA, K., CHINDAPRASIRT, P., et al. 2011. Lightweight geopolymer made of highly porous siliceous materials with various Na2O/Al2O3 and SiO2/Al2O3 ratios. Materials Science and Engineering: A, 528, 6616-6623.

POON, C.-S., AZHAR, S., et al. 2003. Performance of metakaolin concrete at elevated temperatures. Cement and Concrete Composites, 25, 83-89.

PUERTAS, F., MARTíNEZ-RAMíREZ, S., et al. 2000. Alkali-activated fly ash/slag cements: Strength behaviour and hydration products. Cement and Concrete Research, 30, 1625-1632.

PUERTAS, F., PALACIOS, M., et al. 2011. A model for the C-A-S-H gel formed in alkali-activated slag cements. Journal of the European Ceramic Society, 31, 2043-2056.

RAMLOCHAN, T., ZACARIAS, P., et al. 2003. The effect of pozzolans and slag on the expansion of mortars cured at elevated temperature: Part I: Expansive behaviour. Cement and Concrete Research, 33, 807-814.

RANGAN, B. V. 2008. Low calcium fly ash based geopolymer concrete:Concrete construction engineering handbook. Curtin University of Technology, Perth, Australia.

RAPHAEL, J. M. 1984. Tensile strength of concrete. Concrete International Magazine, 81, 158-165.

RATTANASAK, U. & CHINDAPRASIRT, P. 2009. Influence of NaOH solution on the synthesis of fly ash geopolymer. Minerals Engineering, 22, 1073-1078.

RENDELL, F., JAUBERTHIE, R., et al. 2002. Deteriorated concrete: Inspection and physicochemical analysis. Thomas Telford.

RIDDICK, T. M. 1968. Control of Colloid Stability Through zeta potential. ZETA-METER, Incorporated.

RYU, G. S., LEE, Y. B., et al. 2013. The mechanical properties of fly ash-based geopolymer concrete with alkaline activators. Construction and Building Materials, 47, 409-418.

SAGOE-CRENTSIL, K. & WENG, L. 2007. Dissolution processes, hydrolysis and condensation reactions during geopolymer synthesis: Part II. High Si/Al ratio systems. Journal of materials science, 42, 3007-3014.

SARKER, P., GRIGG, A., et al. 2007. Bond strength of geopolymer concrete with reinforcing steel:Recent developments in structural engineering. Mechanics and Computation, 1315-1320.

SARKER, P. K. 2011. Bond strength of reinforcing steel embedded in fly ash-based geopolymer concrete. Materials and structures, 44, 1021-1030.

SARKER, P. K., HAQUE, R., et al. 2013. Fracture behaviour of heat cured fly ash based geopolymer concrete. Materials & Design, 44, 580-586.

SATHONSAOWAPHAK, A., CHINDAPRASIRT, P., et al. 2009. Workability and strength of lignite bottom ash geopolymer mortar. Journal of Hazardous Materials, 168, 44-50.

SCHNEIDER, M., ROMER, M., et al. 2011. Sustainable cement production-present and future. Cement and Concrete Research, 41, 642-650.

SCRIVENER, K. L., CRUMBIE, A. K., et al. 2004. The interfacial transition zone (ITZ) between cement paste and aggregate in concrete. Interface Science, 12, 411-421.

SCRIVENER, K. L. & YOUNG, J. F. 1997. Mechanisms of chemical degradation of cement-based systems. E & FN Spon, London.

SING, K. S. 1985. Reporting physisorption data for gas/solid systems with special reference to the determination of surface area and porosity (Recommendations 1984). Pure and applied chemistry, 57, 603-619.

SINGH, B., ISHWARYA, G., et al. 2015. Geopolymer concrete: A review of some recent developments. Construction and Building Materials, 85, 78-90.

SINSIRI, T., CHINDAPRASIRT, P., et al. 2010. Influence of fly ash fineness and shape on the porosity and permeability of blended cement pastes. International Journal of Minerals, Metallurgy, and Materials, 17, 683-690.

ŠKVÁRA, F., KOPECKÝ, L., et al. 2006. Microstructure of geopolymer materials based on fly ash. Ceramics-Silikaty, 50, 208-215.

SOFI, M., VAN DEVENTER, J., et al. 2007a. Bond performance of reinforcing bars in inorganic polymer concrete (IPC). Journal of Materials Science, 42, 3107-3116.

SOFI, M., VAN DEVENTER, J., et al. 2007b. Engineering properties of inorganic polymer concretes (IPCs). Cement and Concrete Research, 37, 251-257.

SONG, H.-W. & SARASWATHY, V. 2007. Corrosion Monitoring of Reinforced Concrete Structures-A. Int. J. Electrochem. Sci, 2, 1-28.

SONGPIRIYAKIJ, S., KUBPRASIT, T., et al. 2010. Compressive strength and degree of reaction of biomass and fly ash based geopolymer. Construction and Building Materials, 24, 236-240.

STANIFORD, S. 7 November 2012 2012. Cement Production: China and Elsewhere. Early Warning [Online]. Available from: http://earlywarn.blogspot.com.au/2012/11/cement-production-china-and-elsewhere.html.

STANISH, K., HOOTON, R. D., et al. 2005. The Rapid Migration Test—An Alternative to AASHTO T 277. HPC Bridge Views,

STENGEL, T., REGER, J., et al. 2009. LCA of geopolymer concrete – what is the environmental benefit? Proceedings of the 24th biennial conference of the Concrete Institute of Australia, Sydney, Australia.

STEVESON, M. & SAGOE-CRENTSIL, K. 2005. Relationships between composition, structure and strength of inorganic polymers. Journal of Materials Science, 40, 4247-4259.

SUMAJOUW, M. & RANGAN, B. V. 2006. Low-calcium fly ash-based geopolymer concrete: Reinforced beams and columns. Curtin University of Technology, Perth, Australia, 1-121.

SWANEPOEL, J. & STRYDOM, C. 2002a. Utilisation of fly ash in a geopolymeric material. Applied Geochemistry, 17, 1143-1148.

SWANEPOEL, J. C. & STRYDOM, C. A. 2002b. Utilisation of fly ash in a geopolymeric material. Applied Geochemistry, 17, 1143-1148.

TALHA JUNAID, M., KAYALI, O., et al. 2015. A mix design procedure for low calcium alkali activated fly ash-based concretes. Construction and Building Materials, 79, 301-310.

TAYLOR, H. & GOLLOP, R. 1997. Some chemical and microstructural aspects of concrete durability. E & FN Spon, London.

TEMUUJIN, J., VAN RIESSEN, A., et al. 2010. Preparation and characterisation of fly ash based geopolymer mortars. Construction and Building Materials, 24, 1906-1910.

TENNAKOON, C., DE SILVA, P., et al. 2014a. Influence and role of feedstock Si and Al content in Geopolymer synthesis. Journal of Sustainable Cement-Based Materials, 1-13.

TENNAKOON, C., NAZARI, A., et al. 2014b. Distribution of oxides in fly ash controls strength evolution of geopolymers. Construction and Building Materials, 71, 72-82.

THOKCHOM, S., GHOSH, P., et al. 2009. Effect of water absorption, porosity and sorptivity on durability of geopolymer mortars. Journal of Engineering & Applied Sciences, 4, 28-32.

VALCKE, S. L., PIPILIKAKI, P., et al. 2014. FT-IR and 29-Si-NMR for evaluating aluminium–silicate precursors for geopolymers. Materials and Structures, 48, 557-569.

VAN JAARSVELD, J G S, V. D., et al. 2002. The effect of composition and temperature on the properties of fly ash-and kaolinite-based geopolymers. Chemical Engineering Journal, 89, 63-73.

VAN JAARSVELD, J. & VAN DEVENTER, J. 1999. Effect of the alkali metal activator on the properties of fly ash-based geopolymers. Industrial & engineering chemistry research, 38, 3932-3941.

VAN JAARSVELD, J. G. S., VAN DEVENTER, J. S. J., et al. 2003. The characterisation of source materials in fly ash-based geopolymers. Materials Letters, 57, 1272-1280.

VICROADS-2007. Technical Note 89: Test methods for the assessment of durability of concrete. VicRoads, Australia.

WALLAH, S. & RANGAN, B. V. 2006. Low-calcium fly ash-based geopolymer concrete: Long-term properties. Res. Report-GC2, Curtin University of Technology, Perth, Australia, 1-107.

WALLIS, C. 2013. Geopolymer concrete for construction. Concrete in Australia 39, 4-5.

WANG, H., LI, H., et al. 2005. Synthesis and mechanical properties of metakaolinite-based geopolymer. Colloids and Surfaces A: Physicochemical and Engineering Aspects, 268, 1-6.

WANG, K., SHAH, S. P., et al. 2004. Effects of curing temperature and NaOH addition on hydration and strength development of clinker-free CKD-fly ash binders. Cement and Concrete Research, 34, 299-309.

WANG, S. D., SCRIVENER, K. L., et al. 1994. Factors affecting the strength of alkali-activated slag. Cement and Concrete Research, 24, 1033-1043.

WARDHONO, A. 2015. The Durability of Fly Ash Geopolymer and Alkali-Activated Slag Concretes. Ph.D. Thesis, School of Civil, Environmental and Chemical Engineering, RMIT University, Melbourne, Australia.

WARDHONO, A., LAW, D., et al. 2012. Strength of alkali activated slag and fly ash-based geopolymer mortar. Second International Conference on Microstructural-related Durability of Cementitious Composites, Amsterdam, Netherlands.

WARNER, R. F., RANGAN, B. V., et al. 1998. Reinforced Concrete. Addison Wesley Longman.

WILLIAMS, R. P., HART, R. D., et al. 2011. Quantification of the Extent of Reaction of Metakaolin-Based Geopolymers Using X-Ray Diffraction, Scanning Electron Microscopy, and Energy-Dispersive Spectroscopy. Journal of the American Ceramic Society, 94, 2663-2670.

WONGPA, J., KIATTIKOMOL, K., et al. 2010. Compressive strength, modulus of elasticity, and water permeability of inorganic polymer concrete. Materials & Design, 31, 4748-4754.

WOOD, R. 2009. Structural decomposition analysis of Australia's greenhouse gas emissions. Energy Policy, 37, 4943-4948.

XIE, J. & KAYALI, O. 2014. Effect of initial water content and curing moisture conditions on the development of fly ash-based geopolymers in heat and ambient temperature. Construction and Building Materials, 67, 20-28.

XIE, Z. & XI, Y. 2001. Hardening mechanisms of an alkaline-activated class F fly ash. Cement and Concrete Research, 31, 1245-1249.

XU, H. & VAN DEVENTER, J. 2000. The geopolymerisation of alumino-silicate minerals. International Journal of Mineral Processing, 59, 247-266.

XU, H. & VAN DEVENTER, J. S. J. 2002. Geopolymerisation of multiple minerals. Minerals Engineering, 15, 1131-1139.

YAP, S. P., ALENGARAM, U. J., et al. 2013. Enhancement of mechanical properties in polypropylene–and nylon–fibre reinforced oil palm shell concrete. Materials & Design, 49, 1034-1041.

YOUNG, J. F., BENTUR, A., et al. 1998. The science and technology of civil engineering materials. Argentina.

ZHANG, Z., WANG, H., et al. 2012. Quantitative study of the reactivity of fly ash in geopolymerization by FTIR. Journal of Sustainable Cement-Based Materials, 1, 154-166.

ZHENG, L., WANG, W., et al. 2010. The effects of alkaline dosage and Si/Al ratio on the immobilization of heavy metals in municipal solid waste incineration fly ash-based geopolymer. Chemosphere, 79, 665-671.

ZUDA, L., PAVLÍK, Z., et al. 2006. Properties of alkali activated aluminosilicate material after thermal load. International journal of thermophysics, 27, 1250-1263.

APPENDICES

Appendix A 1: Calculate Activator Modulus (AM) and Na_2O dosage

Geopolymer Mix: G1.125

Chemical Consideration :	Activator only						
Type of fly ash:	Gladstone						
According to properties of liquid Sodium Silicate				% Na_2O =	14.7%		
				% SiO_2 =	29.4%		
According to properties of Sodium Hydroxide				% Na_2O =	30.0%		

Mix (Adam A, 2009)	Fly ash	Sand	Water	Sodium Silicate Na_2SiO_3	Sodium Hydroxide NaOH	water / Solid	Na_2SiO_3 / NaOH
G 15 – 1.00	1	2.75	0.067	0.51	0.234	0.37	2.18
Adjustment =	100%	100%	56%	112.5%	93.54%		

Na_2O dosage =	15	AM =	1.125				
Mix Design (Notation)	Fly ash	Sand	Water	Sodium Silicate Na_2SiO_3	Sodium Hydroxide NaOH	water / Solid	Na_2SiO_3 / NaOH
D15 – AM1.125	1.000	2.750	0.038	0.574	0.219	0.370	2.621

Na_2O Content =	14.7%	* Na_2SiO_3 +	30.0%	* NaOH		
Na_2O from Na_2SiO_3 =	0.084	----------	Na_2O content =	15.001	%	
Na_2O from NaOH =	0.066					
Na_2O dosage (%) =	**15.001**					
SiO_2 Content =	29.4%	* Na_2SiO_3				
SiO_2 from Na_2SiO_3 =	0.169	----------	SiO_2 content =	16.868	%	
Activator Modulus (AM) =	**1.125**					

Water/solid ratio

Fly ash (kg)	Sodium Silicate (kg)		Sodium Hydroxide (kg)		added water (kg)	Total water (kg)	Total Solid (kg)
	Solid	water	Solid	water			
1.000	0.253	0.321	0.083	0.136	0.038	0.494	1.336
NaOH (15M) =	37.9%	pellts +	62.1%	water by mass			
Na_2SiO_3 =	44.1%	Solid +	55.9%	water by mass			
NaOH impurity =	99.0%						

Appendix A 2: Calculate Effective Activator Modulus (AM_{eff}) and Effective Na_2O dosage

Geopolymer Mix: G4.5

Chemical Consideration :	Activator + fly ash						
Type of fly ash:	Gladstone						
According to chemical composition of fly ash				% Na_2O =	1.85%		
				% SiO_2 =	49.97%		
According to properties of liquid Sodium Silicate				% Na_2O =	14.7%		
				% SiO_2 =	29.4%		
According to properties of Sodium Hydroxide				% Na_2O =	30.0%		

Mix (Adam A, 2009)	Fly ash	Sand	Water	Sodium Silicate Na_2SiO_3	Sodium Hydroxide NaOH	water / Solid	Na_2SiO_3 / NaOH
G 15 – 1.00	1	2.75	0.067	0.51	0.234	0.37	2.18
Adjustment =	100%	100%	125%	100%	75%		

Eff. Na_2O dosage = 15 Eff. AM = 4.5

Mix Design (Notation)	Fly ash	Sand	Water	Sodium Silicate Na_2SiO_3	Sodium Hydroxide NaOH	water / Solid	Na_2SiO_3 / NaOH
D15 – AM_{eff} 4.5	1.000	2.750	0.084	0.510	0.176	0.370	2.906

Na_2O Content =	14.7%	* Na_2SiO_3 +	30.0%	* NaOH +	1.85%	* fly ash	
Na_2O from Na_2SiO_3 =	0.075	----------	Na_2O content =	14.612	%		
Na_2O from NaOH =	0.053						
Na_2O from fly ash =	0.019						
Effective Na_2O dosage (%) =	**14.612**						
SiO_2 Content =	29.4%	* Na_2SiO_3 +	49.97%	* fly ash			
SiO_2 from Na_2SiO_3 =	0.150	----------	SiO_2 content =	64.964	%		
SiO_2 from fly ash =	0.500						
Effective Activator Modulus =	**4.446**						

Water/solid ratio

Fly ash (kg)	Sodium Silicate (kg)		Sodium Hydroxide (kg)		added water (kg)	Total water (kg)	Total Solid (kg)
	Solid	water	Solid	water			
1.000	0.225	0.285	0.066	0.109	0.084	0.478	1.291
NaOH (15M) =	37.9%	pellts +	62.1%	water by mass			
Na_2SiO_3 =	44.1%	Solid +	55.9%	water by mass			
NaOH impurity =	99.0%						

Appendix B1: Calculate mean compressive strength of geopolymer mortar

Geopolymer Specimen: G1.125

Testing duration: 7 days after casting

Specimen ID	Maximum Load (kN)	Dimensions (mm)			Compressive Strength (MPa)
		Width	Length	Height	
G1.125–7d–S1	100.04	50.0	50.0	50.1	40.0
G1.125–7d–S2	102.46	50.1	50.1	50.0	41.0
G1.125–7d–S3	106.98	50.0	50.0	50.0	42.8
		Mean compressive strength (MPa)			41.3
		Standard deviation (MPa)			1.16

Appendix B2: Calculate element oxide ratio of geopolymer mix

Geopolymer Mix	Oxide composition (mass in kg)									
	NaOH (aq)		Na_2SiO_3 (aq)			Fly ash				Water
	Na_2O	H_2O	Na_2O	SiO_2	H_2O	SiO_2	Al_2O_3	Na_2O	Fe_2O_3	H_2O
G – 1.0	0.0419	0.0705	0.0364	0.0727	0.1383	0.2465	0.1450	0.0	0.0498	0.0325
G – 1.125	0.0390	0.0657	0.0407	0.0815	0.1549	0.2455	0.1444	0.0	0.0496	0.0214
G – 1.25	0.0310	0.0523	0.0451	0.0902	0.1715	0.2443	0.1437	0.0	0.0493	0.0202

Geopolymer Mix	Total oxide composition in geopolymer mix (mass in kg)					Overall element oxide ratio of Mix		
	Na_2O	SiO_2	Al_2O_3	H_2O	Fe_2O_3	SiO_2/Al_2O_3	Al_2O_3/Na_2O	SiO_2/ Na_2O
G – 1.0	0.0782	0.3197	0.1448	0.2413	0.0498	2.20	1.85	4.09
G – 1.125	0.0797	0.3275	0.1442	0.2420	0.0496	2.27	1.81	4.11
G – 1.25	0.0761	0.3351	0.1436	0.2440	0.0493	2.33	1.89	4.40

Appendix C 1: Calculate mean compressive strength of geopolymer concrete

Geopolymer Specimen: G1.375

Testing duration: 28 days after casting

Specimen ID	Maximum Load (kN)	Dimensions (mm)		Compressive Strength (MPa)
		Diameter	Height	
G1.375–28d–S1	635.660	100.1	200.1	80.9
G1.375–28d–S2	656.458	100.0	200.1	83.6
G1.375–28d–S3	651265	100.1	200.0	82.9
		Mean compressive strength (MPa)		82.5
		Standard deviation (MPa)		1.14

Appendix C 2: Calculate mean flexural strength of geopolymer concrete

Geopolymer Specimen: G1.375

Testing duration: 28 days after casting

Specimen ID	Maximum Load (N)	Dimensions (mm)			Compressive Strength (MPa)
		Width	Depth	Span	
G1.375–28d–S1	19113.4	100.0	100.1	300.0	5.73
G1.375–28d–S2	18560.2	100.0	100.0	300.0	5.57
G1.375–28d–S3	16774.8	100.1	100.0	300.0	5.03
		Mean flexural strength (MPa)			5.44
		Standard deviation (MPa)			0.30

Appendix C 3: Calculate mean splitting tensile strength of geopolymer concrete

Geopolymer Specimen: G1.375

Testing duration: 28 days after casting

Specimen ID	Maximum Load (kN)	Dimensions (mm)		Compressive Strength (MPa)
		Diameter	Length	
G1.375–28d–S1	237.284	150.1	300.0	3.36
G1.375–28d–S2	342.512	150.0	300.1	4.85
G1.375–28d–S3	324.007	150.1	300.0	4.59
		Mean splitting tensile strength (MPa)		4.26
		Standard deviation (MPa)		0.65

Appendix C 4: Calculate mean Elastic modulus of geopolymer concrete

Geopolymer Specimen: G1.375

Testing duration: 90 days after casting

Specimen ID	Elastic modulus (GPa)					Dimensions (mm)		Average Elastic Modulus (GPa)
	1	2	3	4	5	Diameter	Height	
G1.375-90d-S1	23.565	239.67	24.080	23.986	24.042	100.1	200.1	24.036
G1.375-90d-S2	22.354	231.45	22.945	23.080	23.039	100.1	200.1	23.021
G1.375-90d-S3	22.787	228.73	22.816	22.810	22.821	100.1	200.0	22.816
						Overall mean Elastic modulus (GPa)		23.291
						Standard deviation (GPa)		0.53

Note: Data between 3rd and 5th attempt considered for the final calculations

Appendix C 5: Calculate mean Poison's ratio of geopolymer concrete

Geopolymer Specimen: G1.375

Testing duration: 90 days after casting

Specimen ID	Poison's ratio					Dimensions (mm)		Average Poison's ratio
	1	2	3	4	5	Diameter	Height	
G1.375-90d-S1	0.16	0.14	0.15	0.14	0.15	100.1	200.1	0.15
G1.375-90d-S2	0.15	0.15	0.15	0.15	0.15	100.1	200.1	0.15
G1.375-90d-S3	0.15	0.15	0.15	0.16	0.16	100.1	200.0	0.16
						Overall mean Poison's ratio		0.15
						Standard deviation		0.0056

Note: Data between 3rd and 5th attempt considered for the final calculations

Appendix C 6: Calculate mean dry density of geopolymer concrete

Geopolymer Specimen: G1.375

Testing duration: 28 days after casting

Specimen ID	Weight (g)			Volume (10^{-3} m^3)	Dry density (kg/m^3)
	Saturated surface dry	Immersed in water	Oven dry		
G1.375–28d–S1	3934.2	2209.1	3756.7	1.725	2178
G1.375–28d–S2	3918.7	2211.1	3736.3	1.708	2188
G1.375–28d–S3	3835.6	2165.3	3654.8	1.670	2188
				Mean dry density(kg/m^3)	2185
				Standard deviation (kg/m^3)	6.0

Appendix D 1: Calculate ultrasonic pulse velocity of geopolymer concrete

Geopolymer Specimen: G1.375

Testing duration: 28 days after casting

G1.375 Specimen Location	Time (µs)			Velocity (km/s)		
	28d–S1	28d–S2	28d–S3	28d–S1	28d–S2	28d–S3
L 1	29.0	27.4	25.7	3.4	3.6	3.9
L 2	29.6	27.2	25.5	3.4	3.7	3.9
L 3	28.6	30.5	26.1	3.5	3.3	3.8
L 4	30.0	27.6	26.2	3.3	3.6	3.8
L 5	25.3	27.6	26.7	4.0	3.6	3.7
L 6	26.7	27.0	27.0	3.7	3.7	3.7
L 7	27.1	27.4	26.5	3.7	3.6	3.8
L 8	27.5	31.0	26.0	3.6	3.2	3.8
L 9	26.7	27.4	28.3	3.7	3.6	3.5
L 10	27.1	27.6	29.5	3.7	3.6	3.4
L 11	27.6	27.2	26.0	3.6	3.7	3.8
L 12	27.5	27.3	25.5	3.6	3.7	3.9
L 13	27.5	29.3	31.4	3.6	3.4	3.2
L 14	28.4	31.3	27.6	3.5	3.2	3.6
L 15	27.4	28.3	30.7	3.6	3.5	3.3
L 16	27.1	27.9	31.4	3.7	3.6	3.2
		Average Velocity (km/s)		3.62	3.55	3.65
				Overall mean ultrasonic pulse velocity (km/s)		3.61
					Standard deviation	0.04

Appendix D 2: Calculate water absorption of geopolymer concrete

Geopolymer Specimen: G1.375

Testing duration: 28 days after casting

Specimen ID	Weight (g)				Immersed Absorption A_i	Boiled Absorption A_b	AVPV
	Oven dry M_1	Saturated surface dry M_{2i}	After boiled M_{3b}	Immersed in water $M4_{ib}$			
G1.375–28d–S1	924.6	976.0	989.5	550.0	5.56	7.02	14.77
G1.375–28d–S2	1052.5	1108.2	1113.1	633.5	5.29	5.76	12.64
G1.375–28d–S3	855.1	904.3	907.4	511.2	5.75	6.12	13.20
G1.375–28d–S4	859.1	908.9	914.1	514.6	5.80	6.40	13.77
G1.375–28d–S5	828.6	877.2	880.0	496.0	5.87	6.20	13.39
G1.375–28d–S6	915.1	964.3	977.6	545.2	5.38	6.83	14.45
G1.375–28d–S7	1087.3	1142.6	1147.0	654.6	5.09	5.49	12.12
G1.375–28d–S8	894.7	944.3	949.2	536.0	5.54	6.09	13.19
G1.375–28d–S9	994.7	1047.0	1050.9	598.9	5.26	5.65	12.43
G1.375–28d–S10	863.6	914.2	918.5	518.6	5.86	6.36	13.73
G1.375–28d–S11	871.9	919.7	933.6	520.3	5.48	7.08	14.93
G1.375–28d–S12	864.1	915.2	919.6	518.5	5.91	6.42	13.84
			Overall mean value		5.57	6.28	13.54
			Standard deviation		0.26	0.49	0.85

Appendix D 3: Calculate water permeability of geopolymer concrete

Geopolymer Specimen: G1.375

Testing duration: 365 days after casting

Time (min)	Water penetration (µL)			Water penetration (m^3x10^{-7})			Mean water penetration (m^3x10^{-7})	√time (√min)
	365d–S1	365d–S2	365d–S3	365d–S1	365d–S2	365d–S3		
0	1	1	1	0.01	0.01	0.01	0.0100	0.0000
1	57	59	46	0.57	0.59	0.46	0.5400	1.0000
2	74	70	59	0.74	0.7	0.59	0.6767	1.4142
3	85	79	68	0.85	0.79	0.68	0.7733	1.7321
4	94	87	76	0.94	0.87	0.76	0.8567	2.0000
5	104	94	83	1.04	0.94	0.83	0.9367	2.2361
6	109	100	87	1.09	1	0.87	0.9867	2.4495
7	117	106	93	1.17	1.06	0.93	1.0533	2.6458
8	122	109	96	1.22	1.09	0.96	1.0900	2.8284
9	128	115	102	1.28	1.15	1.02	1.1500	3.0000
10	132	119	104	1.32	1.19	1.04	1.1833	3.1623
11	137	124	109	1.37	1.24	1.09	1.2333	3.3166
12	141	128	111	1.41	1.28	1.11	1.2667	3.4641
13	145	132	115	1.45	1.32	1.15	1.3067	3.6056
14	148	135	119	1.48	1.35	1.19	1.3400	3.7417
15	152	139	119	1.52	1.39	1.19	1.3667	3.8730

Note: Data between 5th and 15th minute considered for the final calculations

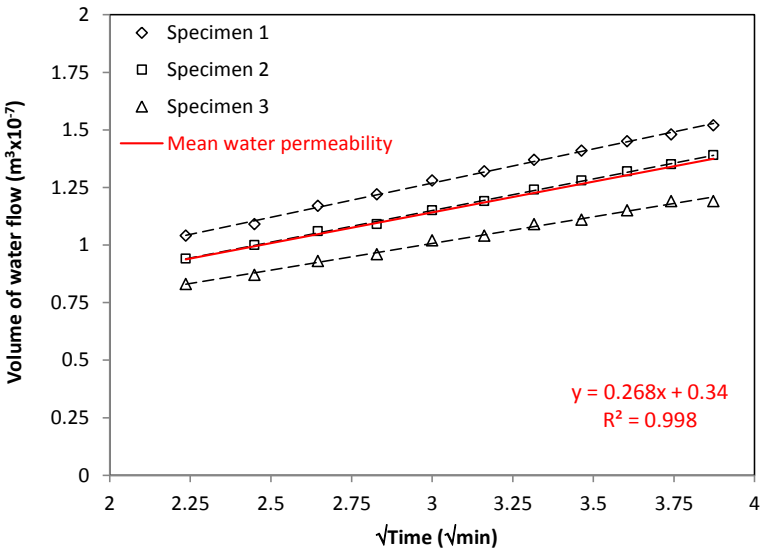

Appendix D 4: Calculate Air permeability of geopolymer concrete

Geopolymer Specimen: G1.375

Testing duration: 28 days after casting

Time (min)	Pressure (mBar)			Ln Pressure (mBar)			Mean Ln Pressure (mBar)
	365d–S1	365d–S2	365d–S3	365d–S1	365d–S2	365d–S3	
0	507	507	523	6.2285	6.2285	6.2596	6.2389
1	464	486	507	6.1399	6.1862	6.2285	6.1849
2	433	463	483	6.0707	6.1377	6.1800	6.1295
3	405	440	459	6.0039	6.0868	6.1291	6.0732
4	380	419	437	5.9402	6.0379	6.0799	6.0193
5	356	399	416	5.8749	5.9890	6.0307	5.9649
6	334	380	397	5.8111	5.9402	5.9839	5.9117
7	314	363	379	5.7494	5.8944	5.9375	5.8604
8	295	346	361	5.6870	5.8464	5.8889	5.8074
9	277	330	345	5.6240	5.7991	5.8435	5.7556
10	260	315	330	5.5607	5.7526	5.7991	5.7041
11	245	301	315	5.5013	5.7071	5.7526	5.6536
12	230	287	301	5.4381	5.6595	5.7071	5.6016
13	216	274	288	5.3753	5.6131	5.6630	5.5505
14	203	262	276	5.3132	5.5683	5.6204	5.5007
15	191	250	264	5.2523	5.5215	5.5759	5.4499

Note: Data between 5th and 15th minute considered for the final calculations

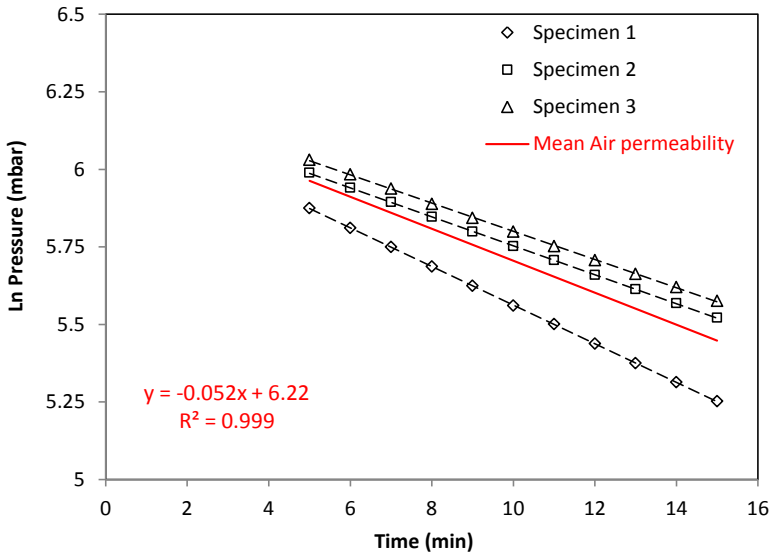

Appendix D 5: Calculate Resistivity of geopolymer concrete

Geopolymer Specimen: G1.375

Testing duration: 28 days after casting

Specimen Location	Resistivity (kΩ.cm)		
	G1.375–28d–S1	G1.375–28d–S2	G1.375–28d–S3
L 1	8.6	9.7	9.7
L 2	5.6	5.8	7.1
L 3	5.4	5.0	6.3
L 4	5.1	4.5	4.9
L 5	5.0	4.3	4.6
L 6	5.2	4.1	5.1
L 7	4.0	3.9	5.3
L 8	5.4	4.1	5.6
L 9	5.9	6.2	6.9
L 10	6.7	6.6	7.6
Average	5.7	5.4	6.3
		Mean Resistivity (kΩ.cm)	5.8
		Standard deviation	0.4

Appendix D 6: Calculate Schmidt Rebound value of geopolymer concrete

Geopolymer Specimen: G1.375

Testing duration: 28 days after casting

Specimen Location	Rebound Number		
	G1.375–28d–S1	G1.375–28d–S2	G1.375–28d–S3
L 1	23	23	23
L 2	24	32	34
L 3	28	31	33
L 4	23	24	24
L 5	30	26	32
L 6	39	38	36
L 7	45	42	38
L 8	34	27	31
L 9	34	28	32
L 10	40	38	42
L 11	37	44	42
L 12	27	31	33
L 13	23	24	22
L 14	39	34	31
L 15	32	29	31
L 16	25	25	23
Average	31	31	32
	Mean Schmidt Rebound value		31
	Standard deviation		0.5